



<https://theses.gla.ac.uk/>

Theses Digitisation:

<https://www.gla.ac.uk/myglasgow/research/enlighten/theses/digitisation/>

This is a digitised version of the original print thesis.

Copyright and moral rights for this work are retained by the author

A copy can be downloaded for personal non-commercial research or study,
without prior permission or charge

This work cannot be reproduced or quoted extensively from without first
obtaining permission in writing from the author

The content must not be changed in any way or sold commercially in any
format or medium without the formal permission of the author

When referring to this work, full bibliographic details including the author,
title, awarding institution and date of the thesis must be given

Enlighten: Theses

<https://theses.gla.ac.uk/>
research-enlighten@glasgow.ac.uk

Complex Torque Coefficient Analysis of Multi-Device Power Systems

Jonathan James Bremner

A THESIS SUBMITTED TO
THE DEPARTMENT OF ELECTRONICS AND ELECTRICAL ENGINEERING
OF
THE UNIVERSITY OF GLASGOW
FOR THE DEGREE OF
DOCTOR OF PHILOSOPHY

September 1996

© Jonathan J. Bremner 1996

ProQuest Number: 13815344

All rights reserved

INFORMATION TO ALL USERS

The quality of this reproduction is dependent upon the quality of the copy submitted.

In the unlikely event that the author did not send a complete manuscript and there are missing pages, these will be noted. Also, if material had to be removed, a note will indicate the deletion.



ProQuest 13815344

Published by ProQuest LLC (2018). Copyright of the Dissertation is held by the Author.

All rights reserved.

This work is protected against unauthorized copying under Title 17, United States Code
Microform Edition © ProQuest LLC.

ProQuest LLC.
789 East Eisenhower Parkway
P.O. Box 1346
Ann Arbor, MI 48106 – 1346

ABSTRACT

This thesis is concerned with the analysis of torsional interaction phenomena which may occur in modern power systems containing high bandwidth power control devices. In particular, it examines the suitability of Complex Torque Coefficient Analysis in providing a powerful yet visually appealing tool for the study of the underlying mechanisms and which overcomes the lack of physical understanding inherent in other methods of analysis.

In its most basic form, the Complex Torque coefficient represents the transfer function between a change in electromagnetic torque and the change in rotor angle which produced it. By recognising that the additional current flowing in the stator windings as a result of this action is composed of a supersynchronous component and a subsynchronous component, the influence of the external network on the behaviour of the machine may be represented by the complex impedance matrix which describes the response of the network at the super- and subsynchronous frequencies.

The first part of the thesis reviews the techniques currently used in the general study of dynamic stability in power systems and the background and mathematical description of the Complex Torque Coefficient is introduced. It is shown that this method of analysis is easily applied to the phenomenon of Subsynchronous Resonance due to the use of series compensation capacitors on long transmission lines.

The second part deals with the extension of the method to the multi-machine problem and to the study of interactions between synchronous machines and power flow controllers including an assessment of the risk posed to turbine shaft fatigue due to noncharacteristic harmonics. The mechanism underlying the Subsynchronous Torsional Interaction phenomena now known to exist between synchronous machines and Static Var compensators is demonstrated. The method of analysis highlights the significant advantages that the use of Thyristor Controlled Series Compensation devices may have over passive compensation schemes.

Table of Contents

List of Figures	viii
List of Tables	xii
Acknowledgements	xiv
1 Power System Dynamic Stability	1
1.1 Introduction.....	1
1.1.1 Definition of Stability as Applied to the Modern Power System.....	1
1.2 The Dynamic Stability Problem	2
1.2.1 History of Dynamic Stability Studies	4
1.2.2 Current Dynamic Stability Techniques and Software	5
1.2.3 Disadvantages of Current Techniques	7
1.3 Importance of Research in this Area	9
1.4 Principle Objectives of this Study	9
1.5 Structure of the Thesis	11
2 Complex Torque Coefficient Analysis	13
2.1 Introduction	13
2.1.1 Background.....	13
2.1.2 Basic Principles	13
2.2 Coefficients of the Synchronous Machine.....	16
2.2.1 Stator Current Components in Oscillating D-Q axes	16
2.2.2 Interpretation of the Complex Impedance Matrix.....	19
2.2.3 Complex Torque Coefficient.....	22
2.3 Influence of Synchronous Machine Parameters on the Complex Torque Coefficient	23
2.3.1 Normalisation of the Complex Torque Coefficient.....	24
2.3.2 Influence of Generator Transient and Subtransient Reactances.....	24
2.3.3 Influence of total system resistance	26
2.4 Summary of Chapter 2.....	28

3	The Power System Model.....	29
3.1	Introduction	29
3.2	Synchronous Machine Models.....	30
3.2.1	Synchronous Generator Model for Machine - Network Interaction Studies.....	31
3.2.2	Synchronous Machine Models for Multi-machine Systems.....	33
3.2.3	Flux Linkage State-Space Model - - Electrical Equations	33
3.2.4	Flux Linkage State-Space Model - - Turbine Shaft Model.....	35
3.2.5	Lower Order E'' State-Space Model.....	39
3.3	Network Model.....	40
3.3.1	Network Transformation and Impedance in d-q coordinates	40
3.3.2	Transmission Line Model.....	41
3.3.3	Transformer Model	43
3.3.4	Load Models.....	44
3.4	Summary of Chapter 3	44
4	Subsynchronous Resonance Analysis.....	45
4.1	Introduction	45
4.1.1	Background	45
4.1.2	Induction Generator Effect	45
4.1.3	Torsional Interaction	47
4.1.4	Causes and Countermeasures of SSR.....	47
4.2	Electromagnetic Complex Torque Coefficients applied to the single machine system	50
4.2.1	Single Machine System.....	51
4.2.2	Effect of Network Capacitors on Electromagnetic Torque Coefficients.....	52
4.2.3	Multiple Transmission Lines	55
4.2.4	Influence of Transmission Line Resistance.....	55
4.3	Mechanical Complex Torque Coefficients of the Multi-Mass System	56
4.3.1	Natural Frequencies using an Analytical Method	57
4.3.2	Natural Frequencies using Eigenanalysis.....	59
4.3.3	Natural and Coupled System Frequencies using Electromechanical Torque Analysis	60
4.4	SSR Analysis of the Single Machine-Compensated Transmission Line—Six Turbine Shaft.....	62

4.4.1	Time Constants for decay of Principle torsional Oscillations.....	64
4.4.2	Graphical Analysis of the Combined Electromagnetic and Mechanical Systems	65
4.5	Consideration of Additional Modelling Detail.....	68
4.5.1	Representation of Additional Excitation Control.....	68
4.5.2	Influence of Transmission System Load Characteristics on Decay of Principle Torsional Oscillations.....	71
4.6	Summary of Chapter 4.....	72
5	Multi-Machine Complex Torque Coefficients	73
5.1	Introduction	73
5.2	Calculation of Coefficients.....	75
5.2.1	State-space approach to Torque Coefficients Algorithm.....	78
5.2.2	Linearised State-Space Multi-Machine Model.....	79
5.2.3	Retention of Higher Frequency Transmission Line effects.....	80
5.2.4	Conversion to System Reference Frame	81
5.2.5	Complex Impedance of the Synchronous Machine - - Simple Shaft Model.....	82
5.2.6	Complex Impedance of the Synchronous Machine - - Full Shaft Model	84
5.3	Three Machine System Study.....	84
5.3.1	Single Rotor Mass Models - - Neglecting Sub- and Super-synchronous Network Effects	86
5.3.2	Single Rotor Mass Models - - Full Network Model.....	88
5.3.3	Multi-Mass Models - - Full Network Model.....	89
5.4	Summary of Chapter 5.....	92
6	Subsynchronous Torsional Interaction Due to Static Var Compensators	93
6.1	Overview of the Static Var Compensator	93
6.2	Typical Applications.....	95
6.2.1	Voltage Control.....	95
6.2.2	Reactive Compensation of HVDC Converters	95
6.2.3	Improvement of System Damping.....	96
6.3	Torsional Interactions between Synchronous Machines and SVCs.....	97
6.4	Static Var Compensator Model	97
6.4.1	Load-Flow Model of the Static Var Compensator	98

6.4.2 Complex Torque Analysis Model of the Static Var Compensator	101
6.5 Analysis of Subsynchronous Torsional Interaction	104
6.5.1 Influence of Voltage Regulator parameters on the Torque Coefficient Loci	105
6.5.2 Influence of SVC Placement.....	107
6.5.3 Influence of SVC Operating Point	108
6.6 Thyristor Controlled Series Compensation devices	113
6.6.1 SSR Mitigation capability of the TCSC	114
6.6.2 Calculation of TCSC Complex Admittance	114
6.6.3 Complex Torque Coefficients for a single machine - TCSC system	115
6.7 Summary of Chapter 6	118
7 Validation of Complex Torque Coefficient Technique	121
7.1 Techniques for validation	121
7.2 Non-linear Simulation of The Series Compensated System.....	122
7.2.1 Case I — 50% Line Compensation	125
7.2.2 Case II — 70% Line Compensation	128
7.2.3 Case III — 91% Line Compensation.....	130
7.3 Summary of Chapter 7	132
8 Torsional Stressing due to HVDC Converters	133
8.1 Introduction	133
8.2 Excitation by Non-characteristic Frequencies	133
8.2.1 Non-characteristic frequencies	134
8.2.2 Modulation frequencies for a 50Hz/60Hz Asynchronous System.....	135
8.2.3 Modulation frequencies for a 50Hz/50Hz asynchronous System	136
8.3 Modal shaft torque due to steady resonant excitation.....	138
8.3.1 660MW Machine A.....	138
8.3.2 1000MW Machine B.....	140
8.4 Generator Scaling Factor (GSF).....	140
8.5 Evaluation of Shaft Torques in Multi-Machine systems	142
8.5.1 System Equivalent Circuit.....	142
8.5.2 System Scaling Factor (SSF)	142
8.5.3 Effect of Damper Representation on Generator Reactance	

-- 500MW Machine D	143
8.6 Shaft Torques due to Noncharacteristic Currents – 50Hz/50Hz Asynchronous	
Link	144
8.6.1 Modulation Product Currents and Shaft Torques – 660MW Machine A	144
8.6.2 Modulation Product Currents and Shaft Torques - 1000MW Machine B	145
8.7 Summary of Chapter 8	146
9 Conclusions	147
9.1 Suggestions for Further Work	150
Appendix 1 Software Development.....	151
A.1 Introduction	151
A.2 Program Structure	151
A.2.1 Main menu's	154
A.2.2 File selection	155
A.2.3 Generator Template Editor	156
A.2.4 System Template Editor	159
A.2.5 Loadflow Analysis and results	162
A.2.6 SVC Status Page.....	164
A.2.7 Torque Coefficient Analysis Page.....	165
A.3 pc-dap Input file format	168
A.3.1 System Input File Format	168
A.3.2 Generator Data Input File Format.....	174
A.4 User interface	176
A.4.1 Pull-Down Menus.....	176
A.4.2 Static Menus.....	179
Appendix B Modeling of Static Var Compensation	181
Appendix C Modal Torque Analysis Algorithms.....	185
C.1 Amplitude of Shaft Torsional Vibrations due to Resonant Excitation	185
C.2 Modal Torque due to Resonant Excitation at Generator Rotor.....	185
C.3 Time Constants for Decay of Torsional Vibration	186

C.4 Generator Scaling Factors (GSF)	187
C.4.1 Method A - - Harmonic Currents completely reflected at rotor surface	187
C.4.2 Method B - - Equivalent circuits neglecting resistance	188
C.4.3 Method C - - Equivalent circuits representing resistance	189
Appendix D Approximate Calculation of Noncharacteristic Current Level.....	191
Appendix E Material Hysteretic Damping	193
References.....	195

List of Figures

Figure 1.1: Range of Dynamical Phenomena	3
Figure 2.1: Mechanical Analogy of Electrical Complex Torque Coefficient	14
Figure 2.2: Transfer Function from Generator Speed to Electrical Torque.....	15
Figure 2.3: Oscillating Rotor Coordinates.....	16
Figure 2.4: Single Transmission Line System	18
Figure 2.5: Electromagnetic damping Coefficient as a function of line reactance – Influence of Transient reactance of synchronous machine	25
Figure 2.6: Electromagnetic damping Coefficient as a function of line reactance.....	25
Figure 2.7: Electromagnetic damping Coefficient as a function of total resistance	26
Figure 2.8: Electromagnetic damping Coefficient as a function of total resistance – Influence of Transmission line reactance	27
Figure 3.1: Power System Schematic	30
Figure 3.2: Equivalent Circuits for Two-axis Model.....	32
Figure 3.3: Lumped Mass-Spring Model of a Turbine-Generator Shaft	36
Figure 3.4: Π Equivalent Circuit Representation of a Transmission Line	41
Figure 3.5: System Admittance Matrix Construction.....	42
Figure 3.6: Equivalent Circuit Model of the Transformer.....	43
Figure 4.1 : Equivalent Circuit for the Induction Machine	46
Figure 4.2 : The Phase Shifter Concept	47
Figure 4.3 : HVDC link	50
Figure 4.4 : Single Machine System	51
Figure 4.5 : Electromagnetic Damping Torque Component vs Rotor Oscillation Frequency	53
Figure 4.6 : Variation of Damping Torque Component with Compensation Level	54
Figure 4.7 : Effect of Parallel Lines.....	54
Figure 4.8 : Effect of Transmission Line Resistance	56
Figure 4.9 : 4-Mass Turbine-Generator-Exciter System	57
Figure 4.10: Natural Frequencies of the 4-Mass System.....	59
Figure 4.11: Mechanical Synchronising Coefficient	63
Figure 4.12: Mechanical Damping Coefficient	63
Figure 4.13: Analysis of the combined systems	66
Figure 4.14: Analysis of the parallel line system.....	67

Figure 4.15: Two Compensated line System.....	67
Figure 4.16: Excitation system with Stabiliser	68
Figure 5.1: Multi-machine Matrix Reduction.....	76
Figure 5.2: Relationship between Common and Machine Reference Axes.....	83
Figure 5.3: Nine bus, 3 machine system	84
Figure 5.4: Impedance Plot - - Single Rotor Mass.....	85
Figure 5.5: Impedance Plot - - Full Shaft Model.....	85
Figure 5.6: Full Shaft Model - - Increased Steam Viscous Damping	86
Figure 5.7: Electromagnetic and mechanical synchronising coefficients.....	87
Figure 5.8: Electromagnetic Damping Coefficient – Three machine system	88
Figure 5.9 : Single rotor mass - Network included.....	89
Figure 5.10: Multi-mass shaft - Network included	90
Figure 5.11: Full shaft model - Capacitor compensated system.....	90
Figure 5.12: Coincidental electrical system and shaft resonant frequencies	91
Figure 6.1: Static Var Compensator	94
Figure 6.2: Voltage/Current Characteristic for the SVC	94
Figure 6.3: Load-Flow Representation of the SVC	99
Figure 6.4a: Voltage Profile before connection of Static Compensator	100
Figure 6.4b: Voltage Profile after connection of Static Compensator	100
Figure 6.5: Primary Voltage Control Loop	101
Figure 6.6: Single Machine - SVC - Infinite Bus System.....	104
Figure 6.7: Influence of SVC Voltage Regulator Lag Time Constant	106
Figure 6.8: Influence of SVC Voltage Regulator Gain	106
Figure 6.9: Combined Electromagnetic and Mechanical SVC system.....	108
Figure 6.10: Influence of Machine to Compensator Line Impedance	109
Figure 6.11: Influence of Compensator to Infinite Bus Line Impedance.....	109
Figure 6.12: Variation of Damping Component with SVC Operating Point	110
Figure 6.13: Variation of Minimum Damping with SVC Operating Point	111
Figure 6.14a: Influence of Generator Real Power – Constant SVC Reactive Power Injection	112
Figure 6.14b: Influence of Generator Real Power Demand – Variation of SVC Reactive Power Injection	112
Figure 6.15: Thyristor Controlled Compensation Scheme	114
Figure 6.16: SSR Mitigation using TCSC Device.....	115

Figure 6.17: Influence of Voltage Regulator Lag Time Constant – TSCS System	117
Figure 6.18: Influence of Thyristor Firing Delay – TSCS System	117
Figure 7.1: Test system for Validation using PSCAD.....	123
Figure 7.2: Torque coefficient analysis for Case I – 50% compensation	125
Figure 7.3: Electromagnetic Torque – 50% compensation	126
Figure 7.4: FFT of torque waveform due to 50% compensation	126
Figure 7.5: LPA-LPB Shaft section torque – 50% compensation	126
Figure 7.6: Electromagnetic Torque waveform for Case I with increased transmission line resistance	127
Figure 7.7: LPA-LPB Shaft section torque corresponding to electromagnetic torque	127
excitation illustrated in Figure 7.6.....	127
Figure 7.8: Torque coefficient analysis for Case II – 70% compensation.....	128
Figure 7.9: Electromagnetic torque for Case II – 70% compensation	129
Figure 7.10: LPA-LPB Shaft section torque – 70% compensation	129
Figure 7.11: FFT of torque waveform due to 70% compensation	129
Figure 7.12: Torque Coefficient analysis for Case III–91% compensation	130
Figure 7.13: Electromagnetic torque due to 91% compensation	131
Figure 7.14: LPA-LPB Shaft section torque - 91% compensation	131
Figure 7.15: Electromagnetic torque due to 92% compensation	131
Figure 8.1 : Asynchronous HVDC Link.....	134
Figure A.1: Flow Diagram of PC-DAP	152
Figure A.2: Initial PC-DAP Menu Options	155
Figure A.3: Main Menu Options.....	156
Figure A.4: File Selection Box.....	157
Figure A.5: PC-DAP Error Messaging	157
Figure A.6: Generator Template Editor	157
Figure A.7: PC-DAP System Template Editor.....	159
Figure A.8: Component definition.....	160
Figure A.9: Loadflow results page	163
Figure A.10: Voltage Distribution display	163
Figure A.11: Power flow distribution display	164
Figure A.12: SVC Display Box.....	164
Figure A.13: Torque Coefficient Analysis Page.....	166
Figure A.14: PC-DAP Eigenanalysis results	167
Figure A.15: PC-DAP Pull Down Menu.....	177

Figure A.16: Sub-menu's.....	178
Figure B.1 : SVC Primary Voltage Control Loop.....	181
Figure E.1 : Hysteresis Loop.....	193

List of Tables

Table 2.1: Generator Constants.....	23
Table 4.1: Generator and Transmission Line Parameters	51
Table 4.2: Rotor Inertias and Stiffnesses	52
Table 4.3 : Effect of Load Characteristics on Net Damping.....	71
Table 4.4 : Effect of Load Characteristics on Time Constants	71
Table 5.1: Eigenvalues for 3 Machine System.....	87
Table 6.1 : Iterative SVC Voltage Scheme	
-- Set point = 1.0p.u. voltage.....	99
Table 6.2 : Typical Parameters for SVC Model.....	103
Table 7.1 : Machine electrical parameters.....	124
Table 7.2 : Rotor Inertias and stiffnesses	124
Table 8.1 : Modulation Product Harmonics for a 50Hz/60Hz HVDC Link.....	136
Table 8.2 : Modulation Product harmonics for a 49.75Hz/50.5Hz HVDC Link	136
Table 8.3 : Generator Constants and Steam Torque Data	137
Table 8.4 : Rotor Inertias and Stiffnesses.....	137
Table 8.5 : Shaft Torques for 0.004p.u. Torque Excitation Acting on Generator Rotor	
-- 660MW Machine A at Full-load	139
Table 8.6 : Shaft Torques for 0.004p.u. Torque Excitation Acting on Generator Rotor	
-- 660MW Machine A at No-load	139
Table 8.7 : Shaft Torques for 0.004p.u. Torque Excitation Acting on Generator Rotor	
-- 1000MW Machine B at Full-load.....	139
Table 8.8 : Shaft Torques for 0.004p.u. Torque Excitation Acting on Generator Rotor	
-- 1000MW Machine B at No-load.....	140
Table 8.9 : Generator Scaling Factors - Machine A, B, and C	141
Table 8.10 : Effect of Damper Representation on Generator Scaling Factors	
-- 500MW Machine D.....	141
Table 8.11 : Typical System Scaling Factors (SSF) - - 250MW Link	143
Table 8.12 : Effect of Damper Representation on Generator Harmonic Impedance	
-- 500MW Machine D at Full-load.....	143
Table 8.13 : Shaft Torque due to Resonant Excitation acting on Generator Rotor	
-- 660MW Machine A.....	145
Table 8.14 : Shaft Torque resulting from Resonant Excitation acting on Generator Rotor	

-- 1000MW Machine B.....	146
Table A.1: Generator template editor Mechanical parameters.....	158
Table A.2: Generator template editor Electrical parameters.....	158
Table A.3: System template editor Busbar parameters.....	160
Table A.4: System template editor Transmission Line parameters	161
Table A.5: System template editor Generator parameters	161
Table A.6: System template editor Shunt parameters	161

Acknowledgements

Firstly, I thank my supervisor Dr Enrique Acha for his unwavering guidance and encouragement over the last three years. I must also thank Professor T.J.E. Miller for his support of the project and for providing the facilities to allow me to carry out this research. I also thank Dr T.J. Hammons for his useful input and advice.

I acknowledge the joint financial support of Scottish Power PLC and the Science and Engineering Research Council. Special acknowledgement is due to Mr Ken Trantor and Mr Jim Toal of Scottish Power PLC for their support and advice.

I thank all my colleagues in the Scottish Power Electronics and Electric Drives Consortium (SPEED) and in the Department of Electronics and Electrical Engineering at Glasgow for providing the unique working environment which makes working at Glasgow a truly enjoyable experience.

Finally, I thank my family and friends whose support and encouragement I knew I could always count on.

POWER SYSTEM DYNAMIC STABILITY

1.1 INTRODUCTION

The reliability of modern power systems is something which we, perhaps, take for granted. But the continually expanding demand for power makes it increasingly more difficult for electricity utilities to maintain system integrity in terms of availability, voltage regulation, and frequency regulation. From the most basic fundamental point of view, the first requirement of reliability is to maintain the synchronous generators running concurrently and with adequate capacity to meet the load demand. The second requirement is to maintain the integrity of the high voltage transmission system along which the power is transmitted to the load centres. Consequently, in the event of a disturbance or a change in operating point which would cause the system to oscillate, the system should settle to a new point of equilibrium in which both of the above requirements are satisfied. If this were the case, the system would be described as *stable*. If, however, the system continues to oscillate about its operating point, or one or both of the above requirements is not met, the system would be described as *unstable*. To ensure a reliable service therefore, being able to predict the *stability* of a power system under many feasible operating conditions is an important aspect of power system planning.

1.1.1 Definition of Stability as Applied to the Modern Power System

The term *stability* is a very general expression when applied to electric power systems. As the systems evolved, so too has the most appropriate definition of stability at that time. It is useful at this point to briefly examine the classical definitions of stability that were valid during the early period of power systems analysis.

Transient stability referred to the stability of a power system subject to a sudden and severe disturbance, such as a 3-phase line to ground fault, which was beyond the capability of the linear and continuous stability control. Of particular interest was the behaviour of the synchronous generators in the system, their rotor angles, internal electromotive forces, terminal voltages, and currents. These, in turn, determined the network parameters such as real and reactive power flow in the transmission lines, busbar voltages, and so on.

- *Steady-state stability* referred to the stability of a power system which was subject to a relatively small or gradual change, particularly focusing on the dynamics of synchronous machines following a transition from one operating point to another, to adjust for load changes.

In more recent times, dynamic stability has received increased attention. This is due mainly to the use of wide bandwidth controlled devices which extend the region of possible instability from a few milliseconds up to several minutes. In a more general form, dynamic stability refers to the stability of a power system which is subject to a small disturbance; the system can be described by linear differential equations, if the size of disturbance allows it, and the oscillations may be stabilised by conventional control techniques.

1.2 THE DYNAMIC STABILITY PROBLEM

The dynamic stability problem is often confused with the earlier steady-state problem, but as alluded to above, the two are not the same; steady-state stability is a subset of the former and essentially questions long term stability. The dynamic stability problem differs from the transient problem in several ways. By dynamic stability we mean the ability of all machines in the system to adjust to small load changes or impacts. To illustrate, consider a multi-machine system feeding a constant load. At a given instant the load is changed by a small amount. Assume that this change in load is large enough to be recognised as such by a group of machines in the system. The machines nearest the load will experience the biggest change and those farther away will experience a smaller change. Since it is a load increase, there is an immediate increase in the output power requirements from each of the machines. Since step changes in power to turbines are not possible, this

increased power requirement will come first from stored energy in the machines, initially from the magnetic field and then from the rotational energy. Because of differences in size, design and electrical distance from the load, each machine will respond differently, each having its own natural frequency of response, and will oscillate until damping forces decay the oscillations. Thus the one change in load sets up all kinds of oscillatory responses and the system “rings” for a time with many frequencies present. The dynamic stability study assesses the possibility of dynamical phenomena such as self-excitation of generators, network torsional interactions, and control system related oscillations as a consequence of the small change in load or disturbance. Figure 1.1 illustrates the range of dynamical phenomena that may affect the correct operation of a typical power system. In this illustration, dynamic stability studies would encompass the range of phenomena between Subsynchronous Resonance and Long Term dynamics. The Daily Loadflow entry is a quasi-steady state condition and is included simply for comparison.

The detailed study of dynamic stability for a typical power system, operating in a three-phase mode, is complicated by the size and complexity of the networks involved. In addition, machines interact with each other across the network, and control systems are present, adding further complexity to the study. On the basis of these considerations, the analysis invariably requires the proper formulation of the mathematical model of the complete system, machines, network, and other controlled plant. There are several ways of achieving this, each one with its own advantages, and indeed disadvantages.

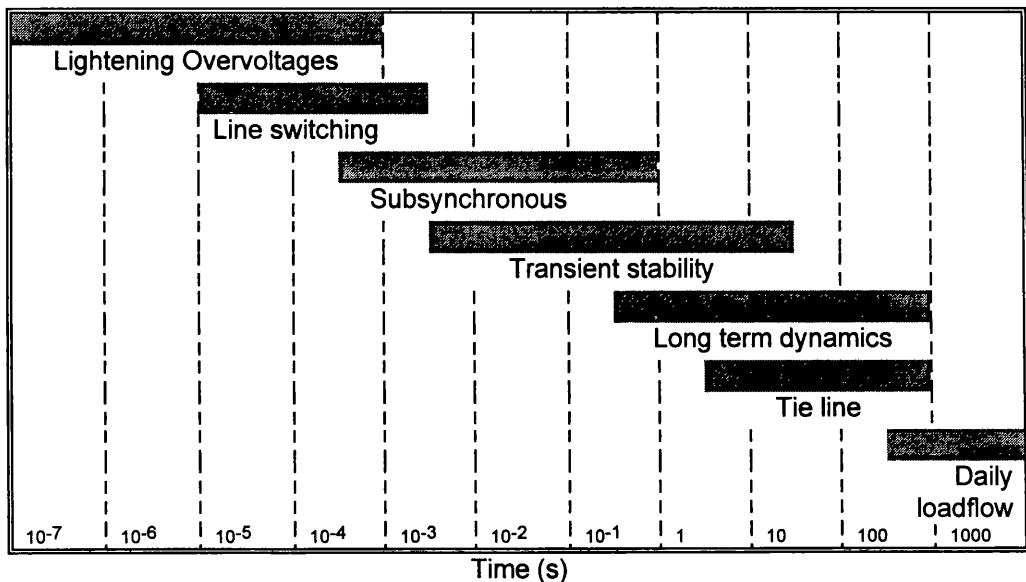


Figure 1.1: Range of Dynamical Phenomena

1.2.1 History of Dynamic Stability Studies

Power system stability was first recognised as an important problem in the 1920's by Steinmetz [1], in which the short term or transient period after a large disturbance was the subject of research. Much of the electric utility industry effort and interest related to system stability to date however, has been concentrated on the short term response, and as a result the system is designed and operated so as to meet a set of reliability criteria concerning stability in the transient sense. Well established analytical techniques and computer programs exist for the analysis of transient stability but these methods will not be discussed here. There is however, a wealth of literature on the subject as described for example by Young [2], Kimbark [3], Anderson [4], and Kakimoto [5].

In recent years, the need for studying the response of the system for longer periods of time has been recognised, and analytical tools for studying these aspects have been evolving. In dynamic stability analysis, the problem is usually one of ensuring sufficient damping of system oscillations. In general, the stability properties of an oscillatory system do not depend on the size of the disturbance if that system is inherently unstable and hence can be analysed by considering the system linearised about a point of equilibrium. This, of course, excludes problems which are of a transient nature for example the loss of synchronism following a large shock to the system which clearly does depend on the size of the initial disturbance. This has allowed the use of powerful analytical techniques applicable to linear systems to determine the stability characteristics of the system. Eigenvalue analysis is by far the most extensively employed technique, although other methods, especially those used frequently in determining control system stability, for example Nyquist and Routh's criteria, have been used successfully for power system stability analysis also.

The analysis of dynamic stability is nowhere near as widespread as transient stability, and as a result there are no standard study procedures with which to follow. Many utilities take dynamic stability for granted and carry out no studies at all, or simply depend on transient studies to reveal possible problem areas. This is primarily because, in the past, a system which remained stable for the first few seconds after a large disturbance was almost certain to remain stable for small perturbations about the post-fault condition. This, however, is not the case for today's power systems. As the systems developed and increased in complexity, the need to conduct dynamic stability studies as part of the

routine planning procedures was recognised. In reflection of this, much attention has been devoted in recent years to the development of analysis tools specifically designed to answer questions relating to dynamic stability issues.

1.2.2 Current Dynamic Stability Techniques and Software

A number of dynamic stability software packages have emerged over the years as described by Byerly [8], Wang [9], Uchida [10], Verghese [11], and Stadnicki [13]. These are all based on essentially the same approach of describing the power system in a state-space form,

$$\dot{x} = Ax \quad [1.1]$$

and determining the eigenvalues belonging to the matrix A. The imaginary part of the eigenvalue is equal to the frequency of the mode in rad/s, or in per unit with respect to the base frequency if the system has been described in per unit, and the real part indicates the stability of that mode; a negative number indicates a stable mode, and a positive number indicates an unstable mode. However, one of the deterrents of this approach to the wide spread analysis of dynamic stability has been the computational limitations, a situation which in recent years has begun to dissolve.

Conventional 'eigenanalysis' programs, such as described by Alden et al [7] form the state-matrix of the entire system explicitly and then use a general routine to determine the eigenvalues of that system. Most commonly, these routines employ the QR transformation method, originally developed by Francis [6]. The method is robust, but is limited to systems of only a few hundred dynamic states. To overcome these limitations of the conventional approach, much work has been expended to develop improved eigenvalue routines which focus on determining a selected subset of eigenvalues. Further, these methods avoid constructing the A matrix explicitly which improves the computational aspects of the problem.

One such technique is the AESOPS algorithm [8] which uses a novel frequency response approach based on the application of an external torque to a particular generator in a multi-machine system from which the eigenvalues associated with the rotor swing modes of that multi-machine system may be calculated. Essentially, it is an eigenvalue

search technique which relies on a given estimate of a single eigenvalue belonging to the system to compute a more accurate estimate of that eigenvalue. If a particular generator participates in more than one mode of oscillation, then the computed eigenvalue depends on the initial eigenvalue estimate used. For this reason, the authors recommend that a classical eigenanalysis be completed before the AESOPS algorithm is applied. A number of other powerful methods have emerged in the literature

Wang and Semlyen [9] describe the application of two sparsity based techniques to the small signal stability of large power systems; simultaneous iterations and the modified Arnoldi method. Both these methods belong to a class of methods known as the Krylov method described by Ruhe [12] which are high performance alternatives to the QR method. There are two important features of these methods. First, they are both aimed at finding a few of the dominant eigenvalues of the system A matrix, which can be useful when applied to power system analysis since usually only a small number of modes are relevant to system wide stability, and secondly, it is not necessary to form the A matrix explicitly, which helps to preserve the full sparsity of the problem.

The S-Matrix method, described by Uchida [10], transforms the original A matrix into the 'S' matrix according to Eqn. 1.2 in such a way that eigenvalues with poor damping (small negative real parts) become greater in absolute value than eigenvalues with good damping (large negative real parts).

$$S = (A + hI)(A - hI)^{-1} \quad [1.2]$$

h: a positive real number

I: the unit matrix

The stability of the system is then judged on the absolute value of the largest absolute eigenvalue $|\lambda_s|$ of the S-matrix according to the following set of rules:

unstable if $|\lambda_s| > 1$

critical if $|\lambda_s| = 1$

stable if $|\lambda_s| < 1$

As shown in [10], the computations can be arranged to take advantage of the sparse nature of the overall system equation.

The Selective Modal Analysis (SMA) approach developed by Verghese [11] attempts to identify system states that are relevant to the selected modes of interest. A reduced order model of the system is then constructed which retains only those relevant states. Standard eigenanalysis techniques may then be applied to this reduced order system.

Stadnicki and Van Ness [13] proposed an interesting approach to eigenvalue calculation founded on the idea of the invariant subspace which permits the calculation of eigenvalues belonging to an overall system matrix A by calculating the eigenvalues of subsystems M, N, \dots which are subsets of the entire eigenvalue set. Since the subsystems will be of a lower order than the overall system, calculation of subset eigenvalues will be considerably faster than simply calculating the eigenvalues directly from the A matrix.

The contributions highlighted above are predominately concerned with the calculation of dominant inter-machine or inter-area modes and do not address the issues of higher frequency interactions such as will be found on systems containing series compensation and high bandwidth power flow controllers. Gross et al [14] partly addressed this with the development of the EISEMAN package which is capable of studying a wide range of dynamic stability phenomena including subsynchronous resonance, inter-machine interactions and the effect of excitation and turbine-governor systems on stability although no attention was given to high bandwidth controllers such as Static Var compensators and their influence on system stability.

1.2.3 Disadvantages of Current Techniques

The techniques described above, although being inherently powerful, do have two significant drawbacks:

1. The analyses relies on mere mathematical sophistication and do not yield a good physical explanation to the complex processes at work. Even the more sophisticated techniques reviewed above still present the results in the same quantitative manner, their only gain over the more conventional approach being that these techniques effectively filter the system modes to reveal only those modes which play a dominant part in system stability. This indeed spares the engineer the task of identifying these modes by 'post-processing' the raw eigenvalues, but he still bases his/her analysis on what is a statement rather than an explanation of stability.

2. Eigenanalysis does not lend itself to the study of any one machine in particular – a ‘system’ solution is always obtained. In systems containing many machines, this itself can make a detailed analysis a time consuming process, producing, for even a moderately sized system, many hundreds of eigenvalues most of which have little or no impact on system damping.

Much of this thesis describes the development of a multi-machine, multi-device Dynamic stability program based on the Complex Torque Coefficient technique which has not been discussed in-depth in the literature heretofore. Unlike the conventional techniques discussed, this approach aims to give a clearer explanation of the complex mechanisms that are responsible for Synchronous machine instability for the full range of dynamic stability phenomena including self-excitation, Subsynchronous Resonance, Subsynchronous Torsional Interaction, and intermachine interactions. It should be noted that the dynamic Stability programs discussed in the previous section, although being able to analyse systems of many generators, and in some cases, other controlled power system components, cannot be used to predict or study the SSR phenomena, as this would require explicit representation of the network dynamics, which due to the high level of complexity, are neglected in all.

Oscillatory problems caused by Subsynchronous Resonance and Subsynchronous Torsional Interaction are well documented in power systems literature. However, it is noted that most reported analyses to date have concentrated on the eigenanalysis of highly simplified power system representations. The IEEE SSR Working Group proposed a standard model known as the IEEE First Benchmark model for Computer Simulation in 1977 [15], followed by the second Benchmark Model [16] in 1985 which extended the original model to a two machine system. These models have been extensively employed for more than a decade by many authors although they only represent simple configurations rarely encountered in practical power systems. The primary use of these models is simply to assess possible SSR mitigation schemes. The detailed SSR analysis of a typical large multi-machine power system requires the use of a much more comprehensive power system model, with explicit representation of all generators, controlled devices and network dynamics. The Complex Torque Coefficient technique described in this thesis can be applied to any arbitrary power system with representation of machine dynamics,

transmission line dynamics, shunts, transformers, loads, and dynamic devices, such as Static Compensators.

1.3 IMPORTANCE OF RESEARCH IN THIS AREA

In recent years, the global power demand has shown a steady but geographically uneven growth. The available power generation is often remote to the growing load centres and locations of new power generation plants are largely determined by environmental acceptability and the cost of available energy. In order to meet the power demand, the utilities increasingly rely on the utilisation of existing generation facilities via power import and export arrangements. This requires the interconnection of previously independent power systems into an ever increasing grid. For the connection of remote energy sources or for the transfer of power over long distances, the most cost effective method is by HVDC transmission. Furthermore, the desire to increase line loadability of existing transmission corridors and the need to maintain transient and dynamic stability throughout the network has dictated the need for faster, more flexible control of power flow and reactive compensation in the transmission system using solid-state power flow and compensation controllers i.e. FACTS devices. As a result of the increasing density of both HVDC systems and compensation schemes, it is important that suitable analysis tools are developed which provide the engineer with a good physical picture of system damping in both the subsynchronous and supersynchronous frequency ranges.

1.4 PRINCIPLE OBJECTIVES OF THIS STUDY

The principle objective of this project was the development of a fully comprehensive small-signal dynamic stability package based on the concept of Complex Torque Coefficient analysis.

This thesis has extended the concept of Complex Torque coefficient analysis, previously developed with reference to simple system configurations, to form the basis for the interpretation of more comprehensive stability analyses containing an unlimited number of synchronous machines and controlled devices. It has been illustrated that the method provides a valuable means for studying the fundamental mechanisms involved in not only the subsynchronous resonance phenomenon, but all torsional interaction

phenomenon encompassing inter-machine characteristics and machine-device characteristics.

The development of complex torque coefficients in the context of multi-machine power systems has been presented, for which all relevant machine and system equations have been developed. Unlike the eigenanalysis approach, complex torque coefficients allow an enhanced view of the mechanisms involved in the multi-machine interactions. Contrary to previously published work on the subject, which does not take full account of the low frequency coupling between synchronous machines, this thesis utilises the rigorous state-space formulation of the interconnected multi-machine system such that the calculation of the torque coefficients are based on a full modal analysis of the system which, to the best of the authors knowledge, has not been discussed in the literature heretofore.

It has demonstrated that this form of analysis can be used successfully to analyse potential instants of interactions between rotating machinery and static compensators. It has been shown that the principle source of the interaction is through the voltage regulator action of the compensator. The extent of the interaction depends on the specific operating point of both the machine and the compensator and on the location of the compensator relative to the machine.

An investigation of the damping characteristics of the recently developed Thyristor controlled series compensation device has been presented. It has been demonstrated by complex torque coefficient analysis that the TCSC device offers considerable advantage over conventional fixed compensation schemes. However, the possibility of unfavourable interaction with nearby machines still exists such that detailed investigations of damping characteristics should be thoroughly studied before implementing such a scheme.

This thesis has presented an in-depth analysis of the excitation of shaft torsional vibrations by variable frequency ripple currents superimposed on DC currents in asynchronous HVDC Links. Equivalent circuits of the synchronous machine are employed to correlate HVDC disturbance current impressed on the generator stator with steady-state torque excitation from which magnitude of turbine shaft torque is found. It has been concluded that such superimposed currents can excite sympathetic vibrations in the turbine-generator shaft. The susceptibility of the turbine shaft to excitation by variable frequency currents depends on the mechanical and electrical parameters of each specific case.

1.5 STRUCTURE OF THE THESIS

The Chapter structure of this thesis is as follows:

Chapter 2 describes the technique known as Complex Torque Coefficients, its background, basic principles, and method of calculation when applied to synchronous generators.

Chapter 3 develops the power system model which constitutes the comprehensive modelling ability required for the useful and accurate study of multi-element power systems.

Chapter 4 discusses the application of Complex Torque Coefficients, when used in conjunction with the power system model developed in Chapter 3, to the problem of Subsynchronous Resonance.

Chapter 5 extends the analysis technique to the area of multi-machine interactions, in particular how turbine-generator-exciter shaft modes of other machines can influence the stability of shaft modes on the machine under study.

Chapter 6 introduces the relatively recent problem known as Subsynchronous Torsional Interaction, a possible problem associated with Static Var Compensators and other high bandwidth power controllers, and how the method of Complex Torque Coefficients can highlight possible unfavourable interactions.

Chapter 7 discusses the issue of validation of the Complex Torque Coefficient technique by Eigenanalysis and time-domain methods.

Chapter 8 analyses the possibility of torsional resonances due to noncharacteristic harmonics produced by the phase modulation behaviour of asynchronous HVDC Links.

Chapter 9 concludes the study.

A detailed description of the software tool PC-DAP, based on the work discussed in this thesis is given in Appendix 1.

COMPLEX TORQUE COEFFICIENT ANALYSIS

2.1 INTRODUCTION**2.1.1 Background**

The idea of synchronising and damping torque components of the synchronous machine has been around for quite a long time. The original idea was proposed by R.H. Park [17,18] in the 1930's and subsequently became a useful tool for investigating hunting phenomena and self-excitation of the synchronous machine as reported by Bodine, Concordia, and Kron in 1943 [19], and later by Concordia in 1951 [20]. In these early works, the interest was in the stability of the machine at low frequencies of oscillation, in particular, how the behaviour was influenced by tie line resistance and inductance, amortisseur windings, and operating point of the machine. It is also of note that in these early works, the coupling that exists between the electrical and mechanical systems was ignored.

In recent times, the technique has found use in the study of machine stability at the electromechanical frequencies of oscillation as influenced by excitation systems and power system stabilisers [21], and Static Var Compensators [22,23], and more recently in the study of torsional interaction between HVDC systems and turbine-generators [24].

2.1.2 Basic Principles

Under certain conditions a synchronous machine, connected to a supply system and otherwise operating normally at synchronous speed, may oscillate in speed about the mean value. When this occurs the currents in all the windings also pulsate at the same frequency, which is usually at a subsynchronous frequency. The rotor of the machine, instead of running exactly in synchronism at a constant angle δ ahead of or behind the no-

load reference axis, oscillates about a mean position. The oscillations may be forced, caused by pulsating torques originating from an external source, as is the case with a diesel driven generator; or free oscillations arising from within the machine itself as is the case with self-excitation.

The analysis of small oscillations is analogous to an equivalent mechanical system having stiffness and damping, as illustrated in Figure 2.1 below.

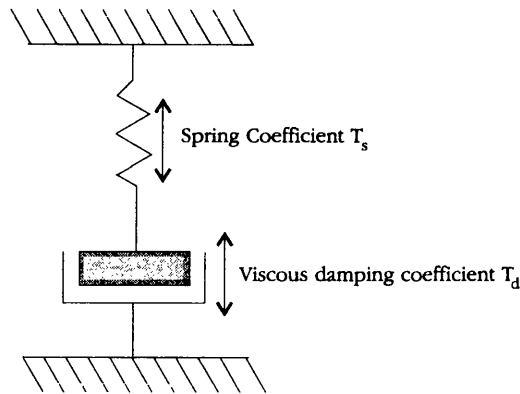


Figure 2.1: Mechanical Analogy of Electrical Complex Torque Coefficient

Suppose that the angular position of the rotor, defined by the angle δ , oscillates sinusoidally about its mean position. The electrical torque developed by the machine also pulsates at the same frequency, and if the oscillations are sufficiently small, the torque pulsations can be considered to be sinusoidal also. However, the torque pulsations do not necessarily have to be in-phase with the rotor angular position pulsations, but can be resolved into two components, one in-phase with the rotor pulsations, and one in quadrature. The component of the torque which is in-phase with the rotor angular position is known as the synchronising torque, and is equivalent to the elastic torque of the spring illustrated in Figure 2.1, while the quadrature component, which is in-phase with the angular velocity pulsations of the rotor is known as the damping torque component, and is equivalent to the damping torque of the viscous damper in Figure 2.1. Clearly then, the additional electrical torque due to the rotor oscillation can be written as

$$\Delta T_e = T_s \Delta \delta + T_d \Delta \omega \quad [2.1]$$

where ΔT_e is the additional electrical torque acting on the rotor, $\Delta\delta$ is the oscillatory component of rotor angle position, $\Delta\omega$ is the oscillatory component of rotor speed about its mean value, T_s is the synchronising torque coefficient, and T_d is the damping torque coefficient. Expressing $\Delta\omega$ as the derivative of rotor angle position in the p-domain, $p\Delta\delta$, Eqn. [2.1] becomes

$$\begin{aligned}\Delta T_e &= (T_s + pT_d)\Delta\delta \\ &= (T_s + j\lambda T_d)\Delta\delta\end{aligned}\quad [2.2]$$

From Eqn. [2.2], it is clear that the complex quantity can be described in terms of the transfer function between ΔT_e and $\Delta\delta$, as illustrated in Figure 2.2.

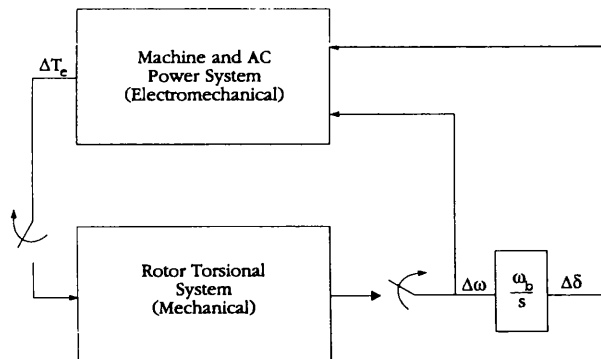


Figure 2.2: Transfer Function from Generator Speed to Electrical Torque

Of particular interest in the Dynamic stability problem is the imaginary part of Eqn. [2.2], T_d the damping torque component. If this component is positive at a given rotor oscillation frequency λ , then this would indicate that as the rotor speed increases, the electrical torque would also increase by an amount proportional to the value of the damping component. This will oppose the original perturbing force, and cause the succeeding oscillations to decay. However, if the damping component is negative, then this would indicate that as the rotor speed increases, the electrical torque would decrease. This will tend to sustain the original oscillations and the system will exhibit unstable behaviour.

2.2 COEFFICIENTS OF THE SYNCHRONOUS MACHINE

The torque coefficients derived by Park [17] and used by Concordia et al [19] dealt only with the rotor frequency corresponding to the electromechanical swing mode. To be of use in the study of torsional interaction phenomena, torque coefficients which are valid over the entire subsynchronous frequency range must be used. Canay [25] suggested and developed the appropriate equations for these coefficients.

2.2.1 Stator Current Components in Oscillating D-Q axes

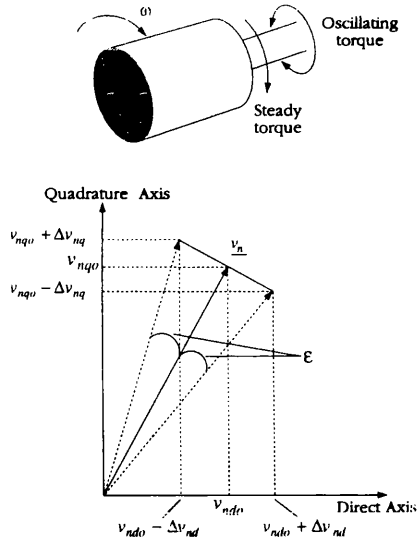


Figure 2.3: Oscillating Rotor Coordinates

If the rotor of a machine exhibits oscillations with an amplitude $\hat{\delta}$ at a frequency λ , then to an observer rotating at synchronous speed, all the stator quantities of the machine in this oscillating reference frame would appear to contain oscillatory components, irrespective of whether in reality they oscillate or are in steady-state.

For example, the infinite bus voltage, v_n as illustrated in Figure 2.3 exhibits oscillating components in this reference frame which only have sheer mathematical significance.

In a similar manner, the terminal voltage, stator current, and flux linkage of the machine expressed in this oscillating reference frame will also have oscillatory components:

$$\begin{aligned}
 v_d &= v_{do} + \Delta v_d \\
 v_q &= v_{qo} + \Delta v_q \\
 \\
 i_d &= i_{do} + \Delta i_d \\
 i_q &= i_{qo} + \Delta i_q \\
 \\
 \psi_d &= \psi_{do} + \Delta \psi_d \\
 \psi_q &= \psi_{qo} + \Delta \psi_q
 \end{aligned} \tag{2.3}$$

The per unit rotor speed ω of an oscillating synchronous machine can be expressed as

$$\omega = 1 + \frac{d\delta}{dt} \tag{2.4}$$

where δ is the rotor angle deviation in Figure 2.3. The direct- and quadrature axis voltage equations of the synchronous machine can be written as

$$\begin{aligned}
 v_d &= -r_a i_d + \omega \psi_q - \frac{d\psi_d}{dt} \\
 v_q &= -r_a i_q - \omega \psi_d - \frac{d\psi_q}{dt}
 \end{aligned} \tag{2.5}$$

which, using Eqn. [2.4] and linearising, become

$$\begin{aligned}
 \Delta v_d &= -r_a \Delta i_d + \Delta \psi_q + \psi_{qo} \frac{d\delta}{dt} - \frac{d}{dt} \Delta \psi_d \\
 \Delta v_q &= -r_a \Delta i_q - \Delta \psi_d + \psi_{do} \frac{d\delta}{dt} - \frac{d}{dt} \Delta \psi_q
 \end{aligned} \tag{2.6}$$

The incremental change in flux linkage $\Delta \psi$ can be expressed as a function of incremental stator current and field voltage in the Laplace domain,

$$\begin{aligned}
 \Delta \psi_d &= x_d(p) \Delta i_d - G(p) \Delta v_f \\
 \Delta \psi_q &= x_q(p) \Delta i_q
 \end{aligned} \tag{2.7}$$

where $x_d(p)$, $x_q(p)$ and $G(p)$ are the well known synchronous machine operational impedances [26].

By substituting Eqn. [2.7] into Eqn. [2.6], the following voltage equation is obtained:

$$\begin{bmatrix} \Delta v_d \\ \Delta v_q \end{bmatrix} = \begin{bmatrix} \psi_{qo} \\ -\psi_{do} \end{bmatrix} p\delta + \begin{bmatrix} p \\ 1 \end{bmatrix} G(p)\Delta v_f - \begin{bmatrix} r_a + px_d(p) & -x_q(p) \\ x_d(p) & r_a + px_q(p) \end{bmatrix} \begin{bmatrix} \Delta i_d \\ \Delta i_q \end{bmatrix} \quad [2.8]$$

Consider the simple transmission line shown in Figure 2.4 comprising a net resistance r_e , a net inductive reactance X_e , and a capacitive reactance X_c between the machine terminals and the infinite-bus.

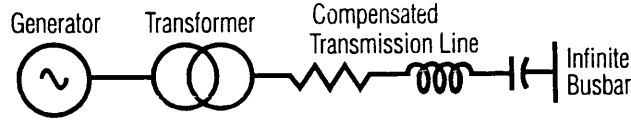


Figure 2.4: Single Transmission Line System

Using the voltage equations of this network as a basis, Canay [25] showed that the components of oscillating current in the machine stator windings were related to the oscillating components of machine voltage by the following equation:

$$\begin{bmatrix} \Delta i_d - i_{qo}\delta \\ \Delta i_q + i_{do}\delta \end{bmatrix} = \begin{bmatrix} Z_{de}(j\lambda) & -X_{qe}(j\lambda) \\ X_{de}(j\lambda) & Z_{qe}(j\lambda) \end{bmatrix}^{-1} \begin{bmatrix} \Delta v_d - v_{qo}\delta \\ \Delta v_q + v_{do}\delta \end{bmatrix} \quad [2.9]$$

where $Z_{de}(j\lambda)$, $Z_{qe}(j\lambda)$, $X_{de}(j\lambda)$ and $X_{qe}(j\lambda)$ are functions of both the machine and the external network and i_{do} and i_{qo} are the machine initial stator currents.

Combining Eqn. [2.9] with Eqn. [2.8], together with $\Delta v_f = g(p)\delta$ relating the change in field voltage due to the rotor oscillation, the expression giving oscillating machine currents due to a rotor oscillation of amplitude $\hat{\delta}$ at a frequency λ are given by:

$$\begin{bmatrix} \Delta i_d \\ \Delta i_q \end{bmatrix} = \begin{bmatrix} i_{qo} \\ -i_{do} \end{bmatrix} \delta + \begin{bmatrix} Z_{de}(j\lambda) & -X_{qe}(j\lambda) \\ X_{de}(j\lambda) & Z_{qe}(j\lambda) \end{bmatrix}^{-1} \begin{bmatrix} j\lambda & -1 \\ 1 & j\lambda \end{bmatrix} \begin{bmatrix} \psi_{d\delta o} \\ \psi_{q\delta o} \end{bmatrix} \delta \quad [2.10]$$

where

$$\begin{aligned} \psi_{d\delta o} &= G(p)g(p) + (x_q - x_d(p))i_{qo} \\ \psi_{q\delta o} &= v_{fo} - (x_d - x_q(p))i_{do} \end{aligned}$$

This is a very important equation. It shows that for a given machine operating point, the effect of an external network on the additional current components present in the stator windings of the machine is given only by the resulting combined Thevenin Impedance matrix Z_n evaluated at each frequency of rotor oscillation, which for the simple network configuration illustrated in Figure 2.4 is given by:

$$\begin{bmatrix} r_a + r_n + j\lambda \left(X_d(j\lambda) + X_n + \frac{X_{cn}}{1 - \lambda^2} \right) & - \left(X_q(j\lambda) + X_n - \frac{X_{cn}}{1 - \lambda^2} \right) \\ \left(X_d(j\lambda) + X_n - \frac{X_{cn}}{1 - \lambda^2} \right) & r_a + r_n + j\lambda \left(X_q(j\lambda) + X_n + \frac{X_{cn}}{1 - \lambda^2} \right) \end{bmatrix} \quad [2.11]$$

2.2.2 Interpretation of the Complex Impedance Matrix

It is useful at this point to examine the matrix equation given in Eqn. [2.10]. Each of the additional currents (direct- and quadrature-axis) are composed of two terms; the first term, when expressed in the steady stator reference frame, is a steady component given only by the magnitude of initial steady current in the stator and the magnitude of the rotor oscillation; the second term in the same steady reference frame yields an oscillatory component of current. For rotor oscillations with relative frequency λ , these additional

oscillatory currents in the stator windings due to the second term in Eqn. [2.10], can be written as

$$\begin{aligned}\Delta \underline{i}_d &= i_{d\delta}(j\lambda)e^{j\lambda t} \\ \Delta \underline{i}_q &= i_{q\delta}(j\lambda)e^{j\lambda t}\end{aligned}\quad [2.12]$$

Substituting these current components into the expression for the transformation into the phase-domain using Park's transformation [17,18] with a nominal synchronous frequency of ω_s , which for phase-a is given by

$$\Delta \underline{i}_a = \Delta \underline{i}_d \cos \omega_s t - \Delta \underline{i}_q \sin \omega_s t \quad [2.13]$$

and rearranging, the following expression is obtained:

$$\begin{aligned}\Delta i_a &= \frac{1}{2} [i_{d\delta}(j\lambda) + j i_{q\delta}(j\lambda)] e^{j(\lambda + \omega_s)t} + \frac{1}{2} [i_{d\delta}(j\lambda) - j i_{q\delta}(j\lambda)] e^{j(\lambda - \omega_s)t} \\ &\text{or} \\ \Delta \underline{i}_a &= \underline{i}_{super} + \underline{i}_{sub}\end{aligned}\quad [2.14]$$

Clearly the additional oscillatory stator current has two components; a supersynchronous current component at a relative frequency of $(\lambda + \omega_s)$, and a subsynchronous current component at a relative frequency of $(\lambda - \omega_s)$. This is the inverse of the well-known case in Induction machine theory where an oscillating stator quantity gives rise to a forward rotating component and a backward rotating component on the rotor.

Returning to the original expression in Eqn. [2.10], the additional direct- and quadrature-axis stator current components, composed of the steady term and the oscillatory term in each, may be written as

$$\begin{aligned}\Delta i_d &= i_{qo} \underline{\delta} + i_{super} e^{-jt} + i_{sub}^* e^{jt} \\ \Delta i_q &= -i_{do} \underline{\delta} - j \left[i_{super} e^{-jt} - i_{sub}^* e^{jt} \right]\end{aligned}\tag{2.15}$$

where the oscillatory term associated with the phasor e^{jt} has now been expressed as a sum of a supersynchronous and a subsynchronous component. Similar equations can be derived for the additional voltage components, i.e.

$$\begin{aligned}\Delta v_d &= v_{qo} \underline{\delta} + v_{super} e^{-jt} + v_{sub}^* e^{jt} \\ \Delta v_q &= -v_{do} \underline{\delta} - j \left[v_{super} e^{-jt} - v_{sub}^* e^{jt} \right]\end{aligned}\tag{2.16}$$

Substitution of Eqns. [2.15] and [2.16] into Eqn. [2.9] yields:

$$\begin{aligned}\frac{v_{super}}{i_{super}} &= Z_{super} = Z_n(j\lambda) + j X_n(j\lambda) \\ \frac{v_{sub}}{i_{sub}} &= Z_{sub} = Z_n(j\lambda)^* + j X_n(j\lambda)^*\end{aligned}\tag{2.17}$$

The terms Z_{sub} and Z_{sup} denote the network impedances for the stator frequencies $(1+\lambda)f_s$ and $(1-\lambda)f_s$ for system frequency f_s . The frequency operators $Z_n(j\lambda)$ and $X_n(j\lambda)$ can be determined from:

$$\begin{aligned}Z_n(j\lambda) &= \frac{1}{2} \left[Z_{sub}^* + Z_{super} \right] \\ X_n(j\lambda) &= \frac{1}{2} \left[Z_{sub}^* - Z_{super} \right]\end{aligned}\tag{2.18}$$

Hence, the full influence of the network on the behaviour of the synchronous machine to rotor oscillations can be assessed if the impedance of the system to which the machine is connected, for both the supersynchronous and subsynchronous frequencies relative to the frequency of rotor oscillation, is known. From a computational point of

view, the complex impedance matrix operators $Z_n(j\lambda)$ and $X_n(j\lambda)$ can only be computed using the equations of [2.18] if the network contains only passive elements. The reason for this statement is that, referring to Eqn. [2.10], $Z_{de}(j\lambda) \equiv Z_{qe}(j\lambda) \equiv Z_n(j\lambda)$ and $X_{de}(j\lambda) \equiv X_{qe}(j\lambda) \equiv X_n(j\lambda)$ are only true when considering non-active elements such as resistors, inductors, and capacitors. For active elements, the Direct- and Quadrature-axis impedance operators are not equal, and equations [2.18] are not sufficient.

2.2.3 Complex Torque Coefficient

The instantaneous per-unit power output of a three-phase synchronous machine is given by [4]

$$P_o = \frac{2}{3}(v_a i_a + v_b i_b + v_c i_c) \quad p.u. \quad [2.19]$$

which in terms of Direct-, Quadrature, and Zero-axis quantities is

$$P_o = v_d i_d + v_q i_q + 2v_o i_o \quad p.u. \quad [2.20]$$

By eliminating the voltage terms according to Eqn. [2.5], the expression for power becomes

$$P_o = \left(i_d \frac{d\psi_d}{dt} + i_q \frac{d\psi_q}{dt} + 2i_o \frac{d\psi_o}{dt} \right) + (i_d \psi_q - i_q \psi_d) \omega - r(i_d^2 + i_q^2 + 2i_o^2) \quad p.u. \quad [2.21]$$

in which the first term represents the rate of change of magnetic energy, the second term represents air-gap power, and the third term represents armature losses. Dividing the air-gap power by the rotor velocity ω gives the general expression for electrical torque:

$$T_e = i_d \psi_q - i_q \psi_d \quad p.u. \quad [2.22]$$

By linearising Eqn. [2.22] for small deviations about an operating point, and applying the Laplace transformation, the deviation in electrical torque as a function of the oscillating d-q axis current components becomes

$$\Delta T_e = [\psi_{qo} - i_{qo}x_d(j\lambda)]\Delta i_d - [\psi_{do} - i_{do}x_q(j\lambda)]\Delta i_q \quad p.u. \quad [2.23]$$

Returning to Eqn. [2.2], it was stated that the transfer function between electrical torque and the rotor oscillation that produced it yields the Complex Torque Coefficient. By substituting the expression for D-Q axis oscillating currents from Eqn. [2.10] into the above expression for torque, this transfer function may be calculated for each frequency of oscillation of the rotor.

2.3 INFLUENCE OF SYNCHRONOUS MACHINE PARAMETERS ON THE COMPLEX TORQUE COEFFICIENT

Using Eqns. [2.10] and [2.23], applied to the simple system illustrated in Figure 2.4, the dependency of the Complex Torque Coefficient on typical synchronous machine parameters is illustrated in the following sections. Table 2.1 summarises generator constants for a typical machine. All generator and transmission line constants have been normalised on the generator apparent power rating of 600MVA. Transmission line total resistance and total reactance parameters are varied as indicated on Figures 2.5 - 2.8.

Table 2.1: Generator Constants

<i>Apparent Power, MVA</i>	600
<i>Number of Poles</i>	2
<i>Supply Frequency</i>	60
<i>Direct Axis:</i>	
<i>Synchronous Reactance Xd, p.u.</i>	1.790
<i>Transient Reactance, Xd', p.u.</i>	0.169
<i>Subtransient Reactance Xd'', p.u.</i>	0.135
<i>Open Circuit Transient Time Constant Tdo', s</i>	4.300
<i>Open Circuit Subtransient Time Constant Tdo'', s</i>	0.032
<i>Stator Resistance Ra, p.u.</i>	0.005
<i>Stator Leakage Reactance Xa, p.u.</i>	0.130
<i>Characteristic Reactance Xchar, p.u.¹</i>	0.220
<i>Quadrature Axis:</i>	
<i>Synchronous Reactance Xq, p.u.</i>	1.710
<i>Transient Reactance Xq', p.u.</i>	0.228
<i>Subtransient Reactance Xq'', p.u.</i>	0.200
<i>Open Circuit Transient Time Constant Tqo', s</i>	0.850
<i>Open Circuit Subtransient Time Constant Tqo'', s</i>	0.050

All constants have been normalised on machine apparent power rating

¹ The characteristic reactance takes account of the true magnetic coupling between the field and the damper circuit of a synchronous machine [67].

2.3.1 Normalisation of the Complex Torque Coefficient

Before proceeding to study the characteristics of the Complex Torque Coefficient, it is appropriate at this point to indicate the units that will be used throughout.

The Complex torque coefficient has been defined as the ratio of change in torque for a given change in rotor angle. It is usual in such studies to use a common base for all data, whether electrical or mechanical. For the normalisation of the Complex Torque Coefficient, the base units of angular velocity and torque must be known. Base angular velocity, ω_{base} in Rad/sec, is taken to be 2π multiplied by the system frequency. Base torque, in MVA, is defined by

$$T_{base} = \frac{S_{base}}{\omega_{base}}$$

where S_{base} is the base power.

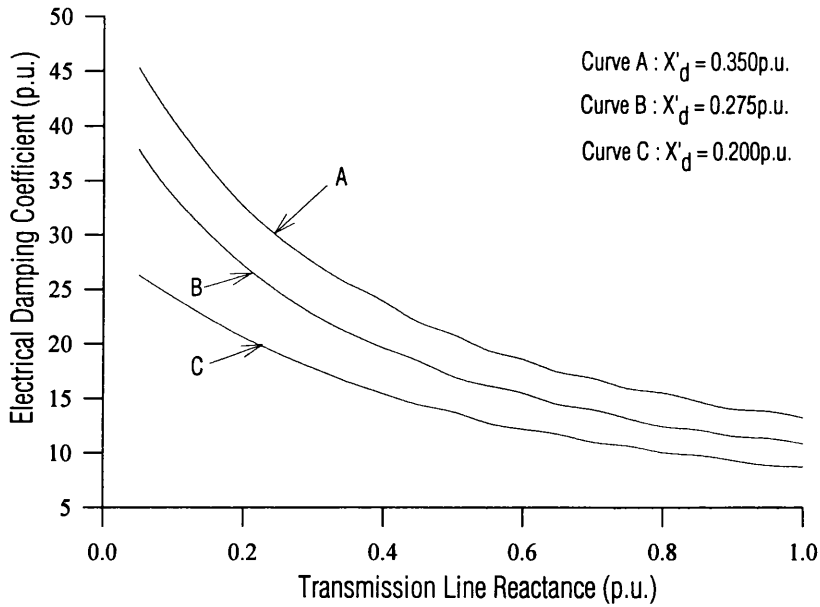
From Eqn. [2.2], the base synchronising and damping coefficients are given by

$$T_{sbase} = \frac{S_{base}}{\omega_{base}} \text{ MVA-sec}$$

$$T_{dbase} = \frac{S_{base}}{\omega_{base}^2} \text{ MVA-sec}^2$$

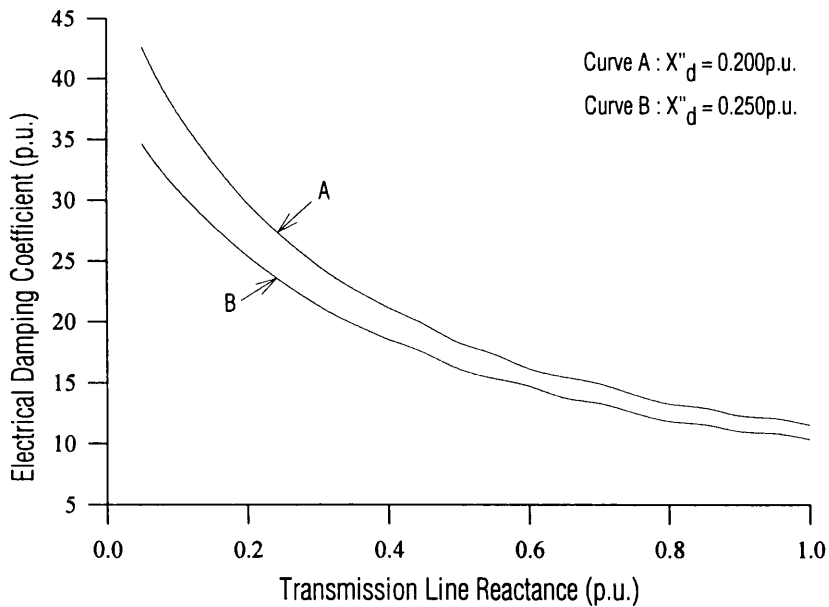
2.3.2 Influence of Generator Transient and Subtransient Reactances

Figure Error! Reference source not found. depicts electromagnetic damping coefficient as a function of the transmission line reactance at several values of synchronous machine transient reactance, X'_d . Increased line reactance has a detrimental effect on the damping of oscillations. The coefficients have been calculated at frequencies corresponding to the zeroth or rotor swing frequency, which varies slightly as the reactance of the line is increased. The transient reactance of the machine has a significant impact on electromagnetic damping for low values of line reactance. For higher values, the effect becomes less significant. A higher transient reactance will result in improved damping.



Electromagnetic damping coefficients correspond to rotor swing frequency calculated at each value of transmission line impedance. Synchronous machine operating at one half of full-load ($P_o=0.5$ p.u., $Q_o=0.0$ p.u.). Transmission line resistance $R_s=0.0236$ p.u. Coefficients are normalised on machine apparent power rating of 600MVA and base angular velocity of 120π Rad/sec.

Figure 2.5: Electromagnetic damping Coefficient as a function of line reactance -- Influence of Transient reactance of synchronous machine



Electromagnetic damping coefficients correspond to rotor swing frequency calculated at each value of transmission line impedance. Synchronous machine operating at one half of full-load ($P_o=0.5$ p.u., $Q_o=0.0$ p.u.). Transient reactance of synchronous machine $X'_d=0.275$ p.u. Transmission line resistance $R_s=0.0236$ p.u. Coefficients are normalised on machine apparent power rating of 600MVA and base angular velocity of 120π Rad/sec.

Figure 2.6: Electromagnetic damping Coefficient as a function of line reactance -- Influence of Subtransient reactance of synchronous machine

Figure 2.6 depicts similar curves for electromagnetic damping as a function of transmission line reactance at several values of machine subtransient reactance, X_d'' . From Figures 2.5 and 2.6 it can be seen that the damping coefficient is actually a function of $(X_d' - X_d'')$. As the difference term increases, the damping coefficient increases; as the difference term decreases, the damping coefficient decreases.

2.3.3 Influence of Total System resistance

Figure 2.7 illustrates the variation of electromagnetic damping across the subsynchronous frequency range with total system resistance, $r_a + r_e$, where r_a is the generator stator resistance given in Table 2.1.

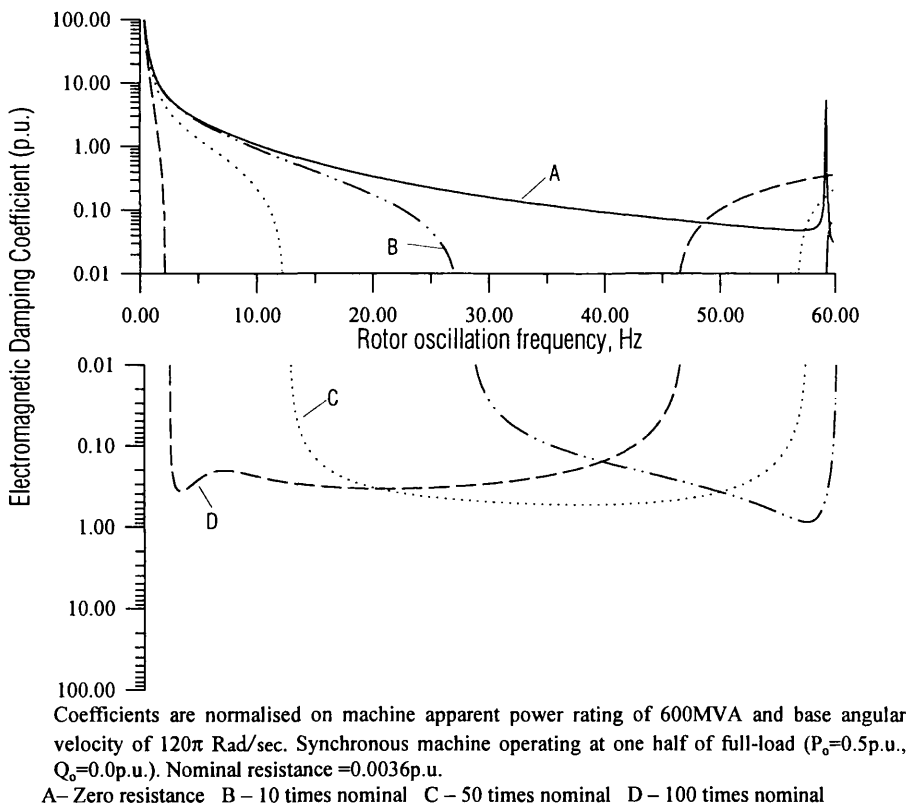
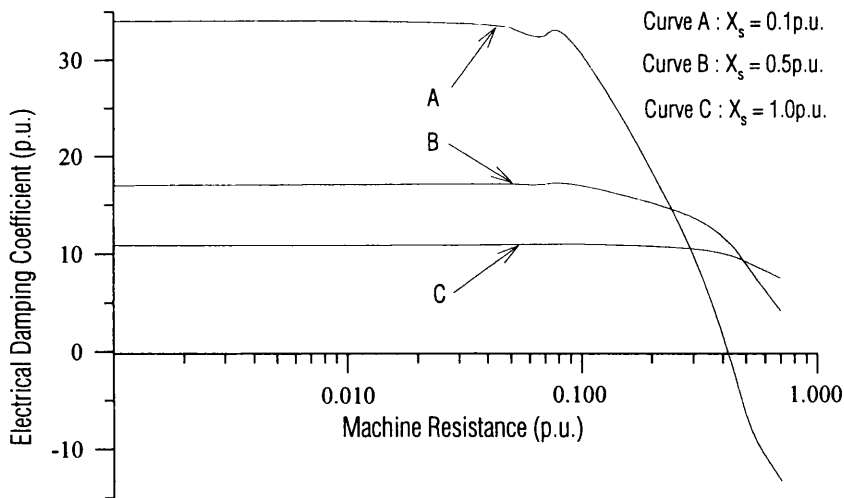


Figure 2.7: Electromagnetic damping Coefficient as a function of total resistance

Clearly, for low values of total resistance, electromagnetic damping remains positive throughout the range. However, for total resistance values greater than 10 times

Clearly, for low values of total resistance, electromagnetic damping remains positive throughout the range. However, for total resistance values greater than 10 times the nominal value, the impact on electromagnetic damping is significant. It can be observed that as the resistance is increased a large region of negative electromagnetic damping is present. That is, for rotor oscillations within the range of this region, the electromagnetic torque would act to encourage the oscillations to build up. In the absence of the mechanical characteristics of the shaft, however, the description of the system is incomplete and no predictions of overall stability can be made. However, it is true to say that during light loads, when steam viscous damping is negligible, machines which exhibit high stator resistance or machines which are connected to a line with high resistance may experience oscillatory torque problems.

Figure 2.8 illustrates the impact of total resistance on the electromagnetic damping for the rotor oscillation frequency corresponding to the rotor swing mode for increasing system impedance. This demonstrates that a weaker system, denoted by a higher impedance, will degrade the damping of this mode.



Electromagnetic damping coefficients correspond to rotor swing frequency calculated at each value of transmission line impedance. Synchronous machine operating at one half of full-load ($P_o=0.5$ p.u., $Q_o=0.0$ p.u.). Coefficients are normalised on machine apparent power rating of 600MVA and base angular velocity of 120π Rad/sec.

Figure 2.8: Electromagnetic damping Coefficient as a function of total resistance -- Influence of Transmission line total reactance

2.4 SUMMARY OF CHAPTER 2

This Chapter has discussed the background and basic principles and equations underlying Complex Torque Coefficient analysis. Using the voltage equations of the synchronous machine as a basis, the complex impedance matrix of the machine has been derived and its significance discussed.

The influence of the transient and subtransient reactances of the machine and the transmission line reactance on the damping characteristic of the rotor swing mode has been studied. It has been shown that the electromagnetic damping which acts along the active length of the generator rotor decreases as the system strength decreases

The influence of total system resistance has been found to have a significant effect of the electromagnetic damping. For large resistances in excess of 10 times the nominal value of resistance, the electromagnetic damping exhibits a large negative region which would lead to an increase in the time constants for decay of the principle torque oscillations especially during periods of light load.

CHAPTER THREE

THE POWER SYSTEM MODEL

3.1 INTRODUCTION

The detailed stability analysis of a modern, large power system requires the use of a comprehensive power system model, with explicit representation of all generators, controlled devices, loads, and network dynamics. In conventional stability analyses which consider the problem of electromechanical modes of oscillation, including transient studies, the key mathematical equations were those which described the dynamic behaviour of the synchronous generators. The power system model used therefore, was that which emphasised the modelling of the torques influencing the motion of the machine rotors and their associated controls. The rest of the system would be modelled only in a simplified form¹, sufficient to represent the influence of the electrical system on the mechanical torques. For analyses which must predict all forms of torsional interaction, including subsynchronous resonance, the 'network' model cannot be quite so simplified. In addition, modern power networks often have dynamic devices other than synchronous machines whose behaviour can play a significant part in system stability. These devices must also be modelled with a sufficient level of detail. This chapter describes the equations used in this study to model :

- i) Synchronous generators
- ii) Transmission lines, including static compensation
- iii) Shunt elements
- iv) Transformers
- v) Static Loads

¹ Usually as an admittance matrix in which only power frequency positive sequence admittance would be considered.

3.2 SYNCHRONOUS MACHINE MODELS

A schematic diagram of a power system is illustrated in Figure 3.1. It shows 4 synchronous machines interconnected through an arbitrary system of nodes, each node being connected to at least one transmission line, some of these nodes also being connected to static loads. As was discussed in the previous chapter, Complex Torque Coefficient analysis concentrates on one machine in the system taking into account the influence of all other machines. This machine is illustrated as Machine A. It would be modelled with a high degree of detail including the rotor circuit, stator circuit, and excitation system (AVR). If a Power System Stabiliser (PSS) is also fitted to the machine under study then it too should be included in the model.

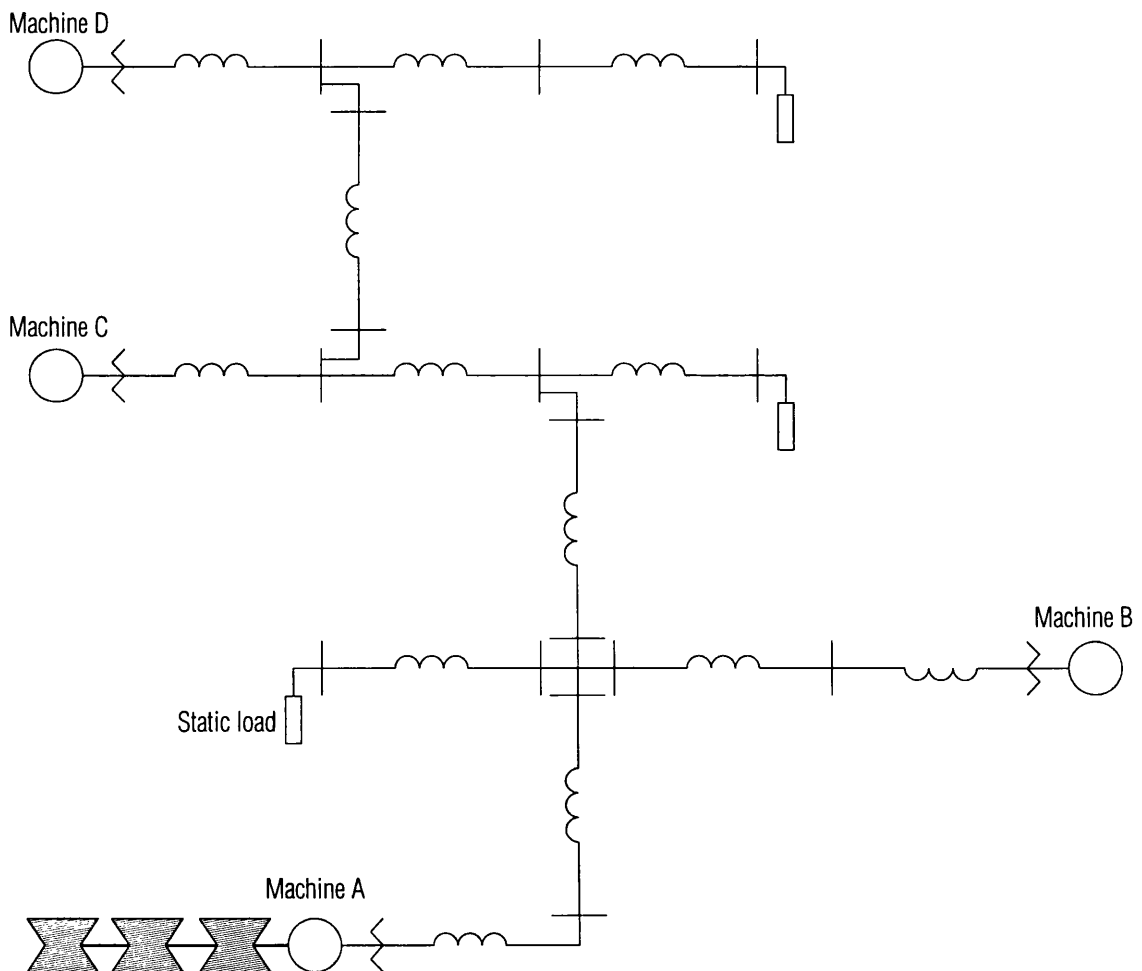


Figure 3.1: Power System Schematic

The other machines would be modelled with varying degrees of detail depending on their perceived contribution to the stability of the machine under study. This contribution will depend on a number of factors; generators which have a significantly smaller capacity than the machine under study will have a lesser influence than generators of approximately the same rating or greater; electrical distance between machines can play a significant part, especially for systems of a low density. The representation of the mechanical system for each machine will also vary from the simplest case of a single rotor mass to the full multi-mass model. The mechanical system model will be discussed in a later section.

There are two general types of system studied:

- i. Systems containing only one machine
- ii. Systems containing more than one machine

For type (i) systems, only the interaction between the machine and the network (including both passive and active elements) is present. For this type of system, the machine model described in Section 3.2.1 is adequate.

For type (ii) systems, there are two distinct interactions to consider; the interaction between the machine and the network; and the interaction between the machine and other machines in the system. For this type of system, the machine models in Section 3.2.1 through Section 3.2.3 must be used.

3.2.1 Synchronous Generator Model for Machine - Network Interaction Studies

For studies of systems containing only one machine, a two-axis model based on Park's equations [17] with one damper-winding on each axis has been used, as was described in Section 2.2 in the derivation of the Complex Torque Coefficients. Figure 3.2 illustrates the equivalent circuits for each axis.

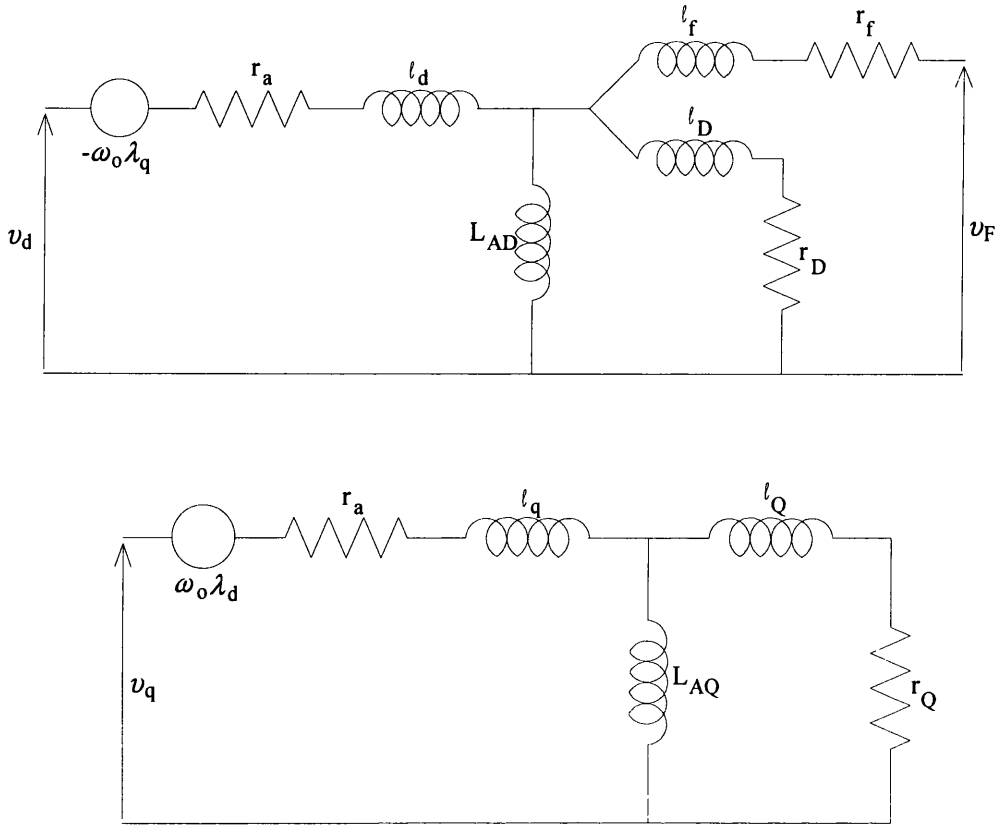


Figure 3.2: Equivalent Circuits for Two-axis Model

The d- and q-axis voltage equations for these circuits were given in Eqn. [2.8] in which the well-known operational impedances in terms of transient, subtransient and subsubtransient reactances and time constants, as described for example by Krauss [27], are given by

$$x_d(s) = x_d \frac{\left(1 + \frac{x'_d}{x_d} \tau'_{do} s\right) \left(1 + \frac{x''_d}{x'_d} \tau''_{do} s\right)}{(1 + \tau'_{do} s)(1 + \tau''_{do} s)}$$

$$x_q(s) = x_q \frac{\left(1 + \frac{x'_q}{x_q} \tau'_{qo} s\right) \left(1 + \frac{x''_q}{x'_q} \tau''_{qo} s\right)}{(1 + \tau'_{qo} s)(1 + \tau''_{qo} s)}$$

[3.1]

The model of the excitation system and any additional excitation control or power system stabilisers can be incorporated through the transfer function

$$G(p)\Delta v_f$$

where $G(p) = \frac{(1 + p\tau_{do})}{(1 + p\tau'_{do})(1 + p\tau''_{do})}$ and $\Delta v_f = g(p)\delta$. The function $g(p)$ is derived from the model of the excitation system being used.

The equations used for the excitation system, and their effect on the stability coefficients of the machine will be discussed in a later section.

3.2.2 Synchronous Machine Models for Multi-machine Systems

In order to calculate correctly the influence of other synchronous machines operating in the system on the machine under investigation, a different approach to that employed for the case of a single machine is required. This approach is described fully in Chapter 5 and consists of two parts; in performing the *machine-network interaction* calculations, the other machines in the system must be included within the network model²; discrepancies in the calculated low-frequency *inter-machine*³ *interactions* introduced in the first part of the calculations must be corrected by additional calculations which are concentrated on the lower frequency range. The synchronous machine models for the first part of the multi-machine calculations are described in Section 3.2.3. The synchronous machine models for the second part of the multi-machine calculations are described in Section 3.2.5.

3.2.3 Flux Linkage State-Space Model - - Electrical Equations

The synchronous machine model is expressed in a state-space form based on the equivalent circuits illustrated in Figure 3.2 in which the state-variables are the flux-linkages λ_d , λ_f , λ_D , λ_q , and λ_Q .

² This is achieved by constructing the Complex Admittance matrices for each machine and appending them to the network admittance matrix equation as described in Section 5.2

³ Inter-machine interactions are most dominant at the low-frequency 'swing' modes, typically 0.5~2Hz.

The voltage equations of the d-axis may be rearranged into the form

$$\dot{\lambda}_d = -\frac{r_a}{\ell_d} \lambda_d + \frac{r_a}{\ell_d} \lambda_{AD} - \omega \lambda_q - v_d \quad [3.2]$$

Repeating the procedure for the remaining circuits on both axes, gives the following first order equations,

$$\begin{aligned} \dot{\lambda}_f &= -\frac{r_f}{\ell_f} \lambda_f + \frac{r_f}{\ell_f} \lambda_{AD} + v_f \\ \dot{\lambda}_D &= -\frac{r_D}{\ell_D} \lambda_D + \frac{r_D}{\ell_D} \lambda_{AD} \\ \dot{\lambda}_q &= -\frac{r_a}{\ell_q} \lambda_q + \frac{r_a}{\ell_q} \lambda_{AQ} + \omega \lambda_d - v_q \\ \dot{\lambda}_Q &= -\frac{r_Q}{\ell_Q} \lambda_Q + \frac{r_Q}{\ell_Q} \lambda_{AQ} \end{aligned} \quad [3.3]$$

If saturation is neglected, then it can be shown [4] that the following relations hold between the currents and the flux-linkages:

$$\begin{aligned} i_d &= \left(1 - \frac{L_{MD}}{\ell_d}\right) \frac{\lambda_d}{\ell_d} - \frac{L_{MD}}{\ell_d} \frac{\lambda_f}{\ell_f} - \frac{L_{MD}}{\ell_d} \frac{\lambda_D}{\ell_D} \\ i_f &= -\frac{L_{MD}}{\ell_f} \frac{\lambda_d}{\ell_d} + \left(1 - \frac{L_{MD}}{\ell_f}\right) \frac{\lambda_f}{\ell_f} - \frac{L_{MD}}{\ell_f} \frac{\lambda_D}{\ell_D} \\ i_D &= -\frac{L_{MD}}{\ell_D} \frac{\lambda_d}{\ell_d} - \frac{L_{MD}}{\ell_D} \frac{\lambda_f}{\ell_f} + \left(1 - \frac{L_{MD}}{\ell_D}\right) \frac{\lambda_D}{\ell_D} \end{aligned} \quad [3.4]$$

where $\frac{1}{L_{MD}} = \frac{1}{\ell_d} + \frac{1}{L_{AD}} + \frac{1}{\ell_f} + \frac{1}{\ell_D}$

Substituting Eqn. [3.4] into the voltage Eqns. [3.2] and [3.3], the linearised equations for the d-axis can be computed as

$$\dot{\lambda}_d = -r_a \left(1 - \frac{L_{MD}}{\ell_d}\right) \frac{\lambda_d}{\ell_d} + r_a \frac{L_{MD}}{\ell_d} \frac{\lambda_f}{\ell_f} + r_a \frac{L_{MD}}{\ell_d} \frac{\lambda_D}{\ell_D} - \omega \lambda_q - v_d \quad [3.5]$$

$$\dot{\lambda}_f = r_f \frac{L_{MD}}{\ell_f} \frac{\lambda_d}{\ell_d} - r_f \left(1 - \frac{L_{MD}}{\ell_f}\right) \frac{\lambda_f}{\ell_f} + r_f \frac{L_{MD}}{\ell_f} \frac{\lambda_D}{\ell_D} + v_f \quad [3.6]$$

$$\dot{\lambda}_D = r_D \frac{L_{MD}}{\ell_D} \frac{\lambda_d}{\ell_d} + r_D \frac{L_{MD}}{\ell_D} \frac{\lambda_f}{\ell_f} - r_D \left(1 - \frac{L_{MD}}{\ell_D}\right) \frac{\lambda_D}{\ell_D} \quad [3.7]$$

Similarly the q-axis linearised equations can be written as

$$\dot{\lambda}_q = -r_a \left(1 - \frac{L_{MQ}}{\ell_q}\right) \frac{\lambda_q}{\ell_q} + r_a \frac{L_{MQ}}{\ell_q} \frac{\lambda_Q}{\ell_Q} + \omega \lambda_d - v_q \quad [3.8]$$

$$\dot{\lambda}_Q = r_Q \frac{L_{MQ}}{\ell_Q} \frac{\lambda_q}{\ell_q} - r_Q \left(1 - \frac{L_{MQ}}{\ell_Q}\right) \frac{\lambda_Q}{\ell_Q} \quad [3.9]$$

Eqns. [3.5]-[3.9] are the required electrical state equations.

3.2.4 Flux Linkage State-Space Model - - Turbine Shaft Model

In order to correctly predict the influence that one machine will have on another, especially at frequencies corresponding to shaft resonant modes, the mechanical shaft-train dynamics must also be included in the model for each machine. For the state-space model described here, there are two parts to this; the *mechanical* equations, which couple adjacent turbines together; and the swing or electromagnetic torque equation which couples the mechanical and electrical systems together.

Figure 3.3 illustrates a schematic of the multi-mass shaft train. Each turbine mass I_i connects to its adjacent turbine masses through a spring constant K_{ij} and a dashpot D_{ij} . This dashpot, although easily incorporated into the shaft equations, is seldom used given that these elements have very little effect on the shaft dynamics. A second dashpot element D_i connects each turbine mass with the fixed reference. This element attempts to

represent the effect of steam damping which acts on each mass and has a significant influence on shaft dynamics. Material hysteretic damping⁴ is usually neglected.

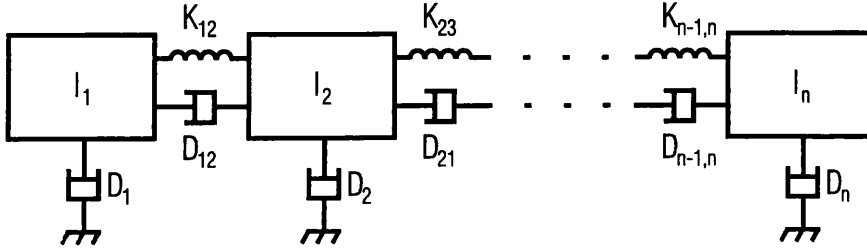


Figure 3.3: Lumped Mass-Spring Model of a Turbine-Generator Shaft

The torque equations for each shaft section comprising a turbine mass and spring sections are the fundamental relations that determine the dynamic performance of the shaft system. For the m^{th} mass connected to mass l and mass n through spring constants K_{ml} and K_{mn} , the following equation based on Newton's second law for rotating bodies applies.

$$I_m \frac{d\omega_m}{dt} = T_m - K_{mn}(\theta_m - \theta_n) - K_{ml}(\theta_m - \theta_l) - D_m \omega_m \quad [3.10]$$

In common with all other model equations, these torque equations must be normalised by dividing by a base quantity equal to the rated torque at rated speed which is defined as:

$$T_B = \frac{S_{VA}}{\omega_{\text{rated}}} \quad [3.11]$$

where S_{VA} is the 3-phase VA rating of the machine and ω_{rated} is the rated shaft speed in rad/s. From the definition of kinetic energy of a rotating body,

⁴ If time constants for resultant steam viscous damping are small, material hysteretic damping of the shaft may be ignored.

$$W_m = \frac{1}{2} I_m \omega_m^2 \quad [3.12]$$

the normalised torque equation may be written as

$$\frac{2W_m}{S_{VA}\omega_{rated}} \dot{\omega}_m = T_m^u - \frac{K_{mn}^u}{s} \left(\frac{\omega_m - \omega_n}{\omega_{rated}} \right) - \frac{K_{ml}^u}{s} \left(\frac{\omega_m - \omega_l}{\omega_{rated}} \right) - D_m^u \left(\frac{\omega_m}{\omega_{rated}} \right) \quad [3.13]$$

or more commonly as

$$2H\dot{\omega}_m = T_m^u - K_{mn}^u(\theta_m - \theta_n) - K_{ml}^u(\theta_m - \theta_l) - D_m^u \omega_m \quad [3.14]$$

where quantity H , the inertia constant, is in seconds. The normalised coefficients for the stiffness and damping parameters are defined as

$$D_i^u = \frac{D_i \omega_{rated}^2}{S_{VA}} \quad [3.15]$$

$$K_{ij}^u = \frac{K_{ij} \omega_{rated}}{S_{VA}}$$

Then for a system of 3 masses consisting of two turbines (masses 1 and 2) and a generator (mass 3) from Eqn. [3.14] the appropriate per-unit *mechanical* equations in the correct form for inclusion in the complete state-space model would be

$$\dot{\omega}_1 = \frac{T_{m1}}{\tau_1} - \frac{D_1}{\tau_1} \omega_1 - \frac{K_{12}}{\tau_1} (\theta_1 - \theta_2)$$

$$\dot{\omega}_2 = \frac{T_{m2}}{\tau_2} - \frac{D_2}{\tau_2} \omega_2 + \frac{K_{12}}{\tau_2} (\theta_1 - \theta_2) - \frac{K_{23}}{\tau_2} (\theta_2 - \theta_3) \quad [3.16]$$

$$\dot{\omega}_3 = \frac{T_e}{\tau_3} - \frac{D_3}{\tau_3} \omega_3 - \frac{K_{23}}{\tau_3} (\theta_2 - \theta_3)$$

To complete the model of the electromechanical system, the coupling equation between the mechanical and electrical systems is required. The electromagnetic torque equation is defined as

$$T_e = i_q \lambda_d - i_d \lambda_q \quad [3.17]$$

Eliminating the current terms i_d and i_q using the current Eqn. [3.4], the electromagnetic torque equation becomes

$$T_e = \lambda_d \lambda_q \left(\frac{L_{MD} - L_{MQ}}{\ell_d^2} \right) - \lambda_d \lambda_Q \frac{L_{MQ}}{\ell_q \ell_Q} + \lambda_q \lambda_F \frac{L_{MD}}{\ell_d \ell_F} + \lambda_q \lambda_D \frac{L_{MD}}{\ell_d \ell_D} \quad [3.18]$$

Substituting Eqn. [3.18] into the electromechanical equation which couples the electrical and mechanical systems⁵ completes the model. The arrangement of the equations for an 11th order model is illustrated in Eqn. [3.19]:

$$\begin{bmatrix} \dot{\lambda}_d \\ \dot{\lambda}_f \\ \dot{\lambda}_D \\ \dot{\lambda}_q \\ \dot{\lambda}_Q \\ \dot{\omega}_1 \\ \dot{\omega}_2 \\ \dot{\omega}_3 \\ \dot{\delta}_1 \\ \dot{\delta}_2 \\ \dot{\delta}_3 \end{bmatrix} = \begin{bmatrix} -\frac{r}{\ell_d} \left(1 - \frac{L_{MD}}{\ell_d} \right) & \frac{r}{\ell_d} \frac{L_{MD}}{\ell_f} & \frac{r}{\ell_d} \frac{L_{MD}}{\ell_f} & -\omega & 0 & 0 & 0 & 0 & 0 & 0 & 0 & 0 \\ \frac{r_f}{\ell_d} \frac{L_{MD}}{\ell_f} & -\frac{r_f}{\ell_f} \left(1 - \frac{L_{MD}}{\ell_f} \right) & \frac{r_f}{\ell_D} \frac{L_{MD}}{\ell_f} & 0 & 0 & 0 & 0 & 0 & 0 & 0 & 0 & 0 \\ \frac{r_D}{\ell_d} \frac{L_{MD}}{\ell_D} & \frac{r_D}{\ell_D} \frac{L_{MD}}{\ell_f} & -\frac{r_D}{\ell_D} \left(1 - \frac{L_{MD}}{\ell_D} \right) & 0 & 0 & 0 & 0 & 0 & 0 & 0 & 0 & 0 \\ \omega & 0 & 0 & -\frac{r}{\ell_q} \left(1 - \frac{L_{MQ}}{\ell_q} \right) & \frac{r}{\ell_d} \frac{L_{MD}}{\ell_Q} & 0 & 0 & 0 & 0 & 0 & 0 & 0 \\ 0 & 0 & 0 & \frac{r_Q}{\ell_Q} \frac{L_{MD}}{\ell_q} & -\frac{r_Q}{\ell_Q} \left(1 - \frac{L_{MQ}}{\ell_Q} \right) & 0 & 0 & 0 & 0 & 0 & 0 & 0 \\ 0 & 0 & 0 & 0 & 0 & -\frac{D_1}{\tau_1} & 0 & 0 & -\frac{K_{12}}{\tau_1} & \frac{K_{12}}{\tau_1} & 0 & 0 \\ 0 & 0 & 0 & 0 & 0 & 0 & -\frac{D_2}{\tau_2} & 0 & \frac{K_{12}}{\tau_2} & -\left(\frac{K_{12} + K_{23}}{\tau_2} \right) & \frac{K_{23}}{\tau_2} & 0 \\ -\frac{L_{MD}}{3\tau_3 \ell_d^2} \lambda_q & -\frac{L_{MD}}{3\tau_3 \ell_d \ell_f} \lambda_q & -\frac{L_{MD}}{3\tau_3 \ell_d \ell_D} \lambda_q & -\frac{L_{MQ}}{3\tau_3 \ell_q^2} \lambda_q & -\frac{L_{MQ}}{3\tau_3 \ell_q \ell_Q} \lambda_q & 0 & 0 & -\frac{D_3}{\tau_3} & 0 & \frac{K_{23}}{\tau_3} & -\frac{K_{23}}{\tau_3} & 0 \\ 0 & 0 & 0 & 0 & 0 & 1 & 0 & 0 & 0 & 0 & 0 & 0 \\ 0 & 0 & 0 & 0 & 0 & 0 & 1 & 0 & 0 & 0 & 0 & 0 \\ 0 & 0 & 0 & 0 & 0 & 0 & 0 & 1 & 0 & 0 & 0 & 0 \end{bmatrix} \begin{bmatrix} \lambda_d \\ \lambda_f \\ \lambda_D \\ \lambda_q \\ \lambda_Q \\ \omega_1 \\ \omega_2 \\ \omega_3 \\ \delta_1 \\ \delta_2 \\ \delta_3 \end{bmatrix} \quad [3.19]$$

⁵ The factor of 1/3 in the substitution for T_e arises from the need to use p.u. torque on a three-phase basis.

3.2.5 Lower Order E'' State-Space Model

In order to reproduce the correct low frequency dynamics of interaction between machines, an additional calculation, described in Chapter 5, is employed. This calculation uses a subtransient machine model which has lower order than the model described in Section 3.2.3, which reduces computational labour.

The reduction in order is made by neglecting the transformer voltage terms in the stator voltage Eqns. [3.2] and [3.3], since they are numerically smaller than the speed voltage terms. Although being a simplified model, the field effects and the effects of the damper circuits are included in the representation.

Anderson and Fouad [4] provide a thorough derivation of this model. Based on the assumptions stated above, it can be shown that the system equations may be reduced to the following form:

$$\begin{aligned}
 \dot{e}_d'' &= -\frac{1}{\tau_{qo}''} e_d'' - \frac{1}{\tau_{qo}''} (x_q - x_q'') i_q \\
 \dot{\Lambda}_D &= -\frac{1}{\tau_{do}''} \Lambda_D + \frac{1}{\tau_{do}''} e_q' + \frac{1}{\tau_{do}''} (x_d' - x_f') i_d \\
 \dot{e}_q' &= -\frac{1}{\tau_{do}'} e_d'' + \frac{1}{\tau_{do}'} e_f - \frac{1}{\tau_{do}'} K_d e_q' + \frac{1}{\tau_{do}'} x_{xd} i_d + K_d \Lambda_D \\
 e_q'' &= K_1 e_q' + K_2 \Lambda_D
 \end{aligned}
 \tag{3.20}$$

in which the constants are defined as

$$\begin{aligned}
 K_1 &= \frac{x_d'' - x_f}{x_d' - x_f} \\
 K_2 &= 1 - K_1 \\
 K_d &= \frac{(x_d - x_d')(x_d' - x_d'')}{(x_d' - x_f)^2} \\
 x_{xd} &= \frac{(x_d - x_d')(x_d'' - x_f)}{x_d' - x_f}
 \end{aligned}
 \tag{3.21}$$

The mechanical system representation in this model has been limited to an equivalent rotor mass to keep the complete system (many machines) order to a lower value. The interest with this calculation is only on the low frequency response, so higher order shaft modes, which would require the fully detailed shaft model, do not need to be represented. The remaining equations then are

$$\begin{aligned}\dot{\omega}_i &= \frac{T_m}{\tau} - \frac{1}{\tau} (e_q'' i_q + e_d'' i_d) - \frac{D_i}{\tau} \omega_i \\ \dot{\delta}_i &= \omega_i - 1\end{aligned}\tag{3.22}$$

With appropriate substitutions made for the current terms, these equations are arranged into a suitable form similar to that used for the more detailed machine model in Eqn. [3.19].

3.3 NETWORK MODEL

The classical model of the power network for stability studies represents all transmission lines as positive sequence admittances at the power frequency. For studies which do not take the dynamics of the network into account, such as is the case with conventional eigenanalysis for low-frequency machine interactions, this is perfectly adequate. However, for studies where higher frequency phenomena is of importance, the network dynamics cannot be so simplified.

3.3.1 Network Transformation and Impedance in d-q coordinates

In Section 2.2.2, the form of the complex impedance matrix was discussed. It was shown that the additional stator currents due to the rotor oscillation has two components; a subsynchronous component at frequency $(\omega_o - \omega)$; and a supersynchronous component at frequency $(\omega_o + \omega)$. This indicates that if the impedance of a line at both these frequencies is known, the impedance in d-q coordinates may be deduced. The transformation from stationary to oscillating d-q coordinates is defined by

$$\begin{bmatrix} v_d(j\omega) \\ v_q(j\omega) \end{bmatrix} = \frac{1}{2} \begin{bmatrix} 1 & 1 \\ -j & j \end{bmatrix} \begin{bmatrix} v^+(j(\omega_o + \omega)) \\ v^-(j(\omega_o - \omega)) \end{bmatrix} \quad [3.23]$$

where v^- and v^+ represents sub- and supersynchronous components respectively and $v_{d,q}$ represents d-q axis components. The inverse transformation is

$$\begin{bmatrix} v^+(j(\omega_o + \omega)) \\ v^-(j(\omega_o - \omega)) \end{bmatrix} = \begin{bmatrix} 1 & j \\ 1 & -j \end{bmatrix} \begin{bmatrix} v_d(j\omega) \\ v_q(j\omega) \end{bmatrix} \quad [3.24]$$

Thus, using Eqn. [3.23], an impedance in stationary coordinates, Z_s , can be transformed to oscillating d-q coordinates by

$$Z_{dq} = T^{-1} Z_s T \quad [3.25]$$

where T represents the transformation matrix in Eqn. [3.23].

3.3.2 Transmission Line Model

The transmission line model used in this study is based on the standard Π equivalent model common to loadflow analysis of power systems, consisting of lumped resistance and inductance parameters, with the equivalent shunt admittance split between both ends of the line as illustrated in Figure 3.4.

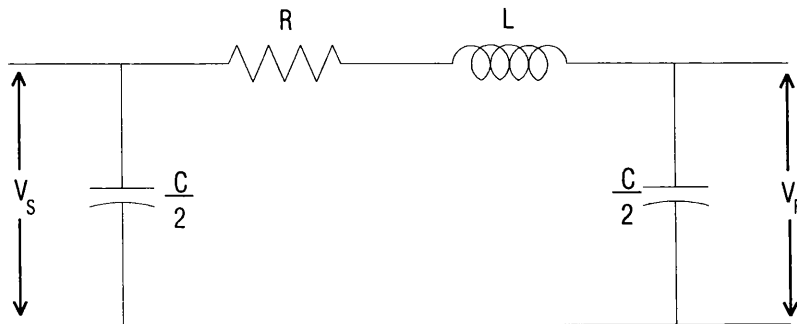


Figure 3.4: Π Equivalent Circuit Representation of a Transmission Line

For the RLC segment of the transmission line, matrix Z_s in stationary coordinates may be written as

$$\begin{bmatrix} v^+(j(\omega_o + \omega)) \\ v^-(j(\omega_o - \omega)) \end{bmatrix} = \begin{bmatrix} r_n + j(\omega_o + \omega)L_n + \frac{j}{(\omega_o + \omega)C_n} & 0 \\ 0 & r_n + j(\omega_o - \omega)L_n + \frac{j}{(\omega_o - \omega)C_n} \end{bmatrix} \begin{bmatrix} i^+(j(\omega_o + \omega)) \\ i^-(j(\omega_o - \omega)) \end{bmatrix} \quad [3.26]$$

Applying Eqn. [3.26] to [3.25] results in the following 2x2 complex impedance matrix,

$$\begin{bmatrix} r_n + j\lambda \left(X_n + \frac{X_{cn}}{1 - \lambda^2} \right) & - \left(X_n - \frac{X_{cn}}{1 - \lambda^2} \right) \\ \left(X_n - \frac{X_{cn}}{1 - \lambda^2} \right) & r_n + j\lambda \left(X_n + \frac{X_{cn}}{1 - \lambda^2} \right) \end{bmatrix} \quad [3.27]$$

where λ is relative frequency of rotor oscillation, $\frac{\omega}{\omega_o}$, X_n is inductive reactance, and X_{cn} is series capacitive reactance. This is inverted to an admittance form whereby it can be included in the overall network admittance equation⁶, illustrated in Figure 3.5.

In this construction, the negative of the complex admittance matrix corresponding to the RLC series element connecting nodes i and j will make up the off-diagonal elements Y_{ij} and Y_{ji} and the positive complex admittance matrix will be added to the diagonal elements Y_{ii} and Y_{jj} .

$$\begin{bmatrix} \Delta i_d^1 \\ \Delta i_q^1 \\ \downarrow \\ \Delta i_d^n \\ \Delta i_q^n \end{bmatrix} = \begin{bmatrix} Y_{11}^{dd} & Y_{11}^{dq} & \dots & Y_{1n}^{dd} & Y_{1n}^{dq} \\ Y_{11}^{qd} & Y_{11}^{qq} & \dots & Y_{1n}^{qd} & Y_{1n}^{qq} \\ \vdots & \vdots & \ddots & \vdots & \vdots \\ Y_{n1}^{dd} & Y_{n1}^{dq} & \dots & Y_{nn}^{dd} & Y_{nn}^{dq} \\ Y_{n1}^{qd} & Y_{n1}^{qq} & \dots & Y_{nn}^{qd} & Y_{nn}^{qq} \end{bmatrix}^{-1} \begin{bmatrix} \Delta v_d^1 \\ \Delta v_q^1 \\ \downarrow \\ \Delta v_d^n \\ \Delta v_q^n \end{bmatrix}$$

Figure 3.5: System Admittance Matrix Construction

⁶ Each element Y_{ij} is a 2x2 matrix in which each sub-element is complex

Shunt capacitance elements of the same line represented in the form

$$\begin{bmatrix} j\lambda \frac{X_{cn}}{1-\lambda^2} & \frac{X_{cn}}{1-\lambda^2} \\ \frac{X_{cn}}{1-\lambda^2} & j\lambda \frac{X_{cn}}{1-\lambda^2} \end{bmatrix} \quad [3.28]$$

and inverted, are also added to the diagonal elements Y_{ii} and Y_{jj} .

Similarly, inductive shunt elements are represented by their impedance matrix form

$$\begin{bmatrix} j\lambda X_n & -X_n \\ X_n & j\lambda X_n \end{bmatrix} \quad [3.29]$$

3.3.3 Transformer Model

The transformer model used is illustrated in Figure 3.6, in which both primary and secondary windings are represented by equivalent impedances $R_p + jX_p$ and $R_s + jX_s$ which may be incorporated into the analysis in exactly the same manner as is used for transmission lines. Magnetising reactance and core loss are represented by admittance G_m and conductance B_m respectively. Saturation of the core is neglected. A tap-changing facility is included during loadflow calculations, from which the primary and secondary equivalent impedances are updated.

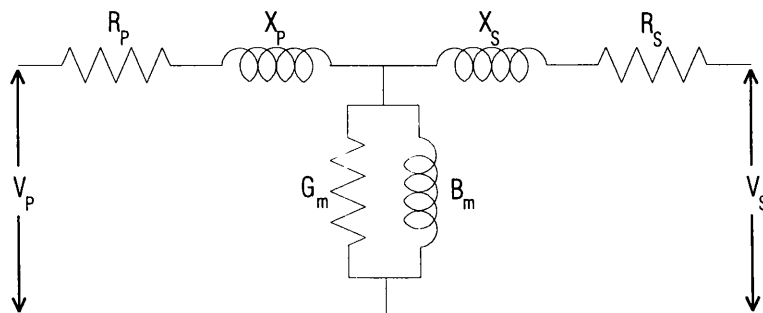


Figure 3.6: Equivalent Circuit Model of the Transformer

3.3.4 Load Models

A number of studies in the past have shown there is no single load characteristic that leads to accurate results for all system configurations [28]. Stability studies have traditionally used static models which represented constant power, constant current or constant impedance configurations. The model considered here takes the exponential form

$$P_L = P_o \left(\frac{V}{V_o} \right)^\alpha \quad Q_L = Q_o \left(\frac{V}{V_o} \right)^\beta \quad [3.30]$$

where V_o and P_o (Q_o) are nominal voltage of the bus and the corresponding active (reactive) power of the load respectively. The exponential terms α and β are generally in the range 1 to 3, depending on which configuration of load is being modelled.

After determining P_L and Q_L the equivalent load admittance is calculated from

$$P_L + jQ_L = V_L^2 (G_L - jB_L) \quad [3.31]$$

and transformed to d-q coordinates in a similar manner to that used for shunt components (Eqns. [3.28] and [3.29]).

3.4 SUMMARY OF CHAPTER 3

This Chapter has described the dynamic equations governing the behaviour of the interconnected power system, the main elements of which are synchronous machines including the mechanical shaft train, transmission lines, transformers, shunt elements and loads.

The equations of the synchronous machine and shaft train have been arranged in state-space form which is necessary to facilitate a rigorous approach to multi-machine analysis as will be discussed in Chapter 5.

All of the described elements will be used in the analysis of torsional interaction in subsequent chapters.

SUBSYNCHRONOUS RESONANCE ANALYSIS**4.1 INTRODUCTION****4.1.1 Background**

It has long been known that the phenomenon of Torsional Oscillations in turbine-generator shafts is a direct consequence of the use of compensating equipment [29,30], and more recently, power system controllers in electrical power systems [32,33]. This phenomenon is a subset of the general dynamic stability problem. There are two general categories of the phenomenon, Subsynchronous Resonance (SSR) and Subsynchronous Torsional Interaction (SSTI). This chapter discusses the application of Complex Torque Coefficient analysis to SSR while the latter will be discussed in Chapter 6.

Subsynchronous Resonance is a condition¹ that may exist on power systems wherein the transmission network has natural frequencies of oscillation that fall below the nominal (50Hz or 60Hz) power frequency of the system. The phenomenon manifests itself in two distinct mechanisms; *Induction Generator* effect and *Torsional Interaction*.

4.1.2 Induction Generator Effect

When a resonance occurs in an electrical transmission network to which a synchronous generator is connected, there will be a revolving magnetic field in the generator air-gap corresponding to the resonant frequency f_e . If this frequency is subsynchronous i.e $f_e < f_s$ where f_s is the system frequency, the revolving field will be rotating at a subsynchronous speed. Since the generator rotor itself is rotating at synchronous or base speed, the synchronous machine will behave like an induction generator with respect to the subsynchronously rotating field due to the electrical

¹ The formal definition of Subsynchronous Resonance is provided by the IEEE SSR Working Group [30]

resonance. The well-known equivalent circuit of the induction machine is illustrated in Figure 4.1. By the definition of slip² as given by Eqn. 4.1

$$s = \frac{(f_e - f_s)}{f_e} \quad [4.1]$$

it can be seen that for a field rotating at a subsynchronous speed, the equivalent rotor resistance in Figure 4.1 will be negative. This will have the effect of reducing the total resistance to subsynchronous currents which are induced as a result of system disturbances. These currents themselves induce additional torques acting on the generator rotor and result in the time constants for the decay of exciting torques becoming greater thus exacerbating the oscillatory problem.

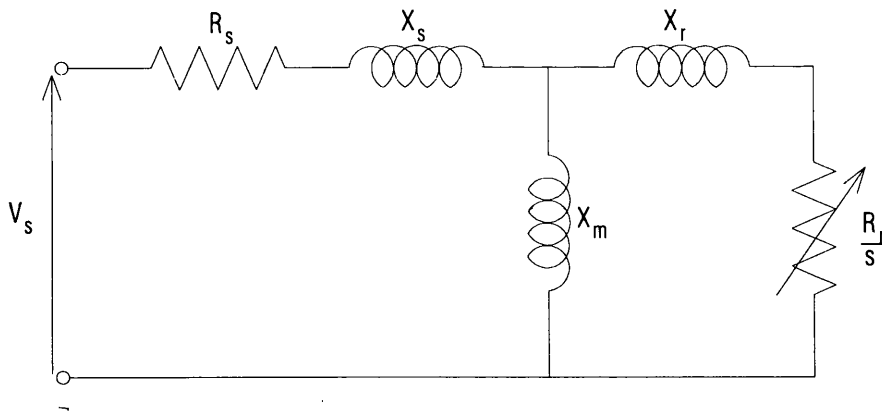


Figure 4.1 : Equivalent Circuit for the Induction Machine

If this 'negative' resistance is greater in magnitude than the equivalent resistance of the network as viewed from the terminals of the Synchronous machine³, and further, the equivalent reactance of the network as viewed from the same location is close to zero, an electrical resonance will occur [34,35], and the system will self excite. The induction generator mode of SSR is the dominant factor in machine oscillations following system disturbances.

² The per-unit relative speed of the rotor with respect to the rotating magnetic field in the airgap.

4.1.3 Torsional Interaction

The induction generator effect is solely an electrical phenomenon and does not take proper account of the influence of the mechanical system to which the generator rotor is connected. The Torsional Interaction phenomenon however, embraces the interplay between the electrical and mechanical systems that may occur in resonant electric transmission systems. It can be shown that currents flowing in a transmission network which exhibits points of resonance will be composed of two components; one component at the nominal power frequency and one component resulting from the sum of the natural resonant frequencies of the network, or mathematically

$$i(t) = k \left(A \sin(\omega_1 t + \psi_1) + \sum_{m=2}^n B e^{-\zeta \omega_m t} \sin(\omega_m t + \psi_m) \right) \quad [4.2]$$

in which all the parameters except ω_1 , the system base frequency, are functions of the transmission network. The stator windings of Synchronous generators which are connected to the transmission network will also contain these two components of current. Fluctuations of the airgap MMF will induce additional rotor currents which will produce additional oscillatory torque components superimposed upon the steady torque, at the supersynchronous and subsynchronous frequencies. The high-, intermediate-, and low-pressure turbines, the generator rotor, and the exciter are usually arranged on the same shaft, constituting a linear mass-spring system. The frequencies of oscillation of a typical multi-mass shaft system which is coupled to the electrical network via the generator rotor are very close to the natural frequencies of oscillation of the uncoupled multi-mass shaft, and generally lie below the base frequency. Should the additional torque component at the subsynchronous frequency coincide with any one of these shaft frequencies, the shaft system and the electrical system resonance could be mutually excited, causing fatigue life expenditure, damage or even complete failure of the shaft.

4.1.4 Causes and Countermeasures of SSR

SSR most commonly occurs when compensating capacitors in the power network interact with the inductive transmission lines to form a resonant circuit. Typically the

³ The impedance of the Synchronous Machine cannot be correctly calculated using the equivalent circuit of the induction machine, thus doing so will give an approximate solution only.

resonant frequencies will produce additional rotor torques with frequencies in the range of 10Hz to 40Hz providing the conditions for an exchange of energy between the electrical network and the mechanical system with possible torsional fatigue damage to the shaft.

To prevent SSR and to protect the system, countermeasures of SSR have been developed. Of these, the simplest is the Static Blocking Filter, tuned to the transmission system natural frequency, which blocks the path of harmonic currents and prevents the build up of oscillatory torques. However, the major drawbacks of this form of countermeasure are high cost and inflexibility in tuned frequency, which can be a problem in systems which are continually changing in topology (line switching and load demands).

More advanced techniques have since been developed [36,37] which attempt to regulate the reactive power output or demand of the machine. By modulating the VAR's such that the resulting rotor torque oscillation is in anti-phase with the original oscillatory component due to SSR, the problem can be eliminated. Excitation control of the generator and active reactors located close to the generator are examples of such schemes. However, in a system containing many machines, providing countermeasures for all can be very costly. This is further compounded by problems of coordinating the control of machines to prevent unfavourable interactions.

A better approach, perhaps, may be to tackle the problem at its source. Thyristor switching compensation capacitors have received a great deal of attention. The basic idea is to modulate the capacitance in such a way as to reduce the amplitude of harmonic currents. Recent studies [38] on unbalanced systems has indicated that unbalancing the compensation capacitors in each phase eliminates the troublesome oscillations and thus removes the threat for all machines in the system.

The use of Flexible AC Transmission System (FACTS) components has shown to have good potential, not only for increasing the utilisation of existing transmission corridors without change in loading of parallel paths, but also as an SSR countermeasure. The range of possible FACTS devices is diverse, but of those investigated for countermeasure service, three in particular demonstrate promise:

Static Phase Shifters

The Static Phase Shifter is a device which can inject a voltage with a controllable phase angle and/or magnitude under no-load and load conditions. The principle of

operation is illustrated in schematic form in Figure 4.2. By introducing a phase shift in the generator terminal voltages which is proportional to the rotor speed deviations, with proper phase and gain, the effective phase angle between the generator rotor and the system voltage changes forcing the generator to modulate reactive power. The phase shift is obtained by injecting a quadrature voltage into the line. The phase of the injected voltage is determined by controlling the switching instants of a thyristor bank. Iravani et al [39] demonstrated that such a system could help to eliminate subsynchronous oscillations.

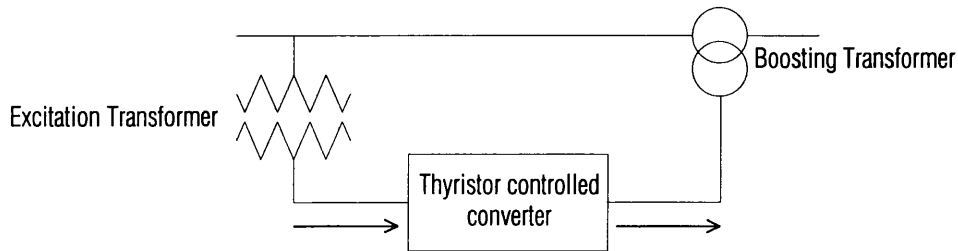


Figure 4.2 : The Phase Shifter Concept

HVDC Converters

HVDC links permit interlinking of AC power systems in cases where it might otherwise be prohibited, either by technical or economic constraints. In addition, it has been well known [40] that, in general, HVDC systems provide a significant level of stability due to their fast response capabilities. HVDC therefore has an increasing, albeit specialised, role to play in power transfer. However, the possibility of interaction between HVDC links and turbine-generator shafts should be borne in mind. An investigation into the impact that non-characteristic harmonics generated by HVDC links could have on shaft oscillations on turbine generators is discussed in Chapter 7.

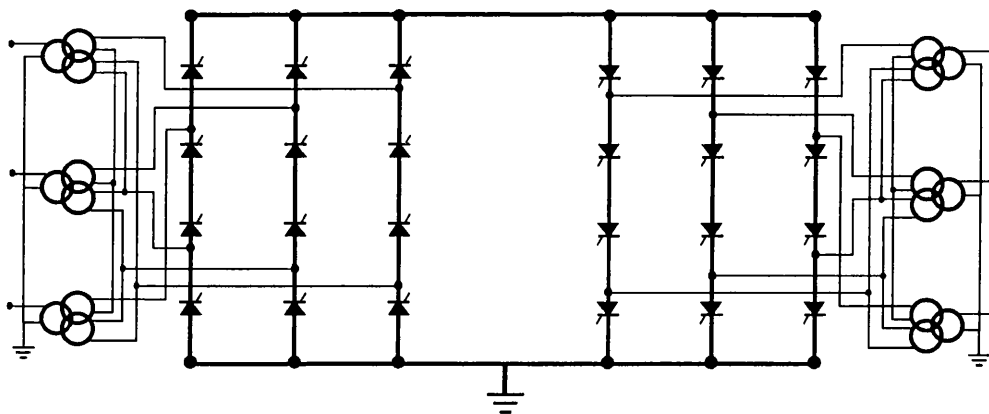


Figure 4.3 : HVDC link

TCSC Systems

Thyristor controlled series capacitor systems, rather than being devices employed to mitigate subsynchronous resonance caused by transmission lines compensated using fixed capacitors, can be used as a direct replacement for the traditional scheme providing the same level of compensation but without any subsynchronous resonance problems [41,42,43].

TCSC controllers use thyristor controlled reactors in parallel with capacitor banks. This combination allows the capacitive reactance to be continuously controlled over a wide range. At subsynchronous frequencies, the TCSC assumes an inductive-resistive impedance thus allowing TCSC's to provide higher levels of series compensation with significantly reduced risk of SSR interaction.

Such a scheme will be studied using complex torque coefficient analysis in Chapter 6.

4.2 ELECTROMAGNETIC COMPLEX TORQUE COEFFICIENTS APPLIED TO THE SINGLE MACHINE SYSTEM

The following sections aim to demonstrate the applicability of Complex Torque Coefficient Analysis to the study of Subsynchronous Resonance.

4.2.1 Single Machine System

The system illustrated in Figure 4.4 consists of a synchronous machine, a transformer, and a compensated transmission line in parallel with an uncompensated line. The synchronous machine and transmission line data is given in Table 4.1.

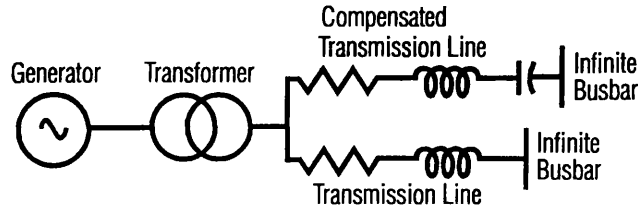


Figure 4.4 : Single Machine System

Table 4.1: Generator and Transmission Line Constants

Apparent Power, MVA	600
Number of Poles	2
Supply Frequency	60
<i>Direct Axis:</i>	
Synchronous Reactance X_d , p.u.	1.790
Transient Reactance, X_d' , p.u.	0.169
Subtransient Reactance X_d'' , p.u.	0.135
Open Circuit Transient Time Constant T_{do}' , s	4.300
Open Circuit Subtransient Time Constant T_{do}'' , s	0.032
Stator Resistance R_a , p.u.	0.005
Stator Leakage Reactance X_a , p.u.	0.130
Characteristic Reactance X_{char} , p.u. ⁴	0.220
<i>Quadrature Axis:</i>	
Synchronous Reactance X_q , p.u.	1.710
Transient Reactance X_q' , p.u.	0.228
Subtransient Reactance X_q'' , p.u.	0.200
Open Circuit Transient Time Constant T_{qo}' , s	0.850
Open Circuit Subtransient Time Constant T_{qo}'' , s	0.050
Transmission Line n1 resistance, p.u.	0.024
Transmission Line n2 resistance, p.u.	0.024
Transmission Line n1 inductive reactance, p.u.	0.140
Transmission Line n2 inductive reactance, p.u.	0.075
Transmission Line n1 shunt capacitance, p.u.	0.5
Transmission Line n2 shunt capacitance, p.u.	0.5
Transformer T1 resistance, p.u.	0.003
Transformer T1 reactance, p.u.	0.062
Series capacitance on line n1, % of line reactance	50%

All constants have been normalised on generator apparent power rating of 600MVA and base voltage of $13.6kV_{L-L}$.

⁴ The characteristic reactance takes account of the true magnetic coupling between the field and the damper circuit of a synchronous machine.

Table 4.2 : Rotor Inertias and Stiffnesses

<i>Inertia, MW-s/MVA</i>	
<i>HP turbine</i>	<i>0.104</i>
<i>IP turbine</i>	<i>0.284</i>
<i>LP1 turbine</i>	<i>1.558</i>
<i>LP2 turbine</i>	<i>1.540</i>
<i>Generator</i>	<i>0.727</i>
<i>Exciter1</i>	<i>0.021</i>
<i>Stiffness, MW/MVA-rad</i>	
<i>HP/IP</i>	<i>48.5</i>
<i>IP/LP1</i>	<i>106.0</i>
<i>LP1/LP2</i>	<i>3940.0</i>
<i>LP2/GEN</i>	<i>58.3</i>
<i>GEN/EX1</i>	<i>28.5</i>
<i>Damping, MW-s/MVA-rad</i>	
<i>HP turbine</i>	<i>0.002</i>
<i>IP turbine</i>	<i>0.002</i>
<i>LP1 turbine</i>	<i>0.002</i>
<i>LP2 turbine</i>	<i>0.002</i>
<i>Generator</i>	<i>0.002</i>
<i>Exciter1</i>	<i>-</i>

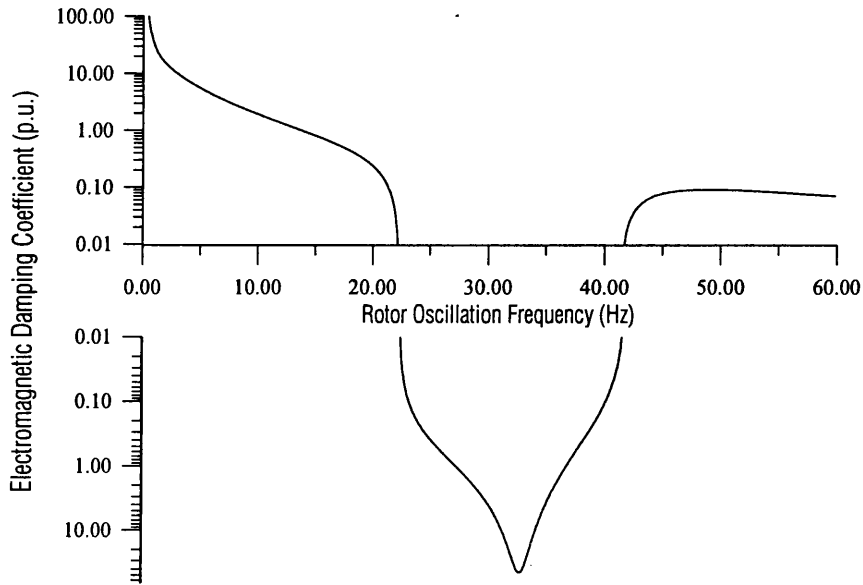
All constants have been normalised on generator apparent power rating of 600MVA. Unit torque corresponds to apparent power at unity power factor.

The analysis consists of essentially two parts. Firstly, the rotor of the synchronous machine is assumed to be subjected to small oscillations about its mean operating point. The origin of these oscillations is completely arbitrary and is of no relevance to the analysis, simply that they exist. Using the theory of Torque Coefficients developed in Chapter 2, the possibility of these oscillations being sustained or amplified assuming zero mechanical damping influence is investigated. This is the Electromagnetic Torque Coefficient, discussed for this specific case in § 4.2.2 . Secondly, the influence of the mechanical system is evaluated by defining a complementary Mechanical Torque Coefficient. The origin of this quantity and its interpretation is discussed in § 4.3.

4.2.2 Effect of Network Capacitors on Electromagnetic Torque Coefficients

The usefulness of the Complex Torque coefficients in the analysis of Subsynchronous Resonance is easily appreciated from Figure 4.5, which depicts damping torque component, which if recalled from Chapter 2, is the imaginary component of the electromagnetic torque coefficient, as a function of rotor oscillation frequency for 50% capacitor compensation⁵ with the uncompensated transmission line disconnected.

⁵ Percentage of capacitor compensation refers to the reactance of the capacitor expressed as a percentage of the line inductive reactance. It is worth noting that the *effective* compensation is



Damping Coefficient is normalised on machine apparent power rating of 600MVA divided by (base angular velocity)². Angular velocity is normalised on 120π rad/sec.

Figure 4.5 : Electromagnetic Damping Torque Component for 50% Line Compensation

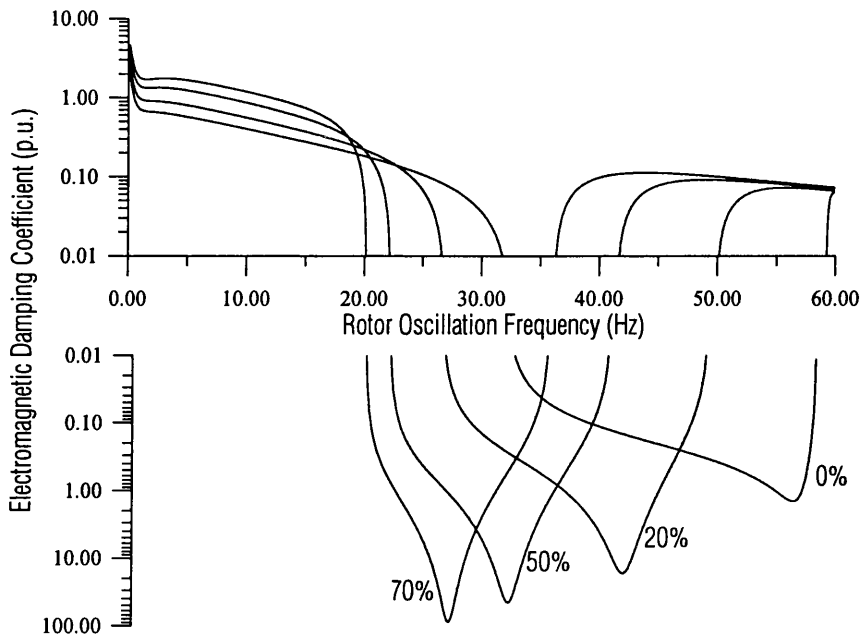
Clearly, the presence of the capacitor induces a region of negative electrical damping on the machine rotor which, assuming no external damping component, would tend to encourage rotor oscillations to build up. Examining the curve more closely, it can be observed that the peak negative damping occurs at a frequency of approximately 32 Hz. The transmission line, with its series LC combination, will have a natural frequency, on the stator side of the machine, defined by Eqn. [4.3]:

$$\omega_n = \sqrt{\frac{1}{LC}} \quad \text{rad / sec} \quad [4.3]$$

where the inductance L of the transmission line includes the leakage inductance of the transformer and the subtransient inductance of the machine.

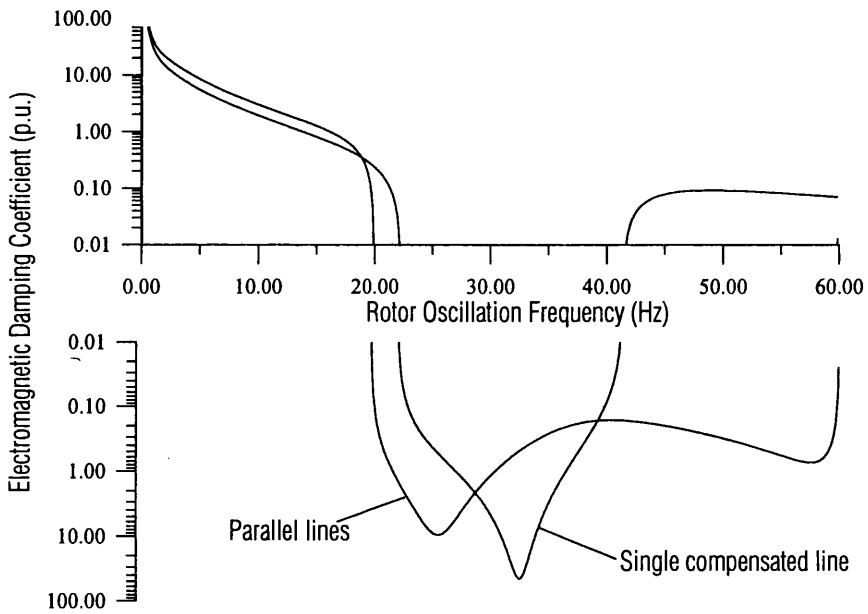
Substituting the system parameters as given in Table 4.1 into Eqn. [4.3] gives an estimated resonant frequency of 32.5 Hz, which is in good agreement with that predicted by Figure 4.5.

considerably reduced when the impedance of machine transformers and effective load impedance are taken into account.



Damping Coefficient is normalised on machine apparent power rating of 600MVA divided by $(\text{base angular velocity})^2$. Angular velocity is normalised on 120π rad/sec.

Figure 4.6 : Variation of Damping Torque Component with Compensation Level



Damping Coefficient is normalised on machine apparent power rating of 600MVA divided by $(\text{base angular velocity})^2$. Angular velocity is normalised on 120π rad/sec. Series compensation of 50% in compensated line.

Figure 4.7: Effect of Parallel Lines

Figure 4.6 depicts the change in the damping torque component curve as the percentage of capacitor compensation is varied between 0% and 70% of the line inductance in transmission line n1. As one would expect from the simple equation of resonance, the frequency of least electrical damping decreases as the line compensation is increased, thereby putting the lower torsional modes of oscillation at risk. However, the bandwidth of possible interaction is reduced significantly as compensation is increased. It should also be noted that effective damping at the lower end of the scale is improved as compensation is increased.

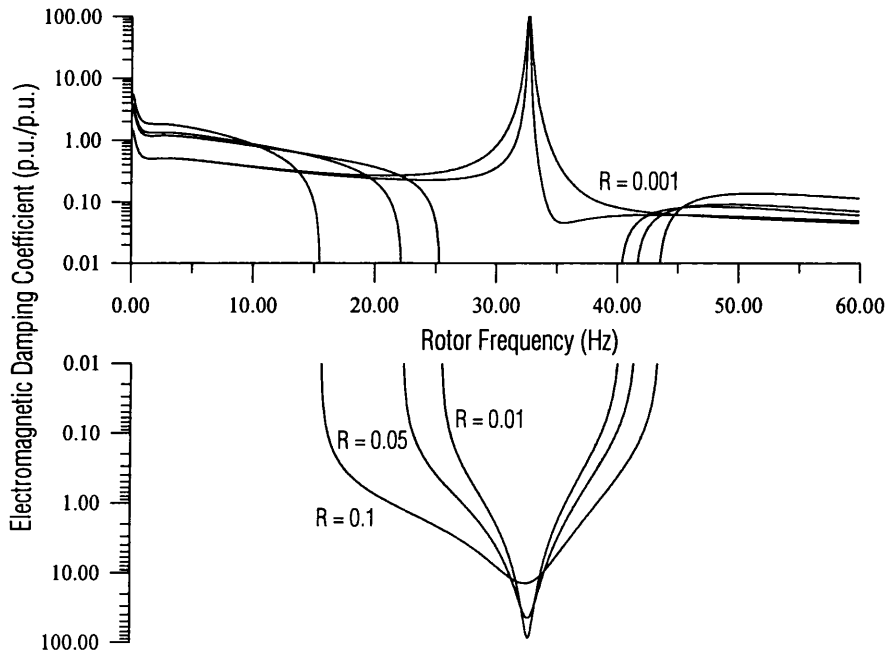
4.2.3 Multiple Transmission Lines

The effect of increasing the connectivity of the system is illustrated in Figure 4.7. In this case, the uncompensated transmission line n2 was connected in parallel to the original compensated line n1. This effect has been well experienced in many large compensated systems and is often used to mitigate any possible oscillations. This effect explains why problems of subsynchronous resonance involving capacitor compensated lines is much more common in areas where the system is inherently weak.

4.2.4 Influence of Transmission Line Resistance

In Chapter 2, the influence of synchronous machine resistance on the calculated electromagnetic torque coefficient was discussed. In systems involving series compensation of transmission lines, resistance of the line, often regarded as being a relatively insignificant parameter, has a significant impact on the damping coefficients. Figure 4.8 illustrates the sensitivity of the damping coefficients to variations in the transmission line resistance parameter.

The curves demonstrate that as the machine resistance is decreased from 0.1p.u to 0.001p.u., the electromagnetic damping coefficient becomes more onerous, with the bandwidth of the negative region decreasing, the minimum value coinciding with the natural frequency of the transmission line.



Damping Coefficient is normalised on machine apparent power rating of 600MVA divided by $(\text{base angular velocity})^2$. Angular velocity is normalised on 120π rad/sec. Series compensation of 50% in compensated line. All resistances are normalised on machine apparent power rating and base voltage.

Figure 4.8 : Effect of Transmission Line Resistance

Reducing the resistance further has the effect of eliminating this negative region and replacing it with a region of positive damping, its point of maximum again coinciding with the natural frequency of the line.

4.3 MECHANICAL COMPLEX TORQUE COEFFICIENTS OF THE MULTI-MASS SYSTEM

In Chapter 2, the idea of the Electromagnetic Torque Coefficient and its possible application to the study of machine stability was discussed. However, as pointed out in Chapter 3 during the development of the state-space forms of the synchronous machine, for multi-machine analysis to be discussed in Chapter 5, the mechanical system equations cannot be ignored and must form an integral part of the analysis. The determination of shaft oscillation frequencies is an important part of this. There are essentially three methods that can be used to determine these frequencies: an analytical approach; eigenanalysis applied to the shaft train; or mechanical torque coefficient analysis.

4.3.1 Natural Frequencies using an Analytical Method

The general approach to the solution of the equations of motion is the same for all linear systems. Consider the 4-mass undamped system illustrated in Figure 4.9, for which the system equations may be written as

$$\begin{aligned}
 I_1 \ddot{\theta}_1 &= k_1(\theta_1 - \theta_2) \\
 I_2 \ddot{\theta}_2 &= k_1(\theta_1 - \theta_2) - k_2(\theta_2 - \theta_3) \\
 I_3 \ddot{\theta}_3 &= k_2(\theta_2 - \theta_3) - k_3(\theta_3 - \theta_4) \\
 I_4 \ddot{\theta}_4 &= k_3(\theta_3 - \theta_4) + M_o \cos \omega t
 \end{aligned}
 \tag{4.4}$$

where $M_o \cos \omega t$ represents an exciting torque applied to mass 4.

It is well known that the motion of a linear vibrating system is associated with simple harmonic motion. The solution therefore will take the form

$$\begin{aligned}
 \theta_1 &= \Phi_1 \cos \lambda t \\
 \theta_2 &= \Phi_2 \cos \lambda t \\
 \theta_3 &= \Phi_3 \cos \lambda t \\
 \theta_4 &= \Phi_4 \cos \lambda t
 \end{aligned}
 \tag{4.5}$$

in which the amplitudes Φ_i and the natural frequency λ have to be determined.

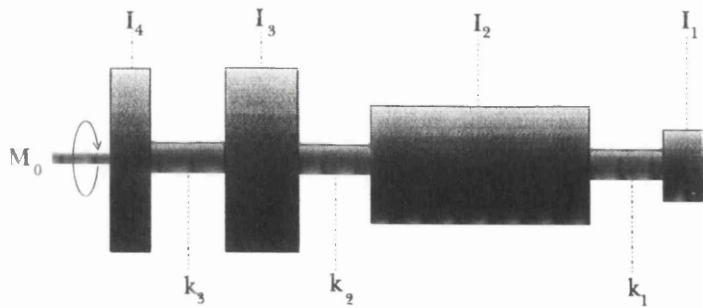


Figure 4.9 : 4-Mass Turbine-Generator-Exciter System

Substituting the solutions [4.5] into the equations of motion [4.4] yields

$$\begin{aligned}
 (k_1 - \lambda^2 I_1)\Phi_1 - k_2 \Phi_2 &= 0 \\
 -k_1 \Phi_1 + (k_1 + k_2 - \lambda^2 I_2)\Phi_2 - k_2 \Phi_3 &= 0 \\
 -k_2 \Phi_2 + (k_2 + k_3 - \lambda^2 I_3)\Phi_3 - k_3 \Phi_4 &= 0 \\
 -k_3 \Phi_3 + (k_3 - \lambda^2 I_4)\Phi_4 &= M_o
 \end{aligned}
 \tag{4.6}$$

The three⁶ natural frequencies of the system are obtained from the solution to these equations when the exciting torque M_o equals zero, i.e a polynomial of the form

$$\lambda^6 - \alpha\lambda^4 + \beta\lambda^2 - \gamma = 0 \tag{4.7}$$

is obtained, where α , β , and γ are functions of I_i and K_i ($1 \leq i \leq 4$).

Classical analysis applied to this for this 4 mass system suggests that the roots of [4.7] are given by

$$\lambda^2 = \frac{1}{3}\alpha - \frac{2}{3}\sqrt{\alpha^2 - 3\beta} \cos \frac{1}{3}(\phi + 2\pi n) \quad (n = -1, 0, 1) \tag{4.8}$$

where

$$\cos \phi = \frac{\frac{\alpha\beta - 9\gamma}{\alpha^2 - 3\beta} - \frac{2}{3}\alpha}{\frac{2}{3}\sqrt{\alpha^2 - 3\beta}} \tag{4.9}$$

The roots may be represented graphically as shown in Figure 4.10.

⁶ The frequency Eqn. [4.6] is a third order equation in λ^2 after the rigid body motion of the system, the root $\lambda^2=0$, is eliminated.

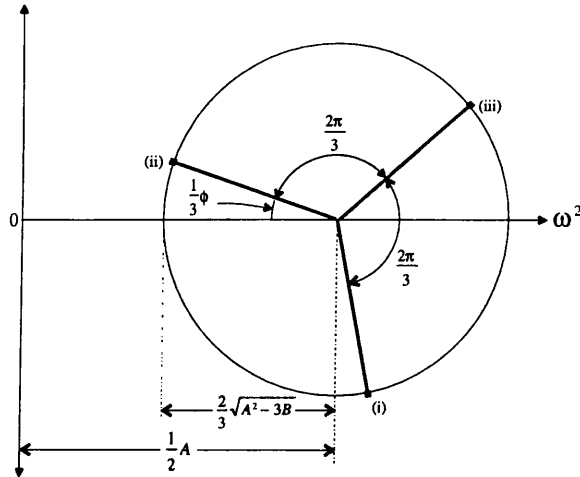


Figure 4.10 : Natural Frequencies of the 4-Mass System

4.3.2 Natural Frequencies using Eigenanalysis

Unfortunately, few turbine-generator-exciter shaft systems consist of only four or less masses making the analytical method somewhat cumbersome. An alternative numerical technique can be used instead, based on determining the eigenvalues of the state-matrix belonging to the shaft system.

The undamped frequency of oscillation of a single mass shaft system is given by:

$$\omega_n = \sqrt{\frac{K}{J}} \text{ rad / sec} \quad [4.10]$$

For the damped case, the frequency is given by:

$$\omega_r = \sqrt{\frac{k}{J} - \frac{D^2}{4J^2}} \text{ rad / sec} \quad [4.11]$$

For most physical shaft systems, the damping factor D is very small and the damped frequency differs insignificantly from the undamped frequency (approx. 0.1Hz). It is therefore feasible to calculate the undamped natural frequencies and assume these to be the same as the damped system frequencies.

Rewriting Eqn. [4.4] in matrix form and rearranging yields

$$\begin{aligned}
 [I][\ddot{\theta}] + [k][\theta] &= 0 \\
 \Rightarrow [\ddot{\theta}] &= -[I^{-1}][k][\theta] \\
 &= [A][\theta]
 \end{aligned} \tag{4.12}$$

The imaginary parts of the eigenvalues of the 'system' matrix A give the natural undamped frequencies of oscillation. Because the solution of Eqn. [4.12] is numerical as compared with the analytical technique of Eqn. [4.8], it can be applied to an arbitrary number of masses, and is in an appropriate form for software implementation.

4.3.3 Natural and Coupled System Frequencies using Electromechanical Torque Analysis

For free oscillations, an electromagnetic torque acting on the rotor of a synchronous machine will be counteracted by a mechanical torque acting in the opposite direction. To determine whether these oscillations will be damped or sustained the mechanical system equations must be solved together with the electrical system equations which are providing the exciting torque. Eqn. [2.2] stated that the electromagnetic torque was related to the rotor oscillation through a complex quantity. Similarly, the responding mechanical torque will also be related to rotor oscillation through a complex quantity $K_m(j\lambda)$ which opposes the effect of the electromagnetic torque coefficient.

Using similar notation then, the complex relationship for the mechanical system may be written as [25]

$$\Delta T_m = (T_{sm} + j\lambda T_{dm})\Delta\delta \tag{4.13}$$

where ΔT_m is the change in mechanical torque acting on the generator rotor mass. The combined electromagnetic and mechanical torques acting on the generator rotor must yield

$$(T_{sm} + j\lambda T_{dm}) + (T_{se} + j\lambda T_{de}) = \Delta T_x \tag{4.14}$$

where ΔT_x is the excess torque required to balance the equation and will equate to zero for free oscillations in which there is no damping. With knowledge of these four coefficients, the problem of predicting sustained oscillations can be solved. Coefficients T_{se} and T_{de} are already known. To determine the mechanical torque coefficient components T_{sm} and T_{dm} the differential equations of the shaft line must be used.

The interrelationships between the n -masses of the shaft system are given in matrix form by Eqn. [4.15], where the 2nd mass is assumed to be the generator rotor

$$\begin{bmatrix} H_1(p) & -K_1(p) & & \\ -K_1(p) & H_2(p) & -K_2(p) & \\ & -K_2(p) & H_3(p) & -K_3(p) \end{bmatrix} \begin{bmatrix} \Delta v_1 \\ \Delta v_2 \\ \Delta v_3 \end{bmatrix} = \begin{bmatrix} 0 \\ -\Delta T_e \\ 0 \end{bmatrix} \quad [4.15]$$

where the coefficients are given by

$$H_i(p) = 2H_i p^2 + (D_i + D_{(i-1)i} + D_{i(i+1)})p + K_{i-1} + K_i \quad [4.16]$$

$$K_i(p) = D_{i(i+1)}p + K_i$$

in which v_i represents the angle of deviation of the i^{th} mass, and all quantities are in per unit. Eliminating v_1 and v_3 from Eqn. [4.15] yields

$$K_m(j\lambda) = T_{sm} + j\lambda T_{dm} = H_2(j\lambda) - \frac{K_1(j\lambda)^2}{H_1(j\lambda)} - K_2(j\lambda)A_2(j\lambda) \quad [4.17]$$

where

$$A_i(j\lambda) = \frac{K_i(j\lambda)}{H_{i+1}(j\lambda) - K_{i+1}(j\lambda)A_{i+1}(j\lambda)}$$

Just like $K_e(j\lambda)$, $K_m(j\lambda)$ is a frequency dependent complex quantity. It defines the resulting response of the entire shaft train to the oscillations of the machine rotor. It is termed the Mechanical Complex Torque Coefficient.

The real part of the Coefficient is termed the Mechanical Synchronising coefficient, and is predominately dependent on turbine inertia and shaft stiffness parameters.

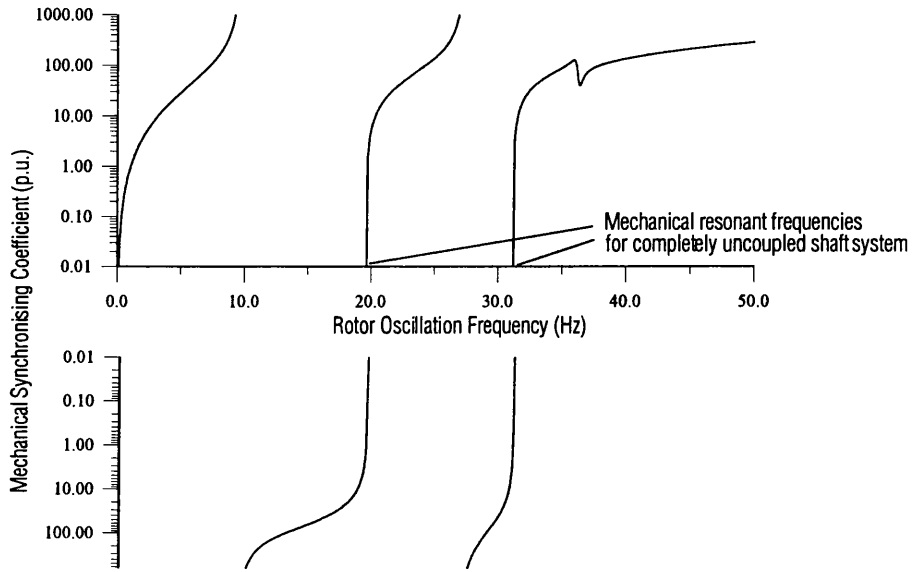
The imaginary part of the coefficient is termed the Mechanical Damping Coefficient. This term reflects the influence of steam viscous damping parameters on the dynamics of the shaft. Steam viscous damping is based on the constant power relationship of the turbine torque/speed characteristic. This leads to viscous damping parameters which are proportional to the instantaneous torque developed by each section of each turbine stage.

The frequency dependency of $K_m(j\lambda)$ of a six mass turbine system as defined in Table 4.2 is illustrated in Figures 4.11 and 4.12. If the steam viscous damping parameters are assumed to be zero, this will lead to a non-complex coefficient. If the shaft line is completely decoupled from the electrical system, the electromagnetic torque, ΔT_e , and the excess torque ΔT_x will both equate to zero, i.e. $(T_{se} + j\lambda T_{de}) = 0$ and the shaft will oscillate freely. Clearly then, Eqn. [4.14] is only satisfied when the only remaining term, T_{sm} , also equals zero. The undamped frequencies of oscillation of the decoupled shaft line therefore are given by the zero crossing points of T_{sm} , as illustrated.

Figure 4.12 illustrates the form of the complex coefficient if steam viscous damping is present. At frequencies close to the undamped natural frequencies of oscillation, the mechanical damping coefficient exhibits a minimum. Between these frequencies, the damping coefficient becomes extremely large.

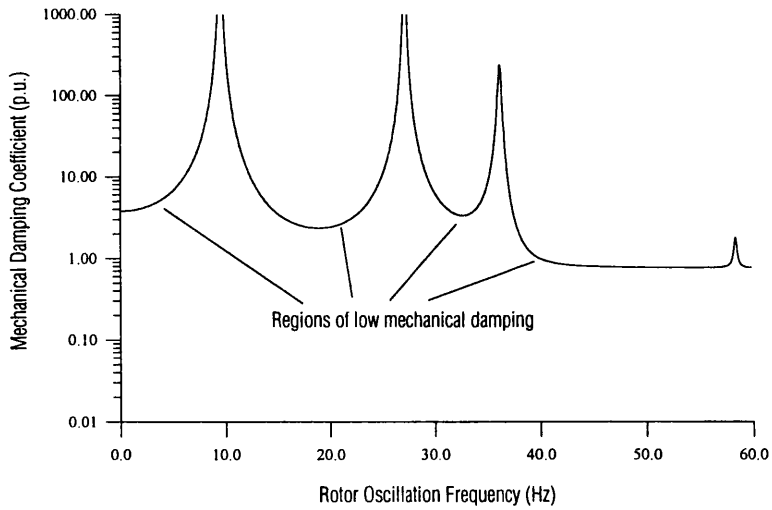
4.4 SSR ANALYSIS OF THE SINGLE MACHINE-COMPENSATED TRANSMISSION LINE—SIX TURBINE SHAFT

In order to predict the occurrence of subsynchronous resonance, it is necessary to combine the electrical and mechanical torque coefficients discussed in the previous sections.



Synchronising Coefficient is normalised on machine apparent power rating of 600MVA divided by (base angular velocity. Angular velocity is normalised on 120π rad/sec.

Figure 4.11: Mechanical Synchronising Coefficient



Damping Coefficient is normalised on machine apparent power rating of 600MVA divided by $(\text{base angular velocity})^2$. Angular velocity is normalised on 120π rad/sec.

Figure 4.12 : Mechanical Damping Coefficient

4.4.1 Time Constants for decay of Principle torsional Oscillations

The interaction between the electrical and mechanical systems can be predicted visually by calculating all four complex torque coefficients over the entire subsynchronous frequency range i.e. rotor oscillations between 0Hz and 50Hz, and plotting them together on the same graph. For the case when electromagnetic damping exactly cancels out mechanical viscous damping, i.e. net damping equals zero, the excess torque will equate to zero and the frequencies of resonance must be given by the points of intersection between the electromagnetic and mechanical synchronising coefficients only. Clearly, due to the high gradient of the mechanical synchronising coefficients at these points of intersection, these frequencies differ very little from the undamped frequencies of oscillation, as predicted by Eqn. [4.11]. According to Eqn. [4.14], the conditions now exist for sustained oscillations of the shaft.

If T_{dm} and T_{de} sum to a positive value then to balance Eqn. [4.14] the excess torque ΔT_x will be positive and the oscillations will decay. If T_{dm} and T_{de} sum to a negative value then to balance Eqn. [4.14] the excess torque ΔT_x will be negative and the oscillations will build.

Of interest here is how quickly the oscillations grow or decay. If an eigenanalysis study was being performed, then Hammons et al. [43] indicate that time constants for decay of torsional vibrations due to steam damping, Γ_m , and due to electromagnetic damping, Γ_e , can be predicted from

$$\Gamma_m = \frac{4 \sum_{i=1}^n H_i(x_{ik})^2}{\omega_o \sum_{i=1}^n D_{i_m}(x_{ik})^2} \quad \Gamma_e = \frac{4 \sum_{i=1}^n H_i(x_{ik})^2}{\omega_o D_{k_e}} \quad [4.18]$$

where H_i represents turbine inertias, x_{ik} represents eigenvectors for modal frequency k , D_{i_m} represents mechanical viscous damping coefficients acting at turbine i , and D_{k_e} represents electrical viscous damping coefficients for modal frequency k . The terms

$\sum_{i=1}^n H_i(x_{ik})^2$ and $\sum_{i=1}^n D_{i_m}(x_{ik})^2$ represent the modal inertias H_{mi} and damping D_{mi} for

each modal frequency. These can be determined easily as part of the Complex Torque Coefficient analysis such that no knowledge of eigenvectors is required.

As discussed by Canay [25], the mechanical synchronising coefficient T_{sm} represents the equation of oscillation for each modal frequency, such that

$$T_{sm} = -2H_{mi}\lambda_i + k_i = 0 \quad [4.19]$$

Taking the derivative of both sides of Eqn [4.19] gives

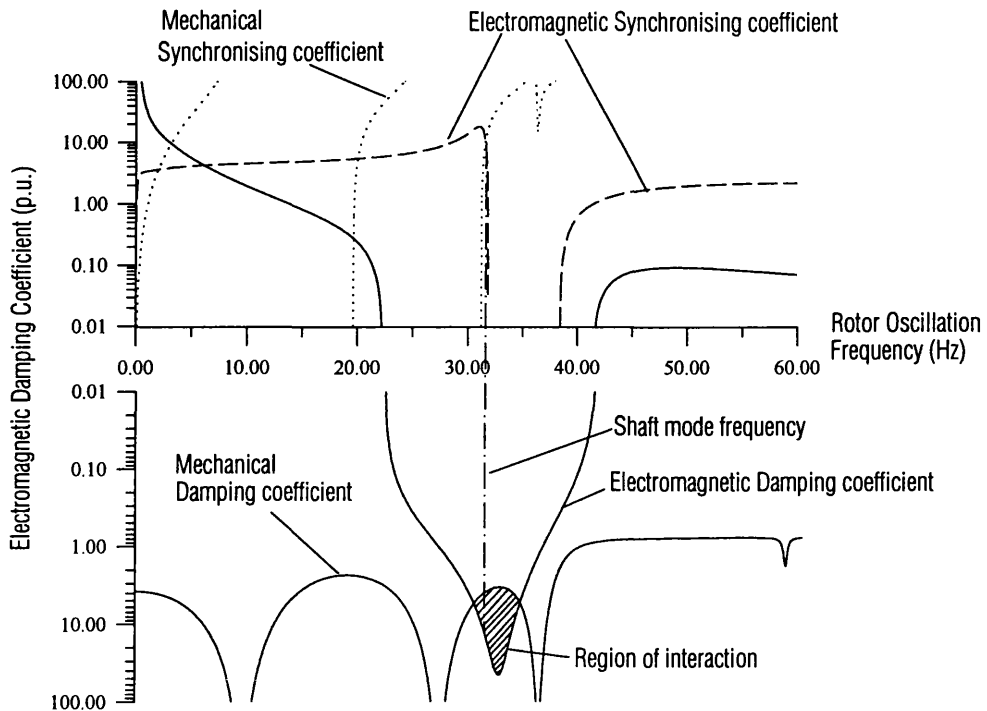
$$H_{mi} = -\frac{1}{4\lambda_i} \left(\frac{dT_{sm}}{d\lambda} \right)_{k_m=0} \quad [4.20]$$

Thus the modal inertias required for calculation of the time constants can be determined from the gradient of the synchronising torque coefficients at the points where the curves cut the abscissa. The modal damping for each mode is given by the net damping at the frequency of the mode.

4.4.2 Graphical Analysis of the Combined Electromagnetic and Mechanical Systems

Figure 4.13 illustrates the graphical analysis of the combined electrical and mechanical systems as defined by Figure 4.4 and Tables 4.1 and 4.2. Transmission line n2 is disconnected. The resonant frequency of the electrical system, indicated by the point of minimum in the electromagnetic damping coefficient, passes through a region of low mechanical steam viscous damping, indicated by the shaded region. The intersection of the electromagnetic and mechanical synchronising coefficients within the frequency range spanned by the shaded region indicates that, according to Eqn. [4.14], the region falls on a resonant mode of the shaft.

At the frequency indicated by the intersection of the synchronising coefficients, the negative electromagnetic damping exceeds the mechanical modal damping by approx. 5.0 p.u., indicating net negative damping. As a result, the shaft oscillations will increase with time. Using Eqn. [4.18] and Eqn. [4.20], the time constant of oscillation for this mode is found to be 3.46 seconds.



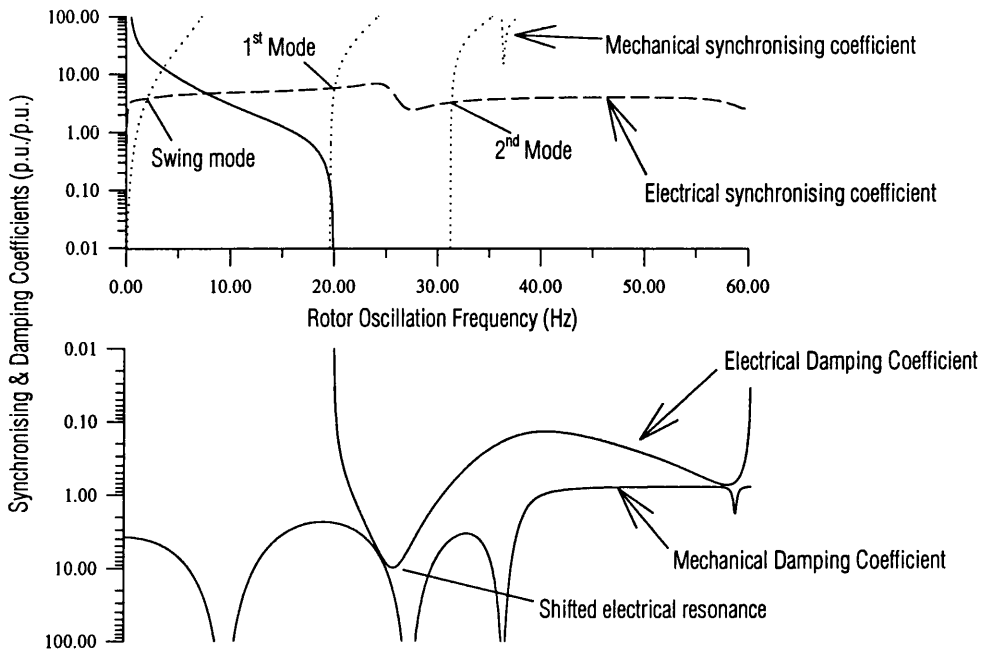
Damping Coefficients are normalised on machine apparent power rating of 600MVA divided by $(\text{base angular velocity})^2$. Synchronising Coefficients are normalised on machine apparent power rating of 600MVA divided by base angular velocity. Angular velocity is normalised on 120π rad/sec.

Figure 4.13: Analysis of the combined systems

Figure 4.14 illustrates the analysis for the case when line $n2$ in Figure 4.4 is switched in. On inspection of this plot, it is clear that the electromagnetic coefficient has shifted to the left and the region of interaction has disappeared.

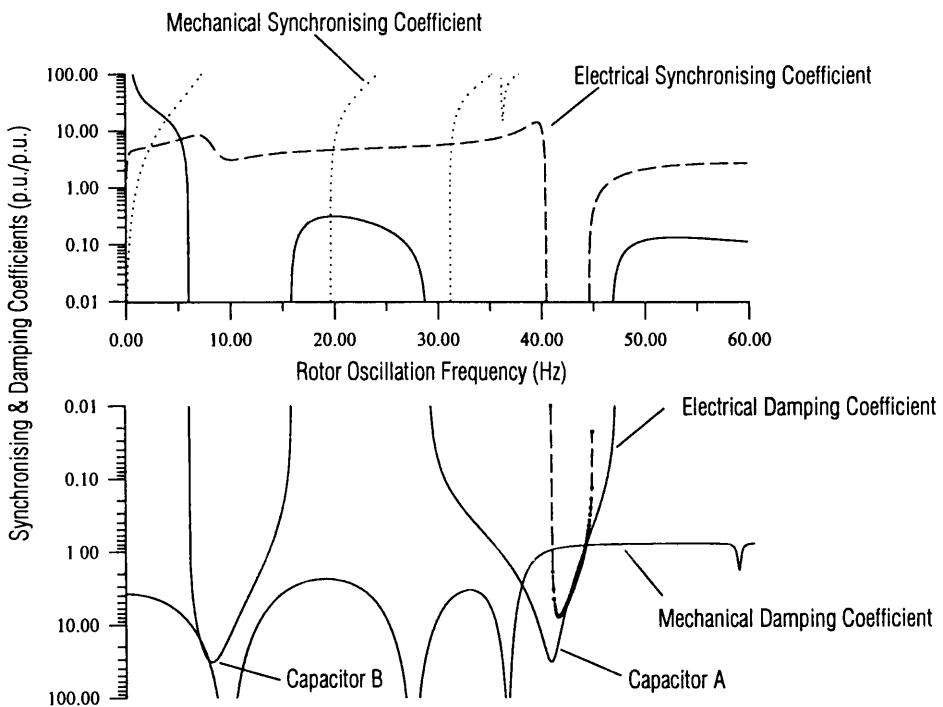
The electrical resonant frequency now lies in a region of high mechanical steam viscous damping.

If a second capacitor, of different rating to the first, was to be inserted in the uncompensated line, two electrical resonant frequencies would appear. Figure 4.15 illustrates such a scenario. Capacitor A is rated at 1200MVA and capacitor B is rated at 400MVA. If both transmission lines are of equal impedance, then capacitors A and B correspond to 30.6% and 91.8% compensation respectively. Although there are now two possible regions for instability, neither falls in a region in which a shaft resonant mode lies. This system would therefore remain stable.



Synchronising and Damping Coefficients are the real and imaginary parts respectively of p.u. change in mechanical torque divided by p.u. change in rotor speed. Torque is normalised on machine apparent power rating of 600MVA. Rotor speed is normalised on 2π times base frequency..

Figure 4.14: Analysis of the parallel line system



Synchronising and Damping Coefficients are the real and imaginary parts respectively of p.u. change in mechanical torque divided by p.u. change in rotor speed. Torque is normalised on machine apparent power rating of 600MVA. Rotor speed is normalised on 2π times base frequency..

Figure 4.15: Two Compensated line System

4.5 CONSIDERATION OF ADDITIONAL MODELLING DETAIL

This section discusses the method of representing several parameters as yet unmentioned in this thesis, namely (i) Automatic Voltage Regulator (AVR) action, (ii) Power System Stabiliser (PSS) action, and (iii) Transmission system load characteristics.

4.5.1 Representation of Additional Excitation Control

The use of additional excitation control is recognised as being one of the most effective ways of increasing the damping of rotor swing oscillations. In any instance, the synchronising and damping torque in the range of electromechanical frequencies of oscillation provide a measure of the generators contribution to power system stability. Figure 4.16 depicts the general configuration of a generator fitted with AVR and PSS systems.

Analysis of the influence of excitation and speed control of the synchronous machine and also the effect of stabiliser control on dynamic stability may be carried out by modifying the equations for the electromagnetic complex torque coefficient already discussed in this study. De Oliveria [21] attempted to do this for an AVR transfer function given by

$$R(p) = \frac{\Delta V_f}{\Delta V_{ref} - \Delta V_t} = \frac{K_r}{1 + pT_r} \frac{1 + pT_{r1}}{1 + pT_{r2}} \quad [4.21]$$

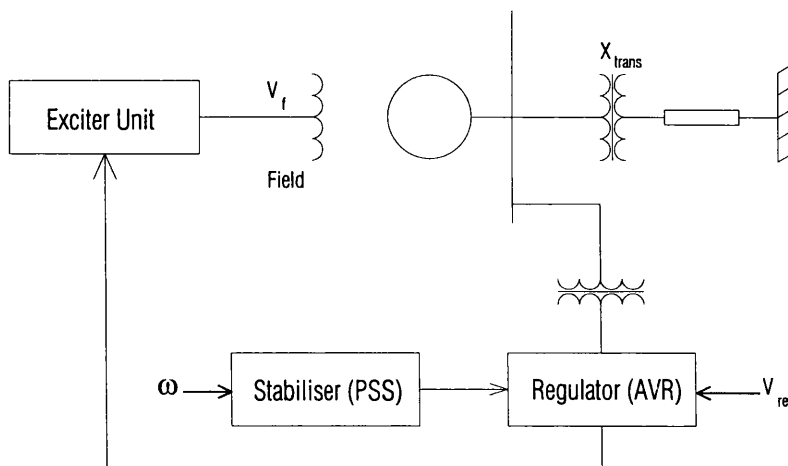


Figure 4.16: Excitation system with Stabiliser

and a power system stabiliser (PSS) transfer function, relating output voltage deviations to speed deviations, represented by

$$S(p) = \frac{\Delta V_{ref}}{\Delta \omega} = \frac{K_s}{1 + pT_s} \frac{1 + pT_{s1}}{1 + pT_{s2}} \frac{1 + pT_{s3}}{1 + pT_{s4}} \quad [4.22]$$

For small deviations, the relationship between the input and output voltage variables can be expressed by:

$$\Delta V_t = e'_d \Delta V_d + e'_q \Delta V_q \quad [4.23]$$

where $e'_d = \frac{V_{d0}}{V_{t0}}$, $e'_q = \frac{V_{q0}}{V_{t0}}$

The deviation of field voltage can now be expressed as:

$$\Delta V_f = -R(p) \left(e'_d \Delta V_d + e'_q \Delta V_q - S(p) p \Delta \delta \right) \quad [4.24]$$

To include the representations for AVR and PSS in the calculation of the complex torque coefficient, ΔV_d and ΔV_q must be eliminated in the above expression. To do this, the linearised voltage equations for a machine connected to the infinite bus must be used:

$$\begin{aligned} \Delta V_d &= V_{nq0} \Delta \delta - X_e i_{q0} p \Delta \delta + (r_e + pX_e) \Delta i_d - X_e \Delta i_q \\ \Delta V_q &= V_{ndo} \Delta \delta + X_e i_{d0} p \Delta \delta + (r_e + pX_e) \Delta i_q + X_e \Delta i_d \end{aligned} \quad [4.25]$$

By deriving expressions for stator current oscillations Δi_d and Δi_q

$$\Delta i_d = i_{q0}\Delta\delta + \frac{1}{[Z_{qe}(p)Z_{de}(p) + X_{qe}(p)X_{de}(p)]} [Z_{qe}(p)(p\varphi_{d\epsilon0}\Delta\delta - \varphi_{q\epsilon0}\Delta\delta) + X_{qe}(p)(p\varphi_{q\epsilon0}\Delta\delta + \varphi_{d\epsilon0}\Delta\delta)]$$

$$\Delta i_q = i_{d0}\Delta\delta - \frac{1}{[X_{de}(p)X_{qe}(p) + Z_{qe}(p)Z_{de}(p)]} [X_{de}(p)(p\varphi_{d\epsilon0}\Delta\delta - \varphi_{q\epsilon0}\Delta\delta) - Z_{qe}(p)(p\varphi_{q\epsilon0}\Delta\delta + \varphi_{d\epsilon0}\Delta\delta)]$$

[4.26]

where $\varphi_{d\epsilon0}\Delta\delta = -X_d(p)i_{q0}\Delta\delta + \varphi_{q0}\Delta\delta + G(p)\Delta V_f$, $\varphi_{q\epsilon0}\Delta\delta = X_q(p)i_{d0}\Delta\delta - \varphi_{d0}\Delta\delta$

the d-q axis voltage components as a function of rotor angle and field voltage fluctuations may be obtained

$$\Delta V_d = A_d(p)\Delta\delta + A_{fd}(p)\Delta V_f$$

$$\Delta V_q = A_q(p)\Delta\delta + A_{fq}(p)\Delta V_f$$

[4.27]

where the coefficients for the direct-axis are given by:

$$A_d(p) = p\varphi_{q0} - Z_d(p) \left[i_{q0} + \frac{1}{X_{dk}(p)X_{qe}(p) + Z_{dk}(p)Z_{qe}(p)} [(pZ_{qe}(p) + X_{qe}(p))(\varphi_{q0} - X_d(p)i_{q0}) + (pX_{qe}(p) - Z_{qe}(p))(X_q(p)i_{d0} - \varphi_{d0})] \right]$$

$$+ X_q(p) \left[i_{d0} - \frac{1}{X_{dk}(p)X_{qe}(p) + Z_{dk}(p)Z_{qe}(p)} [(pX_{dk}(p) - Z_{dk}(p))(\varphi_{q0} - X_d(p)i_{q0}) - (X_{dk}(p) - pZ_{dk}(p))(X_q(p)i_{d0} - \varphi_{d0})] \right]$$

$$A_{fd}(p) = pG(p) - \frac{Z_d(p)}{X_{dk}(p)X_{qe}(p) + Z_{dk}(p)Z_{qe}(p)} [(pZ_{qe}(p) + X_{qe}(p))G(p)] + \frac{X_q(p)}{X_{dk}(p)X_{qe}(p) + Z_{dk}(p)Z_{qe}(p)} [(pX_{dk}(p) + Z_{dk}(p))G(p)]$$

[4.28]

The transfer function for the combined effect of AVR and PSS can then be deduced:

$$\Delta V_f = J(p)\Delta\delta$$

[4.29]

This approach, although providing valuable insight into the behavior of excitation and stabiliser systems is representative only of the single machine-infinite busbar case. To get truly meaningful results, simulation of AVR and PSS systems must be carried out in the context of a multi-machine study in which the terminal conditions of the machine under study reflect the combined behaviour of the entire system. The application of the complex torque coefficient analysis to multi-machine systems is discussed in Chapter 5.

4.5.2 Influence of Transmission System Load Characteristics on Decay of Principle Torsional Oscillations

The influence exerted by various load types was evaluated using the same single machine system of Figure 4.4 in which the load connected to Bus 2 was varied. In this study, frequency dependency in loads was disregarded. Voltage dependency, however, was represented by exponential functions:

$$P_L = P_o (V)^\alpha \quad Q_L = Q_o (V)^\beta$$

Tables 4.3 and 4.4 depict the influence of load characteristics on net damping and time constants for damping, respectively, at the 19.6 Hz shaft mode.

Table 4.3 : Effect of Load Characteristics on Net Damping

Type		Constant Power	Constant Current	Constant Impedance
Load		Net Damping (p.u.)		
MW	MVAR			
115	60	0.49	0.50	0.51
215	100	0.62	0.64	0.65
415	200	0.84	0.85	0.87

Damping factors depict Net Damping at 19.6Hz shaft oscillation for generator connected to Bus 1. No load Net Damping at 19.6 Hz = 0.28 p.u.

Table 4.4 : Effect of Load Characteristics on Time Constants

Type		Constant Power	Constant Current	Constant Impedance
Load		Time Constants (seconds)		
MW	MVAR			
115	60	13.58	13.38	13.17
215	100	10.74	10.56	10.37
415	200	7.98	7.85	7.72

All Time Constants depict rate of decay of 19.6Hz shaft oscillation for generator connected to Bus 1. No load Time Constant = 24.03seconds.

The effect of loads which are local to the generator is to have a significant damping effect. It has been found that the machine is most susceptible to torsional oscillations when operating on or close to no-load. This is further exacerbated by the fact that steam viscous damping is very small when operating on light loads.

For the three load characteristics evaluated, constant impedance loads exert the most influence on damping, although the differences between all three types is marginal in this network.

4.6 SUMMARY OF CHAPTER 4

The phenomenon of subsynchronous resonance in electrical power systems has been discussed and the application of Complex Torque Coefficient analysis to the study of this phenomenon has been demonstrated for a single machine/two transmission line system.

It has been shown that the insertion of series compensation capacitors in transmission lines in close proximity to a synchronous generator induces a region of negative electromechanical damping which may subsequently lead to torsional interaction occurring.

The concept of the mechanical complex torque coefficient, which complements the electromagnetic coefficient and is a necessary component for the determination of the stability of torsional interactions, has been introduced.

A technique for including the effect of excitation control and additional stabilisation control has been outlined, although it should be noted that such an approach is valid only for single machine-infinite busbar systems. If these systems are to be included in the analysis at all, then this should be carried out in the context of multi-machine systems.

The influence of transmission system load characteristics on the damping of torsional oscillations has been examined. Torsional interaction is more likely to occur if the machine is operating at or close to no-load. Differences in computed net damping between loads represented as constant impedance, constant power or constant current are small enough to be considered negligible.

CHAPTER FIVE

MULTI-MACHINE COMPLEX TORQUE COEFFICIENTS

5.1 INTRODUCTION

The traditional technique for studying multi-machine interactions has been Eigenvalue analysis as described by numerous authors including Alden [7] and Gross [14]. Although, admittedly, this is a powerful technique, inter-machine interactions studied using this technique are somewhat obscure and difficult to explain fully and, as highlighted by Alden, no generalisations can be drawn as regards the influence that a torsional mode on one machine will have on a corresponding mode on another machine. Furthermore, the technique does not lend itself to the study of any one machine in particular – a ‘system’ solution is always obtained. In systems containing many machines, this itself can make a detailed analysis a time consuming process, producing, for even a moderately sized system, many hundreds of eigenvalues most of which have little or no impact on system damping.

Complex Torque Coefficient analysis applied to multi-machine systems can alleviate some of the drawbacks of Eigenanalysis:

- Studies are concentrated on individual machines, with full account taken of the influence of the network, other machines, and other dynamic devices present in the system.
- Interactions between machines can be clearly identified and studied in greater depth than is practical with eigenvalue based methods.
- The analysis is graphically based which promotes a clearer understanding of the complex mechanisms involved.

It is commonly assumed that machines only interact at the zeroth or swing mode frequencies. This is not strictly correct. Although the most *dominant* coupling occurs through this mode, unfavourable coupling via higher frequency modes is a possibility. Note that unlike the zeroth modes, which are dependent on both the electrical and mechanical characteristics, the frequencies of belonging to the higher modes will not change significantly from the natural frequencies of each shaft since these are dictated purely by the mechanical characteristics of the shaft train. In a system, for example, of three machines, A, B and C, the question naturally arises: to what extent, if any, do the modes belonging to machines B and C influence the stability of the modes belonging to machine A, and visa-versa. With the exception of the swing mode, the modal frequencies of the shaft are not sensitive to ‘system’ configurations and are determined only by the inertia and stiffness parameters of the shaft. However, the damping of these modes can be influenced significantly by the modes belonging to the other machines, especially if they are at similar frequencies.

With conventional eigenvalue techniques, the mechanism of these couplings is hidden. To obtain a solution, sensitivity studies would have to be conducted using, for example, sparsity based methods such as described by Smed [46], which makes the analysis process more laborious. In effect, post-processing of the eigenvalue analysis results would be required.

Complex Torque coefficient analysis on the other hand does not require any form of post-processing in order to reveal the basic mechanisms at work as was observed, for example, in Chapter 4 regarding the interaction between the machine and a capacitor compensated line. Furthermore, information corresponding to the entire subsynchronous frequency range is provided which promotes a more complete picture.

This chapter aims to demonstrate three things:

- i. Complex Torque Coefficients may be easily calculated for multi-machine systems.
- ii. These coefficients enable an improved insight into the mechanisms of interaction between shaft modes of several machines, not accessible with conventional approaches.
- iii. Network influences (e.g. SSR) are retained in the analysis.

5.2 CALCULATION OF COEFFICIENTS

There has in the past been a number of suggestions on how to evaluate the coefficients with regard to multi-machine systems. Shaltout et al. [47] proposed a technique based on the time responses of the angles, speeds and torques of each machine. They suggested that the electromagnetic torque equation of the machine under investigation could be written in the form

$$e(t) = \Delta T_e - [k_s \Delta \delta(t) + k_d \Delta \omega(t)] \quad [5.1]$$

where $e(t)$ is an error term, k_s is a synchronising coefficient, and k_d is a damping coefficient.

The summation of the errors squared over the interval of oscillation, τ , is given by

$$\int_0^\tau e(t)^2 dt = \int_0^\tau (\Delta T_e - k_s \Delta \delta(t) - k_d \Delta \omega(t))^2 dt \quad [5.2]$$

and can be minimised by satisfying

$$\begin{aligned} \frac{\partial}{\partial k_s} \int_0^\tau e(t)^2 dt &= 0 \\ \frac{\partial}{\partial k_d} \int_0^\tau e(t)^2 dt &= 0 \end{aligned} \quad [5.3]$$

Changing the order of differentiation and integration in [5.2] and partial differentiating by k_s and k_d yields

$$\begin{aligned} \int_0^\tau \Delta T_e \Delta \delta(t) dt &= k_s \int_0^\tau \overline{\Delta \delta(t)^2} dt + k_d \int_0^\tau \Delta \omega(t) \Delta \delta(t) dt \\ \int_0^\tau \Delta T_e \Delta \omega(t) dt &= k_d \int_0^\tau \overline{\Delta \omega(t)^2} dt + k_s \int_0^\tau \Delta \delta(t) \Delta \omega(t) dt \end{aligned} \quad [5.4]$$

Evaluating the integrals provides two equations in k , and k_d which are then solved for each.

The major drawback of this approach is that detailed time domain simulations must be carried out in advance of the coefficient calculations. Further more, the technique yields only one set of synchronising and damping coefficients, presumably corresponding to the compound electromechanical oscillation. It would clearly be an unwieldy approach to use when considering torque coefficients over the entire subsynchronous range.

A more recent approach by Hara et al [48] based the analysis on an approach similar to that used in this study. Their objective was to evaluate the complex admittance matrix which represented the dynamics of a machine as viewed from its terminals. By evaluating every machine except the one under investigation in this way, the complete system matrix incorporating all machines could be constructed by appending the generator matrices to the diagonal (2x2) matrices corresponding to the locations of the generators, as illustrated in Figure 5.1 below.

$$\begin{aligned}
 \begin{bmatrix} \Delta i_d^1 \\ \Delta i_q^1 \\ \downarrow \\ \Delta i_d^n \\ \Delta i_q^n \end{bmatrix} &= \begin{bmatrix} Y_{11}^{dd} & Y_{11}^{dq} & \dots & Y_{1n}^{dd} & Y_{1n}^{dq} \\ Y_{11}^{qd} & Y_{11}^{qq} & \dots & Y_{1n}^{qd} & Y_{1n}^{qq} \\ \vdots & \vdots & \ddots & \vdots & \vdots \\ Y_{n1}^{dd} & Y_{n1}^{dq} & \dots & Y_{nn}^{dd} & Y_{nn}^{dq} \\ Y_{n1}^{qd} & Y_{n1}^{qq} & \dots & Y_{nn}^{qd} & Y_{nn}^{qq} \end{bmatrix}^{-1} \begin{bmatrix} \Delta v_d^1 \\ \Delta v_q^1 \\ \downarrow \\ \Delta v_d^n \\ \Delta v_q^n \end{bmatrix} \\
 &\Downarrow \\
 \begin{bmatrix} \Delta i_d \\ \Delta i_q \end{bmatrix} &= \begin{bmatrix} Y_{equiv}^{11} & Y_{equiv}^{12} \\ Y_{equiv}^{21} & Y_{equiv}^{22} \end{bmatrix}^{-1} \begin{bmatrix} \Delta v_d \\ \Delta v_q \end{bmatrix} \\
 &\Downarrow
 \end{aligned}$$

Figure 5.1: Multi-machine Matrix Reduction

Similar to that which was discussed in Chapter 2, the oscillatory components of stator currents of a synchronous machine may be written in the form

$$\begin{bmatrix} \Delta i_d \\ \Delta i_q \end{bmatrix} = \begin{bmatrix} Y_{11} & Y_{12} \\ Y_{21} & Y_{22} \end{bmatrix} \begin{bmatrix} \Delta v_d \\ \Delta v_q \end{bmatrix} - \begin{bmatrix} Y_{11} & Y_{12} \\ Y_{21} & Y_{22} \end{bmatrix} \begin{bmatrix} -\psi_{qo} \\ \psi_{do} \end{bmatrix} \Delta \omega - \begin{bmatrix} Y_{11} & Y_{12} \\ Y_{21} & Y_{22} \end{bmatrix} \begin{bmatrix} \frac{p}{\omega_o} G(p) \\ G(p) \end{bmatrix} \Delta v_f \quad [5.5]$$

where, from Eqn. [2.8] $\begin{bmatrix} Y_{11} & Y_{12} \\ Y_{21} & Y_{22} \end{bmatrix} = \begin{bmatrix} -r_a - px_d(p) & x_q(p) \\ -x_d(p) & -r_a - px_d(p) \end{bmatrix}^{-1}$

Hara incorporated the shaft system through the incremental rotor speed term, $\Delta \omega$, by substituting the modal form of the shaft equations given by

$$\Delta \omega = - \left[\sum_{i=1}^n Q_{gi}^2 \frac{p}{p^2 H_i + p D_i + \omega_0 k_i} \right] \Delta T_e \quad [5.6]$$

where Q_{gi} represents the i^{th} mode shape factor of the generator mass. Replacing the electromagnetic torque term with the flux-current expression Eqn. [2.23] the admittance matrix equation could be obtained.

This approach however, seems to be much more complicated than it needs to be, especially if the authors intended their machine models to be of variable detail depending on how many turbines were to be modelled or on the relevance of the electrical or excitation properties, typically neglected when modelling ‘distant’ machines. Evaluating models of differing orders would appear to involve a considerable amount of algebra and be overly computationally intensive.

The method employed to represent the AVR is however, unclear. The method of de Oliveria [21] is not suitable in a multi-machine context as pointed out in Chapter 4.

Furthermore, a more serious flaw exists. The authors use the method of matrix reduction to eliminate all nodes other than the one to which the machine under investigation is connected. In a system of only one machine this is easy to accomplish because all nodes excluding that of the machine will have zero net injected current. But in a system of more than one machine the nodes of connection of the other machines, which

will have non-zero current injections, can not be eliminated in this way. The problem will have most effect at the frequencies corresponding to rotor swing since it is at these frequencies that the predominant current fluctuations exist. At higher frequencies, the incremental currents will be smaller in magnitude and the incurred errors will be much smaller.

5.2.1 State-space approach to Torque Coefficients Algorithm

In this study, to retain the true behaviour of the interconnected machines, the multi-machine model is initially formed in the standard multi-machine eigenanalysis construction:

$$\dot{\underline{x}}_{sys} = A\underline{x}_{sys} \quad [5.7]$$

The variables belonging to the mechanical system of the machine under study are separated from the remaining system variables, so that the generator rotor angle and rotor velocity are treated as input variables. The modified Eqn. [5.7] then becomes

$$\dot{\underline{x}}'_{-sys} = A'\underline{x}'_{-sys} + \underline{b}\Delta\delta_i + \underline{c}\Delta\omega_i \quad [5.8]$$

Assuming a sinusoidal solution, Eqn. [5.8] can be solved to give in the Laplace domain

$$\underline{x}'_{-sys}(s) = [sI - A']^{-1} \left(\frac{\underline{b}}{s} + \underline{c} \right) \Delta\omega_i \quad [5.9]$$

The electromagnetic torque of the machine under study can be expressed as a function of the state variables of that machine, which are a subset of the system state vector \underline{x}'_{-sys} , and the rotor velocity:

$$\Delta T_{e_i}(s) = E\underline{x}'_{-sys} + \frac{F}{s} \Delta\omega_i \quad [5.10]$$

Substituting the expression for \underline{x}'_{-sys} given in Eqn. [5.9] into Eqn. [5.10] yields:

$$\frac{\Delta T_{e_i}(s)}{\Delta \omega_i} = E[sI - A']^{-1} \left(\frac{b}{s} + \underline{c} \right) + \frac{F}{s} \quad [5.11]$$

This result provides the Complex Torque Coefficient of the machine under study, with full account taken of the influence of all other machines and devices in the system. The damping coefficient may be obtained from

$$T_d = \operatorname{Re} \left(\frac{\Delta T_{e_i}}{\Delta \omega_i} \right) \quad [5.12]$$

5.2.2 Linearised State-Space Multi-Machine Model

There are two parts to the construction of the state-space model into the form of Eqn. [5.7] required for the above algorithm. The first part involves building the linearised network matrix, in which all nodes are transformed to the same set of reference axes. The second part involves combining these equations with the machine equations, which were detailed in § 3.2.

The network admittance matrix, in which all load nodes have been eliminated, when linearised, will have the form [4]

$$\Delta I = M_0 \Delta V + \Delta M V_0 \quad [5.13]$$

where M_0 is given by the steady components of Eqn. [5.14] evaluated at the initial rotor angles δ_{i0} , $i=1,2,\dots,n$, and V_0 is the initial voltage vector.

Assuming only power frequency admittances, the transformed network equation may be written

$$M = \begin{bmatrix} Y_{11} e^{j\theta_{11}} & Y_{12} e^{j(\theta_{12} - \delta_{120} - \Delta\delta_{12})} & \dots & Y_{1n} e^{j(\theta_{1n} - \delta_{1n0} - \Delta\delta_{1n})} \\ \dots & \dots & \dots & \dots \\ Y_{n1} e^{j(\theta_{n1} - \delta_{n10} - \Delta\delta_{n1})} & Y_{n2} e^{j(\theta_{n2} - \delta_{n20} - \Delta\delta_{n2})} & \dots & Y_{nn} e^{j\theta_{nn}} \end{bmatrix} \quad [5.14]$$

Since $e^{-j\delta_{ij}}$ can be expanded to $\left[\cos(\Delta\delta_{ij}) - j \sin(\Delta\delta_{ij}) \right]$, and for small perturbations $\cos(\Delta\delta_{ij}) \cong 1$ and $\sin(\Delta\delta_{ij}) \cong \Delta\delta_{ij}$, the general incremental term of [5.14] can be reduced to

$$m_{ij} = -jY_{ij}e^{j(\theta_{ij}-\delta_{ij0})}\Delta\delta_{ij} \quad [5.15]$$

The second term in [5.13] may then can be written in the form

$$\Delta MV_0 = -j \begin{bmatrix} \sum_{i=1}^n Y_{1i} e^{j(\theta_{1i}-\delta_{1i0})} V_{i0} \delta_{1i} \\ \sum_{i=1}^n Y_{2i} e^{j(\theta_{2i}-\delta_{2i0})} V_{i0} \delta_{2i} \\ \dots \\ \sum_{i=1}^n Y_{ni} e^{j(\theta_{ni}-\delta_{ni0})} V_{i0} \delta_{ni} \end{bmatrix} \quad [5.16]$$

such that the linearised Eqn. [5.13] becomes

$$\begin{bmatrix} \Delta I_1 \\ \Delta I_2 \\ \dots \\ \Delta I_n \end{bmatrix} = \begin{bmatrix} Y_{11} e^{j\theta_{11}} & \dots & Y_{1n} e^{j(\theta_{1n}-\delta_{1n0})} \\ Y_{21} e^{j(\theta_{21}-\delta_{210})} & \dots & Y_{2n} e^{j(\theta_{2n}-\delta_{2n0})} \\ \dots & \dots & \dots \\ Y_{n1} e^{j(\theta_{n1}-\delta_{n10})} & \dots & Y_{nn} e^{j\theta_{nn}} \end{bmatrix} \begin{bmatrix} \Delta V_1 \\ \Delta V_2 \\ \dots \\ \Delta V_n \end{bmatrix} - j \begin{bmatrix} \sum_{i=1}^n Y_{1i} e^{j(\theta_{1i}-\delta_{1i0})} V_{i0} \Delta\delta_{1i} \\ \sum_{i=1}^n Y_{2i} e^{j(\theta_{2i}-\delta_{2i0})} V_{i0} \Delta\delta_{2i} \\ \dots \\ \sum_{i=1}^n Y_{ni} e^{j(\theta_{ni}-\delta_{ni0})} V_{i0} \Delta\delta_{ni} \end{bmatrix} \quad [5.17]$$

The vector ΔI , expanded into its real and imaginary parts, is substituted for the machine currents ΔI_{d1} , ΔI_{q1} , ... etc. in the machine Eqns. [3.20] which can then be rearranged into the required form of Eqn. [5.8].

5.2.3 Retention of Higher Frequency Transmission Line effects

The above algorithm is suitable for the study of all machine/device interactions throughout the entire frequency range of interest. However, to retain the ability to include

effects due to compensated transmission lines, a network reduction technique similar to that used by Hara [48] is employed.

Contrary to Hara's approach, a more appropriate way of evaluating the admittance matrix of the machine is to begin with the complete state-matrix form of the model, complete with shaft system and excitation. This technique was described by Undrill [48] in the application of Nyquist's criterion to multi-machine stability analysis. Similar to Hara, however, Undrill did not take account of the low frequency inaccuracies incurred by the method.

The machine model was described in detail in Chapter 3, Eqn. [3.19]. Note that unlike in Hara's technique, this form of the machine model lends itself to the relatively easy reduction or expansion of either the electrical, including excitation, or mechanical systems.

The state and auxiliary equations may be written in compact form as

$$\begin{aligned}\dot{\underline{x}} &= A\underline{x} + B\Delta\underline{v} \\ \Delta\underline{i} &= C\underline{x} + D\Delta\underline{v}\end{aligned}\tag{5.18}$$

Since the analysis deals with small perturbations, it is reasonable to assume solutions of a sinusoidal nature. Eqn. [5.18] then may be reduced directly to

$$\Delta\underline{i} = \left(D - C[A - j\omega I]^{-1} B \right) \Delta\underline{v}\tag{5.19}$$

which yields the frequency dependent complex admittance matrix. The auxiliary current equation is provided by Eqn. [3.4].

5.2.4 Conversion to System Reference Frame

The state equations for the synchronous machines are written with respect to their own rotating d-q axes. The network equations however, are with respect to the common synchronously rotating system reference frame.

To obtain general network relationships between all machines, it is desirable to express the various network branch quantities to the same reference. Figure 5.2 illustrates

the relationship between machine terminal voltages with respect to the common reference axes and the same voltages with respect to the machine reference axes.

From the illustration it can be deduced that the common reference frame voltages can be expressed in terms of the machine voltages and the load angle of the machine :

$$V_{Q_i} + jV_{D_i} = (v_{q_i} \sin \delta_i - v_{d_i} \cos \delta_i) + j(v_{q_i} \cos \delta_i + v_{d_i} \sin \delta_i) \quad [5.20]$$

or in a more generalised system form

$$\begin{bmatrix} V_{Q_1} + jV_{D_1} \\ V_{Q_2} + jV_{D_2} \\ \dots \\ V_{Q_i} + jV_{D_i} \end{bmatrix} = \begin{bmatrix} e^{j\delta_1} & 0 & \dots & 0 \\ 0 & e^{j\delta_2} & \dots & 0 \\ \dots & \dots & \dots & \dots \\ 0 & 0 & \dots & e^{j\delta_i} \end{bmatrix} \begin{bmatrix} v_{q_1} + jv_{d_1} \\ v_{q_2} + jv_{d_2} \\ \dots \\ v_{q_i} + jv_{d_i} \end{bmatrix} \quad [5.21]$$

Eqn. [5.21] is non-linear and must be linearised before useful computations can be made. Thus, linearising yields Eqn. [5.22] which can be substituted directly for the voltage terms v_d and v_q in Eqn. [3.19]

$$\begin{bmatrix} \Delta v_{d_1} \\ \Delta v_{q_1} \\ \Delta v_{d_2} \\ \Delta v_{q_2} \\ \dots \\ \Delta v_{d_i} \\ \Delta v_{q_i} \end{bmatrix} = \begin{bmatrix} \cos \delta_1^0 & \sin \delta_1^0 & 0 & \dots & 0 \\ -\sin \delta_1^0 & \cos \delta_1^0 & 0 & \dots & 0 \\ 0 & \cos \delta_2^0 & \sin \delta_2^0 & \dots & 0 \\ \dots & -\sin \delta_2^0 & \cos \delta_2^0 & \dots & \dots \\ 0 & \dots & \dots & \dots & \dots \\ 0 & \dots & 0 & \cos \delta_i^0 & \sin \delta_i^0 \\ \dots & \dots & 0 & -\sin \delta_i^0 & \cos \delta_i^0 \end{bmatrix} \begin{bmatrix} \Delta V_{D_1} \\ \Delta V_{Q_1} \\ \Delta V_{D_2} \\ \Delta V_{Q_2} \\ \dots \\ \Delta V_{D_i} \\ \Delta V_{Q_i} \end{bmatrix} + \begin{bmatrix} v_{q_0}^1 & 0 & \dots & 0 \\ -v_{d_0}^1 & 0 & \dots & 0 \\ 0 & v_{q_0}^2 & 0 & \dots \\ 0 & -v_{d_0}^2 & 0 & \dots \\ \dots & \dots & \dots & \dots \\ 0 & \dots & 0 & v_{q_0}^i \\ 0 & \dots & 0 & -v_{d_0}^i \end{bmatrix} \begin{bmatrix} \Delta \delta_1 \\ \Delta \delta_2 \\ \dots \\ \Delta \delta_i \end{bmatrix} \quad [5.22]$$

5.2.5 Complex Impedance of the Synchronous Machine - - Simple Shaft Model

Using the algorithm described above, the complex impedance matrix of each machine, which includes both the electrical and mechanical systems can be evaluated.

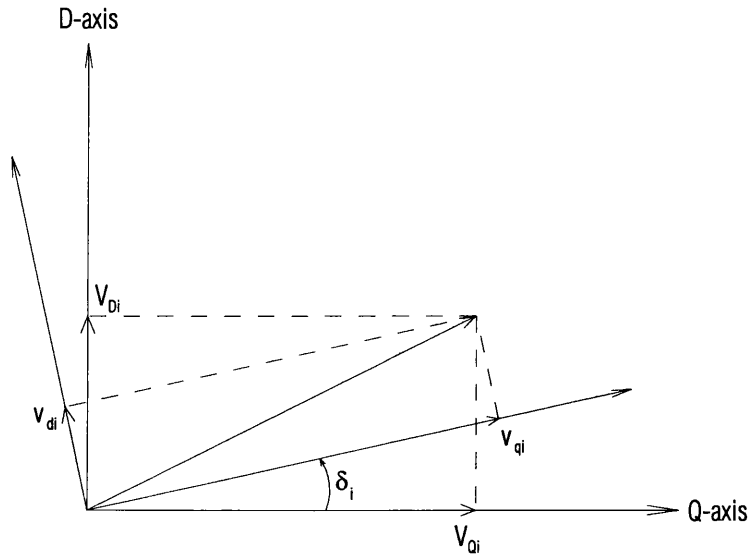


Figure 5.2: Relationship between Common and Machine Reference Axes

At no-load, and with the mechanical system neglected, the impedance matrix is simply that given in Eqn.[5.23]. The diagonal elements correspond to the transformer voltage terms $p\psi$ of the generator stator. These terms are significant only at the higher frequencies of oscillation. The off-diagonal elements follow the loci of the well-known operational impedances.

$$\begin{bmatrix} \Delta v_d \\ \Delta v_q \end{bmatrix} = \begin{bmatrix} r_a + pX_d(p) & -X_q(p) \\ X_d(p) & r_a + pX_q(p) \end{bmatrix} \begin{bmatrix} \Delta i_d \\ \Delta i_q \end{bmatrix} \quad [5.23]$$

Figure 5.4 illustrates the form of the impedance matrix elements when the same machine is assumed to be operating on full-load ($P_o = 1$ p.u., $Q_o = 0$ p.u., $V_t = 1$ p.u.) and with a finite single mass rotor. In all Figures 5.4 - 5.6, Z_{DD} corresponds to element (1,1) of the impedance matrix, Z_{DQ} corresponds to element (1,2), Z_{QD} corresponds to element (2,1), and Z_{QQ} corresponds to element (2,2). Clearly, the most dominant effect occurs at the lower frequencies, especially at or near the frequency corresponding to the natural mode of oscillation of that machine. The impedance elements at the higher frequencies will be virtually unchanged from the case where the mechanical system is neglected.

5.2.6 Complex Impedance of the Synchronous Machine - - Full Shaft Model

Extending the shaft model to represent the individual turbine masses yields the impedance plot illustrated in Figure 5.5. It can be observed that the impedance below ~10Hz is unchanged from the previous case. However, at frequencies above 10Hz, a series of impedance ‘spikes’ has appeared. These correspond exactly to the natural frequencies of oscillation of the turbine shaft and illustrate the coupling between the mechanical system of the machine and the electrical system to which it is connected.

If the steam viscous damping parameters acting on each turbine are increased, the appearance of the resonant modes on the electrical side would be expected to reduce. Figure 5.6 indicates that this is indeed the case. By increasing the damping factors from 0.3 p.u to 1.0 p.u. acting on each turbine mass, the impedance ‘spikes’ have been reduced.

5.3 THREE MACHINE SYSTEM STUDY

The above algorithms were used to study the potential for subsynchronous oscillatory problems in a small, three machine, nine bus system illustrated in Figure 5.3, in which the transmission line between nodes 4 and 6 is series compensated.

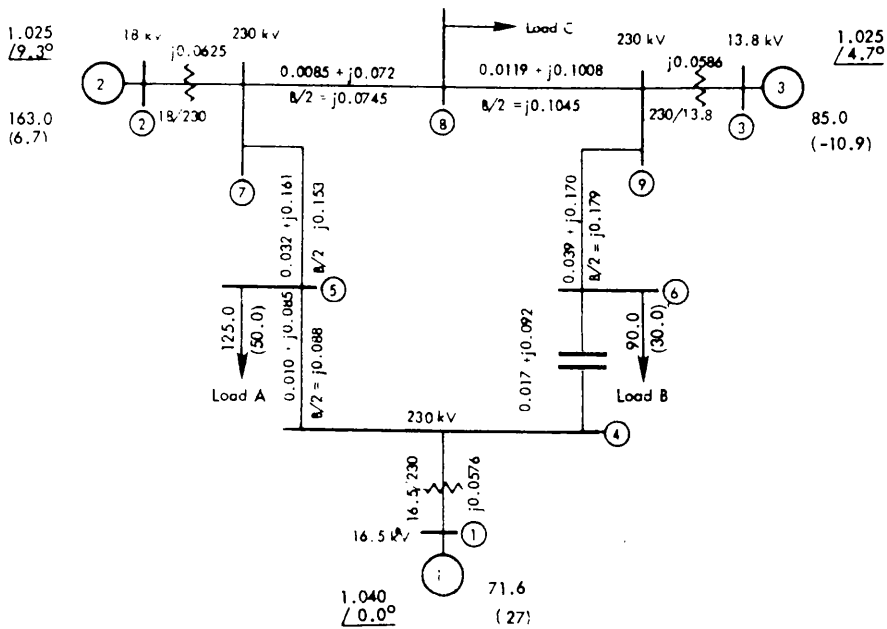
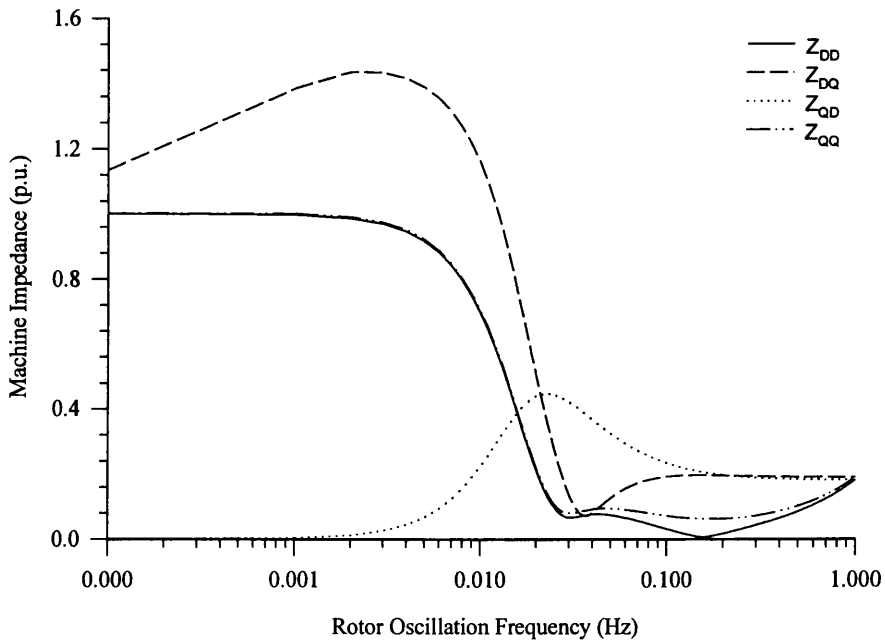
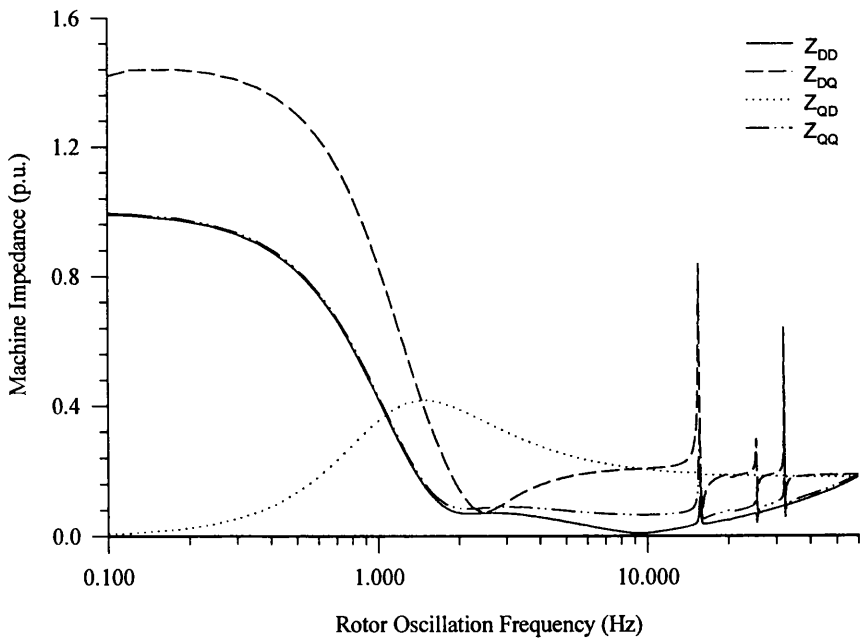


Figure 5.3: Nine bus, 3 machine system



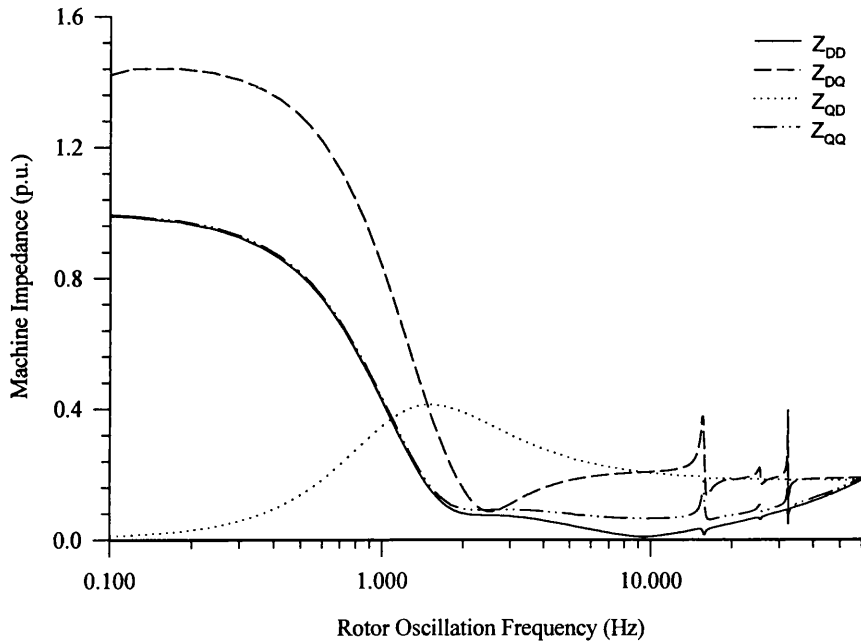
Machine impedance is normalised on a machine apparent power rating of 600MVA

Figure 5.4: Impedance Plot - - Single Rotor Mass



Machine impedance is normalised on a machine apparent power rating of 600MVA

Figure 5.5: Impedance Plot - - Full Shaft Model



Machine impedance is normalised on a machine apparent power rating of 600MVA

Figure 5.6: Full Shaft Model - - Increased Steam Viscous Damping

A preliminary analysis is carried out to determine the operating points of each machine in terms of real and reactive power demand and terminal voltage. The results of this are indicated beside each machine.

5.3.1 Single Rotor Mass Models - - Neglecting Sub- and Super-synchronous Network Effects

Initially, the mechanical systems on each machine were restricted to a single rotor mass on each. Table 5.1 lists the eigenvalues calculated for this system, in which the frequencies are expressed relative to a base frequency of 377rad/s. Of particular interest are the electromechanical oscillatory modes representing rotor swing. In this case, sub- and super-synchronous effects due to network characteristics were neglected, so the algorithm discussed in § 5.2.1 only was used.

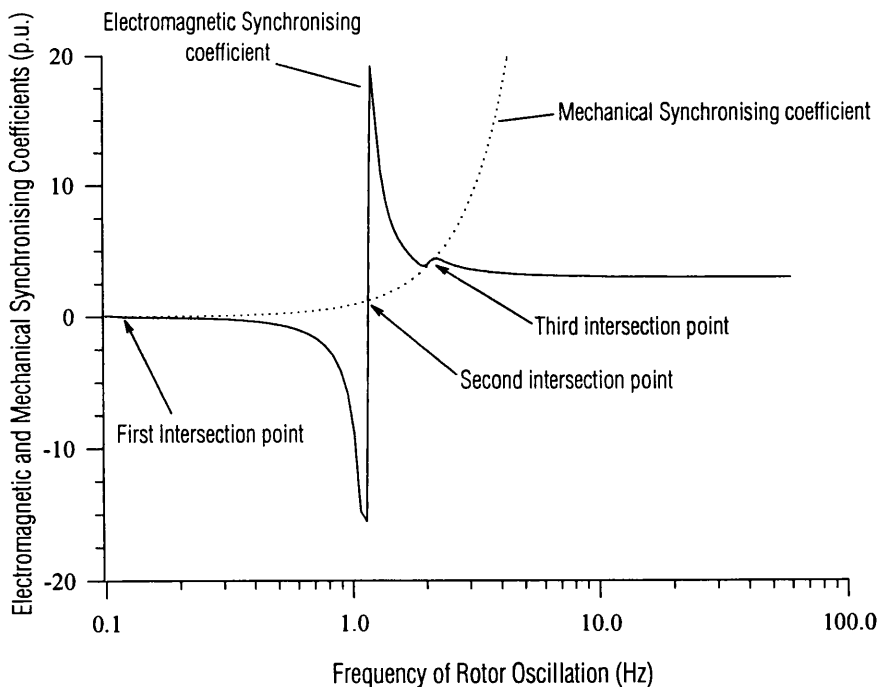
All the eigenvalues have negative real parts indicating that the system is stable. There are three oscillatory modes which correspond to rotor swing. These modes form a composite oscillation for each of the three machines. The dominant frequencies are approximately 2.1Hz and 1.4Hz. The third mode is a long period frequency of 0.01Hz.

Figure 5.7 plots mechanical and electromagnetic synchronising coefficients corresponding to machine 1. As discussed in Chapter 4, the points of intersection of the mechanical and electromagnetic synchronising coefficients will indicate the frequencies of oscillation of the shaft. In this particular case of three machines, three intersections of the synchronising coefficients are observed. The intersections correspond exactly to the oscillatory eigenfrequencies at 2.1Hz, 1.4Hz and 0.01Hz confirming this.

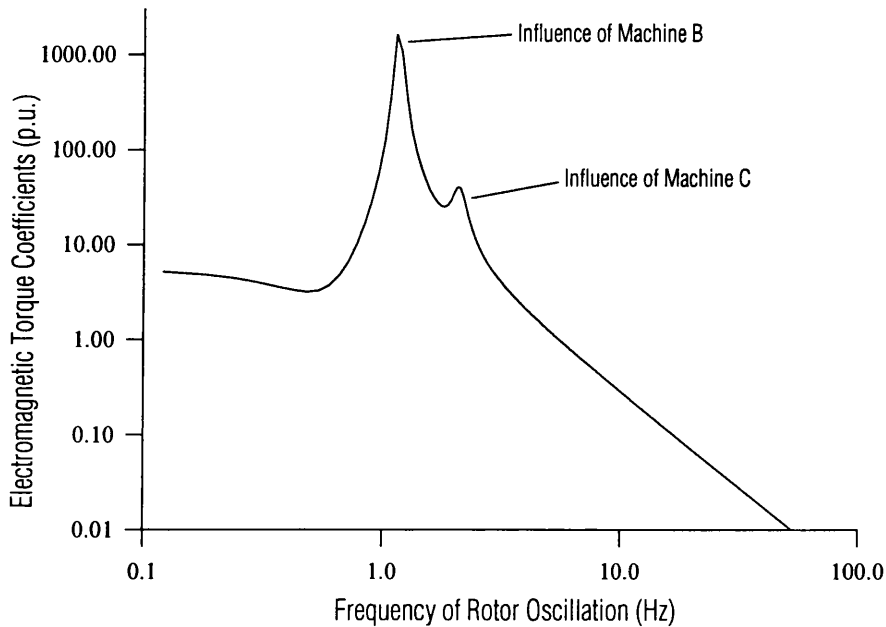
Figure 5.8 depicts the electromagnetic damping coefficient for Machine 1. The influence of Machines 2 and 3 are clearly visible. In both cases, electromagnetic damping is significantly increased at these frequencies. Influence of Machine 2 is greater on account of its higher rotor inertia constant.

Table 5.1: Eigenvalues for 3 Machine System

<i>Machine</i>	<i>Oscillatory Modes</i>	<i>Non-oscillatory</i>
3	-0.002664+j0.03470	-0.016644
2	-0.000622+j0.02290	-0.010373
1	-0.000199+j0.00013	-0.000455



**Figure 5.7: Electromagnetic and mechanical synchronising coefficients
– Three machine system**



**Figure 5.8: Electromagnetic Damping Coefficient – Three machine system
- - Single Rotor Masses : Power frequency network only**

As already pointed out, the algorithm employed above only reveals the system behaviour at low frequencies of oscillation. The damping coefficients calculated at the higher frequencies are not accurate. In order to study higher frequency modes attributable to better turbine shaft modelling and transmission line effects, an additional algorithm must be employed.

5.3.2 Single Rotor Mass Models - - Full Network Model

The above analysis was repeated but including the algorithm detailed in § 5.2.3. The complex admittance matrix for machines 2 and 3 were evaluated for each rotor oscillation frequency and appended to the overall system complex admittance matrix. Evaluating the electromagnetic torque coefficients as per Chapter 2, the coefficients calculated in § 5.3.1 were corrected at the higher frequencies. Figure 5.9 illustrates the modification.

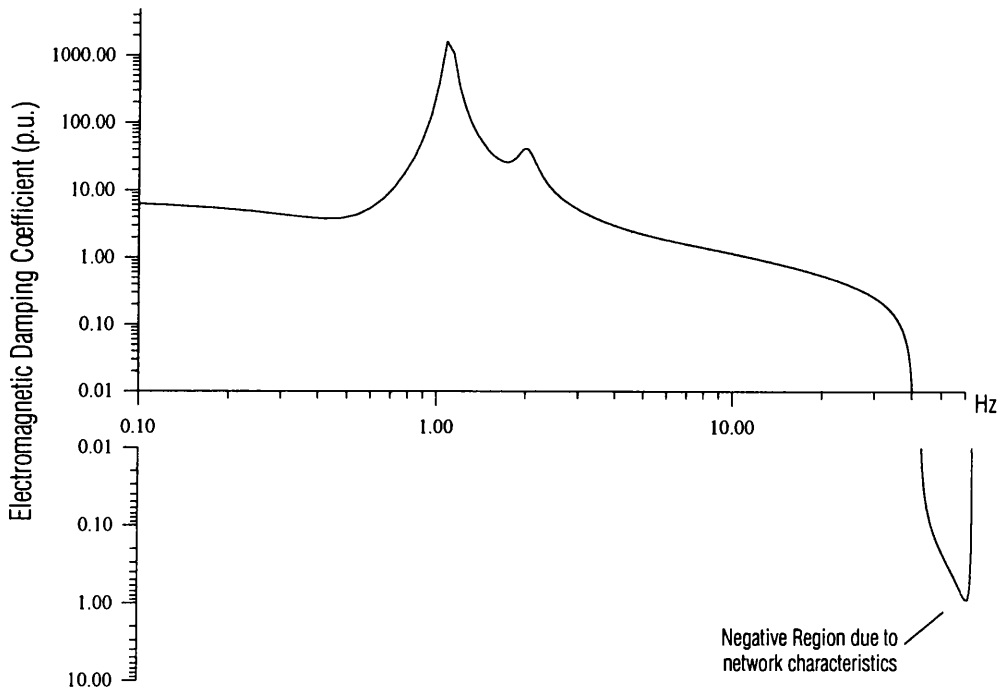


Figure 5.9 : Single rotor mass - Network included, no series compensation

The familiar region of negative damping at the extremity of the sub-synchronous range has reappeared.

5.3.3 Multi-Mass Models - - Full Network Model

The algorithm was applied to the same system but using a lumped-mass turbine shaft model for Machine 2. Machine 3 retained a single rotor mass representation. Figure 5.10 depicts electromagnetic damping coefficient for this case.

In general, each shaft torsional mode of Machine 2 will induce an increase in electromagnetic damping of Machine 1 in the vicinity of the torsional mode. If this mode also lies close to a region of influence from either static or dynamic compensation, then the machine, after taking mechanical damping of the shaft into consideration, may exhibit net positive damping as a result of the shaft mode(s) of the other machine(s). If the influence of these modes were neglected, the analysis may incorrectly predict instability.

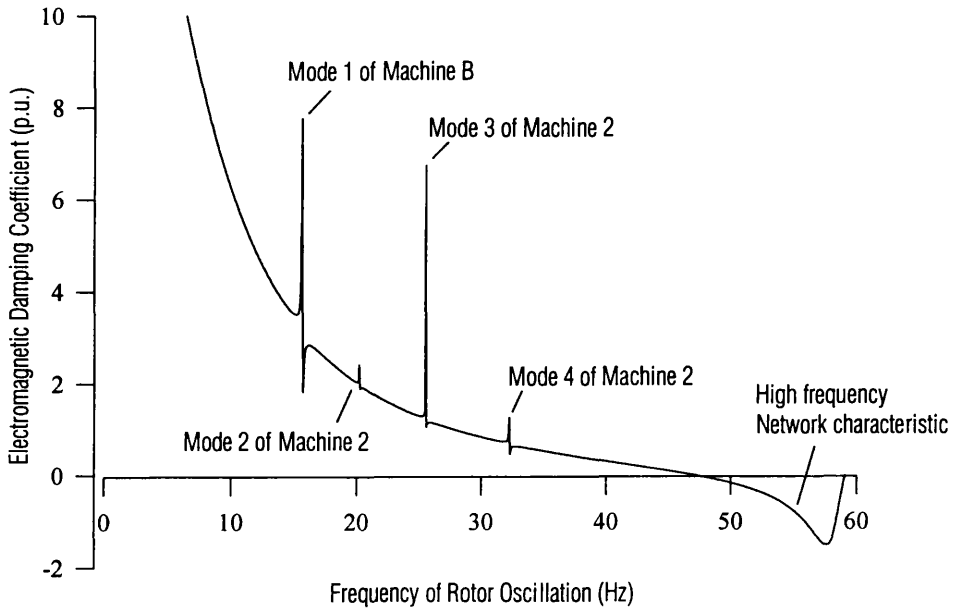


Figure 5.10: Multi-mass shaft - Network included, no series compensation

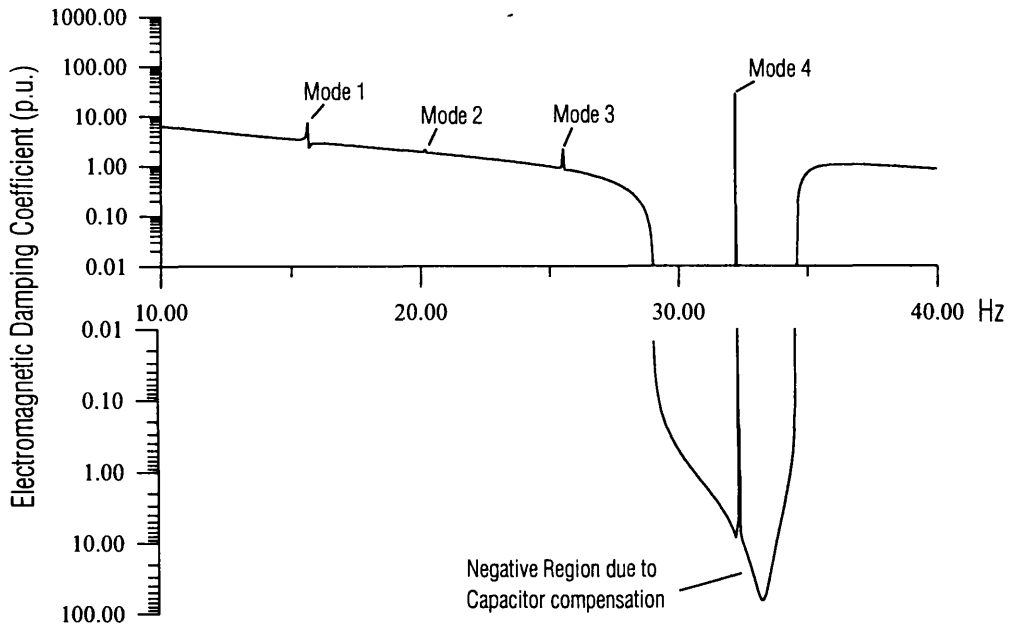


Figure 5.11: Full shaft model - Capacitor compensated system

Figure 5.11 depicts analysis for the same system but with series compensation in one of the transmission lines. As per Chapter 4, the capacitor compensated line induces the large region of negative damping, in this case peaking at 34Hz. On comparison with Figure 5.10, it can be seen that the apparent damping contribution from the 32.2Hz shaft mode of Machine 2 is significantly more than when there is no series capacitor present. This would indicate that damping contributions from different devices are very much dependent on system conditions. The system stability therefore cannot be determined simply by accumulating the damping contributions that prevailed for a previous system configuration. Re-evaluation of the coefficients must be carried out each time the system configuration changes.

Figure 5.12 illustrates the effect of coincidental electrical resonant frequency and shaft modal frequency of Machine 2. In previous cases, the damping contribution from a shaft mode has been confined to a very narrow frequency range. In this case however, the influence of the shaft mode is effective over a marginally wider range, again highlighting the necessity to evaluate each intended operating point.

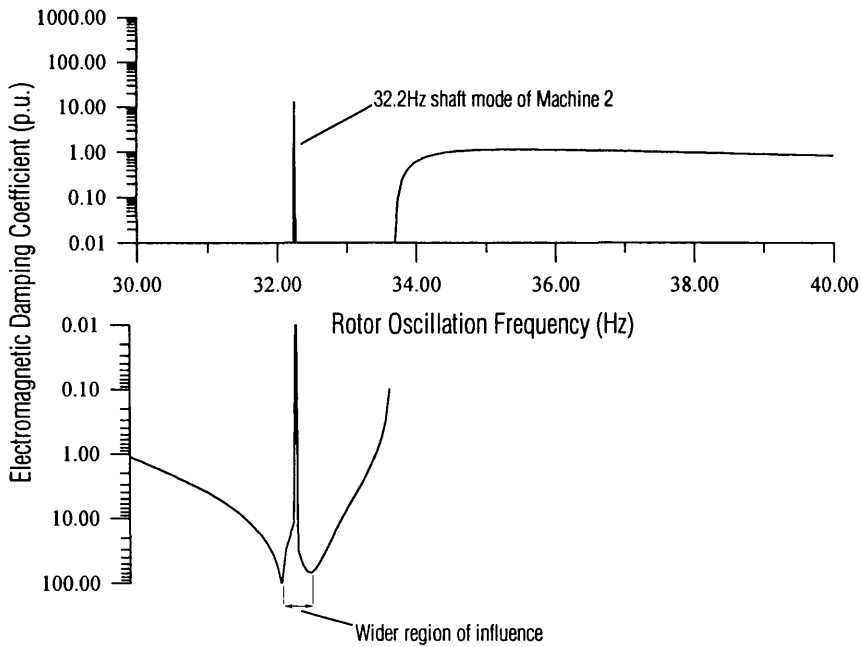


Figure 5.12: Coincidental electrical system and shaft resonant frequencies

5.4 SUMMARY OF CHAPTER 5

This Chapter has discussed the extension of the complex torque coefficient analysis technique to systems containing multiple machines. Application to a three machine system has been demonstrated.

The method is based on the state-space construction of the interconnected power system which provides a rigorous mathematical description which has not been attained using alternative techniques which use network reduction methods for all frequencies of interest.

In this study, low frequency and higher frequency effects are considered separately in order to retain the true coupling of the machines at low electromechanical frequencies. It has been illustrated, by calculation of the electromagnetic synchronising coefficient corresponding to a machine operating within a multi-machine system, that electromechanical rotor oscillations at swing frequencies are composite in nature.

The effect of higher frequency shaft modes belonging to machines other than the one under investigation is, in general, to enhance the damping of rotor oscillations in the very near vicinity of the shaft mode. Frequencies above and below the shaft mode are not influenced significantly by the mode.

The full effect of sub- and super-synchronous network effects have been retained in the analysis. This has been demonstrated for the same three machine system modified to include a series compensated line. Negative electromagnetic damping effects similar to those observed in the case of single machine systems was observed.

The influence of shaft modes belonging to other machines on the induced region of negative electromagnetic damping is most significant if the electrical resonant frequency is coincidental with the frequency of the shaft mode.

SUBSYNCHRONOUS TORSIONAL INTERACTION**DUE TO STATIC VAR COMPENSATORS****6.1 OVERVIEW OF THE STATIC VAR COMPENSATOR**

This Chapter describes the application of Complex Torque Coefficient analysis to the study of Subsynchronous Torsional Interaction, a phenomenon similar to that of subsynchronous resonance as discussed in Chapter 4, which may occur between rotating machines and Static Var Compensator equipment [50,51].

Static Var Compensators (SVCs) are shunt connected static generators and/or absorbers of reactive power whose outputs are varied so as to maintain or control specific parameters of the electrical power system. By continuously controlling the amount of shunt capacitance and inductance connected to a specific node, as illustrated in Figure 6.1, the capacitive and/or inductive current drawn may be used to tailor the net reactive power consumption (positive for absorption, negative for generation). The term 'static' is used to indicate that SVCs unlike synchronous compensators of the past have no moving parts and rely on the switching of thyristor valves for their operation.

Figure 6.2 illustrates a typical voltage-current characteristic of an SVC system. By absorbing or generating reactive power within its working range, the compensator is able to maintain almost constant voltage at its point of connection in the system. This characteristic behaviour is equivalent to an ideal system voltage source being in-phase with the system voltage at the point of connection. The SVC is thus similar to a synchronous compensator in its effect on the system except that it has no mechanical inertia and therefore its speed of response is much faster, an asset which allows the SVC to be effective in solving a wide variety of power system problems.

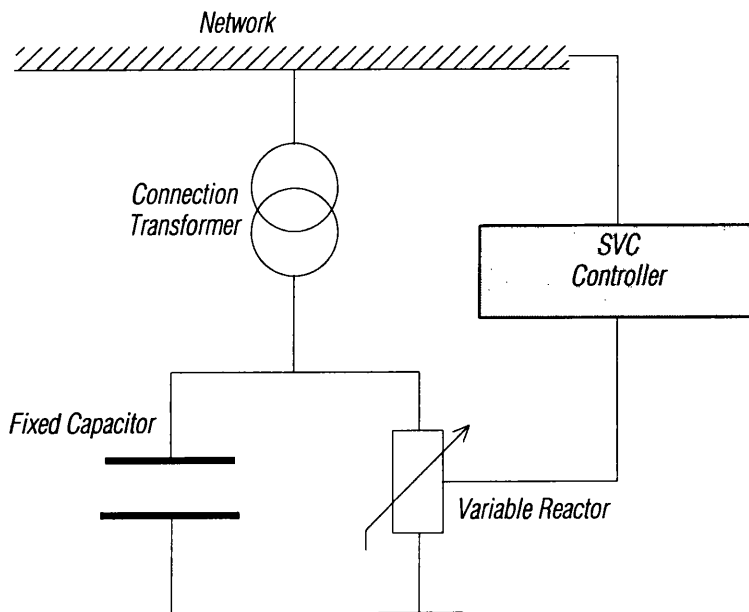


Figure 6.1: Static Var Compensator

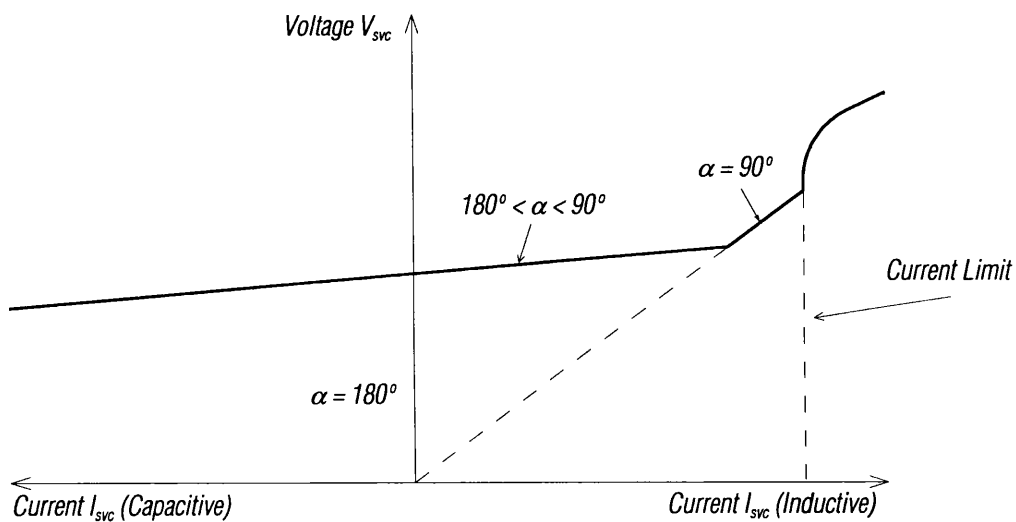


Figure 6.2: Voltage/Current Characteristic for the SVC

6.2 TYPICAL APPLICATIONS

There are many problems encountered in modern power systems to which the Static Var Compensator has been applied with success, the most important of which are briefly discussed here in order of most usage.

6.2.1 Voltage Control

In weak power systems, particularly those which employ long transmission lines, the voltage at the point of load is significantly affected by load variations and switching operations (i.e. transmission lines, transformers etc.). Under heavy loads, the voltage will drop considerably or even collapse in extreme cases, causing significant disruption in service to the consumer. During light loads, the problem becomes that of overvoltages owing to the Ferranti¹ effect on lightly loaded lines. Apart from breaching the voltage regulation agreement² with the consumer, overvoltages cause transformer saturation which leads to an increase in the level of harmonics present in the system, an undesirable outcome that may lead to excessive heating in capacitors and motor loads, harmonic resonances, and possible damage to consumers equipment. To help alleviate such difficulties, the static compensator is often used to dynamically regulate the voltage at the busbar to which it is connected by either absorption or generation of reactive power, as was discussed already.

6.2.2 Reactive Compensation of HVDC Converters

Due to their inherent characteristics, HVDC converters consume reactive power which is typically 60% of their active power [52]. During disturbances, large variations in this reactive power requirement can be experienced. This can cause significant change in the AC side voltage, especially in cases where the AC system impedance at the converter busbar is high.

¹ The Ferranti effect is an interaction between the inductance and the capacitance of a transmission line which results in voltage rise at one end of the line during instances of light loads.

² Currently in the United Kingdom, power generation utilities are required to maintain the 3-phase voltage at consumer locations between the levels of 230V +6%/-10%.

Due to their inherent speed of response, SVCs represent an effective method in controlling such disturbances by allowing more effective control of the AC side voltage.

6.2.3 Improvement of System Damping

Many studies in recent years have made it clear that variable impedance apparatus such as SVCs can improve the small-signal stability of power systems [57,58,59] provided that their location in that system is suitable and, in the case of multiple compensators, that proper coordination is in effect. It can be shown [53] that for the simple system illustrated in Figure 6.6, for which the real and reactive power components can be approximated by

$$P = \frac{V}{X_T} \sin \delta \quad [6.1]$$

$$Q = -\frac{2}{X_T} (V^2 - V \cos \delta)$$

where X_T is the total impedance viewed from the machine busbar, δ is the machine load angle and V is the terminal voltage, the synchronising torque coefficient K for this system is increased by an amount equal to

$$\Delta K = \frac{1}{2X_T} \frac{X_T Y_s (1 - \cos 2\delta) / 4}{V_o + X_T Y_s / 2} \quad [6.2]$$

when the SVC is present where Y_s is the slope admittance. This implies that the natural frequency of oscillation of the synchronous machine will increase since

$$\omega = \sqrt{\frac{K}{M}} \text{ Rad / s} \quad [6.3]$$

where M is the equivalent inertia of the system. De Oliveira [45] showed that for the regulated synchronous machine, the damping component of torque at low frequencies within the range of the zeroth mode would increase as the frequency of oscillation is

increased. This would then imply that the presence of the SVC would improve the damping characteristics.

6.3 TORSIONAL INTERACTIONS BETWEEN SYNCHRONOUS MACHINES AND SVCs

Interactions between machines and series compensation devices is well known and has been discussed in depth in Chapter 4. The possibility of unfavourable interaction between the torsional modes of a synchronous machine and a nearby Static Var compensator however, is something that is not usually considered. Recent investigations in Maine, U.S.A. [32,33] revealed that under certain situations, torsional interaction between the synchronous machine and the controls of a nearby compensator was large enough to warrant closer attention.

Static Var compensator induced SSTI is a mechanism whereby the natural response of the voltage regulator on the SVC degrades the electrical damping of specific torsional modes on nearby steam-turbine units. Essentially, these torsional modes produce slight fluctuations of the terminal voltage of the generator in response to small disturbances on the system. Consequently, these fluctuations of voltage induce control action at the terminals of the compensator which in turn will produce a change in machine torque. If conditions are such that rejection of exciting torques is weak, this action can act to encourage the torque oscillations to build up.

Rostamkolai et al [32] suggested that the interaction could be predicted using damping coefficient techniques similar to those already employed in this study to analyse inter-machine and subsynchronous resonance phenomena. Using this approach in this study would allow the investigation of the combined effects of static var compensators, series compensated transmission lines, and the torsional modes of other nearby turbine generators on the excitation of the torsional modes of the machine under investigation.

6.4 STATIC VAR COMPENSATOR MODEL

There are two models used to represent the static compensator in this study. The first is used during the load-flow analysis which is necessary to compute the correct initial operating conditions in the system, upon which, by the nature of their operation, Static

Var compensators will have a significant effect. The second model is used during the computation of the torque coefficients and must take into account the action of the compensator control system which is known to be instrumental in the interaction phenomenon.

6.4.1 Load-Flow Model of the Static Var Compensator

The general requirements of the load-flow model of the SVC are that the steady-state, balanced fundamental frequency behaviour, including control limits are adequately represented [54]. A three-phase model is required only when considering the problem of voltage imbalance. This is not considered in this study.

The steady-state characteristic of a generalised SVC describes the relationship between the terminal voltage of the compensator and the current that it draws, as was illustrated in Figure 6.2 . The compensator is represented as a shunt component. There are two basic elements needed to achieve the correct characteristic. The slope of the characteristic can be adequately represented by an equivalent reactance, $X_{s'}$ which is added between an imaginary auxiliary node and the point of connection of the compensator, as illustrated in Figure 6.3. This reactance is assumed fixed and will change only if the fundamental characteristic is changed. The second element is a controlled susceptance in parallel with a fixed capacitor, the most common configuration of the SVC. Depending on the voltage at the point of connection of the compensator, the susceptance B_{svc} is increased or decreased in a stepwise fashion according to the error between the computed terminal voltage and the required or reference terminal voltage after each load flow solution. The loop is continued until either the required terminal voltage is achieved or the susceptance limits have been reached. The size of the ΔB_{svc} steps is variable during the analysis so that accuracy is not affected. A more elegant technique, however, would be to include the representation of the Static compensator in the load flow jacobian. It was felt, however, that this would be an unnecessary complication in this study and would not necessarily result in improved accuracy in this particular application.

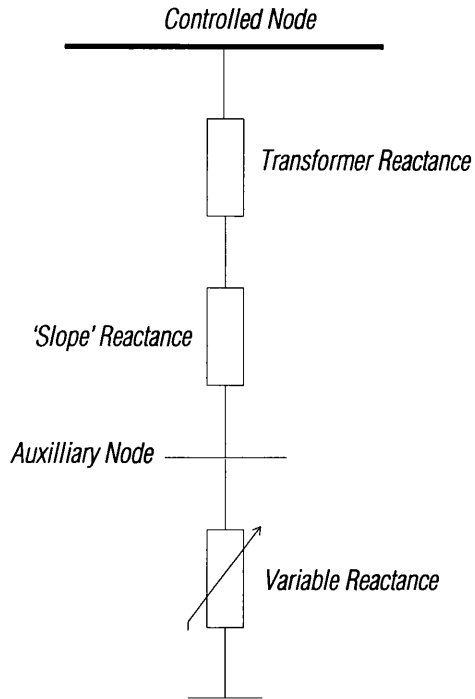


Figure 6.3: Load-Flow Representation of the SVC

Table 6.1 : Iterative SVC Voltage Scheme
 - - Set point = 1.0p.u. voltage

Iteration No.	Calculated Voltage(p.u.)	SVC Tap Position
1	1.0400	0.4600
2	1.0271	0.4329
3	1.0172	0.4158
4	1.0103	0.4055
5	1.0060	0.3995
6	1.0034	0.3961
7	1.0019	0.3942
8	1.0010	0.3932
9	1.0006	0.3926
10	1.0003	0.3923
11	1.0002	0.3921
12	1.0001	0.3920

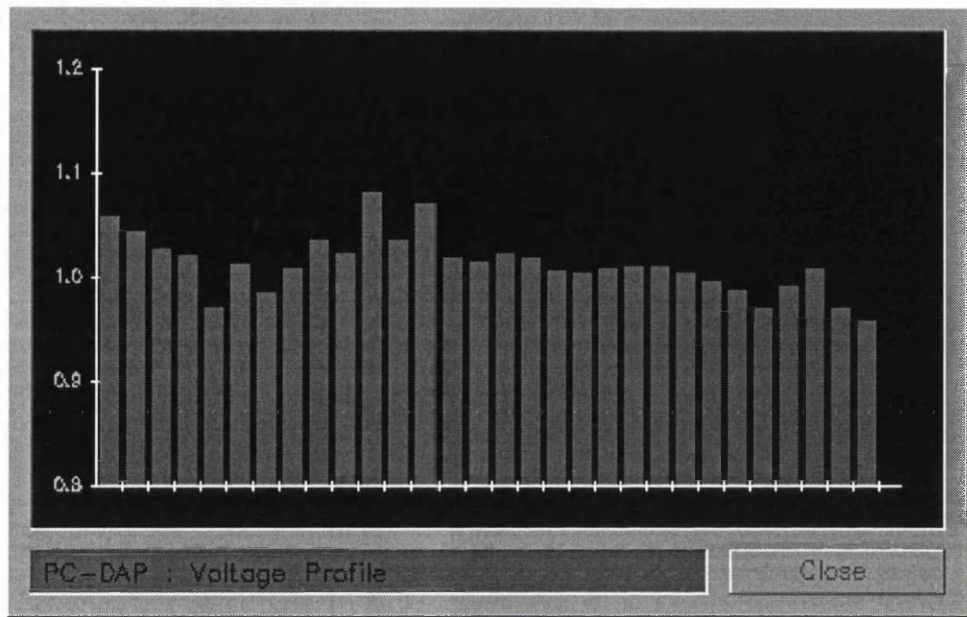


Figure 6.4a: Voltage Profile before connection of Static Compensator

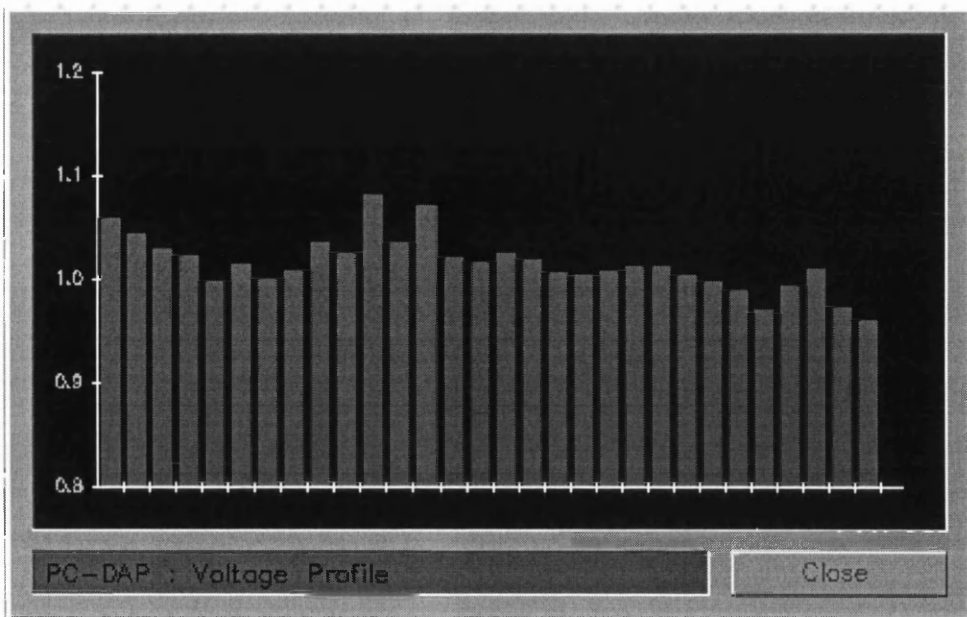


Figure 6.4b: Voltage Profile after connection of Static Compensator

Table 6.1 illustrates the mechanism for a 30 bus system, showing the terminal voltage and the SVC Tap position at the end of each load-flow solution. Figure 6.4a illustrates the voltage distribution before the SVC is introduced and Figure 6.4b illustrates the effect on the voltage distribution after the reference voltage has been attained.

6.4.2 Complex Torque Analysis Model of the Static Var Compensator

The important element in this model is the primary voltage control loop of the variable reactor [55] as depicted graphically in Figure 6.5.

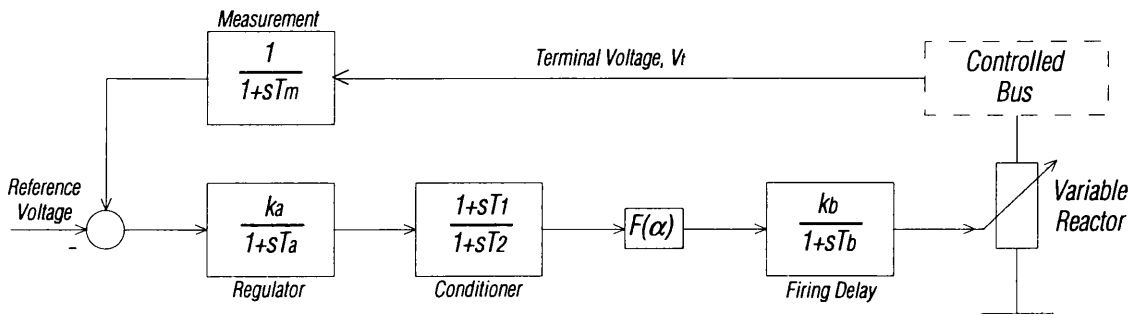


Figure 6.5: Primary Voltage Control Loop

The basic elements consist of :

- a) **Voltage Measuring and Filtering** : Responsible for converting the three-phase voltages to a quasi-dc control signal that is proportional to the positive sequence, fundamental frequency component of the measured quantity. This block is usually modelled as a simple low pass filter, although more elaborate filter representations may be used [52,56] in cases where the network exhibits strong resonances near fundamental frequency.
- b) **Voltage Regulator** : The regulator gain constant represents the 'slope' characteristic of Figure 6.2. Modeling the regulator as either a proportional type controller or as an

integral type controller introduces additional lead/lag components which are often included as an additional signal conditioner block.

- c) **Thyristor susceptance control** : This block is an approximate representation of the control system and physical constraints at the moment of thyristor firing. It has three components associated with it; the thyristor firing sequence control; a gating transport delay; and the non-linear relationship between firing angle and TCR susceptance. The firing sequence control is represented by a lag term with time constant T_b , with a value typically between 4 and six milliseconds. The gating transport delay e^{-sT_d} typically has a value of about 1 millisecond. Given that this parameter is significantly smaller than the firing sequence control delay, it is neglected in this study. The TCR susceptance is a non-linear function of the TCR firing angle α [52]. The relationship is described by

$$B_{TCR} = B_L \frac{2\pi - 2\alpha + \sin(2\pi - 2\alpha)}{\pi} \quad [6.4]$$

where B_L is the susceptance of the linear reactor.

Linearisation of Eqn. [6.4] yields

$$\Delta B_{svc} = \Delta B_{TCR} = F(\alpha)\Delta\alpha \quad [6.5]$$

where $F(\alpha) = -2B_L \frac{1 - \cos(2\alpha)}{\pi}$

If the non-linearity is cancelled by an ideal linearising block, then $F(\alpha)$ becomes a constant equal to $2B_L/\pi$ [52].

- d) **SVC - Network Interface** : Can be modelled either as a variable susceptance or as a controlled current source. The former representation is used in this case .

Table 6.2 : Typical Parameters for SVC Model

SVC Model Parameter	Typical Range of Values
Measurement Module Time constant, T_m	1~8ms
Voltage Regulator Gain constant, k_a	20~100p.u. (SVC Base)
Voltage Regulator Time constant, T_a	20~150ms
Regulator Conditioning lead Time constant, T_1	~0.5s
Regulator Conditioning lag Time constant, T_2	~1s
Firing Angle Delay Time constant, T_b	3~6ms

Typical parameters for the SVC parameters are dependent on the MVA rating and are indicated in Table 6.2 .

The SVC system is included in the Complex Torque analysis by constructing the complex impedance matrix of the SVC by building the model initially in the state-space form (appendix B):

$$\begin{aligned}\dot{\underline{x}} &= A\underline{x} + B\Delta v_{svc} \\ \Delta i_{svc} &= C\underline{x} + D\Delta v_{svc}\end{aligned}\quad [6.6]$$

Proposing a purely sinusoidal solution allows Equation 6.6 to be reduced to

$$\Delta i_{svc} = \left(D - C[A - j\omega I]^{-1} B \right) \Delta v_{svc} \quad [6.7]$$

whereby the (2x2) complex admittance matrix describing the dynamics of the controlled reactor may be obtained by evaluating

$$Y_{svc}(j\omega) = \left(D - C[A - j\omega I]^{-1} B \right) \quad [6.8]$$

at each frequency of rotor oscillation. This matrix can be included in the overall system admittance matrix of Figure 5.1 by appending the $Y_{svc}(j\omega)$ onto the diagonal (2x2) corresponding to the SVC node.

The dynamics of the fixed capacitor may be included in the analysis by evaluating the complex admittance matrix of a capacitor:

$$Y_{cap}(j\omega) = \left(\frac{1}{1-\omega^2} \begin{bmatrix} j\omega & 1 \\ -1 & j\omega \end{bmatrix} X_{cap} \right)^{-1} \quad [6.9]$$

and appending this matrix to the same node as the variable susceptance.

6.5 ANALYSIS OF SUBSYNCHRONOUS TORSIONAL INTERACTION

The SVC models described in the preceding sections were employed to investigate the possibility of torsional interaction for the single machine system illustrated in Figure 6.6.

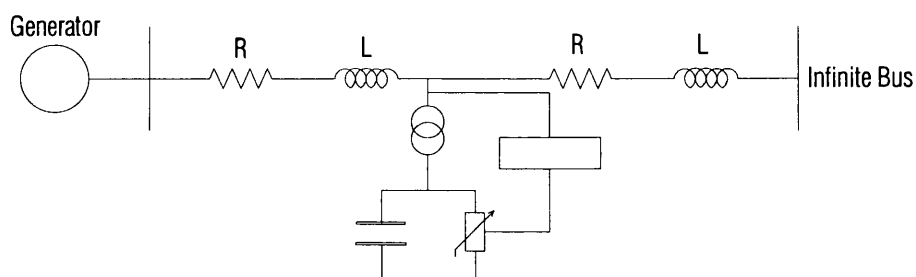


Figure 6.6: Single Machine - SVC - Infinite Bus System

This system represents a worst case scenario. A more highly meshed configuration would be expected to be considerably less sensitive to voltage fluctuation.

6.5.1 Influence of Voltage Regulator parameters on the Torque Coefficient Loci

The influence exerted by each of the SVC parameters on the occurrence of torsional interaction was investigated. The parameters belonging to the voltage regulator block were found to exert the most influence. Variation of all other SVC control parameters resulted in relatively insignificant change to the torque coefficient loci.

Figure 6.7 illustrates the influence of the voltage regulator block of the Static Compensator on the damping coefficient acting on the rotor of the synchronous machine for regulator lag time constants of 0.01s, 0.03s and 0.05s and a regulator gain constant of 50.

The Figure indicates that the compensator may induce regions of negative damping similar to that caused by series compensation capacitors which, under certain electrical and mechanical conditions, could excite oscillations to build up in the turbine-generator shaft. It is found that the region of interaction has a point of maximum associated with the regulator time constant. That is, the interaction region is most severe at a time constant of 0.03s and decreases significantly if the time constant is either increased or decreased from this value. The variation of peak damping frequency is inversely proportional to the increase in time constant. As with all previous studies discussed, the region of negative damping above 35Hz is due to the network characteristics and not to the presence of the compensator.

The influence of SVC voltage regulator gain constant is depicted in Figure 6.8 for the worst case regulator lag time constant of 0.03s identified in Figure 6.7. Clearly, a larger gain results in an amplification of the characteristics. The possibility of adverse interaction is thus increased. Machine electromagnetic damping with the SVC control enabled for steady - state operation but disabled for small disturbances is indicated by curve A. Comparing curve A with curves B, C, and D, it is clear that at all frequencies outwith the narrow region of negative damping below 15Hz, the presence of the compensator tends to improve the electrical damping coefficient acting on the rotor, as observed by de Oliveria [44]. Increasing the regulator gain leads to a general improvement in damping but an increased risk of torsional interaction occurring within the frequency range 5~15Hz.

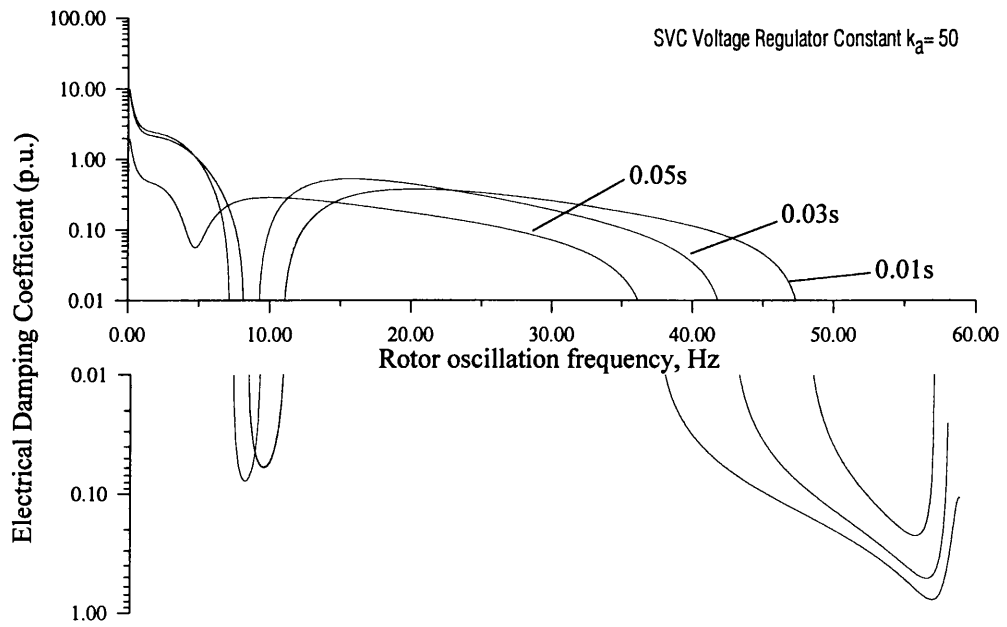


Figure 6.7: Influence of SVC Voltage Regulator Lag Time Constant

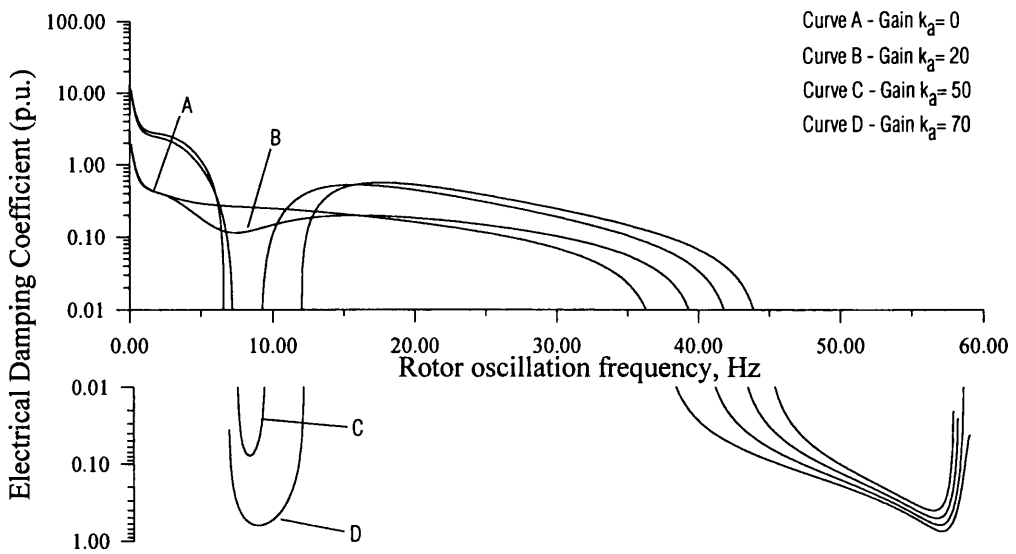


Figure 6.8: Influence of SVC Voltage Regulator Gain

To evaluate the overall system, it is of course necessary to include the mechanical shaft response characteristics as depicted in Figure 6.9. For this specific case, the region of negative electromagnetic damping due to the SVC voltage regulator action falls within a region of high mechanical damping such that no oscillations could take place. It is of note that the presence of the compensator lessens the possibility of interaction within the 40Hz to 60Hz frequency band.

Because the mechanical and electrical systems are conveniently separated in the analysis, the prediction of likely problem systems is intuitively straight forward.

6.5.2 Influence of SVC Placement

Although the SVC regulator parameters play a significant part in the torsional interaction mechanism, the question naturally arises as to what influence the system parameters may have. The question of SVC placement has been addressed by studying the variation of damping component due to (i) generator to SVC line impedance and (ii) SVC to system impedance.

Generator to SVC Impedance

Figure 6.10 depicts the variation of electromagnetic damping for several generator to SVC line impedances. For a low impedance of 0.14p.u., illustrated by curve A indicating close proximity of the generator and the SVC, the region of interaction is very pronounced. As the impedance is increased, effectively moving the SVC further away from the machine, as indicated by curves B, C, and D, the influence of the compensator is significantly reduced as would be expected.

SVC to System Impedance

Variation of line impedance between the point of connection of the SVC and the infinite bus gives a measure of the influence of system strength – a low impedance represents a strong system and a high impedance is representative of a weak system. Variation of the impedance is found to have the opposite effect as illustrated in Figure 6.11.

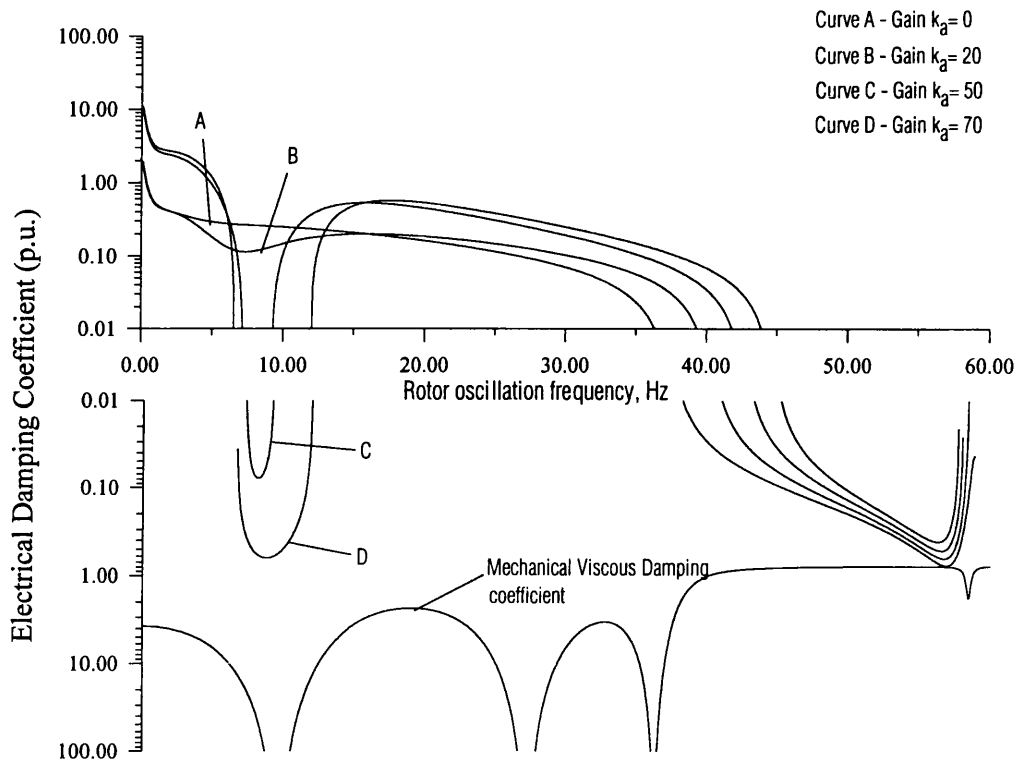


Figure 6.9: Combined Electromagnetic and Mechanical SVC system

As the impedance is decreased from 0.5p.u. to 0.125p.u., i.e. changing from a weak to a strong system, the damping coefficient becomes less onerous.

6.5.3 Influence of SVC Operating Point

The operating point of the SVC was varied by adjusting the specified voltage on the node of connection. For low voltages the net injected MVars would be inductive and for high voltages the net injected MVars would be capacitive. The variation was found to have a significant impact on the damping coefficient as illustrated in Figure 6.12. As the specified voltage is increased from 0.97p.u. to 1.03p.u. the region of interaction is seen to decrease, as shown in curves A to E. However, increasing the specified voltage further results in the negative region increasing again, as shown in curve F. This illustrates that the impact of the interaction exhibits a point of minimum.

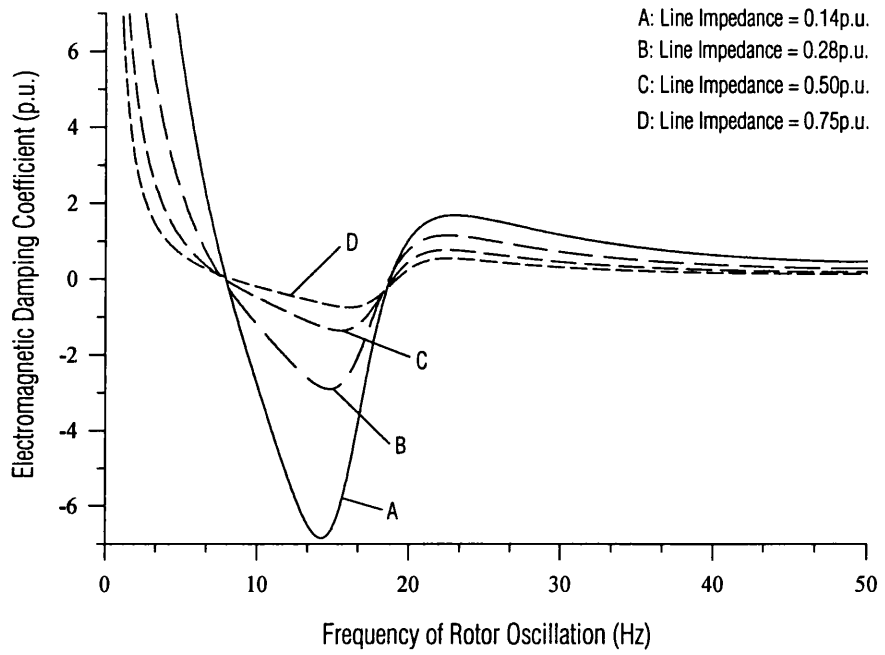


Figure 6.10: Influence of Machine to Compensator Line Impedance

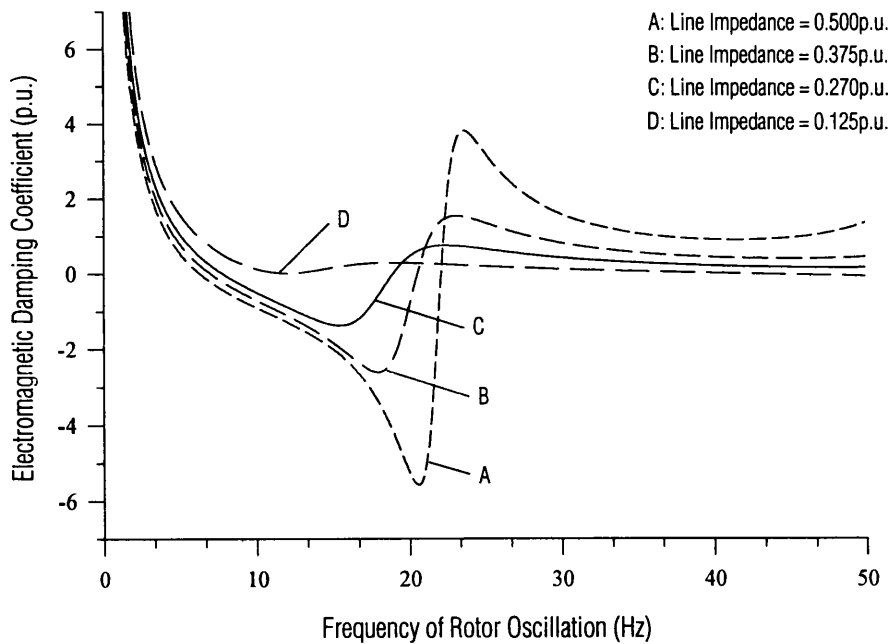


Figure 6.11: Influence of Compensator to Infinite Bus Line Impedance

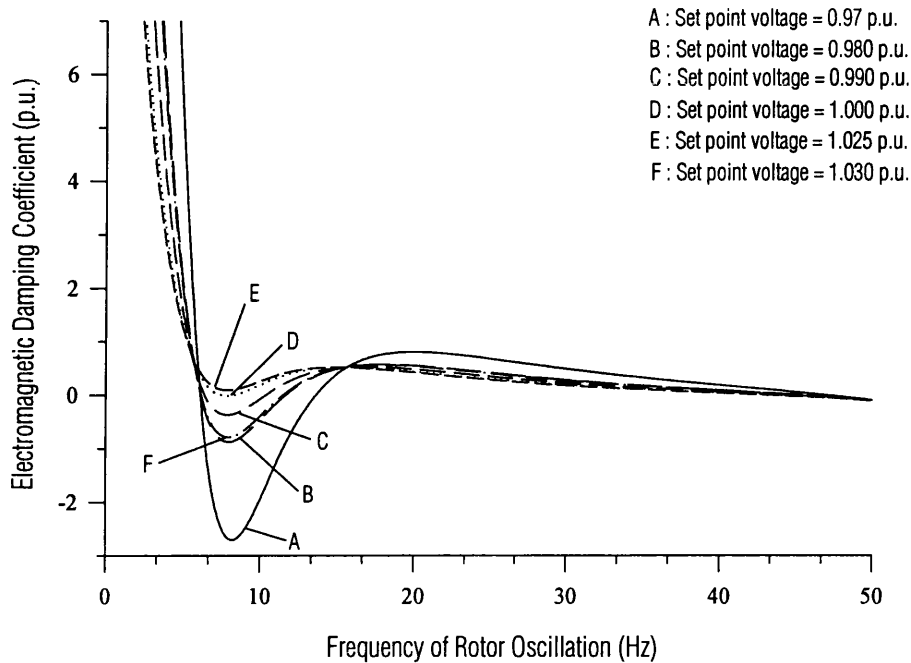


Figure 6.12: Variation of Damping Component with SVC Operating Point

Figure 6.13 shows the variation of minimum damping as a function of the injected reactive power for SVC regulator gain constants of 50, 30, and 10 in curves A, B, and C respectively. In all three cases, the point at which the negative electromagnetic damping is least occurs when the net injected reactive power set to 10MVar. In all three cases, the reactive power load at the infinite bus was 10MVar. Curve D illustrates the variation with a reactive load of 20MVar at the infinite bus. It can be observed that the point of least negative damping now occurs at 20MVar. This demonstrates that the level of interaction is a function of the difference between the reactive power consumed by the load and the reactive power supplied by the SVC. The minimum will occur when the reactive load is completely provided by the compensator i.e. the generator is supplying real power only.

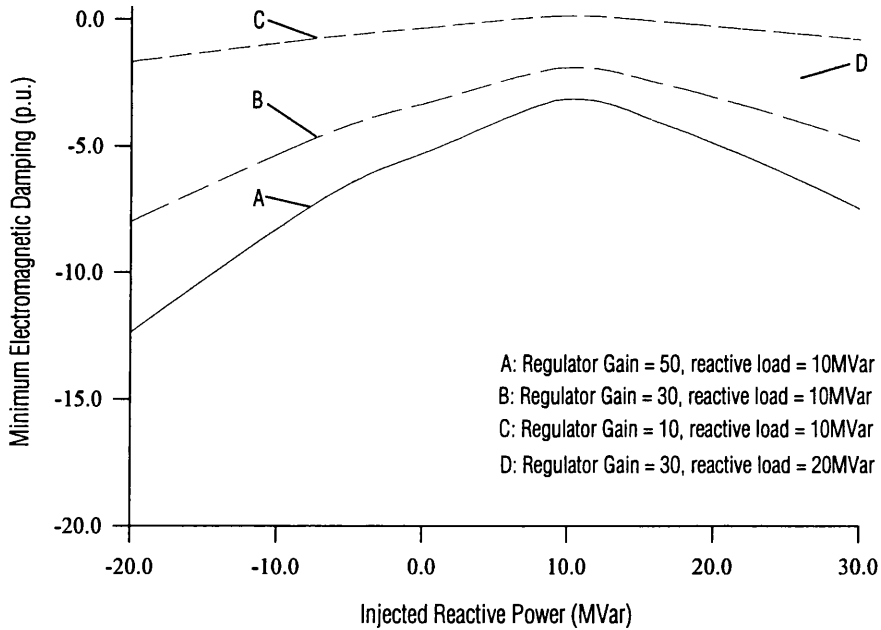


Figure 6.13: Variation of Minimum Damping with SVC Operating Point

Influence of Generator Operating Point

The analysis was repeated but with different generator real power demands. As Figure 6.14a shows, increasing the real power demand on the generator leads to the extent of the negative region becoming greater. It should be noted however, that an increase in real power will lead to increased steam viscous damping. As a result, the overall stability of the machine may not deteriorate. Figure 6.14b depicts the effect of increased SVC reactive power injection. As was previously discussed, matching the SVC reactive power injection with the reactive load demand gives the least effect on the damping coefficient. As the SVC reactive power injection is increased, the damping will become more onerous.

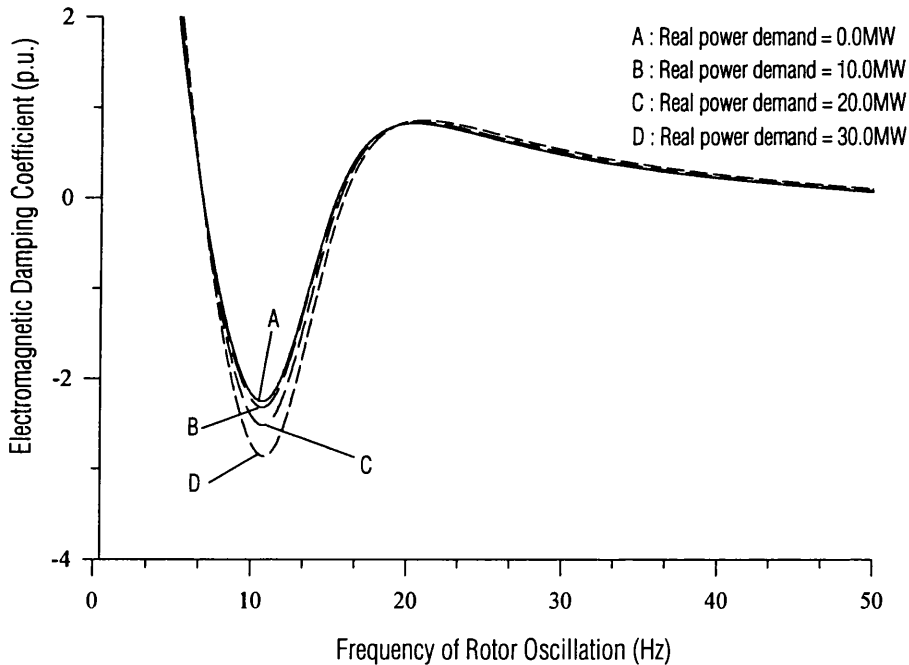


Figure 6.14a: Influence of Generator Real Power Demand - Constant SVC Reactive Power Injection

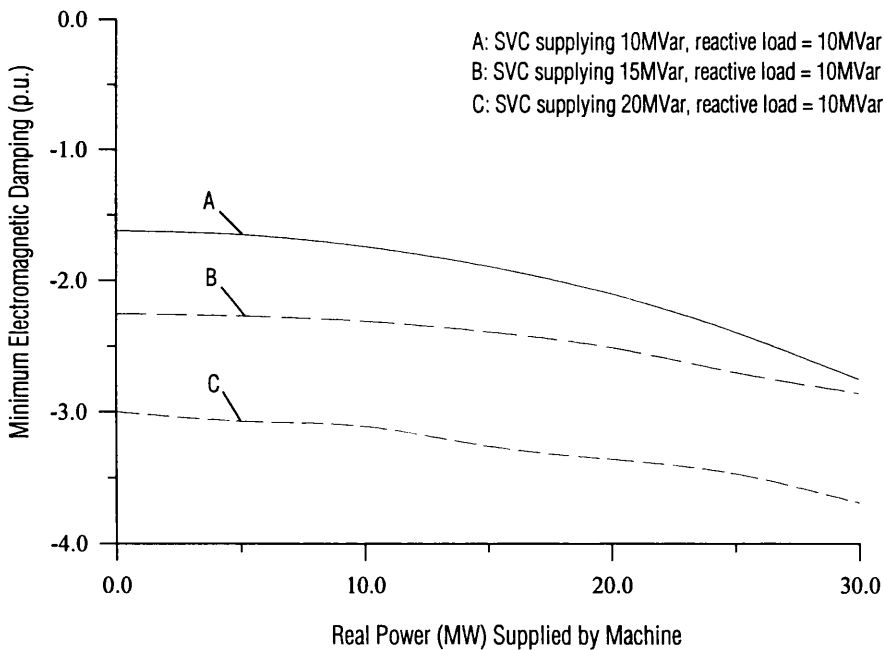


Figure 6.14b: Influence of Generator Real Power Demand - Variation of SVC Reactive Power Injection

6.6 THYRISTOR CONTROLLED SERIES COMPENSATION DEVICES

The preceding sections of this chapter have focused on the controllable shunt element. There is, however, much interest of late in the controllable series element, the TCSC or Thyristor Controlled Series Capacitor. The characteristics of this device in the context of torsional interaction will be studied.

Subsynchronous resonance and the associated turbine-generator torsional interactions are a major constraint for many series compensated transmission systems. As was discussed in an earlier chapter, the use of fixed series compensation devices results in a considerable stability penalty by inadvertently increasing the potential for subsynchronous interactions to take place. Flexible AC Transmission Systems devices such as the TCSC, however, offer compensation levels equalling that which is obtainable with conventional fixed compensation but with suppression of SSR instabilities accomplished through the active control of compensation level, as well as much greater overall flexibility in power flow control.

Conventional series compensation schemes switch capacitors to vary the level of compensation by use of mechanical switching devices. The limitations of using mechanical switching devices force conventional series compensation schemes to be switched in relatively large discrete segments with relatively slow switching times.

Thyristor based controllers for series compensation schemes offer rapid, smooth control of the line impedance over a continuous range. Figure 6.15 illustrates the general configuration of the TCSC. Essentially, the device consists of a parallel combination of a fixed capacitor and a thyristor controlled reactor. By varying the conduction angle of the thyristors the effective inductance of the controlled branch varies which in turn yields a controllable amount of capacitor compensation. The relationship between firing angle and resultant inductive reactance is indicated in Eqn. [6.4].

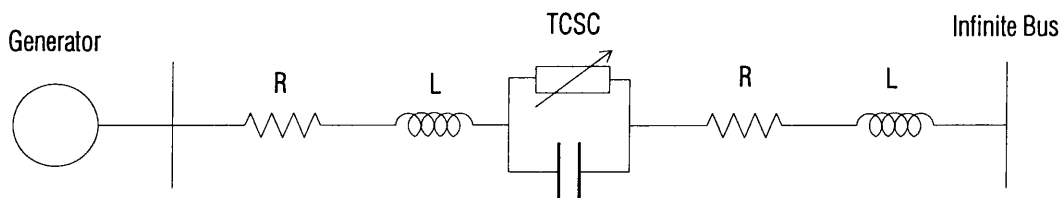


Figure 6.15: Thyristor Controlled Compensation Scheme

6.6.1 SSR Mitigation capability of the TCSC

It has been reported [57,58,59] that, while able to provide series compensation equalling that provided by a fixed capacitor scheme, the TCSC can, at suitable operating points, eliminate completely the problems associated with traditional series compensation schemes.

In this study, the measurable quantity from which control action is derived is TCSC bus voltage. The control will operate so as to minimise the fluctuations in bus voltage. The primary voltage control loop is assumed to be of a similar configuration to that used for the Static Var Compensator, illustrated in Figure 6.5.

6.6.2 Calculation of TCSC Complex Admittance

The complex admittance representing the controlled reactor is derived from the state-space form of the combined controller and network interface equations in a manner similar to that used in §6.4.2 for the static Var compensator. The complex admittance of the fixed capacitor is combined to yield the equivalent admittance matrix of the TCSC. As for all other network components, the admittance matrix is evaluated for each frequency of rotor oscillation. When combined into the overall system matrix, the influence of the controlled branch on machine stability can be studied.

6.6.3 Complex Torque Coefficients for a single machine - TCSC system

The single machine - compensated transmission line system studied in §4.2 was modified by replacing the fixed compensation capacitor with a TCSC element. Figure 6.16 depicts the electromagnetic damping for each rotor oscillation frequency of the machine for increasing TCSC voltage regulator gain constant.

Curve A corresponds to electromagnetic damping with the controlled reactor branch disabled. This corresponds to the fixed compensation scheme. Curve B corresponds to the case of both fixed capacitor and reactor with the TCSC control disabled. As expected, the effective capacitor compensation due to the parallel combination has increased as indicated by the greater amount of negative electromagnetic damping and a lower electrical resonant frequency. Curves C - F depict the effect of increasing voltage regulator gain. For low values of gain the possibility for SSR interaction still exists albeit reduced as compared with the uncontrolled case.

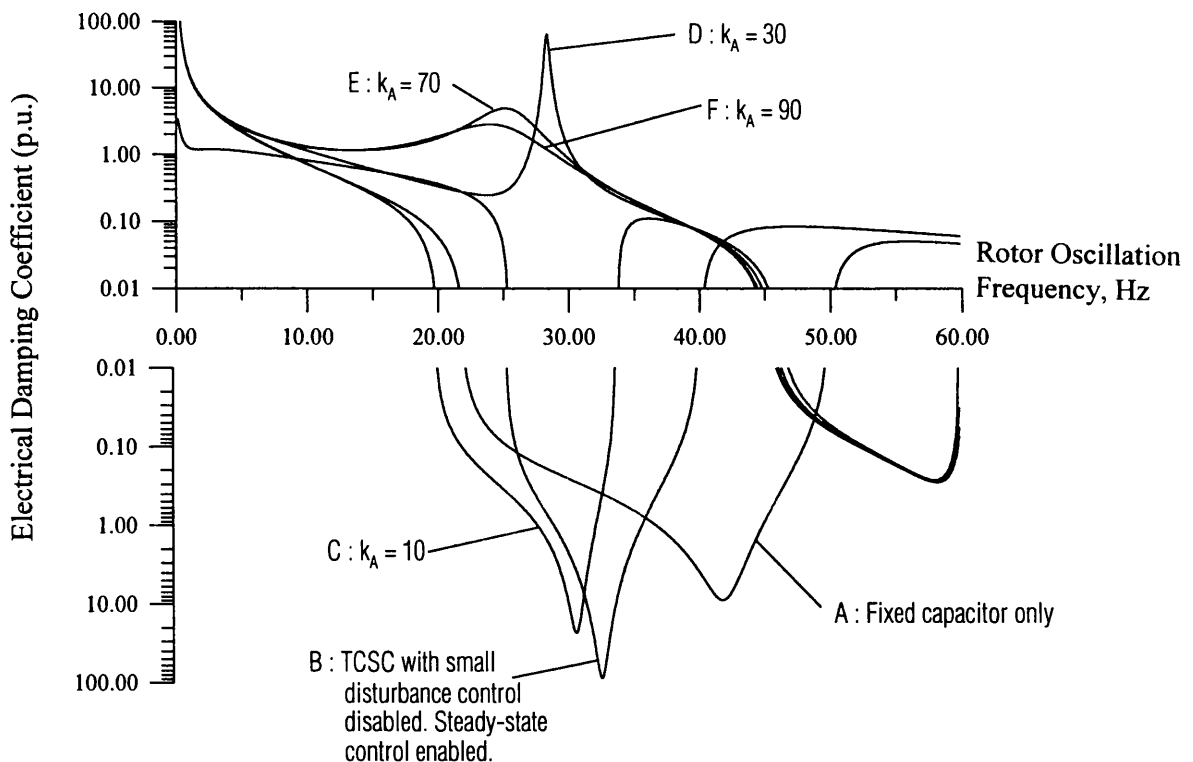


Figure 6.16: SSR Mitigation using TCSC Device

For gain constants greater than 10, the negative region changes polarity to give a large positive region with the same peak frequency. This behaviour is very similar to that of increasing transmission line resistance as discussed in §4.2.4. As the gain is increased further, as depicted by curves E and F, the positive peak region of the electromagnetic damping becomes less pronounced. It can also be observed that the region of negative damping at higher subsynchronous frequencies which was absent for the system containing only a fixed compensation scheme, has returned.

Clearly, when a TCSC device is employed in place of a fixed compensation scheme, the network can be made to exhibit a resistive-inductive characteristic at subsynchronous frequencies. This illustrates that the TCSC can provide power frequency line compensation but without the region of instabilities at subsynchronous frequencies experienced with the use of conventional compensation equipment.

Figures 6.17 and 6.18 illustrates the influence of phase lag on the ability of the TCSC device to mitigate torsional interaction at subsynchronous frequencies.

Increasing the lag time constant due to voltage regulator action, as depicted in Figure 6.17, has an effect which is equivalent to operating the TCSC device at reduced voltage regulator gain. A high time constant would increase the likelihood of torsional interaction.

Figure 6.18 depicts electromagnetic damping for several values of thyristor firing lag time constants. Voltage regulator time constant T_A was maintained at 0.05s. For time constants upto and including 0.007s, the system remains well damped. Increasing the time constant further to 0.009s, however, results in a loss of positive damping. The TCSC device appears as a capacitor to the system at subsynchronous frequencies. The Figure demonstrates that excessive phase lag introduced by the control loop can have a serious impact on the ability of the TCSC to provide series compensation without the possibility of SSR interaction.

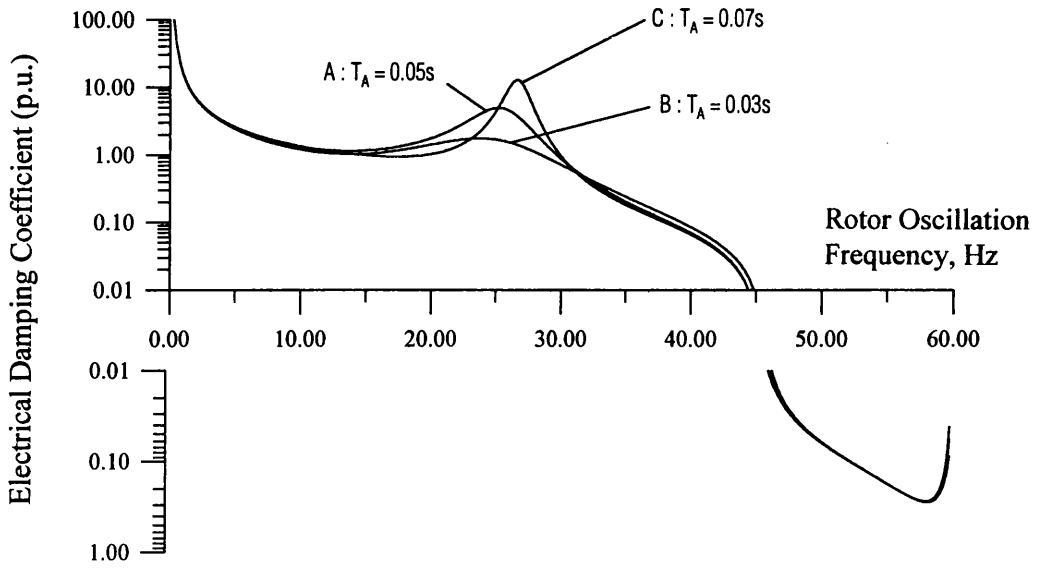


Figure 6.17: Influence of Voltage Regulator Lag Time Constant – TSCS System

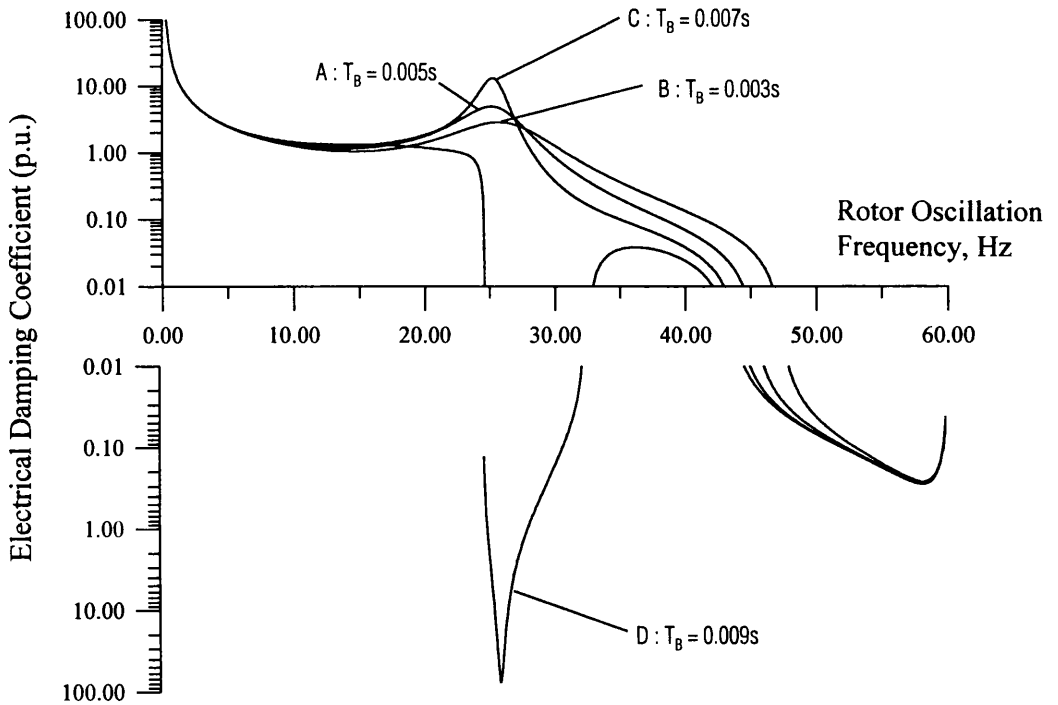


Figure 6.18: Influence of Thyristor Firing Delay – TSCS System

6.7 SUMMARY OF CHAPTER 6

This Chapter has demonstrated that the technique of Complex Torque Coefficient Analysis can be applied successfully to the study of Subsynchronous Torsional Interaction between a synchronous machine and controlled network devices, in this case a Static Var Compensator and a Thyristor Controlled Series Compensator.

It has been shown that, in agreement with the available literature, the mechanism of the interaction between the synchronous machine and the SVC is dominated by the configuration of the voltage regulation on the compensator. Although providing a noticeable improvement in damping over most of the subsynchronous range, unsuitable regulator parameters will induce a region of negative damping not dissimilar to that induced by the use of series compensation capacitors. If the generator under investigation is operating under light load conditions for which steam viscous damping is significantly reduced, the possibility of unfavourable interaction exists.

The influence of 'system' parameters was investigated. It has been demonstrated that location of the SVC has a significant impact on the extent of the negative damping region, with most effect occurring when the SVC is in close proximity to the generator. The system strength was also found to be of significance with weak systems being the most susceptible to the interaction.

Minimisation of the interaction was found to occur when reactive power load demand is matched exactly by SVC reactive power injection. At this point, at least for a single machine system, the generator is supplying the real power demand and the reactive losses only.

Variation of the generator real power demand was found to have a less significant but noticeable influence. Increased real power demand leads to a detriment of the damping coefficient, although it must also be borne in mind that steam viscous damping will increase significantly as real power demand is increased, such that overall machine stability may not be unfavourable.

The Complex Torque Coefficient analysis technique has been applied to the study of a single machine – TCSC system. The ability of the TCSC device to provide line compensation but with no SSR interaction has been illustrated.

Variation of the TCSC voltage regulator parameters was found to have a significant impact on the ability of the device to mitigate regions of negative electromagnetic damping. For the system studied, it has been found that low values of gain do not remove regions of possible torsional coupling. Likewise, excessive phase lag introduced by the control loop, for example by regulator action or thyristor firing delay, may result in the TCSC device being equivalent to a conventional series capacitor at subsynchronous frequencies which would not be desirable.

CHAPTER SEVEN

VALIDATION OF COMPLEX TORQUE COEFFICIENT TECHNIQUE

This chapter verifies the validity of the fundamental concept behind the Complex Torque Coefficient technique — that is, describing the mechanics of the torsional interaction phenomenon by the interplay of two coefficients. The test case focuses on the analysis of subsynchronous resonance.

7.1 TECHNIQUES FOR VALIDATION

The validation and verification of theory and analysis by means of direct measurement and study of a ‘real’ system is a challenging task in any field of scientific and engineering research. In the area of large power systems, however, this task is more formidable than most. The size and complexity of actual power systems forbids the direct approach. It must also be borne in mind that a power system is virtually never off-line except during maintenance schedules. Even while on-line, the operating point is so finely regulated in accordance with consumer agreements that virtually no experimental ‘excitation’ of the system can take place.

The fabrication of a scale model of a multi-machine power system in a laboratory environment is a complex and expensive option. To be of any practical use, the system must replicate the combined behaviour of more than one synchronous generator, transformers, transmission lines and, particularly for the study of torsional interaction, the mechanical characteristics and damping mechanism of steam turbines. More modern systems bring the added complication of power electronic based equipment such as the Static Var compensator. It is not surprising therefore that very few such scale models have been reported in power systems research literature.

A more appropriate option has been the use of power system simulators in which the behaviour of most or all of the power system components are synthesised electronically. Originally, the simulators were analogue in nature but these have since been superseded by all-digital, software based non-linear simulation packages. Having been

validated many times over by researchers studying many fields of power systems research, these tools now commonly form the basis for the validation of power system theory and analysis.

7.2 NON-LINEAR SIMULATION OF THE SERIES COMPENSATED SYSTEM

For the purpose of validation, the non-linear time-domain simulation package PSCAD/EMTDC [65] was employed for the detailed simulation of the combined synchronous machine and mechanical shaft train dynamics when coupled to the compensated transmission line system illustrated in Figure 7.1.

The system consists of a 892MVA synchronous machine operating on full-load, coupled to a six mass turbine system, which is feeding a single compensated line. A step-up transformer raises the voltage from $26kV_{LL}$ at the machine terminals to a system voltage of $500kV_{LL}$. The operating point of the machine is dictated by the magnitude and phase of the voltage source which terminates the transmission line.

The machine model is consistent with that used throughout the study of complex torque coefficients and has the configuration of 1 damper winding on the direct-axis and two damper windings on the quadrature-axis. Because only the fundamental concepts are being proven, the additional dynamics of machine excitation systems and turbine governor systems have not being included. Table 7.1 states the electrical parameters of the machine. Table 7.2 states the turbine-generator inertia, stiffness and steam viscous damping coefficients. Mutual damping components between the masses have been neglected as has material hysteretic damping.

The system is initialised during the first 0.5 seconds of the simulation during which time the machine is represented by a simple voltage source which is ramped up to the specified terminal voltage. At time equal to 0.5 seconds, the machine electrical dynamics are switched in. The mechanical shaft dynamics are released after 1 second. After 1.5 seconds, a three-phase to ground fault of 0.05s duration is applied to the transmission line in order to excite the system into oscillation. Immediately after the fault has been applied, the rate of decay of the torque oscillations is dictated by the induction generator effect discussed in §4.1.2. in which the effective resistance to subsynchronous currents flowing in the stator windings is very low leading to larger time constants for decay of the principle oscillations.

When the fault is removed, the effective resistance increases and the initial oscillations of the rotor will decay more quickly. When the subsynchronous currents in the stator windings due to the fault have decayed, the system behaviour is dictated by the mechanism of torsional interaction.

Table 7.1 : Machine electrical parameters

<i>Apparent Power</i>	<i>MVA</i>	892.4
<i>Number of poles</i>		2
<i>System Frequency, f_s</i>	<i>Hz</i>	50.0
<i>Direct-axis</i>		
<i>Synchronous reactance, X_d</i>	<i>p.u.</i>	1.952
<i>Transient reactance, X'_d</i>	<i>p.u.</i>	0.275
<i>Subtransient reactance, X''_d</i>	<i>p.u.</i>	0.227
<i>Transient short-circuit time constant, T'_d</i>	<i>s</i>	0.793
<i>Subtransient short-circuit time constant, T''_d</i>	<i>s</i>	0.019
<i>Stator resistance, R_a</i>	<i>p.u.</i>	0.0036
<i>Leakage reactance, X_a</i>	<i>p.u.</i>	0.17
<i>Quadrature-axis</i>		
<i>Transient reactance, X_q</i>	<i>p.u.</i>	1.858
<i>Subtransient reactance, X'_q</i>	<i>p.u.</i>	0.29
<i>Sub-subtransient reactance, X''_q</i>	<i>p.u.</i>	0.235
<i>Subtransient short-circuit time constant, T'_q</i>	<i>s</i>	0.223
<i>Sub-subtransient short-circuit time constant, T''_q</i>	<i>s</i>	0.027

All constants have been normalised on generator apparent power rating of 892.4 MVA and base voltage of 26kV_{L-L}.

Table 7.2 : Rotor Inertias and stiffnesses

<i>Inertia, MW-s/MVA</i>	
<i>HP turbine</i>	0.104
<i>IP turbine</i>	0.284
<i>LPa turbine</i>	1.558
<i>LPb turbine</i>	1.54
<i>Generator</i>	0.727
<i>Exciter</i>	0.021
<i>Stiffness, MW/MVA-rad</i>	
<i>HP/IP</i>	39.5
<i>IP/LPa</i>	105.7
<i>LPa/LPb</i>	113.6
<i>LPb/Gen</i>	86.2
<i>Gen/Exc</i>	32.1
<i>Torque sharing, %</i>	
<i>HP Turbine</i>	30.0
<i>IP Turbine</i>	26.0
<i>LP1 Turbine</i>	22.0
<i>LP2 Turbine</i>	22.0
<i>Damping*, MW-s/MVA-rad</i>	
<i>HP Turbine</i>	0.002
<i>IP Turbine</i>	0.002
<i>LP1 Turbine</i>	0.002
<i>LP2 Turbine</i>	0.002
<i>Generator</i>	0.002

All constants have been normalised on machine apparent power rating of 892.4MVA. Base angular velocity is 314.14rad/s.

*Damping coefficients correspond to steam viscous damping acting on each turbine

7.2.1 Case I — 50% Line Compensation

Figure 7.2 illustrates the complex torque coefficient analysis for the specific case of 49% transmission line compensation for the system illustrated in Figure 7.1. Although the electrical and mechanical resonant frequencies differ by approximately 1.5Hz the complex torque analysis indicates that the negative electromagnetic damping induced by the resonant electrical system, indicated by curve A, falls on a region of low mechanical damping in the vicinity of the 31.5Hz shaft mode such that a build-up of shaft oscillations will take place. With the turbine inertia data stated in Table 7.2 and using Eqn. [4.19], the modal inertias of the first three shaft modes can be calculated to be 1.678s, 2.191s, and 23.981s respectively. The time constant of the rate of build-up of the oscillations can be calculated from Eqn. [4.18]. At this operating point, the electromagnetic damping is -12.0 p.u. at the 31.5Hz rotor oscillation frequency. The corresponding steam viscous damping coefficient has a value of 3.8 p.u. at this frequency. For a modal inertia of 2.191s corresponding to the 31.5Hz shaft mode, the resulting oscillations will increase with a time constant of approximately 1.07s.

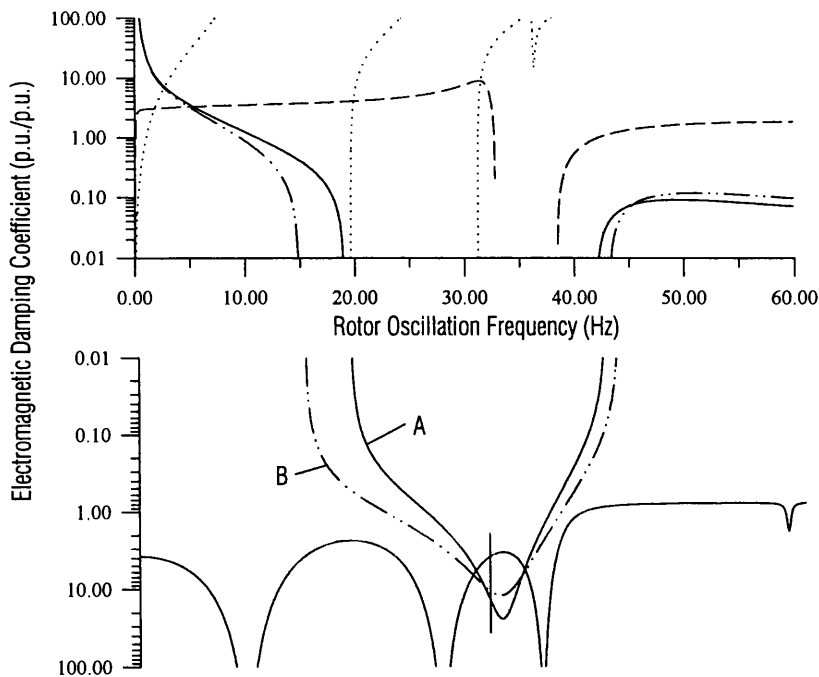


Figure 7.2: Torque coefficient analysis for Case I – 50% compensation
 — Curve A corresponds to nominal transmission line resistance
 — Curve B corresponds to 150% of nominal transmission line resistance
 Synchronising and Damping Coefficients have been normalised on a machine apparent power rating of 892MVA.

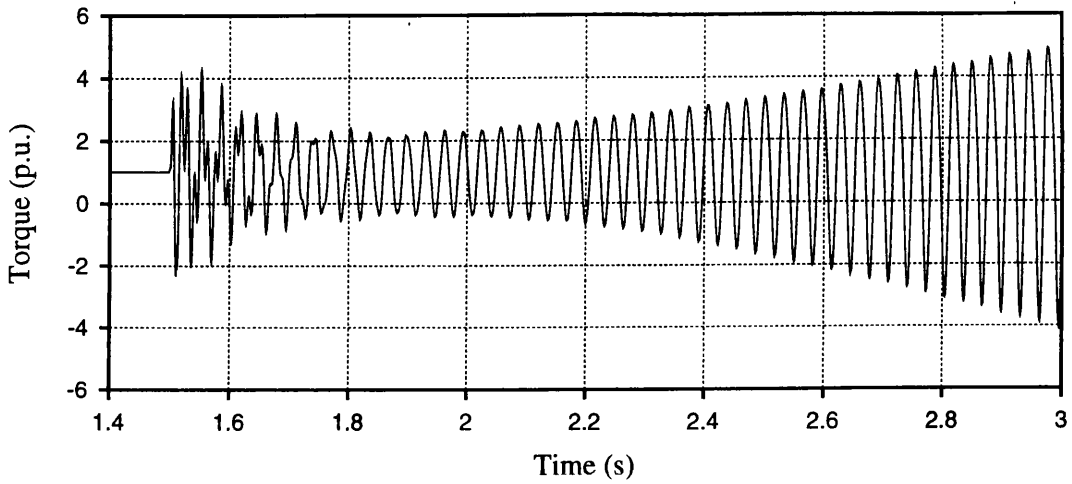


Figure 7.3: Electromagnetic Torque – 50% compensation

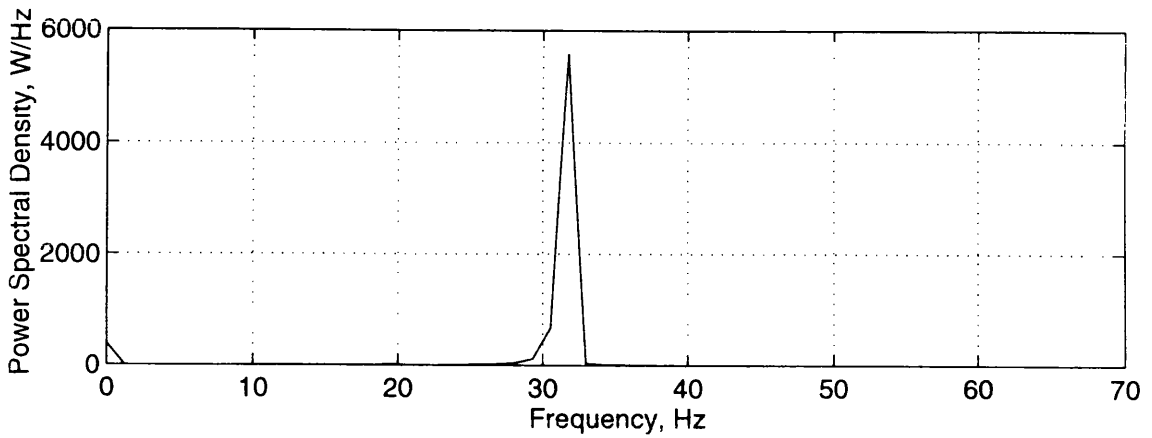


Figure 7.4: Power Spectral Density of torque waveform at 50% compensation

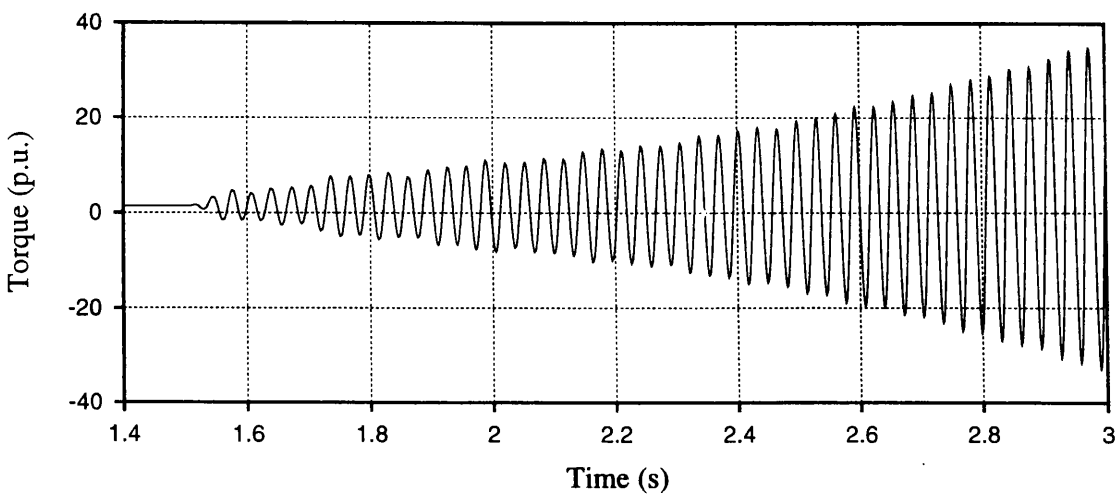


Figure 7.5: LPA-LPB Shaft section torque – 50% compensation

Figure 7.3 illustrates the electromagnetic torque computed from a time-domain simulation of the system at this operating point. A fourier analysis of this waveform, as depicted in Figure 7.4, indicates that the dominant components of the oscillatory torque are at 31.5Hz, due to the mechanical resonant mode, and 32.5Hz, due to the electrical system resonant frequency given by Eqn. 4.3. The torque in this waveform is unstable and is building up at a rate of approximately 1.09s (estimated by inspection of the curve between the 2.0s and 3.0s instants). This shows good agreement with the complex torque coefficient predictions.

If the line resistance is increased by 10%, the system experiences more positive damping and as a result the torque oscillations will increase with a longer time constant as depicted by Figure 7.2 curve B and confirmed by the electromagnetic torque waveform in Figure 7.7 below.

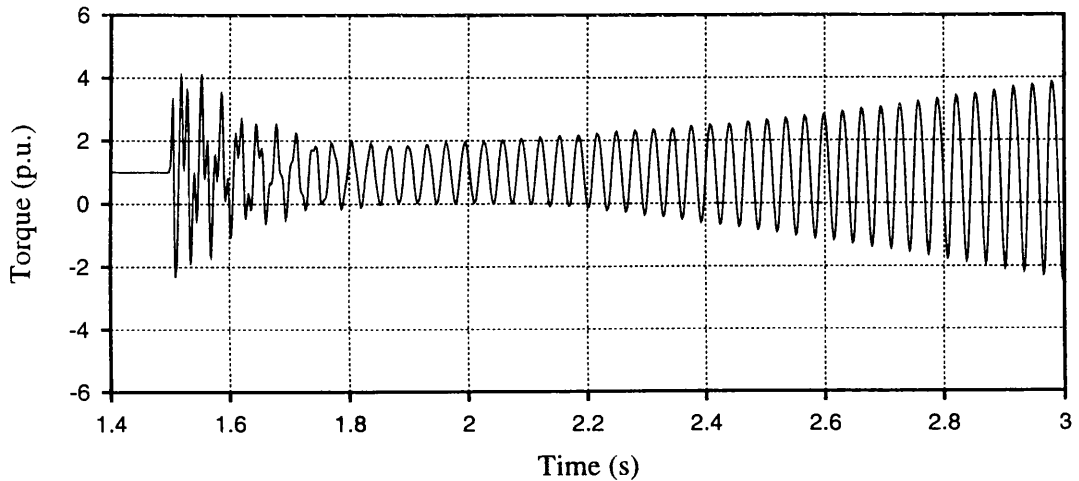


Figure 7.6: Electromagnetic Torque waveform for Case I with increased transmission line resistance

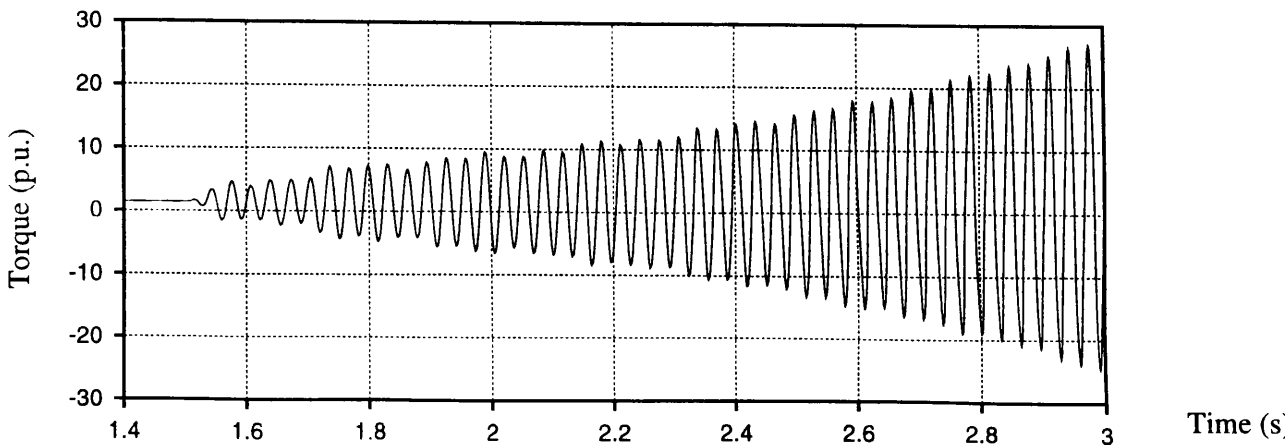
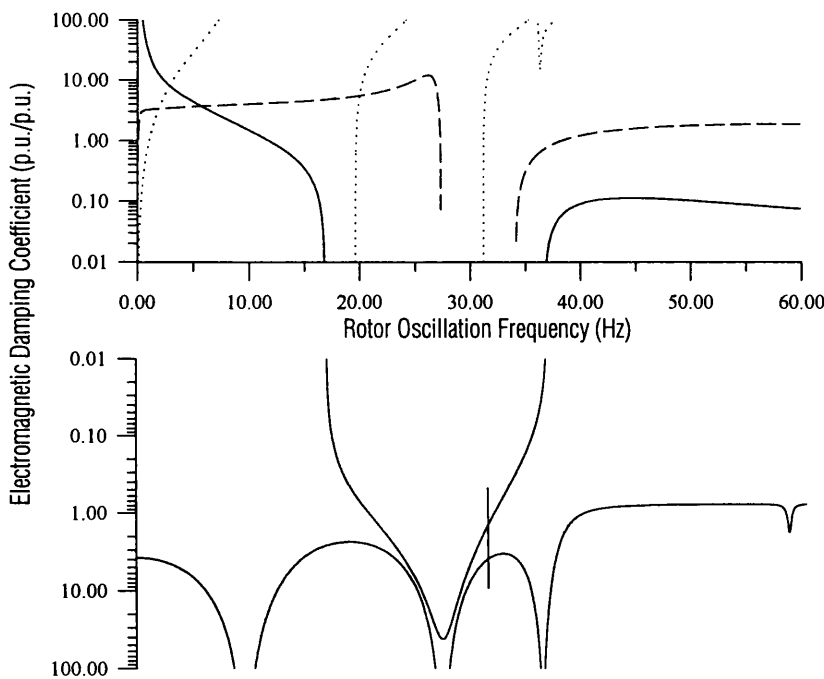


Figure 7.7: LPA-LPB Shaft section torque corresponding to electromagnetic torque excitation illustrated in Figure 7.6

7.2.2 Case II — 70% Line Compensation

Figure 7.8 illustrates the complex torque coefficient analysis for the specific case of 70% transmission line compensation. At this operating point the negative region of electromagnetic damping, which peaks at 27 Hz, falls within a corresponding region of high steam viscous damping. The sum of the electromagnetic and steam viscous damping components yields a net positive damping of approximately 2.6 p.u. As a result, the torque oscillations would be expected to decay with a time constant of approx. 3.4s.

The time-domain simulation of this operating point is illustrated in Figure 7.9. The fourier plot depicted in Figure 7.11 indicates that the dominant frequency of oscillation corresponds to the electrical resonant frequency of this operating point at 27.5Hz. The shaft resonant modes are also visible at 1.5Hz, 20.0Hz and 31.5Hz. After the initial torque oscillations due to the fault have decayed, the oscillations continue to decay. Clearly then, the system is positively damped, even though the compensation level is relatively high. Accurate estimation of the time constant of decay is difficult in this case due to the absence of any significant oscillations.



Synchronising and Damping Coefficients have been normalised on a machine apparent power rating of 892MVA.

Figure 7.8: Torque coefficient analysis for Case II – 70% compensation

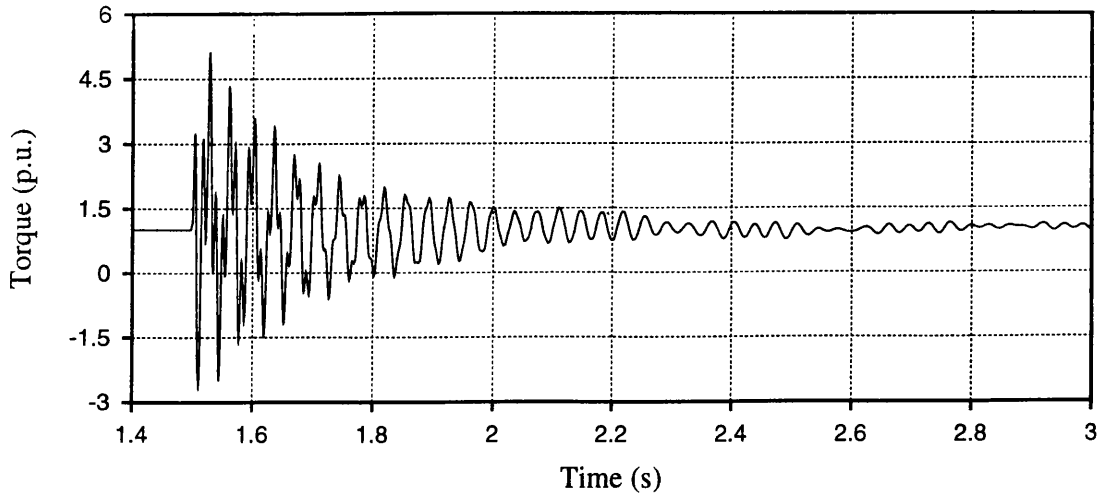


Figure 7.9: Electromagnetic torque for Case II – 70% compensation

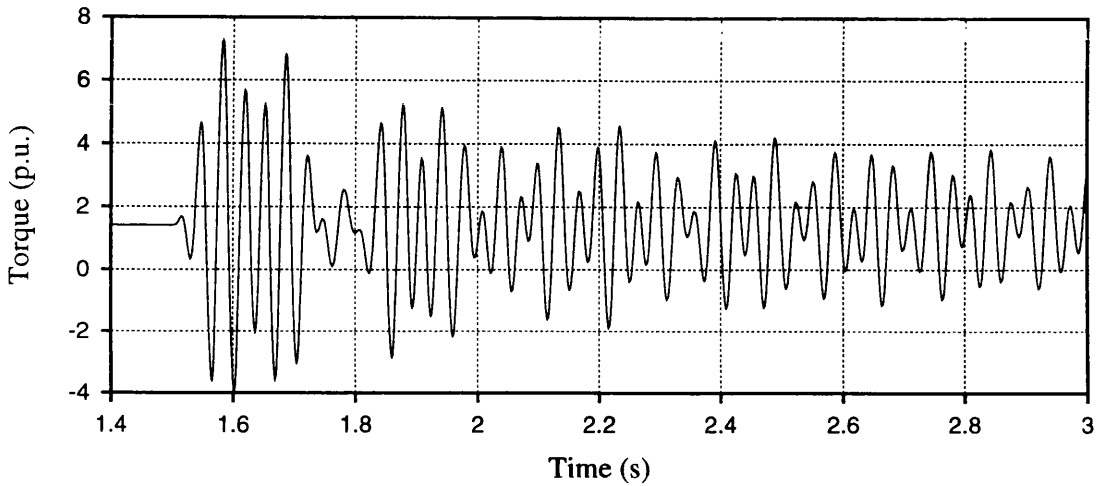


Figure 7.10: LPA-LPB Shaft section torque – 70% compensation

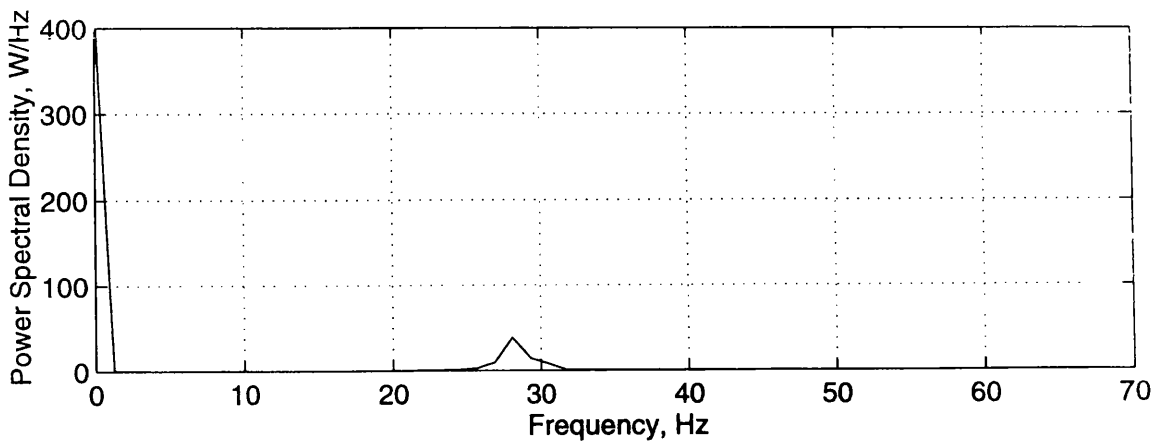
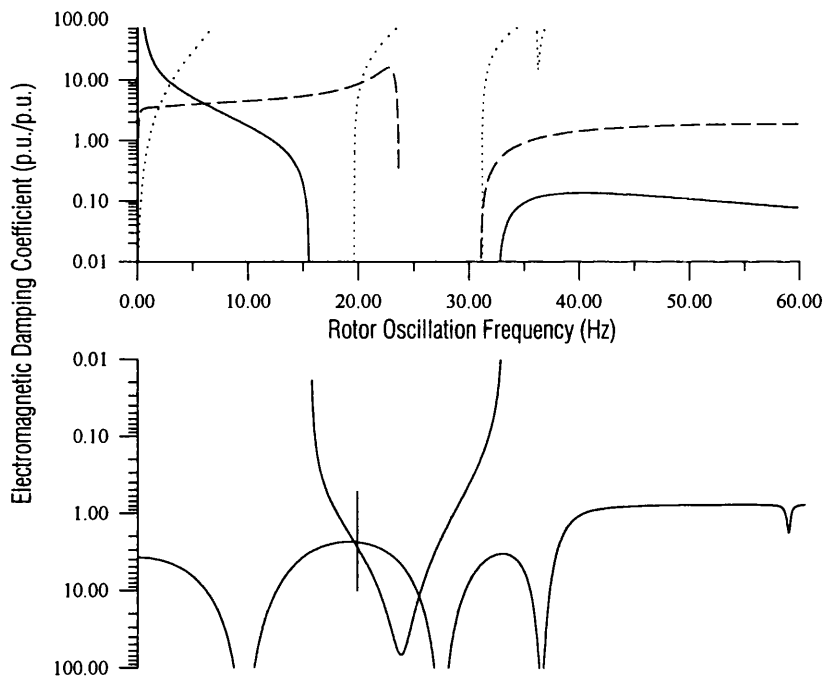


Figure 7.11: Power Spectral Density of torque waveform at 70% compensation

7.2.3 Case III — 91% Line Compensation

Although not a truly practical case given the very high level of compensation, this scenario will be examined to complete the scan of possible operating points at which interaction could occur for this particular system.

The frequency domain-approach, Figure 7.12, indicates that this operating point is just over the point of sustained oscillations — that is oscillations that are neither increasing or decreasing in amplitude — at the 20.5Hz shaft mode even though the electrical resonant frequency is somewhat distant at 22.5Hz. Time domain simulation of this operating point, depicted in Figure 7.13, indicates that the system is marginally stable. Increasing the compensation to 92% however does result in an unfavourable interaction as depicted by Figure 7.15.



Synchronising and Damping Coefficients have been normalised on a machine apparent power rating of 892MVA.

Figure 7.12: Torque Coefficient analysis for Case III—91% compensation

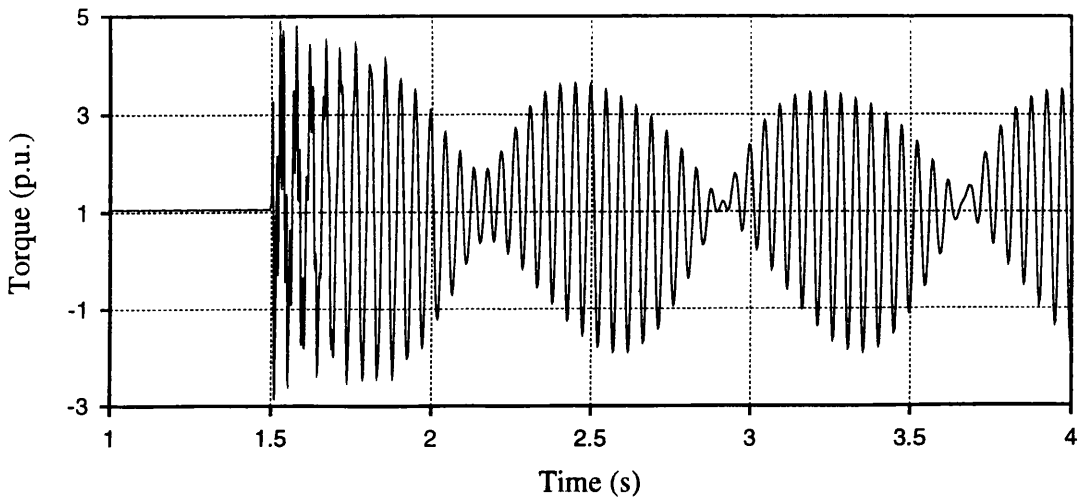


Figure 7.13: Electromagnetic torque due to 91% compensation

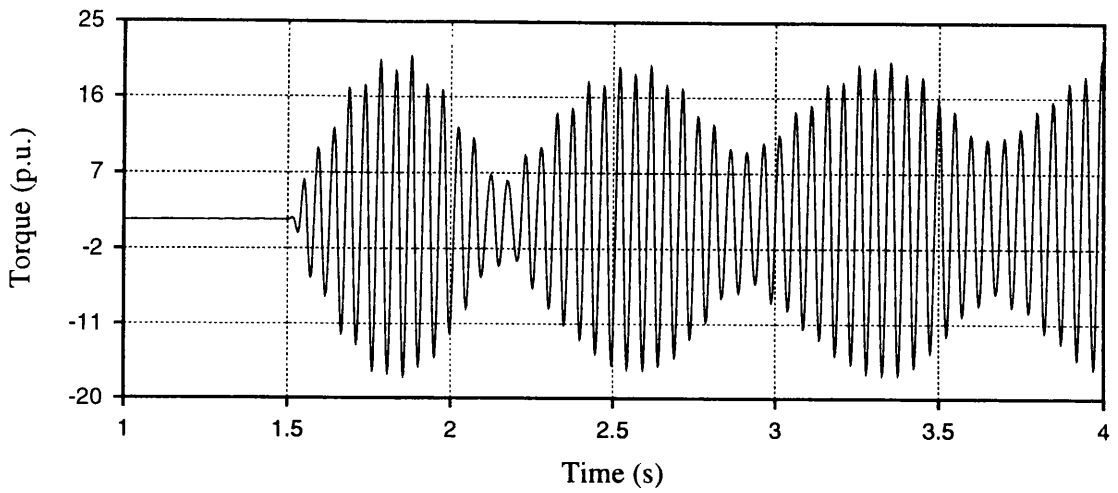


Figure 7.14: LPA-LPB Shaft section torque - 91% compensation

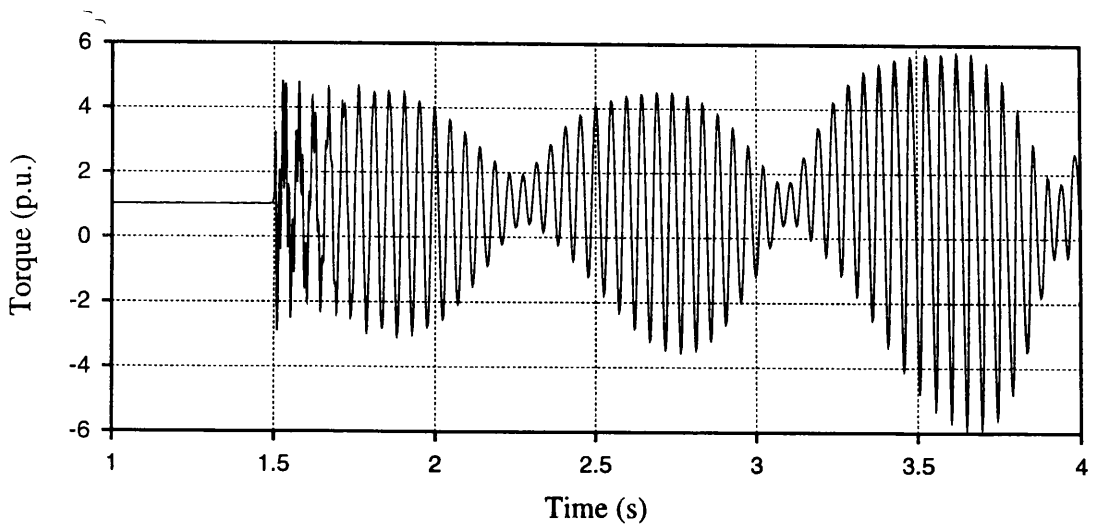


Figure 7.15: Electromagnetic torque due to 92% compensation

7.3 SUMMARY OF CHAPTER 7

This Chapter has verified the method of Complex Torque Coefficient analysis as applied to the prediction of torsional interaction for a range of scenarios within the single machine—capacitor compensated system.

The verification was based on the use of a detailed time domain simulation of the power system using the PSCAD/EMTDC software package.

Within the obvious modelling limitations in comparison with the non-linear time domain simulation, it has been demonstrated that the explicit separation of the electrical and mechanical systems as an aid to visualisation of the complex mechanisms governing the behaviour of the system does not invalidate the analysis as compared with other frequency domain approaches, for example, eigenanalysis, which relies on the mathematical description of the system being arranged into a single unified system matrix. Ease of visualisation aside, the two frequency domain methods are equivalent.

**TORSIONAL STRESSING DUE TO HVDC
CONVERTERS****8.1 INTRODUCTION**

Ripple currents on the DC side of both HVDC asynchronous and synchronous links can, in some circumstances, excite onerous torsional vibrations in large steam-generator-exciter shafts. This problem has assumed increased importance in recent years on account of the increasing number of AC/DC/AC couplers being installed, for example to interconnect the East and West European Grid Systems. This chapter discusses the excitation of torsional vibrations in turbine-generator-exciter shafts that are in close proximity to HVDC converter stations. In common with the torsional analysis discussed in previous chapters relating to subsynchronous resonance, multi-machine effects and Static Var Compensators, the problem will be investigated by examining the electrical and mechanical viscous damping coefficients of the synchronous machine at frequencies corresponding to those theoretically produced by the HVDC converter.

8.2 EXCITATION BY NON-CHARACTERISTIC FREQUENCIES

There are two types of HVDC schemes: synchronous and asynchronous. HVDC schemes which are connected in parallel with an AC line (coupled to both ends) should not generally give rise to enhanced values of characteristic harmonics [60,61]. Indeed the presence of a synchronous scheme generally improves the stability of the system [40]. However, all asynchronous types connecting AC systems of different frequencies and also connecting systems of the same nominal frequency could cause problems on turbine-generator-exciter shafts where the machine is electrically close [60,62]. It is essentially a steady state problem where modest torques acting on the generator rotor can excite sympathetic vibrations in the machine shaft. Amplitude of modal shaft torque is dependent on mechanical viscous damping and electrical damping which acts on each section of the shaft. The amplitude varies significantly from vibration to vibration, with shaft location, and with machine load.

A consequence of operating rectifier and inverter stations asynchronously is that small amounts of non-characteristic frequencies are produced by the converter. These take the form of currents which on the AC side can be considered as a current source which has frequencies which are not integer harmonics of the supply frequency. These noncharacteristic frequencies can be above or below the supply frequency [60] i.e. supersynchronous or subsynchronous. It is the subsynchronous frequencies that can give rise to torsional oscillations of the turbine-generator-exciter shaft.

8.2.1 Non-characteristic frequencies

Consider a 12-pulse asynchronous HVDC scheme which connects two systems with nominal frequencies of ω_1 and ω_2 , as illustrated in Figure 8.1. The rectifier will be subjected to small amounts of ripple current from the inverter. In general, the expected harmonics on the AC side of the rectifier can be derived from:

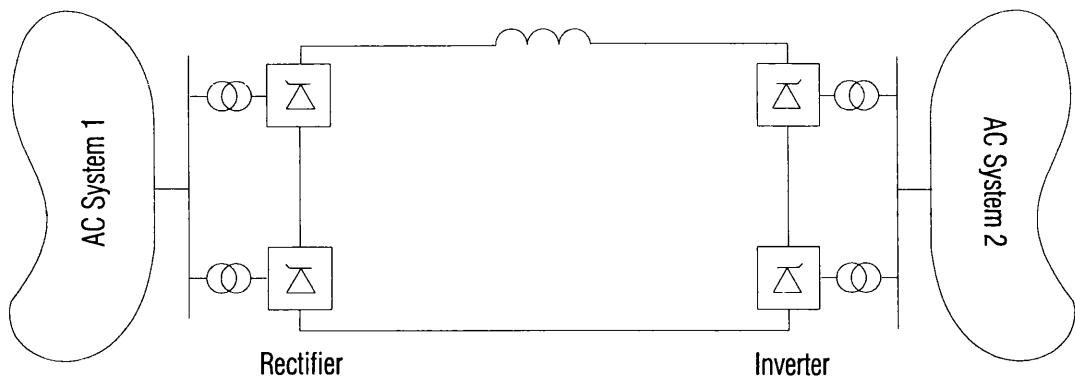


Figure 8.1: Asynchronous HVDC Link

$$\begin{aligned}
 I_{ac_1}(t) = & \left[I_d + b \sin(12\omega_2 t + \beta_{12}) + c \sin(24\omega_2 t + \beta_{24}) + d \sin(36\omega_2 t + \beta_{36}) + \dots \right] \\
 & \cdot \left[\cos(\omega_1 t) - \frac{1}{11} \cos(11\omega_1 t) + \frac{1}{13} \cos(13\omega_1 t) - \frac{1}{23} \cos(23\omega_1 t) + \right. \\
 & \left. \frac{1}{25} \cos(25\omega_1 t) - \frac{1}{35} \cos(35\omega_1 t) + \frac{1}{37} \cos(37\omega_1 t) + \dots \right] \quad [8.1]
 \end{aligned}$$

Eqn. [8.1] yields

$$\begin{aligned}
I_{ac_1}(t) = & kI_d(\text{theoreticals}) + k \frac{b}{2} [\sin(\omega_1 t + 12\omega_2 t + \beta_{12}) - \sin(\omega_1 t - 12\omega_2 t - \beta_{12})] \\
& - k \frac{b}{22} [\sin(11\omega_1 t + 12\omega_2 t + \beta_{12}) - \sin(11\omega_1 t - 12\omega_2 t - \beta_{12})] \quad (i) \\
& + k \frac{b}{26} [\sin(13\omega_1 t + 12\omega_2 t + \beta_{12}) - \sin(13\omega_1 t - 12\omega_2 t - \beta_{12})] \quad (ii) \\
& - k \frac{c}{46} [\sin(23\omega_1 t + 24\omega_2 t + \beta_{24}) - \sin(23\omega_1 t - 24\omega_2 t - \beta_{24})] \quad (iii) \\
& + k \frac{c}{50} [\sin(25\omega_1 t + 24\omega_2 t + \beta_{24}) - \sin(25\omega_1 t - 24\omega_2 t - \beta_{24})] \quad (iv) \\
& - k \frac{d}{70} [\sin(35\omega_1 t + 36\omega_2 t + \beta_{36}) - \sin(35\omega_1 t - 36\omega_2 t - \beta_{36})] \quad (v) \\
& + k \frac{d}{74} [\sin(37\omega_1 t + 36\omega_2 t + \beta_{36}) - \sin(37\omega_1 t - 36\omega_2 t - \beta_{36})] \quad (vi)
\end{aligned}
\tag{8.2}$$

Eqn. [8.2] is applicable to asynchronous systems which connect systems of the same nominal frequency i.e. 50Hz/50Hz or systems of different nominal frequencies i.e. 50Hz/60Hz. Examination of the equation shows that two types of frequency component exist in the asynchronous operation of HVDC converters, namely (i) the sum and (ii) the difference terms.

8.2.2 Modulation frequencies for a 50Hz/60Hz Asynchronous System

Table 8.1 gives modulation product frequencies for a HVDC link which connects systems at 50Hz and 60Hz respectively. The frequencies relate to modulation product harmonics which are injected into the 50Hz and 60Hz systems respectively. The frequencies at which sympathetic shaft torsional vibrations would be excited are given by the difference between the modulation product harmonic frequency and that which corresponds to the respective system supply. Thus, the 70Hz modulation product frequency which is superimposed on the 50Hz system will excite torsional vibrations at 20Hz on the shaft while no subsynchronous vibrations would be excited on the 60Hz system.

Table 8.1 : Modulation Product Harmonics for a 50Hz/60Hz HVDC Link

Equation	50Hz System		60Hz System	
	Modulation frequency, Hz	Rotor Torque frequency, Hz	Modulation frequency, Hz	Rotor Torque frequency, Hz
(i)	170.0	120.0	60.0	0.0
(ii)	70.0	20.0	180.0	120.0
(iii)	290.0	240.0	180.0	120.0
(iv)	190.0	140.0	300.0	240.0
(v)	410.0	360.0	300.0	240.0
(vi)	310.0	260.0	420.0	360.0

8.2.3 Modulation frequencies for a 50Hz/50Hz asynchronous System

Table 8.2 gives the modulation product harmonic frequencies for a nominal 50Hz/50Hz asynchronous system for the specific operating point defined as system A operating at 49.75Hz and system B operating at 50.5Hz. On examination of the Table, it will be noted that the modulation product harmonics produced for this configuration could excite subsynchronous torsional oscillations in either AC system.

Table 8.2 : Modulation Product harmonics for a 49.75Hz/50.5Hz HVDC Link

Equation	49.75Hz System		50.5Hz System	
	Modulation frequency, Hz	Rotor Torque frequency, Hz	Modulation frequency, Hz	Rotor Torque frequency, Hz
(i)	58.75	9.00	41.50	9.00
(ii)	40.75	9.00	59.50	9.00
(iii)	67.75	18.00	32.50	18.00
(iv)	31.75	18.00	68.50	18.00
(v)	76.75	27.00	23.50	27.00
(vi)	22.75	27.00	77.50	27.00

Table 8.3 : Generator Constants and Steam Torque Data

Machine	A	B	C	D	D	D
<i>Model</i>	<i>(1d,1q)</i>	<i>(1d,1q)</i>	<i>(1d,1q)</i>	<i>(2d,3q)</i>	<i>(1d,2q)</i>	<i>(1d,1q)</i>
<i>Rated Power MW</i>	660	982	1300	500	500	500
<i>Rated Power MVA</i>	767	1155	1530	590	590	590
<i>Number of Poles</i>	2	2	2	2	2	2
<i>Supply Frequency, Hz</i>	50	50	50	60	60	60
<i>Magnetising reactance saturation constant k1</i>	0.21	0.21	0.174	0.087	0.087	0.087
<i>Magnetising reactance saturation exponent n</i>	7.70	7.70	6.08	4.36	4.36	4.36
<i>Generator constants:</i>						
<i>Direct-axis synchronous reactance X_d, p.u.</i>	1.780	1.944	2.340	1.770	1.770	1.770
<i>Quadrature-axis synchronous reactance X_q, p.u.</i>	1.690	1.902	2.280	1.650	1.650	1.650
<i>Stator leakage reactance X_σ, p.u.</i>	0.212	0.160	0.150	0.155	0.155	0.155
<i>Field leakage reactance X_f, p.u.</i>	0.061	0.129	0.150	0.245	0.184	0.184
<i>Direct-axis damper leakage reactance X_{kd1}, p.u.</i>	0.013	0.072	0.078	0.455	0.430	0.430
<i>Direct-axis damper leakage reactance X_{kd2}, p.u.</i>	-	-	-	1.039	-	-
<i>Quadrature-axis damper leakage reactance X_{kq1}, p.u.</i>	0.010	0.045	0.046	0.121	0.261	0.188
<i>Quadrature-axis damper leakage reactance X_{kq2}, p.u.</i>	-	-	-	0.509	0.674	-
<i>Quadrature-axis damper leakage reactance X_{kq3}, p.u.</i>	-	-	-	1.126	-	-
<i>Direct-axis mutual leakage reactance X_{mdf}, p.u.</i>	0.0	0.0	0.0	-0.069	-0.021	-0.021
<i>Stator resistance R_a, p.u.</i>	0.002	0.002	0.002	0.002	0.002	0.002
<i>Field resistance R_f, p.u.</i>	0.001	0.001	0.001	0.001	0.001	0.001
<i>Direct-axis damper resistance R_{kd1}, p.u.</i>	0.007	0.017	0.024	0.435	0.060	0.060
<i>Direct-axis damper resistance R_{kd2}, p.u.</i>	-	-	-	0.042	-	-
<i>Quadrature-axis damper resistance R_{kq1}, p.u.</i>	0.023	0.024	0.030	0.247	0.090	0.079
<i>Quadrature-axis damper resistance R_{kq2}, p.u.</i>	-	-	-	0.054	0.015	-
<i>Quadrature-axis damper resistance R_{kq3}, p.u.</i>	-	-	-	0.149	-	-
<i>Steam Torque, * p.u. at rated MVA unity p.f. load:</i>						
<i>HP turbine</i>	0.278	0.278	0.240	0.248	0.248	0.248
<i>IP turbine</i>	0.358	0.313	0.34	0.361	0.361	0.361
<i>LP1f turbine</i>	0.092	0.100	0.140	0.097	0.097	0.097
<i>LP1r turbine</i>	0.090	0.100	0.140	0.098	0.098	0.098
<i>LP2f turbine</i>	0.091	0.100	0.070	0.098	0.098	0.098
<i>LP2r turbine</i>	0.091	0.100	0.070	0.098	0.098	0.098

All constants are normalised on machine apparent power rating. *Damping coefficients are given by normalised steam torque divided by $2p\omega_s$. Steam viscous damping which acts at each turbine is given by the appropriate damping coefficient multiplied by the normalised generator output power.

Table 8.4 : Rotor Inertias and Stiffnesses

Machine	A	B	C	D
<i>Inertia, MW-s/MVA</i>	3.440	4.443	3.671	4.477
<i>HP turbine</i>	0.072	0.059	0.053	0.051
<i>IP turbine</i>	0.314	0.216	0.180	0.215
<i>LP1f turbine</i>	0.573	0.836	0.792	0.843
<i>LP1r turbine</i>	0.570	0.839	0.793	0.843
<i>LP2f turbine</i>	0.574	0.836	0.394	0.840
<i>LP2r turbine</i>	0.570	0.836	0.395	0.839
<i>LP1f blades</i>	-	-	0.100	-
<i>LP1r blades</i>	-	-	0.100	-
<i>LP2f blades</i>	-	-	0.050	-
<i>LP2r blades</i>	-	-	0.050	-
<i>Generator</i>	0.698	0.767	0.707	0.828
<i>Exciter 1</i>	0.017	0.026	0.057	0.020
<i>Exciter 2</i>	0.052	0.027	-	-
<i>Stiffness, MW/MVA-rad</i>				
<i>HP/IP</i>	48.5	37.5	37.2	25.8
<i>IP/LP1f</i>	106.0	82.5	71.1	105.8
<i>LP1f/LP1r</i>	3940.0	3364.0	70.8	2731.0
<i>LP1r/LP2f</i>	93.0	81.3	73.0	132.4
<i>LP2f/LP2r</i>	3990.0	3387.4	1207.0	2731.0
<i>LP2r/GEN</i>	58.3	53.9	47.2	99.4
<i>GEN/EX1</i>	28.5	13.9	16.0	4.56
<i>EX1/EX2</i>	38.6	39.2	-	-
<i>LP1f/blades</i>	-	-	303.8	-
<i>LP1r/blades</i>	-	-	303.8	-
<i>LP2f/blades</i>	-	-	152.1	-
<i>LP2r/blades</i>	-	-	152.1	-

All constants are normalised on machine apparent power rating.

8.3 MODAL SHAFT TORQUE DUE TO STEADY RESONANT EXCITATION

A mathematical model of the generator with (2d,3q) and reduced damper models is employed for simulation of the machine [63]. Discrete mass models of the turbine-generator-exciter shaft are employed to evaluate the torque at specific positions along the turbine-generator-exciter shaft. Modal torque due to steady resonant excitation is evaluated using the algorithms discussed in Appendix C. Analysis is performed on 4 machines, Machine A, Machine B, Machine C and Machine D which are rated at 660MW, 1000MW, 1300MW and 500MW respectively. Modelling detail on Machine D is varied from a (1d,1q) representation to a (2d,3q) representation. Machine data is indicated in Table 8.3. Rotor inertias and shaft stiffnesses are indicated in Table 8.4.

8.3.1 660MW Machine A

Table 8.5 depicts amplitude of modal torque at shaft couplings of the 660MW machine A following a continuous torque excitation of 0.004p.u. applied to the generator rotor. Amplitudes relate to torque excitation at different modal frequencies. They correspond to assumptions where amplitude of torque pulsations are limited by both steam viscous and electrical damping.

Material hysteretic damping is ignored. The machine is assumed to be operating at full-load.

Table 8.5 shows that for torque pulsations which correspond to the frequency of the rotor swing, amplitude of torque at the LP1R/LP2F, IP/LP1F, and HP/IP couplings decreases almost directly as inertia of the rotor to be accelerated is decreased.

Table 8.5 also shows that amplitude of modal torque for this torque excitation of 0.004p.u. varies significantly from vibration to vibration. Electrical damping is the effective mechanism for limiting shaft torque for the vibration which corresponds to rotor swing, but its effect becomes insignificant at the higher frequencies of torsional vibration of the shaft, and may in fact become slightly negative at the higher frequencies as was illustrated in an earlier chapter.

Table 8.6 depicts corresponding amplitude of modal torque at shaft couplings of the same machine when the generator operates on no-load. In this case, there is no steam viscous damping. Comparison of amplitude of the 37.92Hz pulsation is much more onerous on no-load. This is on account of electrical damping for this vibration being extremely small. The electrical damping is more effective when the generator operates at a

small load angle. The difference in amplitude of modal torque at full-load and no-load is of particular note.

Table 8.5 : Shaft Torques for 0.004p.u. Torque Excitation Acting on Generator Rotor -- 660MW Machine A at Full-load

Frequency, Hz	0.924	16.21	26.81	35.59	37.92
Location	<i>STEAM AND ELECTRICAL DAMPING</i>				
HP/IP	0.0003	0.0609	0.0854	0.4137	0.0256
IP/LP1f	0.0014	0.3246	0.3602	1.3779	0.0781
LP1r/LP2f	0.0052	1.0302	0.6467	1.226	0.0362
LP2r/GEN	0.0092	0.8843	0.5176	1.6144	0.0101
GEN/EX	0.0003	0.1033	0.1131	3.4834	0.0049

Torque in p.u. on machine rating.

$P_o=0.860p.u.$, $Q_o=0.510p.u.$, at Full-load. $V_r=1.0p.u.$ Impedance stator terminals to infinite busbar (0.002+j0.170)p.u.

Table 8.6 : Shaft Torques for 0.004p.u. Torque Excitation Acting on Generator Rotor -- 660MW Machine A at No-load

Frequency, Hz	0.790	16.21	26.81	35.59	37.92
Location	<i>ELECTRICAL DAMPING ONLY</i>				
HP/IP	0.0	0.0351	0.4135	0.4224	11.6663
IP/LP1f	0.0005	0.1740	1.7468	1.4070	35.6032
LP1r/LP2f	0.0024	0.5524	3.1369	0.1259	16.5304
LP2r/GEN	0.0041	0.4752	2.5084	1.6500	4.6010
GEN/EX	0.0	0.0552	0.5469	3.5634	2.2091

Torque in p.u. on machine rating.

$P_o=0.000p.u.$, $Q_o=0.000p.u.$, at Full-load. $V_r=1.0p.u.$ Impedance stator terminals to infinite busbar (0.002+j0.170)p.u.

Table 8.7 : Shaft Torques for 0.004p.u. Torque Excitation Acting on Generator Rotor -- 1000MW Machine B at Full-load

Frequency, Hz	0.803	14.486	22.634	32.183	35.034
Location	<i>STEAM ELECTRICAL DAMPING</i>				
HP/IP	0.0003	0.0307	0.0761	0.2400	0.0041
IP/LP1f	0.0008	0.1539	0.2982	0.7570	0.0120
LP1r/LP2f	0.0052	0.8992	1.2134	0.7087	0.0030
LP2r/GEN	0.0098	0.6508	1.1120	3.1029	0.0054
GEN/EX	0.0003	0.0285	0.1479	6.6497	0.003

Torque in p.u. on MVA rating

$P_o=0.850p.u.$, $Q_o=0.526p.u.$, at Full-load. $V_r=1.0p.u.$ Impedance stator terminals to infinite busbar (0.002+j0.170)p.u.

Table 8.8 : Shaft Torques for 0.004p.u. Torque Excitation Acting on Generator Rotor -- 1000MW Machine B at No-load

Frequency, Hz	0.660	14.486	22.634	32.183	35.034
Location	<i>ELECTRICAL DAMPING ONLY</i>				
HP/IP	0.0	0.0177	0.0908	0.0876	29.680
IP/LP1f	0.0003	0.0772	0.3561	0.2767	85.460
LP1r/LP2f	0.0024	0.4512	1.4491	0.2593	20.930
LP2r/GEN	0.0043	0.3281	1.3260	1.1346	3.7564
GEN/EX	0.0	0.0272	0.1759	2.4356	1.0968

Torque in p.u on machine rating.

$P_o=0.000$ p.u., $Q_o=0.000$ p.u., at Full-load. $V_f=1.0$ p.u. Impedance stator terminals to infinite busbar $(0.002+j0.170)$ p.u.

8.3.2 1000MW Machine B

Tables 8.7 and 8.8 give corresponding torques for continuous torque excitations of 0.004p.u. applied to the generator rotor of the 1000MW Machine B. It will be seen that shaft torques are particularly onerous in the case of the 35.03Hz vibration when the generator is operating on the system at no-load. At full-load, shaft torques corresponding to this modal vibration are extremely small.

8.4 GENERATOR SCALING FACTOR (GSF)

This relates to the rate of torque excitation which sets up modal torsional vibrations in the turbine-generator-exciter shaft to the per unit harmonic disturbing current impressed on the generator stator. The factor is frequency dependent and varies with the load conditions of the machine. It is evaluated from the direct- and quadrature-axis equivalent circuits of the generator and two axis currents I_d , I_q , and I_f which define the real and reactive load which is carried by the machine.

The generator scaling factor may be evaluated (a) by assuming harmonic currents are completely reflected at the surfaces of the rotor (Method A), or (b) by using direct- and quadrature-axis equivalent circuits to simulate the rotor of the machine where rotor circuit resistance is neglected (Method B) or (c) by using detailed equivalent circuits where rotor circuit resistance is represented (Method C). Relevant equations for evaluating generator scaling factors are developed in the Appendix C.

Machines A, B, and C -- (1d,1q) Damper Simulation

Table 8.9 illustrates generator scaling factors for the 660MW Machine A, the 1000MW Machine B, and the 1300MW Machine C at (a) full-load and (b) no-load respectively. The damper simulation assume a (1d,1q) configuration.

Table 8.9 : Generator Scaling Factors - Machine A, B, and C

Machine	A [†]		B [‡]		C [‡]	
	Rotor Freq.	GSF	Rotor Freq.	GSF	Rotor Freq.	GSF
<i>Full-load</i>						
Method A	-	1.125	-	1.125	-	1.089
Method B	-	1.131	-	1.150	-	1.116
Method C	16.21	1.168	14.49	1.199	12.60	1.187
	26.81	1.153	22.63	1.181	21.90	1.156
	35.59	1.147	32.18	1.171	30.07	1.144
	37.92	1.146	35.03	1.161	39.67	1.129
	61.05	1.140	61.04		64.66	
<i>No-load</i>						
Method A	-	1.000	-	1.000	-	1.000
Method B	-	1.000	-	1.000	-	1.000
Method C	-	1.000	-	1.000	-	1.000

[†] At Full-load P_o=0.860p.u., Q_o=0.510p.u.

[‡] At Full-load P_o=0.850p.u., Q_o=0.527p.u.

Table 8.10 : Effect of Damper Representation on Generator Scaling Factors -- 500MW Machine D

Damper Representation	(2d,3q)	(1d,2q)	(1d,1q)
<i>Full-load</i>			
Method A [†]	1.091	1.091	1.091
Method B [†]	1.149	1.212	1.212
Method C [‡]			1.315
20.26Hz	1.309	1.283	1.273
31.56Hz	1.283	1.254	1.266
34.60Hz	1.276	1.250	1.256
41.40Hz	1.263	1.242	1.240
63.19Hz	1.230	1.231	
<i>No-load</i>			
Method A	1.000	1.000	1.000
Method B	1.000	1.000	1.000
Method C	1.000	1.000	1.000

[†] All frequencies.

[‡] Rotor vibration frequencies.

Table 8.9 shows that generator scaling factors can typically vary by 20% or more for different rotor vibration frequencies, and as different assumptions for evaluating scaling factors are made.

Machine D - Effect of Damper Simulation

Table 8.10 illustrates the effect damper representation has on generator scaling factors for the 500MW Machine D. Damper representation will be seen to have a small effect on generator scaling factors corresponding to the principle modes of torsional vibrations of the shaft.

8.5 EVALUATION OF SHAFT TORQUES IN MULTI-MACHINE SYSTEMS

HVDC links embedded in multi-machine networks affect generators in close proximity to the converter station. It is necessary to proportion HVDC link disturbance currents to each machine in the network appropriately to determine whether or not a particular generator might be at risk. System network data, fault analysis data, and loadflow data is used to evaluate the proportion of converter station infeed which would be imposed on a particular machine. This scaling factor is calculated for different scenarios of system operation and system load.

8.5.1 System Equivalent Circuit

A single machine-infinite busbar equivalent is employed for the analysis. The impedance between the stator terminals and the infinite busbar is divided into two sections. The converter station is connected to the centre junction of the impedance. The impedance is divided such that the converter station disturbance current is proportioned appropriately to the generator and the system.

8.5.2 System Scaling Factor (SSF)

The ratio of the converter station disturbance current impressed on the generator to the total converter station disturbance current is defined as the system scaling factor. It is expressed in per unit on the generator apparent rating.

System scaling factors for a projected 250MW converter station for different machines in different system operating conditions are given in Table 8.11 . These system

scaling factors are evaluated using the subtransient reactance of the generators. They may be evaluated more accurately using generator impedance to harmonic currents corresponding to each harmonic frequency as summarised in § 8.5.3

Table 8.11 : Typical System Scaling Factors (SSF) - - 250MW Link

Location	System Scaling Factor	
	210MW Machine rating	200MW Machine rating
<i>Ballylumford</i>		
<i>1 x 120MW + 3 x 200MW</i>	0.1465	0.1425
<i>2 x 120MW + 3 x 200MW</i>	0.1347	0.1311
<i>3 x 120MW + 3 x 200MW</i>	0.1245	0.1211
<i>3 x 120MW + 1 x 200MW</i>	0.1645	0.1600
<i>3 x 120MW + 2 x 200MW</i>	0.1417	0.1379
<i>Kilroot</i>		
<i>1x300MW</i>	0.2212	-
<i>2x300MW</i>	0.1133	-

8.5.3 Effect of Damper Representation on Generator Reactance -- 500MW Machine D

Table 8.12 compares the effect damper representation has on effective generator impedance as a function of rotor torque frequency for different damper models of Generator D. Reactances are referred to equivalent values at system supply frequency. Table 8.12 shows that variation of the generator impedance with rotor torque frequency using detailed (2d,3q) and reduced (1d,2q) and (1d,1q) damper representations is of the order of 20%. Variation of generator impedance therefore has a noticeable effect on system scaling factors for Machine D.

Table 8.12 : Effect of Damper Representation on Generator Harmonic Impedance -- 500MW Machine D at Full-load

Damper Representation	(2d,3q)	(1d,2q)	(1d,1q)
Rotor Frequency, Hz	Generator impedance referred to system supply frequency, p.u.		
20.26	-0.0973+j0.3172	-0.0778+j0.3060	-0.1321+j0.3032
31.56	-0.1086+j0.2965	-0.0612+j0.2963	-0.0986+j0.2947
34.60	-0.1110+j0.2917	-0.0582+j0.2950	-0.0932+j0.2937
41.40	-0.1151+j0.2819	-0.0530+j0.2931	-0.0839+j0.2921
63.19	-0.1190+j0.2608	-0.0433+j0.2904	-0.0674+j0.2901
0.92	-0.2209+j0.5173	-0.2439+j0.5070	-0.2218+j0.8954

Reactances expressed as equivalent reactances at system supply frequency.

Resistances and reactances are averaged for the direct- and quadrature-axis equivalent circuits.

Effective generator impedance shown in Table 8.12 is evaluated using classical induction motor theory. Direct- and quadrature-axis equivalent circuits which correspond to frequency of the harmonic impressed on the stator winding where rotor circuit resistance is divided by slip given the difference between harmonic frequency impressed on the generator stator winding and speed of the generator rotor corresponding to system supply frequency are employed. Effective generator impedance is given by the average impedance corresponding to impressed harmonic frequency for the direct- and quadrature-axis equivalent circuits of the machine. Reactances are referred to equivalent values at frequency of the system supply. Resistances, however, differ.

The average of the direct- and quadrature-axis generator subtransient reactances for this Machine are 0.349p.u., 0.289p.u. and 0.289p.u. for the (2d,3q), (1d,2q) and (1d,1q) damper models respectively. Respective sub-transient reactance for the (2d,3q) damper model is 0.230p.u.; the average of the sub-subtransient and subtransient reactances is 0.290p.u. Error in using average generator subtransient reactance for effective generator impedance will be seen to be up to 34% for the (2d,3q) damper model (10% using the average of the sub-subtransient and subtransient reactances), and up to 6% for the (1d,2q) and (1d,1q) damper models, respectively. For approximate calculations, average supply frequency subtransient generator reactance etc. may be used to evaluate the proportion of the converter station harmonic disturbance current which is impressed on a generator in a multi-machine network.

8.6 SHAFT TORQUES DUE TO NONCHARACTERISTIC CURRENTS -- 50Hz/50Hz ASYNCHRONOUS LINK

Shaft torques due to noncharacteristic converter station currents are given by

$$F_{lk} = [Amplitude\ of\ current] \cdot [GSF] \cdot [SSF] \cdot T_{lk}$$

where T_{lk} is the torque at shaft section l for unit torque excitation and k is the modal frequency.

8.6.1 Modulation Product Currents and Shaft Torques -- 660MW Machine A

Table 8.13 depicts shaft torque at different shaft sections of Machine A which could be at risk for a 50Hz/50Hz asynchronous link. Shaft torques correspond to resonant

harmonic modulation product currents corresponding to term 2(i) of Eqn. [8.2] assuming a ripple current at the converter which gives a 12th harmonic voltage of 10% [64]. Table 8.13 also indicates amplitude of the modulation product current at the secondary of the converter transformer produced by term 2(i) of Eqn. [8.2]. The modulation current impressed on the generator stator at rotor torque frequency given in Table 8.13 is not unreasonable for a typical HVDC link. It is assumed that the modulation current at the secondary of the converter transformer is impressed on the stator of the synchronous machine (i.e. the system scaling factor has been ignored). Generator scaling factors are evaluated by Method B using data given in Table 8.9 . A stiffness-adjusted lumped mass model of the machine has been used.

Table 8.13 : Shaft Torque due to Resonant Excitation acting on Generator Rotor -- 660MW Machine A

Frequency, Hz	16.21	26.81	35.59	37.92
Location	<i>ELECTRICAL AND STEAM DAMPING</i>			
<i>Full-load, Term 2(i)</i>				
<i>HP/IP</i>	0.0015	0.0206	0.0999	0.0062
<i>IP/LP1f</i>	0.0784	0.0870	0.3327	0.0189
<i>LP1r/LP2f</i>	0.2488	0.1562	0.0293	0.0087
<i>LP2r/GEN</i>	0.2135	0.1250	0.3898	0.0024
<i>GEN/EXC</i>	0.0249	0.0273	0.8411	0.0049
<i>No-load, Term 2(i)</i>				
<i>HP/IP</i>	0.0075	0.0883	0.0902	2.5666
<i>IP/LP1f</i>	0.0371	0.3729	0.3004	7.6013
<i>LP1r/LP2f</i>	0.1179	0.6697	0.0269	3.5292
<i>LP2r/GEN</i>	0.1015	0.5355	0.3523	0.9823
<i>GEN/EXC</i>	0.0118	0.1168	0.7608	0.4716

Resonant excitation refers to Term (i) of equation [2] for conditions which gives ratio of harmonic to fundamental current at full-load of 0.0854%. Generator scaling factor employed corresponds to Method B.

8.6.2 Modulation Product Currents and Shaft Torques - 1000MW Machine B

Table 8.14 illustrates corresponding shaft torque for modulation currents which relate to rotor torque frequencies in respect of terms 2(i) and term 2(ii) of Eqn. [8.2] for the 1000MW Machine B.

Tables 8.13 and 8.14 demonstrate that resonant excitation by variable frequency currents superimposed on DC currents in asynchronous HVDC links could result under certain circumstances in onerous torques in turbine-generator-exciter shafts.

Table 8.14 : Shaft Torque resulting from Resonant Excitation acting on
Generator Rotor -- 1000MW Machine B

Frequency, Hz	14.49	22.63	32.18	35.03	0.803
Location					
Full-load	<i>ELECTRICAL AND STEAM DAMPING</i>				
Term 2(i)					
HP/IP	0.0075	0.0187	0.0589	0.0010	0.0001
IP/LP1f	0.0378	0.0732	0.1859	0.0029	0.0002
LP1r/LP2f	0.2208	0.2979	0.1740	0.0007	0.0013
LP2r/GEN	0.1598	0.2730	0.7618	0.0013	0.0024
GEN/EXC	0.0070	0.0363	1.6327	0.0001	0.0001
Term 2(ii)					
LP1r/LP2f	0.1623	0.2190	0.1279	0.0005	0.0009
LP2r/GEN	0.1175	0.2007	0.5601	0.0010	0.0018
GEN/EXC	0.0051	0.0267	1.2002	0.0001	0.0001
No-load	<i>ELECTRICAL DAMPING ONLY</i>				
Term 2(i)					
HP/IP	0.0038	0.0194	0.0187	6.3367	0.0000
IP/LP1f	0.0165	0.0760	0.0591	18.2457	0.0001
LP1r/LP2f	0.0963	0.3094	0.0554	4.4686	0.0005
LP2r/GEN	0.0700	0.2831	0.2422	0.8020	0.0009
GEN/EXC	0.0058	0.0376	0.5200	0.2342	0.0000
Term 2(ii)					
IP/LP1f	0.0139	0.0643	0.0499	15.4255	0.0001
LP1r/LP2f	0.0814	0.2616	0.0468	3.7780	0.0004
LP2r/GEN	0.0592	0.2393	0.2048	0.6780	0.0008
GEN/EXC	0.0049	0.0317	0.4396	0.1980	0.0000

8.7 SUMMARY OF CHAPTER 8

This Chapter has assessed the possibility of variable frequency ripple currents superimposed on the DC current in asynchronous Links exciting sympathetic torsional vibrations in the turbine-generator-exciter shaft.

It has been found that susceptibility of turbine-generators to excitation of torsional vibrations by injected harmonic currents depends very much on machine mechanical and electrical design. The amplitude of shaft torque at corresponding shaft sections and corresponding modal frequencies for a given resonant exciting torque differ significantly for machines of different design.

When evaluating the rate of torque excitation due to injected harmonics, detailed (2d,3q) rotor equivalent circuits should be employed. Simpler (1d,1q) and (1d,2q) models incur significant error. Generator scaling factors which relate the rate of torque excitation to harmonic disturbing current vary significantly with generator real and reactive power.

Although the exciting non-characteristic currents are very small, the possibility exists for serious damage to the turbine-generator shaft, especially when operating on light load for which time constants for steam viscous damping are very large.

CONCLUSIONS

This thesis has discussed the background, principles and fundamental equations underlying Complex Torque Coefficient analysis. This form of analysis provides a completely graphical basis for the prediction and evaluation of all forms of torsional interaction in electric power systems. In doing so, this approach enables clearer visualisation and a better understanding of the complex mechanisms by which torsional interaction operates, which is so often hidden by alternative analysis techniques.

A prime objective of this thesis was to demonstrate that this technique can easily be applied to the study of systems of any arbitrary configuration containing many synchronous machines and controlled devices. As a means of demonstrating this, the dynamic equations governing the behaviour of the interconnected power system, the main elements of which are synchronous machines including the mechanical turbine-generator-exciter shaft train, transmission lines, transformers, shunt elements and loads, have been presented.

The influence of transient and subtransient reactances of the machine and the transmission line reactance on the damping characteristic of the rotor swing mode has been studied. It has been shown that the electromagnetic damping which acts along the active length of the generator rotor decreases as the system strength decreases. The influence of total system resistance has been shown to have a significant effect on the electromagnetic damping. The influence of transmission system load characteristics on the damping of torsional oscillations has been examined. Torsional interaction is more likely to occur if the machine is operating at or close to no-load. Differences in computed net damping between loads represented as constant impedance, constant power or constant current are small enough to be considered negligible.

The application of Complex Torque Coefficient analysis to the study of subsynchronous resonance in electrical power systems has been discussed and demonstrated for a single machine/two transmission line system. It has been shown that the insertion of series compensation capacitors in transmission lines in close proximity to a

synchronous generator can induce a region of negative electromagnetic damping which may subsequently lead to torsional interaction occurring.

The development of complex torque coefficients in the context of multi-machine power systems has been presented, for which all relevant machine and system equations have been developed. Unlike the eigenanalysis approach, complex torque coefficients allow an enhanced view of the mechanisms involved in the multi-machine interactions. Application to a three machine system has been demonstrated. The method utilises the rigorous state-space mathematical formulation of the interconnected multi-machine system such that the calculation of the torque coefficients are based on a full modal analysis of the system

In this study, low frequency and higher frequency effects are considered separately in order to retain the true coupling of the machines at low electromechanical frequencies. The effect of higher frequency shaft modes belonging to machines other than the one under investigation is, in general, to enhance the damping of rotor oscillations in the very near vicinity of the shaft mode. Frequencies above and below the shaft mode are not influenced significantly by the mode.

This thesis has demonstrated that the technique of Complex Torque Coefficient Analysis can be applied successfully to the study of Subsynchronous Torsional Interaction between a synchronous machine and controlled network devices, in this case a Static Var Compensator and a Thyristor Controlled Series Compensator. It has been shown that, in agreement with recent literature, the mechanism of the interaction between the synchronous machine and the SVC is dominated by the configuration of the voltage regulation on the compensator. Although providing a noticeable improvement in damping over most of the subsynchronous range, unsuitable regulator parameters will induce a region of negative damping not dissimilar to that induced by the use of series compensation capacitors. If the generator under investigation is operating under light load conditions for which steam viscous damping is significantly reduced, the possibility of unfavourable interaction exists.

The influence of 'system' parameters was investigated. It has being demonstrated that location of the SVC has a significant impact on the extent of the negative damping region, with most effect occurring when the SVC is in close proximity to the generator. The system strength was also found to be of significance with weak systems being the most susceptible to the interaction. Minimisation of the interaction was found to occur when reactive power load demand is matched exactly by SVC reactive power injection. At this point, at least for a single machine system, the generator is supplying real power only.

Variation of the generator real power demand was found to have a less significant but noticeable influence. Increased real power demand leads to a detriment of the damping coefficient, although it must also be borne in mind that steam viscous damping will increase significantly as real power demand is increased, such that overall machine stability may not be unfavourable.

The Complex Torque Coefficient analysis technique has been applied to the study of a single machine – TCSC system. The ability of the TCSC device to provide line compensation but with no SSR interaction has been illustrated.

Variation of the TCSC voltage regulator parameters was found to have a significant impact on the ability of the device to mitigate regions of negative electromagnetic damping. For the system studied, it has been found that low values of gain do not remove regions of possible torsional coupling. Likewise, excessive phase lag introduced by the control loop, for example by regulator action or thyristor firing delay, may result in the TCSC device being equivalent to a series capacitor at subsynchronous frequencies which would not be desirable.

With the aid of non-linear time domain simulation, it has been demonstrated that the explicit separation of the electrical and mechanical system representations as an aid to visualisation of the complex mechanisms governing the behaviour of the system does not invalidate the analysis as compared with other frequency domain approaches, for example, eigenanalysis, which relies on the mathematical description of the system being arranged into a single unified system matrix. Ease of visualisation aside, the two frequency domain methods are equivalent.

A technique for including the effect of excitation control and additional stabilisation control has been outlined, although it should be noted that such an approach is valid only for single machine-infinite busbar systems. If these systems are to be included in the analysis at all, then this should be carried out in the context of multi-machine systems. This can be easily achieved within the state-space formulation of the interconnected power system as has been described in numerous publications on eigenanalysis of power systems.

The thesis has assessed the possibility of variable frequency ripple currents superimposed on the DC current in asynchronous Links exciting sympathetic torsional vibrations in the turbine-generator-exciter shaft.

It has been found that susceptibility of turbine-generators to excitation of torsional vibrations by injected harmonic currents depends very much on machine mechanical and electrical design. The amplitude of shaft torque at corresponding shaft sections and

corresponding modal frequencies for a given resonant exciting torque differ significantly for machines of different design.

When evaluating the rate of torque excitation due to injected harmonics, detailed (2d,3q) rotor equivalent circuits should be employed. Simpler (1d,1q) and (1d,2q) models incur significant error. Generator scaling factors which relate the rate of torque excitation to harmonic disturbing current vary significantly with generator real and reactive power.

Although the exciting non-characteristic currents are very small, the possibility exists for serious damage to the turbine-generator shaft, especially when operating on light load for which time constants for steam viscous damping are very large.

This method of analysis as applied to the prediction of torsional interaction has been verified for a range of scenarios within the single machine—capacitor compensated system. The verification was based on the use of a detailed time domain simulation of the power system using the PSCAD/EMTDC software package.

SUGGESTIONS FOR FURTHER WORK

The Complex Torque Coefficient technique utilised in this thesis is based on direct- and quadrature-axis components of current and torque only. By taking proper account of the negative and zero sequence components of current, the method could be extended to the analysis of full three-phase unbalanced networks. As illustrated by Iravani [37], there exists the potential to reduce SSR effects by unbalancing the series compensation capacitors in each phase of the transmission line.

There exists significant scope for the modeling and analysis of additional FACTS devices including Static Phase Shifters, Unified Power Flow Controllers and Static Synchronous Compensators. This topic will merit considerable attention in the near future on account of the significant level of interest in this area [39].

The incidence of Induction generators connected to mainstream power networks has increased over the last decade. Most of the available literature has concentrated on the transient behaviour of these machines during synchronisation with the power grid. The possibility of unfavourable interaction with the power network during steady operation has, however, not been examined. The Complex Torque coefficient analysis technique could be utilised here since the induction generator model is easily derived from the synchronous generator model simply by removing the influence of the field winding.

SOFTWARE DEVELOPMENT**A.1 INTRODUCTION**

This chapter describes the design of the software tool, PC-DAP, which incorporates all of the theory of analysis presented in the preceding chapters. PC-DAP is designed for prediction and analysis of torsional oscillations in the shaft systems of turbine-generators connected to large networks, including Subsynchronous Resonance (SSR). In the past, engineers have analysed such problems using the eigenvalue technique, which could be said to hide physical insight behind sophisticated mathematics. PC-DAP attempts to overcome this drawback by presenting the user with a completely graphical analysis.

PC-DAP's code makes advanced use of sparsity techniques, so that even large power systems containing hundreds of nodes can be analysed efficiently. Template editors for both the power system (busbars, transmission lines, transformers, etc.) and for the turbine-generator units (rotor circuits, shaft system, AVR, PSS, etc.) are provided so that the effects of changes in the system parameters can be quickly and easily assessed.

A.2 PROGRAM STRUCTURE

PC-DAP can be divided into the following main sections:

1. System file selection
2. System and Turbine-Generator Template Editors
3. Loadflow analysis including calculation of device initial conditions
4. Loadflow analysis output
5. Eigenanalysis
6. Torque Coefficient analysis
7. Torque Coefficient analysis output

Figure A.1 illustrates the sequence of computations in the software program PC-DAP. The calculations can be divided into several distinct steps. All the code has been written in Fortran-77.

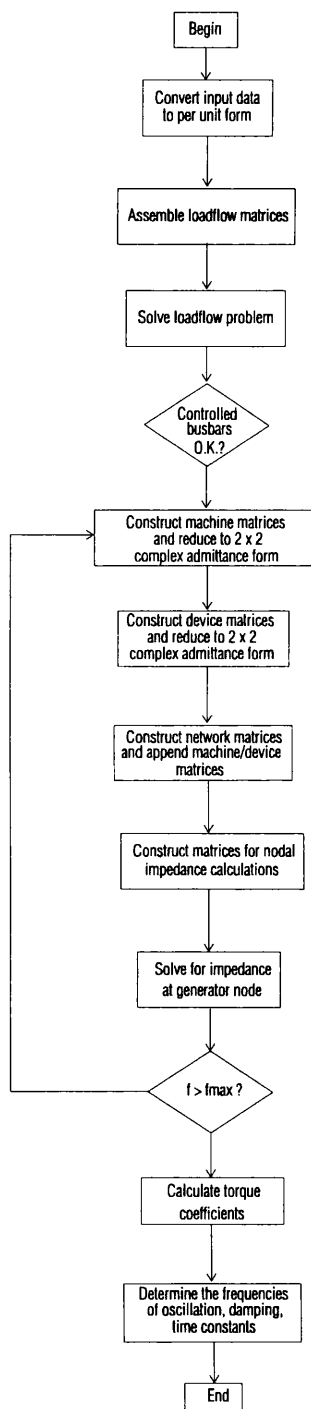


Figure A.1: Flow Diagram of PC-DAP

The initial step is to process the input parameters for both the network elements and the synchronous machines, converting them all to the same p.u. base. All subsequent calculations use the p.u. parameters so no further conversions of the data are necessary.

The torque coefficients of each machine depends on its specific operating point. The steady-state operating point of controllable devices embedded in the system depends on the condition of the surrounding network. In order to determine the operating points of all machines and devices in the system for a given loadbus profile, a comprehensive loadflow must be performed. The routines in PC-DAP use a fast Newton-Raphson algorithm which gives rapid convergence. The operating points of controllable devices are determined in a stepwise fashion by solving for an initial operating point, comparing with the controlled parameter, for example bus voltage, with its reference value and adjusting the operating point appropriately before re-running the loadflow. Although it is possible to combine the control characteristics of these devices into the loadflow jacobian matrix structure on which the algorithm operates such that the solution is obtained first time round, to do so was beyond the scope of this study.

Once the operating points of the system have been determined, the torque coefficient analysis can begin. Each element in the system, whether it is a machine and its associated mechanical system, a transmission line, a load or a controllable device, has to be represented by its 2×2 complex admittance matrix. The matrices of each machine and controlled device are constructed first using the methods described in Chapters 5 and 6. The network admittance matrix must now be constructed from the network element matrices in standard form. That is, the diagonal elements represent the total admittance on each node of the system, and the off-diagonal elements correspond to the transfer admittances between nodes. After this has been constructed, the device matrices previously calculated are appended to the total network admittance matrix to create the system matrix.

The torque coefficient analysis relies on performing a frequency scan of the system as seen from the terminals of the machine under study. This section of the program makes use of modified fault analysis routines which solve the network equations for a fault on the busbar of the machine under investigation having first set the impedance of the machine to infinity. The solution includes a vector containing the Thevenin impedance seen from all nodes.

The frequency scanning routines use Zollenkopf's Bi-factorisation algorithm [66] which takes advantage of the sparse nature of the network matrix.

The problem is to determine the solution vector of

$$x = A^{-1}b$$

without explicitly inverting A . The method used here is to factor the inverse into the product of n factor matrices, or

$$A^{-1} = R^1 R^2 \dots R^{n-1} R^n L^n L^{n-1} \dots L^2 L^1$$

As the matrix A is very sparse in this case, significant savings in storage and computation time can be obtained if a programming scheme is used which stores and processes only the non-zero terms. In order to maintain the benefits of sparsity as far as possible, an optimal ordering scheme is built into the algorithm. The purpose of the scheme is to select at each step of the reduction process that column as pivot which contains the fewest number of non-zero terms thus reducing overall computation time. A packed matrix storage scheme in which only the non-zero terms are stored is employed in the algorithm.

The process of forming the complex impedance matrices and solving the system equations must be repeated for every frequency of interest.

With the torque coefficients calculated, the frequencies of oscillation, the net damping and the time constants associated with the oscillations at the modal frequencies of the shaft must be determined. As discussed in earlier Chapters, all these quantities can be determined from synchronising and damping coefficients of the electrical and mechanical systems.

A.2.1 Main menu's

The main PC-DAP menu provides access to the main options available in the program. There are two such menu's used. The first, illustrated in Figure A.2, is concerned only with the selection of the system file. Once this task is completed, the second main menu, Figure A.3, will appear and all subsequent operations will be initiated from here.

Note that some of the menu options in the main menu will be disabled (indicated by being displayed in a lighter colour) until the correct preceding operations have been completed. The user can return to the first menu at any time in order to either select a different system file, or to quit the program.

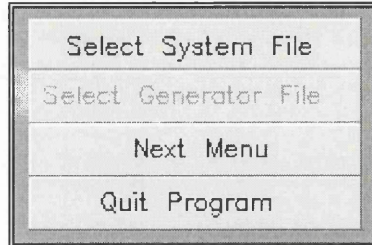


Figure A.2: Initial PC-DAP Menu Options

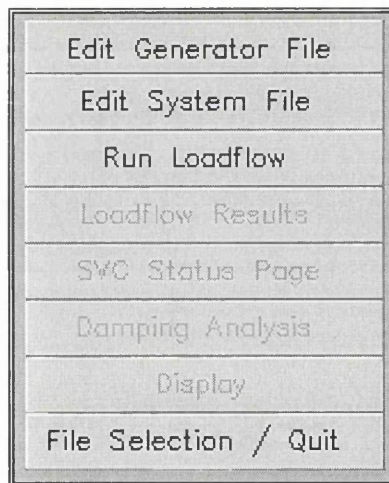


Figure A.3: Main Menu Options

A.2.2 File selection

Depressing the first key on the menu initially displayed invokes the file selection box, as illustrated in Figure A.4. All system files used in PC-DAP have the filename extension .NET. The default directory for system files is c:\NET. The required file may be selected either by using the [↑] and [↓] keys or by depressing the 'up' or 'down' buttons

using the mouse left-button. Pressing either [RETURN] on the keyboard or depressing the 'Close' button will confirm the selection.



Figure A.4: File Selection Box

At this point, PC-DAP will perform an initial check on the selected file to locate any obvious errors. Any such discrepancies located will be brought to the users attention in the error message box, as illustrated in Figure A.5. Depressing the 'Directory' button allows selection of an alternative directory. The keyboard and mouse operations are identical to the procedure for file selection.

A.2.3 Generator Template Editor

Option 1 of the main menu enters the **Generator Template Editor**, Figure A.6, which allows the modification of generator electrical parameters and/or mechanical turbine system parameters.

The editor is arranged as an array of parameter buttons with the current value of each parameter displayed to the left of the button for generator electrical parameters, and below the button for turbine parameters. The template editor was designed to enable the convenient access to parameters for all the turbine-generators in a multi-machine system. The directional buttons at the top left and right corners of the electrical parameter area allow the user to scroll through the parameters of each machine. The turbine section has two pairs of directional buttons; the outermost scroll from one turbine system to the next;

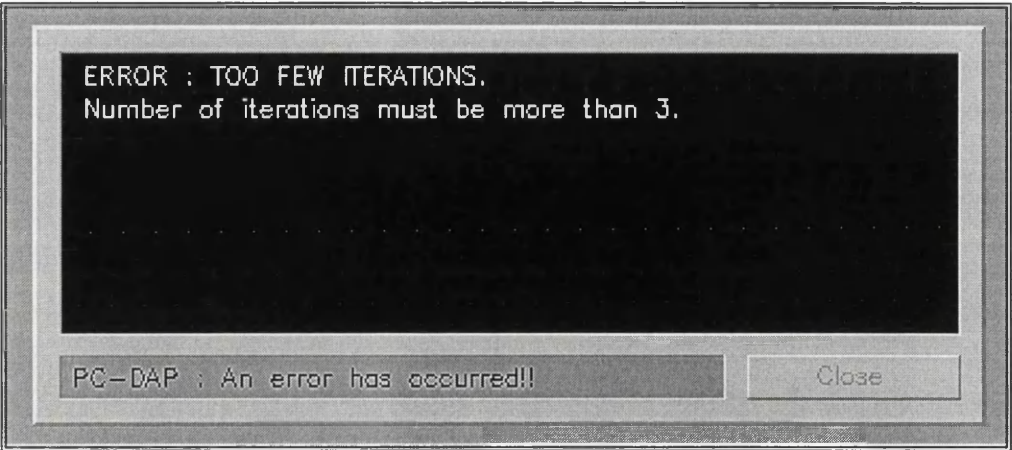


Figure A.5: PC-DAP Error Messaging

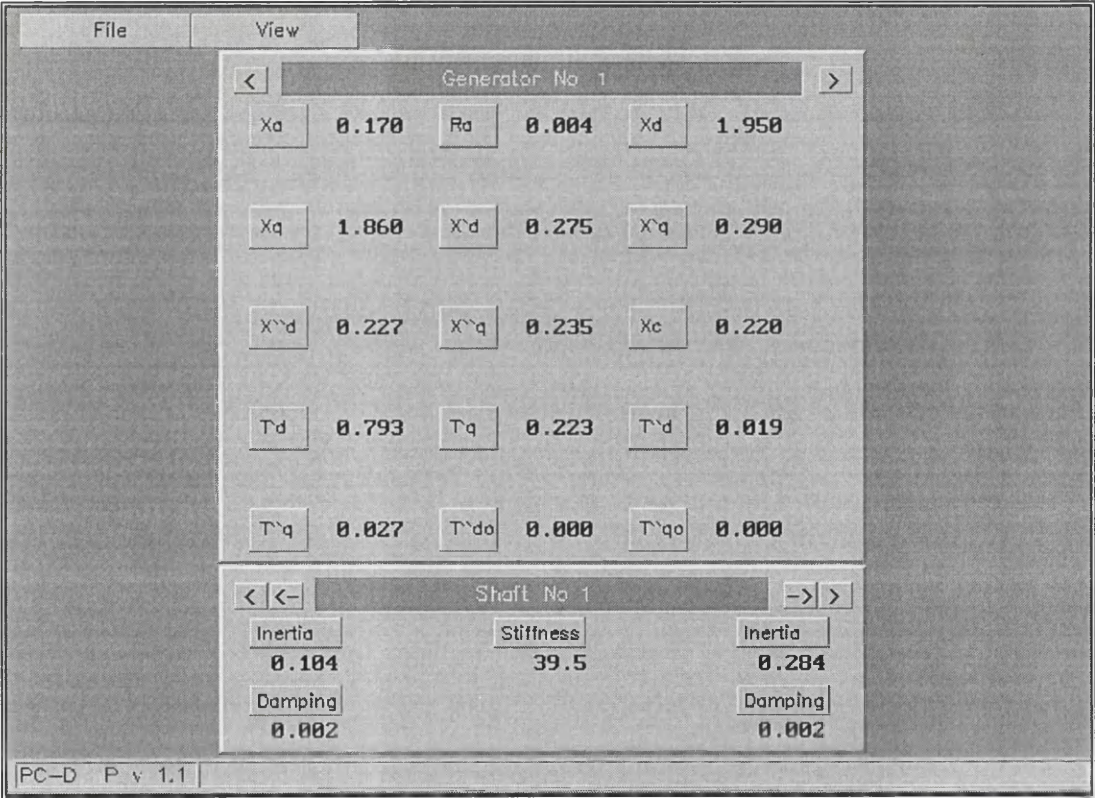


Figure A.6: Generator Template Editor

the innermost display the turbine parameters along the length of the selected turbine system. The turbine parameters are displayed in the form of two inertias I_j and I_k , connected together by a shaft of stiffness S_{kj} , and damping constants D_k acting on I_k and D_j acting on I_j .

Depressing the button corresponding to a parameter allows the user to change the current value of that parameter. [ESC] will abort the operation.

The 'View' pull-down menu allows quick access to a specific generator or turbine through the appropriate [NEXT], [PREVIOUS] or [GOTO..] options. This is particularly useful in the event of a large number of machines being included in the analysis. Selecting the 'File' pull-down and option 'Close' saves the template and returns the user to the main menu.

Generator mechanical and electrical parameter definitions (Generator template editor)

The turbine system parameters listed in the template editor are defined in Table A.1. The generator electrical parameters listed in the template editor are defined in Table A.2.

Table A.1: Generator template editor Mechanical parameters

<i>Inertia</i>	<i>Inertia constant of turbine k in MW-s/MVA (p.u.)</i>
<i>Stiffness</i>	<i>Stiffness constant of turbine shaft k_j, MW/MVA-rad</i>
<i>Damping</i>	<i>Steam viscous damping acting on turbine k, MW-s/MVA-rad</i>

Table A.2: Generator template editor Electrical parameters

X_a	<i>Stator leakage reactance, p.u.</i>
R_a	<i>Stator resistance, p.u.</i>
X_d	<i>Direct axis reactance, p.u.</i>
X_q	<i>Quadrature axis reactance, p.u.</i>
X'_d	<i>Direct axis Transient reactance, p.u.</i>
X'_q	<i>Quadrature axis Transient reactance, p.u.</i>
X''_d	<i>Direct axis sub-transient reactance, p.u.</i>
X''_q	<i>Quadrature axis sub-transient reactance, p.u.</i>
X_c	<i>Canay's reactance, p.u.</i>
T'_d	<i>Direct axis transient short circuit time constant, s</i>
T'_q	<i>Quadrature axis transient short circuit time constant, s</i>
T''_d	<i>Direct axis sub-transient short circuit time constant, s</i>
T''_q	<i>Quadrature axis sub-transient short circuit time constant, s</i>
T''_{do}	<i>Direct axis sub-transient open circuit time constant, s</i>
T''_{qo}	<i>Quadrature axis sub-transient open circuit time constant, s</i>

A.2.4 System Template Editor

Option 2 of the main menu enters the **system template editor**, Figure A.7, which follows a similar format to the generator/turbine editor described in the preceding section. In this case, the displayed sections are 1) busbars, 2) transmission lines, 3) generator loading, and 4) shunt elements. As for the previous editor, all parameters can be modified by selecting the button corresponding to that parameter. The parameters belonging to the 'next' or 'previous' element (i.e. busbar, transmission line etc) can be displayed either by using the directional buttons at the top of each section or by using the 'View' pull-down and selecting the element followed by [NEXT], [PREVIOUS] or [GOTO..].

Additional elements can be added to the system via the edit pull-down. This option also allows the deletion of any of the elements. Note however, that it is up to the user to ensure that the system described in the editor is complete. Figure A.8 illustrates the format of the 'Add busbar' dialogue box. Other elements are added in a similar fashion.

The current system dimensions are indicated on the bar located in the top right of the screen.

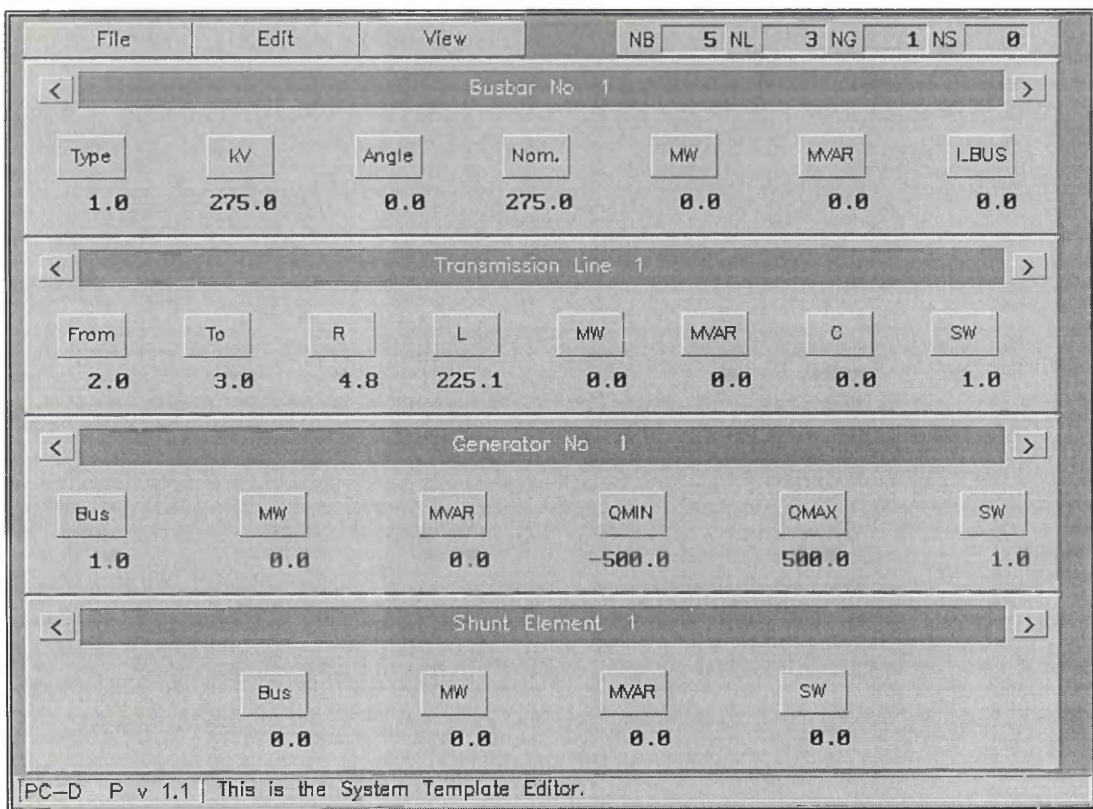


Figure A.7: PC-DAP System Template Editor

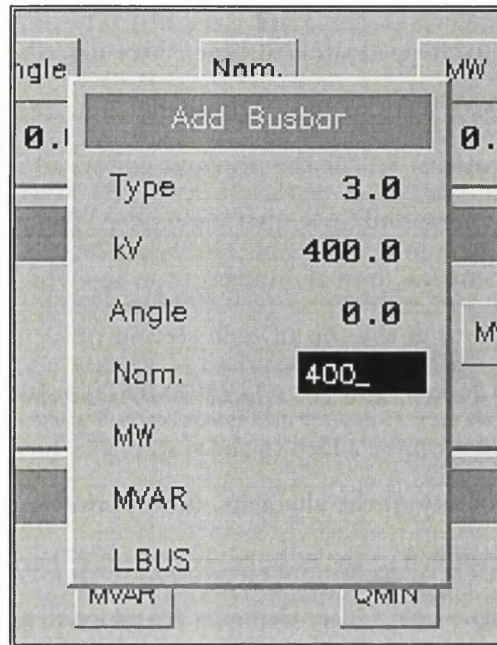


Figure A.8: Component definition

Busbar parameters

The busbar parameters listed in the first section of the template editor are defined as follows:

Table A.3: System template editor Busbar parameters

Type	<p>The 'type' of bus refers to the loadflow classification of busbars:</p> <ul style="list-style-type: none"> • Type 1 is a swing or slack bus, i.e. a bus at which the real and reactive power injection is left unspecified. These values will be calculated by the loadflow algorithm. There can be only one swing bus in a system. • Type 2 bus is a 'PQ' or load bus. This refers to a bus at which there is no net injected power. • Type 3 bus is a 'PV' or generator bus. Any node that has a net injection of either real or reactive power is classed as type 3.
kV	Initial 'guess' voltage on the busbar. The true value will be computed by the loadflow algorithm.
Angle	Initial 'guess' voltage angle with respect to the reference (usually taken to be the swing bus). This parameter is normally set to zero. The actual value will be computed by the loadflow algorithm.
Nom.	The nominal voltage of the busbar.
MW	Real power consumed by a load connected to the busbar. Any busbar can have a load connected to it, regardless of type.
MVAR	Reactive power consumed by a load connected to the busbar.
I_Bus	Should be set to 1 if the bus bar is an infinite bus; 0 otherwise.

Transmission Line parameters

The transmission line parameters listed in the second section of the template editor are defined as follows:

Table A.4: System template editor Transmission Line parameters

<i>From</i>	<i>The sending end busbar of the line.</i>
<i>To</i>	<i>The receiving end busbar of the line.</i>
<i>R</i>	<i>The resistance of the line, ohm</i>
<i>L</i>	<i>The inductive reactance of the line, ohm.</i>
<i>MW</i>	
<i>MVAR</i>	<i>Represents 'charging' capacitance of the line.</i>
<i>C</i>	<i>Series capacitor, measured in MVAR.</i>
<i>SW</i>	<i>Switch state of line: 1 for line connected, 0 for line disconnected.</i>

Generator parameters (system template editor)

The generator parameters listed in the third section of the template editor are defined as follows:

Table A.5: System template editor Generator parameters

<i>Bus</i>	<i>The bus to which the generator is connected.</i>
<i>MW</i>	<i>The real power injected by the generator. If the generator is connected to the swing bus, this parameter should be set to zero.</i>
<i>MVAR</i>	<i>The reactive power in MVAR injected by the generator. As for parameter MW, this parameter should be set to zero if connected to the swing bus.</i>
<i>QMIN</i>	<i>The maximum leading (capacitive) VAR capability of the generator. This parameter should be negative.</i>
<i>QMAX</i>	<i>The maximum lagging (inductive) VAR capability of the generator. This parameter should be positive.</i>
<i>SW</i>	<i>Switch state of generator: 1 for connection, 0 for disconnection</i>

Shunt parameters

The shunt element parameters listed in the final section of the template editor are defined as follows:

Table A.6: System template editor Shunt parameters

<i>Bus</i>	<i>The bus to which the generator is connected.</i>
<i>MW</i>	<i>The resistive component of the shunt element.</i>
<i>MVAR</i>	<i>The reactive component of the shunt element. For an inductive shunt, the parameter should be positive. For a capacitive shunt this parameter should be negative.</i>
<i>SW</i>	<i>The switch state of the shunt: 1 for connection, 0 for disconnection.</i>

A.2.5 Loadflow Analysis and results

The study of the system begins with the loadflow analysis, initiated by pressing option 3, 'Run Loadflow'. Note that this option remains disabled until a valid system data file has been entered. Convergence of the Newton Raphson technique employed is usually fast, even for large networks. When the loadflow analysis has been completed, PC-DAP informs the user via the status bar along the bottom of the screen. Option 4, 'Loadflow Results' now becomes a valid option and may be selected. This is, however, optional and simply provides information regarding the state of the network.

Figure A.9 illustrates the loadflow results page. This is divided into three sections; node status, transmission line status, and transformer status. The node status includes information regarding the p.u. voltage, the angle relative to the reference, which is always taken to be the swing node, and real and reactive power injected into the node. Transmission line information includes the begin and end nodes, real and reactive power flow along the line, and the real and reactive power loss on the line. The transformer section details the connection nodes, the power throughput, and the copper and iron losses (real and reactive).

In exactly the same way as for the template editors, the user can scroll through the information using the directional buttons, or jump to a particular element using the [VIEW] [GOTO...] option.

Option [VIEW] [VOLTAGE PROFILE] displays a chart showing the voltage profile across the network, as illustrated in Figure A.10 for a 30 bus network. Option [VIEW] [POWER PROFILE] displays a chart showing the distribution of real and reactive power flows throughout the network, Figure A.11.

File		View					
NODE STATUS							
Node No	Voltage (p.u.)	Angle (Deg.)	Real (MW)	Reactive (MVAR)			
1	1.00	0.00	10.03	10.67			
TRANSMISSION LINE STATUS							
Line No	From Node	To Node	Real (MW)	Reactive (MVAR)	P Loss (MW)	Q Loss (MVAR)	
1	2	3	10.03	10.66	0.01	0.30	
TRANSFORMER STATUS							
No	From Node	To Node	Real (MW)	Reactive (MVAR)	Copper		Q Loss
					P Loss	Q Loss	
1	1	2	10.03	10.67	0.00	0.00	0.00
					Iron		
					0.00	0.00	
PC-D P v 1.1 This is the Loadflow Results Page.							

Figure A.9: Loadflow results page

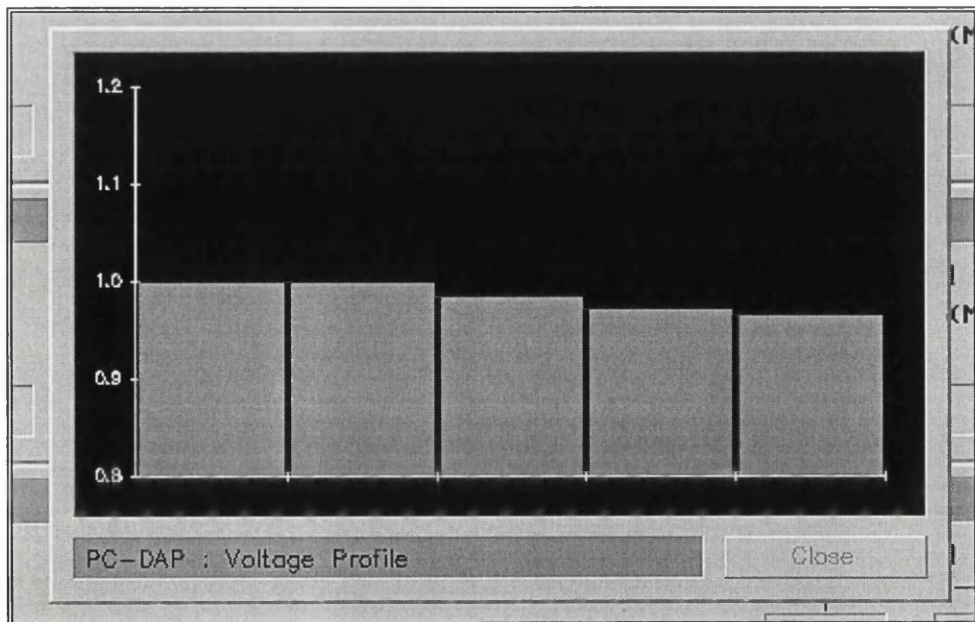


Figure A.10: Voltage Distribution display

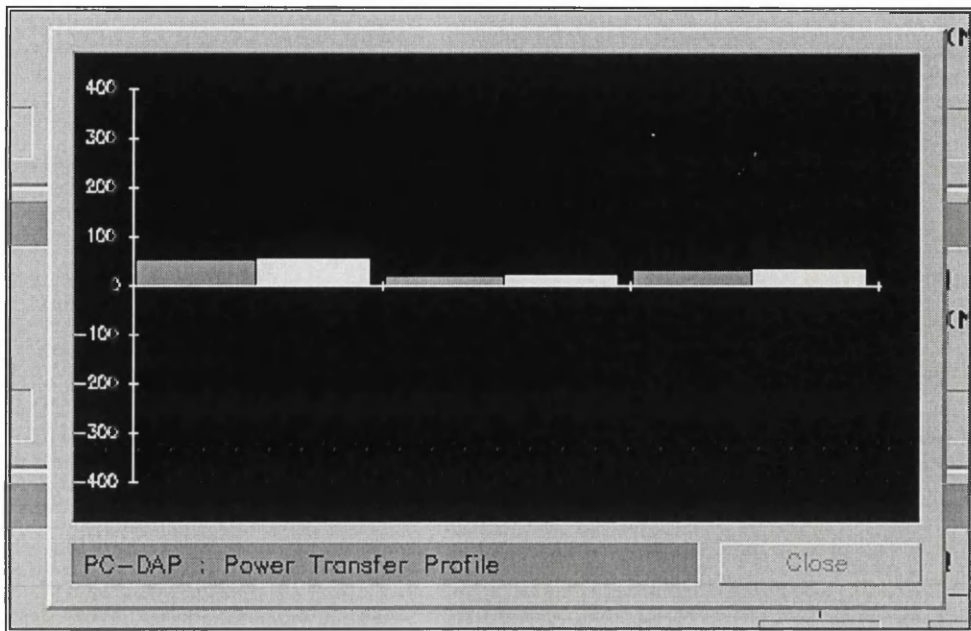


Figure A.11: Power flow distribution display

A.2.6 SVC Status Page

If the system contained busbars controlled with static compensators, the operating point of the compensators will be output in the 'SVC Status page', Option 5. This page, Figure A.12, indicates the percentage of maximum inductive power of the compensator being utilised, and the specified and achieved voltage on the busbar. This information can also be obtained from the SVC template, which is found in the SYSTEM TEMPLATE EDITOR, option [EDIT] [SVC].

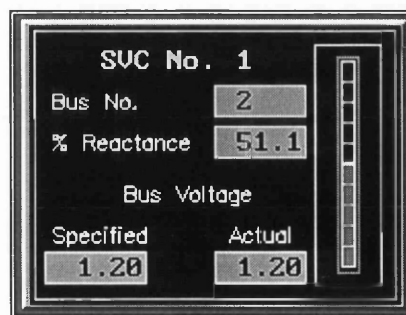


Figure A.12: SVC Display Box

A.2.7 Torque Coefficient Analysis Page

Option 6 ‘Damping Analysis’ initiates the calculation of the complex torque coefficients for the current system and selected generator. This option remains disabled until a loadflow analysis has been completed. The default generator is taken to be generator number 1. On completion of the calculations, pressing option 7 ‘Display Results’ opens the output graphs page, Figure A.13.

This page is divided into 6 sections which are defined as follows:

1. **Maximum Negative Electrical Damping** — displays the frequency at which the lowest value of electrical damping was recorded. The value of damping at this frequency is displayed.
2. **Mechanical Resonant Modes** — displays the frequency and modal inertia of each resonant mode of the turbine connected to the machine under investigation. If the frequency of the mode is within the Subsynchronous range, the position of the mode is highlighted on the graph (see No. 3 below)
3. **Graphical display** — displays the electrical and mechanical damping coefficients for the system and machine under study. The mechanical mode selected is indicated by a vertical line on the display. The current electrical damping coefficient is displayed in red. The current mechanical damping coefficient is displayed in yellow. If the current analysis is not the first to be run, the results of the previous analysis are displayed : previous electrical coefficient is displayed in blue; previous mechanical coefficient is displayed in white.
4. **Interaction status** — displays the net damping and time constant of oscillation for the mechanical mode selected.
5. **Capacitor Location** — displays the location (sending and receiving busbars of the transmission line containing the capacitor) and compensation level of each series compensation capacitor in the system. The compensation level is displayed in both MVA and % formats.
6. **Current System and generator files** — Displays the current files.

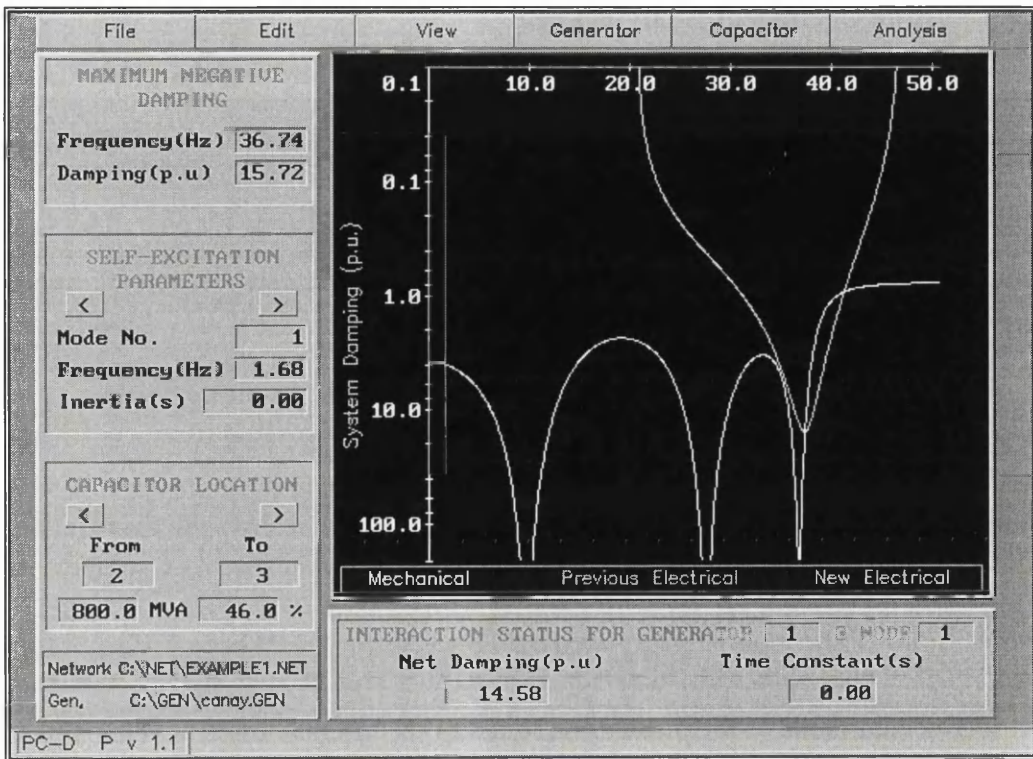


Figure A.13: Torque Coefficient Analysis Page

The main menu bar along the top of the display has six options which are defined as follows:

- File** — *Print* : Screen dumps the display to a user selected file in .PCX format.
Save : Saves the current system and generator configuration via the file selection box (§A.2.2).
Close : Closes the results page and returns the user to the main menu.
- Edit** — *Generator Template* : Invokes the **Generator Template editor** (§A.2.3). Closing the editor after parameter changes have been made returns the user to the graphical display page.
System Template : Invokes the **System Template editor** (§A.2.4). Closing the editor after parameter changes have been made returns the user to the graphical display page.
- View** — *Logarithmic* : Displays the damping coefficients on logarithmic axes. In this mode, both electrical and mechanical coefficients are displayed.

Linear : Displays the electrical damping coefficient on linear axes.

Loadflow results : Invokes the loadflow results page (§A.2.5). Closing the page returns the user to the graphical display page.

Eigenanalysis results : If the system contains more than one synchronous machine, an eigenanalysis will have been carried out as part of the damping coefficient analysis algorithm. The results of the eigenanalysis may be viewed using this option. The results are displayed in a dialogue box (Figure A.14). By pressing the directional buttons , or [PAGE -UP]/[PAGE-DOWN] the user can scroll through the eigenvalues.

Zoom : Allows the user to zoom in or out by modifying the x, y, or x & y axes range.

- Generator** — Changes the selected generator (default 1).
- Capacitor** — Changes the compensation level of the selected series compensation capacitor.
- Analysis** — Runs the damping analysis for the current system and generator configuration, including the initial loadflow.

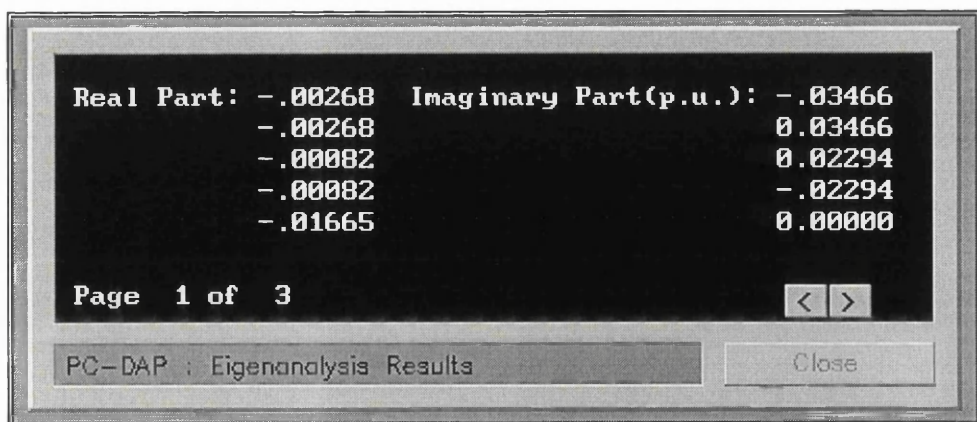


Figure A.14: PC-DAP Eigenanalysis results

A.3 PC-DAP Input file format

PC-DAP input files are in standard ASCII text format and as such may be edited by any standard text editor. There are two files required: a system file with extension .NET; a generator file with extension .GEN. Examples of the input files for a three machine system are described here.

A.3.1 System Input File Format

General System Dimensions

This is the first section in the system datafile. It lists the number of each element in the system.

The parameters are defined as:

- NB :** The total number of buses in the system.
NG : The total number of generators.
NL : The total number of transmission lines in the system.
NT : The total number of transformers in the system.
NSH : The total number of shunt elements in the system
NSVC : The total number of static Var compensators in the system

Busbar Information

The busbar information is arranged as indicated below.

BUSBARS INFORMATION				
BTYPE	VMAG (KV)	VANG (DEG)	KV NOM	INF_BUS
1	239.2	0.00	230.0	0
3	230.0	0.00	230.0	0
3	230.0	0.00	230.0	0
3	230.0	0.00	230.0	0
2	235.75	0.00	230.0	0
3	230.0	0.00	230.0	0
3	230.0	0.00	230.0	0
2	235.75	0.00	230.0	0
3	230.0	0.00	230.0	0
9999	0.0	0.0	0.0	0

The definitions for the parameters are identical to those already discussed in §A.2.4.

Generators information

This section of the datafile details the loading of each of the generators in the system. Note that the first generator is set to zero loading because it is connected to the default swing bus. The parameters below are identical to those discussed in §A.2.4.

GENERATORS INFORMATION						
GBUS	PGEN	QGEN	QMIN	QMAX	SWITCH	
	(MW)	(MVAR)	(MVAR)	(MVAR)	STATE	
1	0.0	0.0	-500.0	500.0	1	
5	163.0	6.7	-500.0	500.0	1	
8	85.0	-10.9	-500.0	500.0	1	
9999	0.0	0.0	0.0	0.0	0.0	0

Transmission line information

Transmission line data is entered into the datafile in the format illustrated below. All parameters are defined in §A.2.4.

TRANSMISSION LINES INFORMATION					
SEND	REC	RESISTANCE	REACTANCE	CHARGING	CHARGING
SWITCH		(OHMS)	(OHMS)	(MW)	MVAR)
STATE					
1	2	0.48	30.47	0.0000	0.00
1					
2	3	5.29	44.97	0.0000	0.00
1					
3	4	16.93	85.17	0.0000	0.00
1					
4	5	0.48	33.06	0.0000	0.00
1					
2	6	8.99	48.67	0.0000	0.00
1					
6	7	15.87	89.93	0.0000	0.00
1					
7	8	0.48	30.99	0.0000	0.00
1					
7	9	6.29	53.32	0.0000	0.00
1					
4	9	4.49	38.09	0.0000	0.00
1					
9999	0	0.00	0.00	0.0000	0.00
0					

Transformers Information

The following sections of the system datafile describe the location and configuration of the transformers present in the system. The first part of this section is illustrated below.

TRANSFORMERS INFORMATION							
SEND IRON	REC SWITCH	R-PRIM (OHMS)	X-PRIM (OHMS)	R-SEC (OHMS)	X-SEC	G-IRON	B- IRON
(OHMS)	(SIEMMENS)	(SIEMMENS)	STATE				
9999	0	0.00	0.00	0.00	0.00	0.00	0.00
0							

The parameters are defined as follows:

- Send/Rec** The sending end refers to the node to which the primary winding of the transformer is connected. The receiving end refers to the point of connection of the secondary winding.
- R-Prim/X-Prim** The resistance and reactance of the primary winding in ohm.
- R-Sec/X-Sec** The resistance and reactance of the secondary winding in ohm.
- G-Iron/B-Iron** The conductance and susceptance of the transformer core. Both parameters are entered in units of Siemens.
- Switch State** Set to 1 for transformer connection, set to zero otherwise.

The remaining sections of the transformer data specify the configuration of tap controls on both primary and secondary windings. The initial section, illustrated below, specify the busbars to be controlled and the voltage at which they are to be maintained.

The primary winding tap information is specified as follows:

LOWER-TAP TAP-POSITION	HIGHER-TAP PRIMARY	LOWER-PHASE PRIMARY	HIGHER-PHASE PRIMARY	TAP-STEPS PRIMARY
9999	0.00	0.00	0.00	0
0.00				

Lower and higher tap positions are entered as per unit quantities i.e. the lower tap position may be 0.9 p.u. and the higher tap position may be 1.1 p.u. The tap steps parameter indicates the available resolution in tap position and is entered as an integer. The tap position parameter indicates the initial tap position.

An similar set of parameters are entered for the secondary windings as illustrated below.

LOWER-TAP TAP-POSITION SECONDARY SECONDARY	HIGHER-TAP SECONDARY	LOWER-PHASE SECONDARY	HIGHER-PHASE SECONDARY	TAP-STEPS SECONDARY
9999 0.00	0.00	0.00	0.00	0

Shunt Elements

The shunt elements consist of a static conductance and susceptance connected in shunt to a specified busbar. Both the conductance and the susceptance parameters are entered in units of power (MW and MVAR).

CONNECTED SWITCH TO BUSBAR STATE	SHUNT ELEMENTS INFORMATION	
	SHUNT-CONDUCTANCE (MW)	SHUNT-SUSCEPTANCE (MVAR)
9999 0	0.00	0.00

Load information

Representation of a load on a busbar can be one of three kinds in PC-DAP: constant current, constant power or constant impedance. The most appropriate representation is configured using the PEXP and QEXP parameters in the load section of the input file. The magnitude of the load is configured by specifying the real and reactive power in MW and MVAR respectively. The load may be turned on or off using SWITCH STATE.

LDBUS SWITCH	PLOAD (MW)	LOAD INFORMATION		
		QLOAD (MVAR)	PEXP	QEXP
STATE				
1	0.0	0.0	0.0	0.0
1	2	0.0	0.0	0.0
1	3	125.0	50.0	0.0
1	4	0.0	0.0	0.0
1	5	0.0	0.0	0.0
1	6	90.0	30.0	0.0
1	7	0.0	0.0	0.0
1	8	0.0	0.0	0.0
1	9	100.0	35.0	0.0
0	9999	0.0	0.0	0.0

General information

The tolerance and maximum allowed number of iterations are specified in this section. The base MVA to which all system parameters will be converted is also specified at this point.

GENERAL PURPOSE INFORMATION		
TOLERANCE	MAXIMUM NUMBER OF ITERATIONS	BASE MVA
1.0E-8	50	100.0

Series Capacitor information

Any series compensation capacitors present in the system can be declared in this section of the input file.

SEND	REC	SERIES CAPACITOR (MVAR)
7	9	1200.0
9999	0	0.0000

The sending and receiving busbars of the transmission line(s) containing the capacitor(s) together with the MVAR rating of the capacitor should be entered as shown above.

Static Var Compensator information

The final section in the system datafile specifies information regarding the placement of static Var compensators in the system for voltage control. The data is split into two areas: the first deals with the system details e.g. busbar to be controlled, required voltage level, ratings of the variable inductor and the fixed capacitor and the tap settings; the second area specifies the SVC control system constants for use in the damping coefficient calculations.

STATIC VAR COMPENSATOR INFORMATION								
CONTROLLED BUSBAR	SPECIFIED VOLTAGE	MAXCONDUCTANCE (MW)	MAXSUSCEPTANCE (MVAR)	TAP POSITION	MAXTAP POSITION	SWITCH STATE	CAP. B (MVAR)	
9999	0.00	0.00	0.00	0.00	0	0	0.0	

The parameters are defined as follows:

- Controlled Busbar :** The number of the busbar to be voltage controlled
- Specified voltage :** The p.u. voltage that the busbar must be maintained at.
- Max Conductance/**
- Max Susceptance:** Variable reactor rating including resistance
- Tap position :** The initial tap setting of the variable reactor
- Max Tap position:** The maximum position that the reactor taps may reach.
- CapB** The MVar rating of the fixed capacitor.

The SVC control system parameters are described in § 6.4.2.

STATIC VAR CONTROLLER CONSTANTS						
T1	T2	TA	TR	TM	KA	KB

A.3.2 Generator Data Input File Format

This data file defines the generator electrical parameters and turbine-generator-exciter inertia constants and shaft stiffness constants for all the machines that are present in the system.

Generator Reactances and Electrical Time Constants

The synchronous machine model in PC-DAP uses the reactance parameters indicated below. The parameters are defined in Table A.2 where X1D represents X'_d and X11D represents X''_d etc.

GENERATOR REACTANCES									
GEN	XA	RA	XD	XQ	X1D	X1Q	X11D	X11Q	XCHAR
1	0.170	0.004	1.950	1.860	0.275	0.290	0.227	0.235	0.22
2	0.052	0.001	0.896	0.864	0.120	0.197	0.018	0.018	0.22
3	0.074	0.001	1.312	1.258	0.181	0.250	0.018	0.018	0.22
9999	0.0	0.0	0.0	0.0	0.0	0.0	0.0	0.0	0.0

Similarly, the electrical time constants of the synchronous machines, also defined in Table A.2, are entered into the datafile in the manner indicated below.

GENERATOR TIME CONSTANTS				
GEN	T1D	T1Q	T11D	T11Q
1	0.850	0.114	0.023	0.0085
2	0.850	0.114	0.023	0.0085
3	0.850	0.114	0.023	0.0085
9999	0.0	0.0	0.0	0.0

Automatic Voltage Regulation (AVR) and Power System Stabilisers (PSS)

It is very common to find AVR systems and more recently, PSS systems installed on large synchronous generators. PC-DAP provides the user with the option of including

these systems in the stability analysis. The AVR and PSS constants have been defined in section ? and are entered into the datafile as shown.

GENERATOR AVR CONSTANTS				
GEN	KR	TR1	TR2	TR3
1	0.0	0.0	0.0	0.0
2	0.0	0.0	0.0	0.0
3	0.0	0.0	0.0	0.0
9999	0.0	0.0	0.0	0.0

GENERATOR PSS CONSTANTS						
GEN	SK	TS1	TS2	TS3	TS4	TS5
1	0.0	0.0	0.0	0.0	0.0	0.0
2	0.0	0.0	0.0	0.0	0.0	0.0
3	0.0	0.0	0.0	0.0	0.0	0.0
9999	0.0	0.0	0.0	0.0	0.0	0.0

Turbine-Generator-Exciter Shaft Input Data

Input data for the mechanical systems on all turbine generators is entered in three sections i.e. turbine inertias, shaft stiffnesses, and turbine damping coefficients. The inertia constants are assumed to be in MW-s/MVA format.

INERTIA (S)						
GEN	HP	IP	LPA	LPB	GEN	EXC
1	0.204	0.384	1.858	1.84	2.927	0.021
2	0.104	0.284	1.558	1.54	0.727	0.021
3	0.104	0.284	1.558	1.54	0.727	0.021
4	0.0	0.0	0.0	0.0	0.0	0.0

The stiffness parameters, indicated below, are assumed to be in MW/MVA-rad format.

GEN	STIFFNESS				
1	39.5	105.7	113.6	86.2	32.1
2	39.5	105.7	113.6	86.2	32.1
3	39.5	105.7	113.6	86.2	32.1
4	0.0	0.0	0.0	0.0	0.0

Steam damping coefficients are entered in a per unit format.

GEN	DASHPOT DAMPING					
1	0.002	0.002	0.002	0.002	0.002	0.002
2	0.002	0.002	0.002	0.002	0.002	0.002
3	0.002	0.002	0.002	0.002	0.002	0.002
4	0.0	0.0	0.0	0.0	0.0	0.0

A.4 USER INTERFACE

The User Interface for PC-DAP is based around a series of routines which, when combined, give a flexible menu system which can be easily extended as the need arises. The system essentially consists of

- Pull-down menus
- Static menus
- Dialogue boxes
- One-shot buttons

A.4.1 Pull-Down Menus

The Pull-down menu consists of a series of horizontal cells which, when depressed by holding the left mouse key down, reveal a menu containing any number of buttons. Keeping the left mouse button depressed and dragging the cursor down over the menu buttons selects each of the buttons in turn. Releasing the left mouse button when the

chosen menu button is depressed selects that option. One of the Pull-down menu's used in PC-DAP is illustrated in Figure A.15.

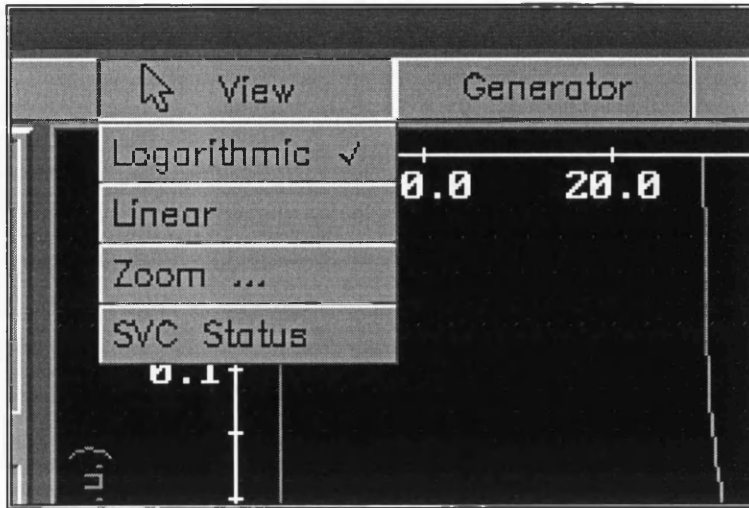


Figure A.15: PC-DAP Pull Down Menu

The following is a description of the variables used in the Call routine for the Pull-down menu. The FORTRAN call is:

```
SUBROUTINE GET_PULL_DOWN(NCELL,SIDE,TOP,WIDTH,M_WIDTH,DPTH,NBUT,
BDPTH,IPOINT,ISTORE,HELP,OUTSIDE,OLD_STATUS,I_EXIT,
IGET,I_TICK,BGRND,SSX,SSY,DISP_BOX,S_PD,S_PDB,S_WIDTH,S_BUT,
LOCK_ABLE,LOCK,PD_POS,P_DWN)
```

The variables are as follows:

NCELL : Number of horizontal cells (or buttons) in the Pull-Down Banner
 SIDE : The left extremity of the PD-Banner
 TOP : The top extremity of the PD-Banner
 WIDTH : Width of the PD-Banner cells
 M_WIDTH : Width of the PD-Menu buttons
 DPTH : Depth of the PD-Banner
 NBUT(i) : Number of PD-Menu buttons corresponding to PD-Banner cell i
 BDPTH : Depth of the PD-Menu Buttons (must not be less than DPTH)

- $I_TICK(i,j)$: Set to 1 if PD-Menu button j corresponding to PD-Banner cell i has a 'tick' to indicate selection. Set to 0 otherwise.
- $DISP_BOX$: Set to 1 if PD-Banner is to be used as a display box.
- $S_PD(i)$: Set to 1 if the PD-Menu corresponding to PD-Banner cell i has any sub-menu's associated with it.
- $S_PDB(i,j)$: Set element (i,j) to 1 if PD-Menu button j corresponding to PD-Banner cell i has a sub-menu. Set element (i,j) to 0 otherwise.
- $S_WIDTH(i,j)$: Width of the sub-menu buttons for PD-Menu button j on PD-Banner cell i
- $S_BUT(i,j)$: Number of sub-menu buttons for PD-Menu button i on PD-Banner cell i
- $PD_TXT(i)$: Text for PD-Banner cell i (this is stored in a separate routine called $GET_TXT(i,PD_TXT,PD_POS,M_TXT)$)
- $PD_POS(i)$: Position of the PD-Banner text for cell i relative to the left-hand edge of *that* cell (used to centre the PD-Banner text)
- $M_TXT(i,j)$: Text for PD-Menu button i corresponding to PD-Banner cell i (this is also stored in the routine GET_TXT)

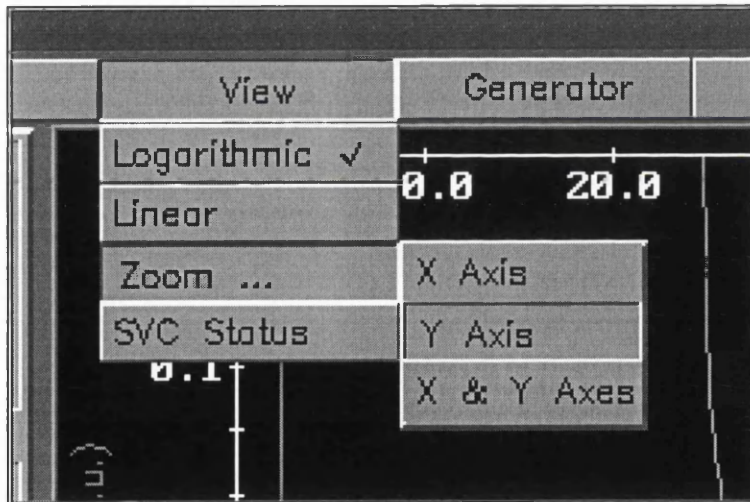


Figure A.16: Sub-menu's

Using the sub-menu variables in the GET_PULL_DOWN routine described above, sub-menu's can be incorporated into the menu system as illustrated in Figure A.16.

A.4.2 Static Menus

The static menu is a subset of the Pull-down routine. The selection of the options is similar to that of the Pull-down routine i.e position the mouse cursor over the chosen menu button and click the left hand mouse button. As for the Pull-down routine, each static menu button can have a sub-menu associated with it. The Call routine for the static menu is very similar to the routine for pull-down menus:

```
SUBROUTINE GET_MENU(SIDE, TOP, WIDTH, C_WIDTH, DPTH, NBUT, M_TXT, I_TICK,
  PD, IGET, AREA, DISP_CODE, BGRND, DISP_BOX, S_PD, S_PDB, S_WIDTH, S_BUT,
  I_BUT, PD_POS)
```

The variables follow an identical format to those described for the pull-down case.

All other button animation used throughout the program is derived from these basic animation routines. This enables expansion of the available options with relative ease, while keeping the size of the program code to a minimum.

APPENDIX B

MODELING OF STATIC VAR COMPENSATION

The primary voltage control loop of Figure 6.5 is repeated here for convenience.

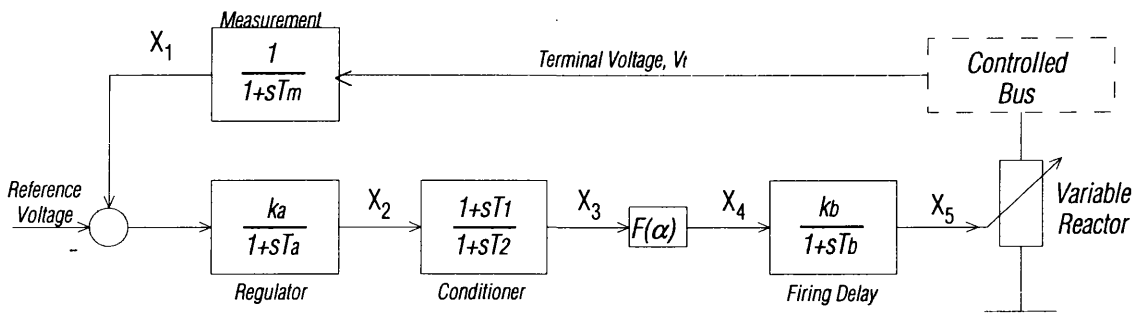


Figure B.1 : SVC Primary Voltage Control Loop

The Static compensator model is constructed in the state-space form

$$\begin{aligned}\dot{\underline{x}} &= A\underline{x} + B\Delta v_{svc} \\ \Delta i_{svc} &= C\underline{x} + D\Delta v_{svc}\end{aligned}\quad [B.1]$$

where the state vector and voltage deviation are defined as

$$\Delta \underline{x} = [\Delta x_1 \quad \Delta x_2 \quad \Delta x_3 \quad \Delta x_4 \quad \Delta x_5]^t \quad [B.2]$$

and

$$\Delta v_{svc} = [\Delta v_d \quad \Delta v_q]^t \quad [B.3]$$

where Δv_d and Δv_q are the real and imaginary components of SVC terminal voltage in the network frame of reference.

The matrices A and B in Eqn. [B.1] are defined as

$$A = \begin{bmatrix} -\frac{1}{T_m} & 0 & 0 & 0 & 0 \\ \frac{K_a}{T_a} & -\frac{1}{T_m} & 0 & 0 & 0 \\ \frac{K_a T_1}{T_2 T_a} & \frac{T_a - T_1}{T_2 T_a} & -\frac{1}{T_2} & 0 & 0 \\ 0 & 0 & \frac{2B_L}{\pi} & 0 & 0 \\ 0 & 0 & 0 & \frac{K_b}{T_b} & -\frac{1}{T_b} \end{bmatrix} \quad [\text{B.4}]$$

$$B = \begin{bmatrix} \frac{v_d^o}{T_m v_{svc}^o} & \frac{v_q^o}{T_m v_{svc}^o} \\ 0 & 0 \\ 0 & 0 \\ 0 & 0 \\ 0 & 0 \end{bmatrix} \quad [\text{B.5}]$$

The auxiliary current equation is obtained by considering that the SVC current is given by

$$\tilde{I}_{svc} = I_d + jI_q = \frac{v_{svc}}{jX_t + \frac{1}{j(\beta_c - B_L)}} \quad [\text{B.6}]$$

where X_t is the SVC connection transformer reactance, β_L and β_c are reactor and fixed capacitor admittances respectively.

Following perturbation then, the auxiliary current matrices C and D become

$$C = \begin{bmatrix} 0 & 0 & 0 & 0 & \frac{v_q^o}{(1 - X_t(\beta_L - \beta)_c)^2} \\ 0 & 0 & 0 & 0 & \frac{-v_d^o}{(1 - X_t(\beta_L - \beta)_c)^2} \end{bmatrix} \quad [\text{B.7}]$$

$$D = \begin{bmatrix} 0 & \frac{\beta_L - \beta_c}{(1 + X_t(\beta_L - \beta_c))^2} \\ \frac{\beta_c - \beta_L}{(1 + X_t(\beta_L - \beta_c))^2} & 0 \end{bmatrix} \quad [\text{B.8}]$$

APPENDIX

C

MODAL TORQUE ANALYSIS ALGORITHMS

C.1 AMPLITUDE OF SHAFT TORSIONAL VIBRATIONS DUE TO RESONANT EXCITATION

For a rigidly-fixed undamped spring/mass system of inertia J , stiffness S , excited by periodic amplitude T_m at resonant frequency $\omega = \sqrt{S/J}$, the amplitude of vibration δ is given by

$$\delta = \frac{T_m t}{2J\omega} \text{ rad} \quad [\text{C.1}]$$

where t is the excitation time in seconds. $T_m t$ is known as the torque excitation.

The corresponding expression for a multi-mass shaft where torque is applied to mass j is [43]

$$\delta_{jk} = \frac{T_{mk} t}{2\omega_k} \frac{(X_{jk})^2}{\sum_{i=1}^n J_i (X_{ik})^2} \text{ rad} \quad [\text{C.2}]$$

Here, j relates to mass, k corresponds to resonant angular frequency, n is the number of masses which simulate the shaft, and X corresponds to the eigenvectors.

C.2 MODAL TORQUE DUE TO RESONANT EXCITATION AT GENERATOR ROTOR

If torque excitation of amplitude T_{mk} is applied continuously to the generator rotor, the initial rate of increase in amplitude of the resulting vibration is given by [43]

$$\frac{d\delta_{jk}}{dt} = \frac{\sum_{l=p}^q (T_{mlk} \omega_l X_{lk} X_{jk})}{4\omega_k \sum_{i=1}^n H_i (X_{ik})^2} \text{ rad(elect)/sec} \quad [\text{C.3}]$$

where $H_i = \frac{J\omega_o}{2}$ in MW-s/MVA and ω_o is the system frequency in rad/s.

The steady amplitude of vibration is then given by

$$\delta_{jk} = \frac{d\delta_{jk}}{dt} T_k \text{ rad.(elect)} \quad [\text{C.4}]$$

where T_k is the time constant for decay of the vibration . The amplitude of the steady pulsating torque between masses r and s is given by

$$T_{rsk} = (\delta_{rk} - \delta_{sk}) S_{rs} \text{ p.u.} \quad [\text{C.5}]$$

where S_{rs} is the stiffness of he shaft between masses r and s.

C.3 TIME CONSTANTS FOR DECAY OF TORSIONAL VIBRATIONS

For a lumped mechanical system consisting of a mass M , spring constant K and viscous damper D , the characteristics of motion in terms of amplitude δ for free vibrations is given by

$$\frac{d^2\delta}{dt} + 2\xi\omega_n \frac{d\delta}{dt} + \omega_n^2\delta = 0 \quad [\text{C.6}]$$

where $\xi = \frac{D\omega_n}{2K}$ and $\omega_n = \sqrt{\frac{K}{M}}$.

The envelope of decay of vibrations of this system can be expressed in the form

$$\delta_i = Ae^{-\xi\omega_n t_i} \quad [\text{C.7}]$$

where δ_i is the amplitude of the i^{th} peak.

The time constant for decay of the vibrations then is given by

$$\Gamma = \frac{1}{\xi\omega_n} = \frac{2M}{D} \quad [\text{C.8}]$$

Inertia constant $H = \frac{M\omega_o}{2}$ in MW-s/MVA where ω_o is the system frequency.

Hence,
$$\Gamma = \frac{4}{\omega_o} \frac{H}{D} \quad [C.9]$$

The corresponding equation for a multi-mass system in terms of the inertia, viscous damping coefficients and the eigenvectors is

$$\Gamma = \frac{4 \sum_{i=1}^n H_i(x_{ik})}{\omega_o \sum_{i=1}^n D_{ik}(x_{ik})} \quad [C.10]$$

C.4 GENERATOR SCALING FACTORS (GSF)

Steady-state torque excitation corresponding to modulation product harmonic currents from which the magnitude of turbine-generator-exciter shaft torques corresponding to resonant excitation conditions are deduced may be evaluated (a) by assuming harmonic currents are completely reflected at the surface of the rotor (Method A), and using direct and quadrature-axis equivalent circuits where winding resistance (b) is ignored (Method B), and (c) is simulated (Method C).

C.4.1 Method A - - Harmonic Currents completely reflected at rotor surface

Airgap torque T_{el} is given by

$$T_{el} = \omega_o [\psi_{do} I_q - \psi_{qo} I_d] \quad [C.11]$$

where ψ_{do} and ψ_{qo} are initial direct- and quadrature-axis flux linkages.

Following perturbation of the current terms and appropriate substitution for the flux linkages in terms of machine reactances, the steady airgap torque is given by

$$\Delta T_{el} = [X_{md} I_{do} + X_{md} I_{fo}] \Delta I_q - X_{mq} I_{qo} \Delta I_d \quad [C.12]$$

But
$$\Delta I_d = I_v \sin[(\nu - \omega_o)t + \phi_d] \quad [C.13]$$

$$\Delta I_q = I_v \sin\left[(\nu - \omega_o)t + \phi_d + \frac{\pi}{2}\right] \quad [C.14]$$

where I_v is the amplitude of injected modulation product current at frequency ν .

The amplitude of steady torque is then given by

$$\Delta T_{el} = I_v \left(\left[X_{md} I_{do} + X_{md} I_{fo} \right]^2 + \left[-X_{mq} I_{qo} \right]^2 \right)^{\frac{1}{2}} \quad [C.15]$$

C.4.2 Method B - - Equivalent circuits neglecting resistance

Consider a (1d,2q) equivalent circuit for the synchronous machine. Active and reactive load on the generator is taken into consideration by the direct and quadrature-axis currents. damper and field winding resistance is neglected.

Using direct- and quadrature-axis equivalent circuits it can be deduced that field and damper currents in terms of perturbations in the direct and quadrature-axis stator currents ΔI_d and ΔI_q are given by

$$I_f = I_{fo} - \frac{X_D}{X_D + X_f} \frac{X_{md}}{X_{mDF} + X_{mD} + \frac{X_F X_D}{X_F + X_D}} \Delta I_d \quad [C.16]$$

or
$$I_f = I_{fo} + K_f \Delta I_d$$

$$I_D = -\frac{X_f}{X_D + X_f} \frac{X_{md}}{X_{mDF} + X_{mD} + \frac{X_F X_D}{X_F + X_D}} \Delta I_d \quad [C.17]$$

or
$$I_D = K_D \Delta I_d$$

$$I_Q = -\frac{X_{Q2}}{X_{Q1} + X_{Q2}} \frac{X_{mq}}{X_{mq} + \frac{X_{Q1}X_{Q2}}{X_{Q1} + X_{Q2}}} \Delta I_q \quad [\text{C.18}]$$

or
$$I_{Q1} = K_{Q1} \Delta I_q$$

$$I_{Q2} = -\frac{X_{Q1}}{X_{Q1} + X_{Q2}} \frac{X_{mq}}{X_{mq} + \frac{X_{Q1}X_{Q2}}{X_{Q1} + X_{Q2}}} \Delta I_q \quad [\text{C.19}]$$

or
$$I_{Q2} = K_{Q2} \Delta I_q$$

Using Eqn. [C.11], the airgap torque can be expressed in the form

$$\Delta T_{el} = A \Delta I_d + B \Delta I_q \quad [\text{C.20}]$$

where

$$A = \left[X_{md} + X_a + X_{md}K_f + X_{md}K_D - (X_{mq} + X_a) \right] I_{qo}$$

$$B = (X_{md} + X_a) I_{do} + X_{md} I_{fo} - \left[X_{mq} + X_a + X_{mq}K_{Q1} + X_{mq}K_{Q2} \right] I_{do}$$

C.4.3 Method C - - Equivalent circuits representing resistance

The constants K_f , K_D , K_{Q1} and K_{Q2} defined in Eqn. [C.20] are complex. They are evaluated using complex impedances where p.u. reactances correspond to rotor vibration frequency and dp.u. resistances are actual values.

The torque constants A and B of Eqn. [C.20] are evaluated using the complex values of K_f , K_D , K_{Q1} and K_{Q2} .

APPENDIX D

APPROXIMATE CALCULATION OF NONCHARACTERISTIC CURRENT LEVEL

The noncharacteristic current level acting on the stator of a synchronous machine can be determined by considering a 2000MW, ± 500 kV double-bipole HVDC Link. The pole current would be 1000A and assume a ripple at the inverter of 10% at the 12th harmonic. Also assume that the DC reactors are 0.5H each.

The 12th harmonic current on the DC line will have a magnitude of

$$\frac{50,000}{(2\pi 60)(12)(0.5 + 0.5)} = 11.05 A_{rms} = 15.6 A_{peak}$$

A direct current of 1000A will give a fundamental alternating current on the secondary of the converter transformer of

$$I_{ac}(50) = 2\sqrt{3} \frac{I_d}{\pi} = 1103 A$$

The modulation product produced by term (i) in Eqn. [8.2] which corresponds to 60Hz on the AC side has an amplitude of

$$I_{ac}(60) = \frac{kb}{22} = 2\sqrt{3} \frac{15.6}{\pi} = 0.782 A$$

The amplitude of the 60Hz component of the modulation current in the 50Hz system will be seen to be approximately 0.071%.

To a first approximation, 1.0 p.u. modulation current will produce 1.0 p.u. torque excitation acting on the generator rotor. It follows therefore that 0.071 p.u. modulation current will produce 0.071 p.u. torque excitation. The amplitude of modulation current acting on the generator stator is significantly reduced as a result of (i) system scaling factors and (ii) transmission line attenuation.

System scaling factors are discussed in Section 8.5.2 and are typically around 10-15% based on the generator apparent power rating. Transmission line attenuation is assumed to reduce the current level by approx. 20%. Taking account of these two factors gives a modulation current level of

$$(0.071)(0.1)(0.8) = 0.0057\%$$

APPENDIX

E

MATERIAL HYSTERETIC DAMPING

Mechanical damping of a turbine shaft is generally represented as viscous in nature having constant values for each section of the lumped mass model. This, however, is a simplification of the true nature of the damping. Mechanical damping is usually associated with steam acting on the turbine blades, hysteresis resulting from differing stress/strain relations on loading and unloading, windage and microslippage although only the two former sources are significant when considering damping of turbine shafts.

Steam damping is based on the constant power relationship of the characteristic which relates turbine speed with torque. This leads to variable damping coefficients acting on each turbine which is in proportion to the machine load.

Material hysteretic damping arises from the occurrence of small plastic strains in the overall elastic response of the material which causes the behaviour of the material on loading to differ slightly from that on unloading producing a hysteresis loop as illustrated in Figure E.1.

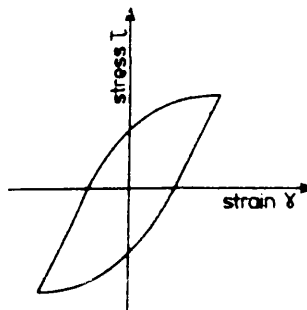


Figure E.1: Hysteresis Loop

The damping is frequency independent but stress-level related. Since in a viscous damper the damping force is proportional to velocity and hence frequency, a viscous damping model can only approximate the actual frequency independent damping. However, the viscous damping representation has the advantage of ease of mathematical formulation.

Smith et al. [67] discuss the variable nature of material damping and derive an equivalent viscous damping to replace the actual damping mechanism which gives identical energy absorption in free oscillations. The authors show that an appropriate damping coefficient is given by

$$D_{eq} = \frac{k_1}{\pi\omega} \left(\beta_1 + \frac{1}{2} \beta_2 \frac{k_1^2}{k_2} \alpha^2 + \dots \right) \quad [E.1]$$

where k_1 , k_2 are material constants, β_1 , β_2 are hysteresis coefficients, α is the strain amplitude of oscillation and ω is the angular frequency.

Equation [E.1] indicates that oscillations with high strain amplitudes will decay much more rapidly than oscillations of a low strain amplitude. In studies of post-fault conditions on turbine shafts where initial oscillations are large, Smith indicates that variable hysteresis damping will be very significant for the first few cycles reducing oscillation levels rapidly to a level at which they persist.

In studies of subsynchronous resonance and related phenomena, the emphasis is placed on oscillations which build gradually from low levels. As material hysteretic damping is not effective at low levels of oscillation, it is a minor source of damping relative to steam damping which is load and not strain level dependent and will not influence to any great extent the initial build-up of oscillations. However, if the oscillations were allowed to increase to significant levels or if the machine was operating on light load for which steam damping is very small, material damping would become a significant component of damping and should be included in shaft fatigue studies of such cases.

REFERENCES

- [1] C.P. Steinmetz, "Power Control and Stability of Electric Generating Stations", *AIEE Trans.*, vol 39, Part 2, pp 1215, July-December 1920
- [2] C. Young, R.M. Webler, "A New Stability Program for Predicting the Dynamic Performance of Electric Power Systems", *Proc. Am. Power Conf.*, pp.1126-1139, 1967
- [3] E.W. Kimbark, "Power System Stability", Vol.1, *Wiley*, New York, 1948
- [4] P.M. Anderson, A.A. Fouad, "Power System Control and Stability", *Iowa State University Press*, 1977
- [5] N. Kakimoto, Y. Ohsawa, M. Hayashi, "Transient Stability Analysis of Large-Scale Power Systems by Lyapunov's Direct Method", *IEEE Trans., Power Apparatus & Systems.*, Vol 103(1), pp. 160-167, January 1978
- [6] J.G. Francis, "The Q-R Transformation - A Unitary Analogue to the LR Transformation", Parts 1 & 2, *Comp. Journal*, Vol. 4, pp.256-271 & 332-345, 1961/62
- [7] R.T.H. Alden, H.M. Zein El-Din, "Multi-Machine Dynamic Stability Calculations", *IEEE Trans. on Power Apparatus & Systems*, Vol. PAS-95, No.5, pp.1529-1534, , Sept. 1976
- [8] R.T. Byerly, R.J. Bennon, D.E. Sherman, "Eigenvalue Analysis of Synchronising Power Flow Oscillations in Large Electric Power Systems", *IEEE Trans. on Power Apparatus & Systems*, Vol. PAS-101, pp.235-243, Jan. 1982
- [9] L.Wang, A. Semlyen, "Application of Sparse Eigenvalue Techniques To The Small Signal Stability Analysis of Large Power Systems", *IEEE Trans. on Power Systems*, PS-5, No.2, pp.635-642, 1990
- [10] N. Uchida, T. Nagao, "A New Eigen-Analysis Method of Steady-State Stability Studies for Large Scale Power Systems: S Matrix Method", *IEEE Trans. on Power Systems*, Vol.PWRS-3, No. 2, pp.706-714, May 1988
- [11] G.C. Verghese, I.J. Perez-Arriaga, F.C. Schweppe, "Selective Modal Analysis with Applications to Electric Power Systems", *IEEE Trans. on Power Apparatus & Systems*, Vol.PAS-101, No.9, pp.3117-3134, Sept.1982

- [12] A. Ruhe, "Rational Krylov Sequence Methods for Eigenvalue Computation", *Linear Algebra and Its Applications*, Vol. 58, pp.391-405, 1984
- [13] D.J. Stadnicki, J.E. Van Ness, "Invariant Subspace Method for Eigenvalue Computation", *IEEE Trans. on Power Systems*, Vol.8, No.2, pp.572-580, May 1993
- [14] G. Gross, C.F. Imparato, P.M. Look, "A Tool for the Comprehensive Analysis of Power System Dynamic Stability", *IEEE Trans. on Power Apparatus & Systems*, Vol. PAS-101, No. 1, pp.226-234, Jan. 1982
- [15] IEEE SSR Working Group, "First Benchmark Model for Computer Simulation of Subsynchronous Resonance", *IEEE Trans. Power Apparatus & Systems*, PAS-96, pp. 1565-1572, 1977
- [16] IEEE SSR Working Group, "Second Benchmark Model for Computer Simulation of Subsynchronous Resonance", *IEEE Trans. on Power Apparatus & Systems*, PAS-104, pp.1057-1066, May 1985
- [17] R.H. Park, "Two-Reaction Theory of Synchronous Machines, Generalised Method of Analysis—I", *AIEE Trans.*, Vol. 48, pp. 716-727, 1929
- [18] R.H. Park, "Two-Reaction Theory of Synchronous Machines—II", *AIEE Trans.*, Vol. 52, pp. 352-354, 1933
- [19] R.B. Bodine, C. Concordia, G. Kron, "Self-excited Oscillations of Capacitor Compensated Long Distance Transmission Systems.", *AIEE Trans.*, Vol. 62, pp. 41-44, 1943
- [20] C. Concordia, "Synchronous Machine Synchronising and Damping Torques", *AIEE Trans.*, Vol 70, pp. 731-737, 1951
- [21] S.E.M. de Oliveira, "Effect of Excitation Systems and Power System Stabilisers on Synchronous Generator Damping and Synchronising Torques", *IEE Proc., Part C*, Vol. 136, No. 5, Sept. 1989
- [22] K.R. Padiyar, R.K. Varma, "Damping Torque Analysis of Static Var System Controllers", *IEEE Trans. on Power Systems*, PS-6, No.2, pp. 458-465, May 1991

- [23] S.E.M. de Oliveira, "Synchronising and Damping Torque Coefficients and Power System Steady-State Stability as Affected by Static Var Compensators", *IEEE Trans. on Power Systems*, PS-9, No. 1, pp. 109-116, Feb. 1994
- [24] A. Kurita et al, "Verification of the Mechanism of Torsional Oscillation caused by the Interactions between Turbine-Generators and HVDC Power Transmission Systems", *Electrical Engineering in Japan*, Vol. 108, No.5, pp. 39-49, 1988
- [25] I.M. Canay, "A Novel Approach to the Torsional Interaction and Electrical Damping of the Synchronous Machine - Part I: Theory", *IEEE Trans. on Power Apparatus & Systems*, PAS-101, No.10, Oct. 1982
- [26] C. Concordia, "Synchronous Machines - Theory and Performance", *General Electric Company*, 1951
- [27] P.C. Krause, "Analysis of Electric Machinery", *McGraw-Hill Book Company*, 1986
- [28] M.H. Kent, W.R. Schmnns, F.A. McCrackie, I.M. Wheeler, "Dynamic Modelling of Loads in Stability Studies", *IEEE Trans. on Power Apparatus & Systems*, Vol. 88, No.5, pp.756-763, 1969
- [29] J.W. Butler, C. Concordia, "Analysis of Series Capacitor Application Problems", *AIEE Trans.*, Vol. 56, pp.975-988, Aug. 1937
- [30] L.A. Kilgore, L.C. Elliott, E.R. Taylor, "The Prediction and Control of Self-Excited Oscillations due to Series Capacitors on Power Systems", *IEEE Trans. on Power Apparatus & Systems*, Vol.90, No.3, pp.1305-1311, May 1971
- [31] IEEE Subsynchronous Working Group, "Terms, Definitions and Symbols for Subsynchronous Oscillations", *IEEE Trans. on Power Apparatus & Systems*, Vol. PAS-104, No.6, June 1985
- [32] K. Mortensen, E.V. Larsen, P.J. Piwko, "Field tests and analysis of Torsional Interaction between the Coal Creek Turbine Generators and the CU HVDC System", *IEEE Trans. on Power Apparatus & Systems*, Vol.PAS-100, No.1, pp.336-344, Jan. 1981
- [33] M. Bahrman, E.V. Larsen, P.J. Piwko, H.S. Patel "Experience with HVDC-Turbine-Generator Torsional Interaction at Square Butte", *IEEE Trans. on Power Apparatus & Systems*, Vol.PAS-99, No.3, pp.966-975, May. 1980

- [34] J.W. Ballance, S. Goldberg, "Subsynchronous Resonance in Series Compensated Transmission Lines", *IEEE Trans. on Power Apparatus & Systems*, Vol.PAS-92, No.5, pp.1649-1658, Sept. 1973
- [35] C.F. Wagner "Self-Excitation of Induction Motors with Series Capacitors", *AIEE Trans.*, Vol.60, pp.1241-1247, 1941
- [36] L. Wang, S. Jan Mau, C. Chen Chuko, "Suppression of Common Torsional mode Interactions using Shunt Reactor Controllers", *IEEE Trans. on Energy Conversion*, Vol.8, No.3, pp.539-545, Sept. 1993
- [37] L. Shun, L. Chun-Chang, "Damping Subsynchronous Resonance using a SIMO Shunt Reactor Controller", *IEEE Trans. on Power Systems*, Vol.9, No.3, pp.1253-1262, Aug. 1994
- [38] M.R. Iravani, A.A. Edris, "Eigenanalysis of series compensation schemes reducing the potential of Subsynchronous Resonance", *IEEE Trans. on Power Systems*, Vol.10, No.2, pp.876-881, 1995
- [39] M.R. Iravani, R.M. Mathur, "Suppressing Transient Shaft Stresses of Turbine Generators using a Static Phase Shifter", *IEEE Trans. on Energy Conversion*, Vol. EC-1, No.1, pp.186-192, March 1986
- [40] IEEE/CIGRE "FACTS Overview", April 1995
- [41] J. Urbanek, R.J.Piwko, E.V. Larsen, B.L. Damsky, "Thyristor Controlled Series Compensation - Prototype Installation at the Slatt 500 kV substation", *IEEE Trans. on Power Delivery*, pp.1460-1469, July 1993
- [42] J.J. Paserba, N.W. Miller, E.V. Larsen, R.J. Piwko, "A Thyristor Controlled Series Compensation Model for Power System Stability Analysis", *IEEE Trans. on Power Delivery*, Vol.10, No.3, pp.1471-1478, 1995
- [43] S. Nyati, C.A. Wegner, R.W. Delmerico, R.J. Piwko, D.H. Baker, A. Edris, "Effectiveness of Thyristor Controlled Series Capacitor in Enhancing Power System Dynamics: An Analog Simulator Study", *IEEE Trans. on Power Delivery*, Vol.9, No.2, pp.1018-1027, April 1994
- [44] T.J. Hammons, M. Istin, A. Crocquevielle, "Analysis of Continuum and Reduced Shaft Models in Evaluating Turbine-Generator Shaft Torsional Response following Severe

- Disturbances on the System Supply”, *Electric Machines and Power Systems*, pp.387-408, Dec. 1987
- [45] S.E.M. de Oliveira, “Synchronising and Damping Torque Coefficients and Power System Steady-state Stability as Affected by Static Var Compensators”, *IEEE Trans. on Power Systems*, Vol.9, No.1, pp.109-116, Feb. 1994
- [46] T. Smed, “Feasible Eigenvalue Sensitivity for Large Power Systems”, *IEEE Trans. on Power Systems*, Vol.8, No.2, pp.555-563, May 1993
- [47] A.A. Shaltout, E.A. Abu-Al-Feilat, “Damping and Synchronising Torque Computation in Multi-machine Power Systems”, *Trans. on Power Systems*, Vol.7, No.1, pp.280-286, Feb. 1992
- [48] T. Hara et al., “Development of a Damping Analysis Program for Multi-Generator Power Systems”, *IEEE Trans. on Power Systems*, Vol.9, pp.1803-1810, 1994
- [49] J.M. Undrill, F.P. de Mello, “Subsynchronous Oscillations — Parts 1 & 2”, *IEEE Trans. on Power Apparatus & Systems*, Vol.PAS-95, No.4, pp.1448-1464, July 1976
- [50] N. Rostamkolai, E.V. Larsen, et al. “Subsynchronous Torsional Interactions with Static Var Compensators - Concepts and Practical Implications”, *IEEE Trans. on Power Systems*, Vol.5, No.4, pp.1324-1332, Nov. 1990
- [51] M. Parniani, M.R. Iravani, “Voltage Control Stability and Dynamic Interaction Phenomena of Static Var Compensators”, *IEEE Trans. on Power Systems*, Vol.10, No.3, pp.1592-1597, Aug. 1995
- [52] Task Force No.2 on Static Var Compensators, “Static Var Compensators”, *Cigre Working Group 38-01*, Sept. 1985
- [53] T. Ohyama et al., “Effective Application of Static Var Compensators to Damp Oscillations”, *IEEE Trans. on Power Apparatus & Systems*, Vol. PAS-104, No.8, pp.1405-1410, June 1983
- [54] IEEE Special Stability Controls Working Group, “Static Var Compensator Models for Power Flow and Dynamic Performance Simulation”, *IEEE Trans. on Power Systems*, Vol.9, No. 1, pp.229-239, Feb. 1994

- [55] A. Roman-Messina, "Enhancement of Dynamic Stability by Coordinated control of Static VAR Compensators", *International Journal of Electrical Power & Energy Systems*, Vol.15, No.2, pp.85-93, 1993
- [56] S. Lefebvre, L. Gerin-Lajoie, "A Static Compensator Model for the EMTP", *IEEE Trans. on Power Systems*, Vol.7, No.2, pp.477-486, May 1992
- [57] R.J. Piwko et al, "Subsynchronous Resonance Performance Tests of the Slatt Thyristor Controlled Series Capacitor", *IEEE Trans. on Power Delivery*, Vol.11, No.2, pp.1112-1119, April 1996
- [58] W. Zhu, R. Spee et al, "An EMTP Study of SSR Mitigation using the Thyristor Controlled Series Capacitor", *IEEE Trans. on Power Delivery*, Vol.10, No.3, pp.1479-1485, 1995
- [59] J.F. Gronquist et al, "Power Oscillation Damping Control Strategies for FACTS Devices using Locally Measurable Quantities", *IEEE Trans. on Power Systems*, Vol.10, No.3, pp.1598-1605, Aug. 1995
- [60] R.Yacamani, "How HVDC Schemes can excite Torsional Oscillations in Turbo-Alternator Shafts", *IEE Proceedings*, Vol.133, Pt. C, No. 6, pp.301-307, 1986
- [61] H. Fick, "Excitation of Subsynchronous Torsional Oscillations in Turbine Generator Sets by a Current-Source Converter", *Siemens Power Engineering IV*, No.2, pp.83-86, 1986
- [62] A. Kurita et al "Verification of the Mechanism of Torsional Oscillation caused by the Interactions between Turbine-Generators and HVDC Power Transmission Systems", *Electrical Engineering in Japan*, Vol.108, No. 5, pp.39-49, 1988
- [63] T.J. Hammons, "Simulation of a Synchronous Generator in Direct Phase Quantities - - Sequential Interruption of Fault Currents and their Effect on Transient Electromagnetic Torque", *Proceedings of the 1984 International Conference on Electric Machines*, Lausanne, Switzerland, Part 2, pp.439-442, 18-21 Sept 1984
- [64] J.C. Read, "The Calculation of Rectifier and Inverter Performance Characteristics", *Journal of the Institution of Electrical Engineers*, Vol.92, No.2, pp.495-509, 1945
- [65] A.M. Gole et al, "A Graphical Electromagnetic Simulation Laboratory for Power Systems Engineering Programs", *IEEE Trans. on Power Systems*, Vol.11, No.2, pp599-606, 1996

- [66] J.K. Reid, "Large Sparse Sets of Linear Equations", *Proceedings of the Oxford conference of the Institute of Mathematics and its Applications*, April 1970, Academic Press 1971
- [67] J.R. Smith et al, "The Effect of Hysteresis Damping on Turbogenerator Shaft Torsional Oscillations", *IEEE Trans. on Energy Conversion*, Vol.EC-1, No.1, pp.152-158, 1986

